Titre: Title:	Comportement dynamique nonlinéaire des structures cylindriques fermées et isotropes, soumises à un écoulement supersonique
Auteur: Author:	Yacine Ben Youssef
Date:	2021
Type:	Mémoire ou thèse / Dissertation or Thesis
Référence: Citation:	Ben Youssef, Y. (2021). Comportement dynamique nonlinéaire des structures cylindriques fermées et isotropes, soumises à un écoulement supersonique [Thèse de doctorat, Polytechnique Montréal]. PolyPublie. https://publications.polymtl.ca/9648/

URL de PolyPublie: PolyPublie URL:	https://publications.polymtl.ca/9648/
Directeurs de recherche: Advisors:	Aouni A. Lakis
Programme: Program:	PhD.

POLYTECHNIQUE MONTRÉAL

affiliée à l'Université de Montréal

Comportement dynamique nonlinéaire des structures cylindriques fermées et isotropes, soumises à un écoulement supersonique

YACINE BEN YOUSSEF

Département de génie mécanique

Thèse présentée en vue de l'obtention du diplôme de *Philosophiae Doctor*

Génie mécanique

Novembre 2021

POLYTECHNIQUE MONTRÉAL

affiliée à l'Université de Montréal

Cette thèse intitulée :

Comportement dynamique nonlinéaire des structures cylindriques fermées et isotropes, soumises à un écoulement supersonique

présentée par **Yacine BEN YOUSSEF**

en vue de l'obtention du diplôme de *Philosophiae Doctor*

a été dûment acceptée par le jury d'examen constitué de :

Shirazi-Adl ABOULFAZL, président

Aouni A. LAKIS, membre et directeur de recherche

Abdelhak OULMANE, membre

Manouchehr NEJAD ENSAN, membre externe

DÉDICACE

الحمد لله الذي بنعمته تتم الصالحات،

(*Louange à ALLAH*)

À mes très chers parents,

À mes chères sœurs et À mon cher beau-frère,

À mon cher neveu et À ma chère nièce,

À la mémoire de ma chère grande mère et mes chers oncles qui ont tous quitté la vie sans que je ne sois présent pour dire au revoir,

À ma chère grande famille

À mes chers frères Abdelhak OULMANE et Youcef KERBOUAA qu'ils n'ont cessé de m'aider sur tous les plans et qui m'ont été un grand soutien avec qui j'ai partagé tous les bons moments et même les moments difficiles.

Croire en un monde extérieur indépendant du sujet qui le perçoit constitue la base de toute science de la nature. Cependant les perceptions des sens n'offrent que des résultats indirects sur ce monde extérieur ou sur la « réalité physique ». Alors seule la voie spéculative peut nous aider à comprendre le monde. Nous devons donc reconnaître que nos conceptions de la réalité physique n'offrent jamais que des solutions momentanées. Et nous devons donc être toujours prêts à transformer ces idées, c'est-à-dire le fondement axiomatique de la physique, si, lucidement, nous voulons voir de manière aussi parfaite que possible les faits perceptibles qui changent. Quand nous réfléchissons même rapidement sur l'évolution de la physique, nous observons bien, en effet, les profondes modifications de cette base axiomatique. ~ ***Albert Einstein***

Quand on observe l'évolution d'une science et qu'on se penche sur la volonté secrète du savant, on s'aperçoit que l'ambition asymptotique fondamentale de toute science est la création d'une théorie aussi totale que possible assumant mathématiquement une part de plus en plus grande du réel. ~ ***Lichnerowicz***

REMERCIEMENTS

Mes premiers remerciements s’adressent tout naturellement et en premier lieu à ALLAH, Le Tout Puissant, de m’avoir donné autant de courage, de patience et de volonté pour achever ce travail malgré toutes les difficultés que j’ai affrontées tout au long de ma thèse de doctorat.

Je tiens par la suite à témoigner ma profonde reconnaissance et mes remerciements les plus sincères à mon directeur de recherche Pr. Aouni A. LAKIS pour les conseils, les encouragements et la confiance qu'il m'a généreusement prodigués tout au long de ce travail. Ils ont été pour moi le stimulant nécessaire à l'accomplissement de ce travail. Je vous remercie également pour l’autonomie que vous m’avez accordée tout au long de ces années afin d’explorer plusieurs axes de recherches et mener à bien ce travail. Vos soins extrêmes, votre expérience scientifique, vos brillantes intuitions et votre éclectisme sont pour moi un exemple.

Ma profonde gratitude et mes vifs remerciements s’adressent à mon Co-encadrant Pr. Youcef KERBOUAA avec qui le travail devient une vraie partie de plaisir. Je vous remercie pour votre soutien indéfectible, pour votre présence qui m’a fait profiter de votre rigueur, de votre expérience scientifique. C’est à ses côtés que j’ai compris ce que rigueur et précision voulaient dire. Je me souviens bien de toutes les heures qu’on a passées travailler et de toutes les discussions enrichissantes que nous avons eues à chaque étape de ce travail. Ils m’ont été trop bénéfiques.

Je tiens aussi à remercier chaleureusement et exprimer ma respectueuse reconnaissance au Pr. Abdelhak OULMANE, ce personnage merveilleux qui a combiné la rigueur scientifique et l'esprit d'altruisme. Je vous remercie infiniment pour votre soutien et pour vos conseils continuels qui ne me cessent d’apporter toujours le plus. J’ai beaucoup bénéficié de votre savoir-faire et de votre expérience et j’ai finalement trouvé la justification pour toute cette énorme quantité de prix et récompenses que vous avez gagnés.

J’adresse aussi mon respect et ma gratitude au professeur ABOULFAZL Shirazi-Adl pour avoir accepté de présider le jury, pour sa participation scientifique ainsi que le temps qu’il a consacré à ma recherche.

Mes vifs remerciements s’adressent également à monsieur NEJAD ENSAN Manouchehr pour l'intérêt qu'il a porté à ce travail en acceptant d'être membre de jury et pour avoir accepté d’évaluer cette thèse.

Parce que la gratitude est la meilleure attitude, je saisie cette occasion pour remercier certains enseignants que j'ai eu la chance d'avoir et qui m'ont amené à faire de la mécanique et de la recherche : Pr. Rachid NASRI, Pr. Ali ZGHAL, Pr. Slim GUERMAZI, Pr. Ahmad MARRAKCHI et Pr. Mekki KSOURI. Qu'ils reçoivent mon meilleur souvenir.

Je tiens aussi à remercier tous mes amis notamment ceux de la section mécanique appliquée, pour la bonne ambiance de travail et pour tous les conseils et les conversations qu'on a pu avoir. Je peux dire qu'un grand nombre de personnes ont eu une part dans ce travail même indirectement mais leur contribution était pour moi un grand apport pour mener cette thèse à son terme car ils ont concouru à rythmer le quotidien et m'écarter positivement de mes obligations doctorantes. Je tiens en ce sens à remercier : Dr. Mohamed, Dr. Abd-ALLAH, Dr. Zakaria, Dr. Aymen, Dr. Hafedh, Anis, Oussema, Abd-ELLATIF, Achraf, Abd-ESSALAM, Ali, Mehdi, Mohamed Bouzouiki Junior, Seifeddine, Samir, Chokri, Houssine, Mohamed Attig et Hichem.

Enfin, les mots sans peu pour exprimer ma profonde reconnaissance et mon énorme gratitude à mes parents qui n'ont jamais cessé de me soutenir et de m'encourager. Je ne serai jamais en mesure de rembourser leurs sacrifices. Peu importe ce que je fais, je ne compenserai jamais une goutte de sueur qui est tombée sur le front de mon père pour nous assurer une belle vie, ou un moment d'anxiété que ma mère a vécu en pensant à moi dans les périodes difficiles. Mes particulières reconnaissances s'adressent également à mes deux sœurs et à mon beau-frère que je les remercie énormément pour leur soutien inestimable et inconditionnel, et pour leur encouragement incessant qui me pousse toujours vers l'avant.

RÉSUMÉ

L’analyse du comportement dynamique géométriquement nonlinéaire des structures cylindriques minces fermées et isotropes, soumises à un écoulement supersonique, a suscité l’intérêt de la communauté scientifique et a mobilisé un grand nombre de chercheurs dans la dernière décennie. Cela est dû, d’une part, à l’utilisation de ces structures dans des domaines de haute pointe telle que l’aérospatiale, l’aéronautique et le nucléaire et d’autre part au besoin de développer des modèles analytiques et numériques capables d’analyser fidèlement le phénomène d’instabilité dynamique afin de pouvoir fournir des prédictions correctes, tant qualitativement que quantitativement surtout avec l’avènement accru des outils numériques.

La majorité des études qui ont été menées emploie l’étude linéaire pour traiter ce genre de problème et un nombre limité de recherches qui a été consacré à l’analyse nonlinéaire du comportement dynamique des coques cylindriques minces soumises à l’effet du flottement supersonique.

Cette thèse a pour but de proposer un modèle capable d’analyser linéairement et nonlinéairement le comportement dynamique des structures cylindriques minces et isotropes lorsqu’elles sont soumises à un écoulement supersonique externe en tenant compte de l’effet des contraintes initiales de raidissement induites par des pressions radiales et/ou des forces axiales. Le modèle développé tient aussi en considération de l’effet des imperfections géométriques initiales, de l’effet de courbure au niveau du champ de déplacement circonférentiel ainsi que de l’effet du couplage nonlinéaire entre les différents modes. Il permet aussi de prédire le début de l’instabilité dynamique de la structure et de décrire son comportement durant les phases qui suivent l’apparition de flottement.

La méthode développée dans cette thèse rallie à la fois la méthode des éléments finis, la théorie des coques minces et la théorie aérodynamique de fluide.

Trois aspects étaient au centre de l'intérêt de ce travail de recherche, réparties sur trois sections stipulant l’effet des contraintes initiales de raidissement sur le comportement dynamique des structures axisymétriques, en premier lieu. Ensuite, une formulation a été développée optant pour l’analyse des vibrations libres géométriquement nonlinéaires des coques cylindriques minces. La troisième partie traite l’effet des forces aérodynamiques induites par un écoulement d’air

supersonique sur le comportement dynamique nonlinéaire des structures cylindriques minces et isotropes en évaluant entre autre leur état de stabilité.

La première partie de ce travail, met en exergue l'analyse détaillée de l'effet des contraintes initiales de raidissement sur le comportement dynamique des structures axisymétriques. Ces dernières sont composées principalement par des éléments de type cylindrique, conique et/ou des éléments axisymétriques à rayon variables. Pour assurer une meilleure consistance géométrique, deux éléments finis de forme cylindrique et conique basés sur la méthode des éléments finis hybrides sont considérés dans cette étude. Cette approche repose sur une combinaison entre la méthode des éléments finis classique et la théorie des coques minces. Les fonctions de déplacement sont dérivées à partir des solutions exactes des équations d'équilibre de Sanders relatives aux cas des coques cylindriques et coniques. Les matrices de masse et de rigidité linéaires sont déterminées en se basant sur l'expression de l'énergie de déformation élastique et de l'énergie cinétique. La matrice de rigidité induite par les contraintes initiales de raidissement, inférées des forces axiales et/ou des pressions radiales, est déterminée à partir de l'expression de l'énergie de déformation élastique associée aux forces membranaires. Les équations de mouvement sont dérivées à partir des équations de Lagrange et résolues en considérant l'approche du système à valeurs propres. Les structures combinées sont aussi prises en considération dans cette étude. Celles-ci se manifestent par un assemblage des éléments cylindriques et d'autres coniques en appliquant les techniques standard des éléments finis. Ces structures combinées tirent, en conséquence, profit des avantages du modèle hybride des éléments finis cylindriques et ceux coniques. L'effet des forces axiales ainsi que des pressions radiales est examiné dans cette étude tout en tenant en compte de la variation des propriétés géométriques des structures. L'analyse tient aussi en compte de l'effet des différentes conditions aux limites sur le comportement dynamique des structures axisymétriques. L'étude a montré que les structures cylindriques soumises à des pressions externes deviennent vulnérables à l'instabilité dynamique (divergence) au fur et à mesure que leurs rayons augmentent. Un effet opposé a été révélé lorsque les structures cylindriques sont sujettes à des forces axiales de compression marquant ainsi l'absence de l'effet de la variation de rayon de courbure sur la charge critique de flambement dynamique des coques cylindriques. Les résultats ont montré aussi que l'augmentation de l'angle du tronc de cône favorise l'instabilité des structures coniques en les comparant aux coques présentant des angles modérés et que l'effet des contraintes initiales de raidissement pour les coques combinées devient prépondérant lorsque le comportement flexionnel gouverne alors qu'il devient minime lorsque le comportement membranaire gouverne. L'étude a montré une excellente concordance entre les résultats issus de cette analyse avec ceux expérimentaux et numériques trouvés dans la littérature.

La seconde partie de cette thèse, est consacrée à l'analyse du comportement géométriquement nonlinéaire (grande amplitude de vibration et petite déformation) des coques cylindriques minces, fermées et isotropes en vibration libre, à travers le développement d'une formulation basée sur les relations cinématiques nonlinéaires de Novozhilov. La théorie, développée dans ce manuscrit, tient en compte de l'effet de courbure au niveau du champ de déplacement circonférentiel et considère l'impact des imperfections géométriques initiales sur la réponse dynamique du système. Le couplage nonlinéaire entre les différents modes est entre autre pris en considération. La formulation prend d'abord une forme générale en considérant le champ de déplacement comme une combinaison entre une fonction temporelle (coordonnée généralisée) et une autre spatiale. Les relations cinématiques nonlinéaires découlent de la théorie de Novozhilov. L'équation de mouvement est inférée des équations de Lagrange en se basant sur une approche énergétique. Les matrices de rigidité nonlinéaires quadratiques et cubiques sont déterminées après intégration analytique des coefficients modaux s'écrivant en termes des fonctions de formes. Le développement d'un modèle hybride a été évoqué dans un second temps, en ralliant à la fois la formulation développée avec la méthode des éléments finis classique. Les matrices élémentaires de masse et de rigidité linéaires et nonlinéaires sont déterminées en remplaçant les fonctions spatiales du champ de déplacement par les fonctions de forme découlant de l'analyse linéaire et dérivés à partir de la solution exacte des équations d'équilibre de Sanders ce qui acquiert au modèle une rapidité de convergence et une précision des résultats. La résolution de l'équation de mouvement se base principalement sur le principe de linéarisation après avoir transformé le système dans sa base modale. L'effet des différents paramètres tel que la variation du nombre d'ondes axiales et circonférentielles, des paramètres géométriques ainsi que des conditions aux limites sur le comportement dynamique des structures cylindriques minces a été examiné. Les résultats décelés à partir de cette étude sont en bonne concordance avec ceux relatifs aux autres auteurs. L'analyse révélée a mis en exergue l'effet prépondérant du couplage nonlinéaire à accentuer le caractère raidissant du comportement dynamique nonlinéaire des coques cylindriques. D'autant plus, l'étude nonlinéaire a apporté quelques amendements en matière de caractérisation des fréquences et modes fondamentaux. L'analyse a aussi exhibé une évolution croissante de la fréquence relative nonlinéaire en fonction de l'augmentation de l'élancement de la structure incité par la chute draconienne de la fréquence linéaire par rapport à celle nonlinéaire.

La troisième partie de cette recherche, présente un modèle permettant d'analyser le comportement dynamique nonlinéaire des coques cylindriques minces fermées et isotropes, soumises à des pressions radiales et/ou des forces axiales et exposées à un écoulement d'air supersonique. Les matrices de masse et de rigidité structurales sont obtenues en se basant sur une approche énergétique. La matrice de rigidité induite par les contraintes initiales de raidissement est calculée en se basant sur l'évaluation de l'énergie de déformations des flux d'efforts membranaires. La matrice de rigidité nonlinéaire cubique est déterminée à partir de l'intégration analytique des coefficients modaux qui dépendent également des fonctions de forme trouvés à partir de l'analyse linéaire. La pression aérodynamique locale exercée par le fluide sur la structure est dérivée de la théorie de piston linéaire avec et sans considération des termes de corrections de courbures. La corrélation entre la pression aérodynamique et la composante radiale, locale du vecteur vitesse de fluide a permet d'exprimer la force aérodynamique en fonction des déplacements calculées en tout point de la structure. Les matrices de rigidité et d'amortissement de fluide sont déterminées par intégration analytique de la force de pression aérodynamique. Les équations de mouvement sont établies à partir des équations de Lagrange et résolues par le biais d'une méthode itérative directe. Plusieurs résultats sont décelés suite à cette recherche mettant en exergue l'effet assouplissant du comportement nonlinéaire traduit par la relation ralliant les rapports des fréquences linéaires et nonlinéaires en fonction des ratios d'amplitude de vibration et de l'épaisseur des parois des coques. L'effet du couplage nonlinéaire ainsi que les effets du nombre d'ondes circonférentiels et des paramètres géométriques de la structure sur le comportement dynamique nonlinéaire des coques pressurisées et non pressurisées pendant le début du flottement et durant les phases d'instabilité sont investigués dans cette étude. L'étude a met l'accent sur l'effet éminent du couplage entre les différents modes nonlinéaires et qui réside dans l'accentuation du caractère assouplissant des coques cylindriques pressurisées en fonction de l'accroissement de l'amplitude de flottement. L'augmentation de l'élancement de la structure favorise l'instabilité de la structure toutefois, son effet sur la tendance du comportement dynamique nonlinéaire des structures cylindriques s'avère négligeable lorsqu'elles sont sujettes aux valeurs limites de flottement en terme de P_{cr} et n_{cr}. Une très bonne concordance a été révélée entre ces résultats et ceux numériques, analytiques et expérimentales trouvés dans la littérature.

Le modèle développé dans cette thèse constitue un outil puissant permettant d'évaluer les caractéristiques vibratoires des structures cylindriques minces fermées et isotropes dans le domaine nonlinéaire et d'offrir, en conséquence, une bonne prédiction de l'instabilité de ces structures lorsqu'elles sont soumises à un écoulement supersonique. Ceci est exaucé grâce à une combinaison entre les avantages de la méthode des éléments finis permettant de traiter les coques avec des formes complexes, avec la précision de la formulation développée admettant comme fonctions de forme les solutions exactes des équations d'équilibre qui découlent de la théorie linéaire des coques. Ces avantages donnent plus de fiabilité aux résultats et offrent plus de robustesse au modèle développé pour traiter les problèmes aéroélastiques.

ABSTRACT

Analysis of the geometrically nonlinear dynamic behaviour of closed and isotropic thin cylindrical structures subjected to supersonic flow has attracted the interest of the scientific community and has been the subject of a large number of research studies during the past decade. The major reason for this is the use of these structures in high-tech fields such as aerospace, aeronautics and nuclear energy. This has created a requirement to develop analytical and numerical models capable of analyzing the phenomenon of dynamic instability and providing accurate predictions, both qualitatively and quantitatively. The advent of new digital tools makes this possible.

The majority of studies that have been conducted in this area use a linear approach to address this type of problem. Only a limited number of studies have been devoted to nonlinear analysis of the dynamic behaviour of thin cylindrical shells subjected to supersonic flutter.

The aim of this thesis is to propose a model capable of analyzing, linearly and nonlinearly, the dynamic behaviour of thin isotropic cylindrical shells subjected to external supersonic flow, including consideration of the effect of initial stiffening stresses induced by radial and/or axial forces. The developed model also takes into account the effect of initial geometric imperfections, the curvature effect in the circumferential direction of the displacement field and the effect of nonlinear coupling between different modes. It also calculates the point of onset of dynamic instability of the structure and describes its behaviour during phases following the onset of flutter.

The method developed in this thesis combines the finite element method, the Novozhilov thin shell theory and aerodynamic fluid theory.

Three aspects were at the centre of interest of this research work and are, therefore, divided into three sections. The first part studies the effect of initial stiffening stresses on the dynamic behaviour of axisymmetrical structures. Following this, a formulation is developed for analysis of geometrically nonlinear free vibration of thin cylindrical shells. The third section deals with the effect of aerodynamic forces induced by supersonic air flow on the nonlinear dynamic behaviour of thin, isotropic cylindrical shells by assessing, among others, their state of stability.

Axisymmetrical structures are mainly composed of cylindrical, conical and/or axisymmetric elements with variable radius. To ensure better geometric consistency, two semi-analytical finite elements (cylindrical and conical) were used in a hybrid finite element method to model

axisymmetric shells. This approach is based on a combination of the classical finite element method and thin shell theory. The displacement functions are derived from exact solutions of Sanders' shell equilibrium equations for cylindrical and conical shells. Linear mass and stiffness matrices are determined based on the expression of elastic strain energy and kinetic energy. The stiffness matrix induced by the initial stiffening stresses, inferred from axial and/or radial forces, is determined from the expression of elastic strain energy associated with the membrane forces. The equations of motion are derived based on the Lagrange method and resolved by considering the eigenvalue system approach. Combined structures are also considered in this study. These are modeled using an assembly of cylindrical and other conical elements and analyzed by applying standard finite element techniques. This modelling approach is advantageous for analysis of combined shells. The effect of axial forces as well as radial pressure is examined. The analysis also includes consideration of variations of the geometric properties and the effect of different boundary conditions on the dynamic behaviour of axisymmetric shells. The critical buckling load is observed to be the lowest in the case of the clamped-free boundary condition of the cylindrical shells. It can be noticed that the conical structure loses its bearing capacity and a significant drop of its total rigidity can be noted when the critical loads corresponding to various semivertex angles are reached. We can also discern that the initial stiffening effect is remarkable for large values of the number of circumferential waves. However, it is minimal when the combined structure membrane behavior governs. The results presented in this study show an excellent agreement with those found in the literature, both experimental and numerical.

The second part of this thesis is devoted to the analysis of the nonlinear dynamic behaviour (large-amplitude vibration) of thin, closed isotropic cylindrical shells. This is accomplished through the development of a formulation based on a hybrid approach combining Novozhilov's non-linear theory with the classical finite element method.

The theory developed in this manuscript is able to include the shell curvature effect in the circumferential direction of the orthogonal displacements and also considers the impact of initial geometric imperfections on the dynamic response of the system. Among others, nonlinear coupling between different modes is taken into consideration. The formulation first takes a general form, expressing shell displacement using a combination of generalized coordinates and spatial functions. Nonlinear kinematic relationships are determined from Novozhilov's theory. The equation of motion is inferred from the Lagrange equations based on an energy approach. Quadratic and cubic nonlinear stiffness matrices are determined after analytical integration of modal coefficients expressed in terms of shape functions.

An application of this model is illustrated in a further step, by adopting the displacement functions derived from exact solutions of linear Sander's theory equilibrium equations for thin cylindrical shells. The governing equations of motion are solved with the help of a direct iterative method. Linear and nonlinear frequencies are validated by comparison with the results in the literature. The effect of different parameters including axial and circumferential wave number, length-to-radius ratio, thickness-to-radius ratio and various boundary conditions, on the nonlinear frequencies of cylindrical shells is investigated. The coupling between nonlinear modes accentuates the hardening character of nonlinear vibrations. It has also been found that the fundamental frequency depends closely on the amplitude of the vibrations once we leave the domain of small vibrations. Excellent agreement is observed between the results derived from this theory and those found in the literature.

The third part of this research presents a model for analyzing the nonlinear dynamic behaviour of closed and isotropic thin cylindrical shells subjected to radial pressures and/or axial forces and exposed to supersonic airflow. The structural mass and stiffness matrices are obtained using an energy approach. The stiffness matrix induced by the initial stiffening stresses is calculated based on the expression of strain energy of the membrane force. A linear analysis is performed to identify natural modes, which are then used in the nonlinear analysis as a spatial function to determine the cubic nonlinear stiffness matrix based on analytical integration of modal coefficients. The local aerodynamic pressure exerted by the fluid on the structure is derived from linear piston theory, with and without consideration of the terms of curve corrections. The correlation between the aerodynamic pressure and the radial component of the fluid velocity vector enables expression of the aerodynamic force according to the calculated displacements at any point of the structure. The fluid stiffness and damping matrices are determined by analytical integration of the aerodynamic pressure force. The governing equations of motion are derived using the Lagrange method and solved numerically with the help of a direct iterative method. Numerical studies are conducted highlighting that the dynamic behaviour’s nonlinear trend is a softening type. Results of these studies also illustrate the effects of different parameters including internal pressure, nonlinear coupling, circumferential wave number, radius-to-thickness ratio, length-to-radius ratio and boundary conditions on the nonlinear dynamic behaviour of the cylindrical shell at the onset of flutter and during the flutter stage. It is revealed that the more slender the structure, the more vulnerable it will be to dynamic instability by flutter. Moreover, the internal pressure has stabilizing influence on the homogeneous isotropic cylindrical shell and the increase in the length to radius ratio of the structure hastens the flutter instability. Good agreement is found between the results obtained using the present approach and those published in the literature.

The model developed in this thesis is a powerful tool for evaluating the vibratory characteristics of closed and isotropic thin cylindrical shells in the nonlinear domain and offering, therefore, a good prediction of the instability of these structures when subjected to supersonic flow. This is achieved through a combination of the advantages of the finite element method for treating shells with complex shapes and the precision of the developed formulation employing exact solutions for the displacement functions. These advantages give more reliability to the results and offer more robustness to the developed model to treat aeroelastic problems.

TABLE DES MATIÈRES

LISTE DES TABLEAUX

LISTE DES FIGURES

LISTE DES SIGLES ET ABRÉVIATIONS

CC	Clamped-Clamped
CNTs	Carbon nanotubes
F.E	Finite element
FEM	Finite Element Method
FG-CNTRC	Functionally graded carbon nanotube-reinforced composite cylindrical shell
FGM	Functionally Graded Materials
FGP	Functionally graded porous cylindrical shells
FSDT	First shear deformation theory
HPM	Homotopy perturbation method
IHB	Incremental Harmonic Balance method
SS	Simply supported- Simply supported
VDQ	Variational differential quadrature method

CHAPITRE 1 INTRODUCTION

1.1. Description du Problème

Les interactions fluide-structure font parvenir deux entités mécaniques distinctes : une structure mobile (rigide ou déformable) et un fluide sous forme gazeuse ou liquide, au repos ou en écoulement autour ou à l’intérieur de cette dernière. Généralement, on peut distinguer les phénomènes hydroélastiques (interaction fluide incompressible/structure) des phénomènes aéroélastiques (interaction fluide compressible/structure). L'hydroelasticité se rencontre souvent dans le domaine biomédical et dans le génie naval. L'aéroélasticité possède, quant à elle, une panoplie d’applications allant de génie civile au domaine aéronautique et spatial. Il en est toutefois de même où l’aéroélasticité fit sa première apparition. C’était dans le début du vingtième siècle, dans le domaine aéronautique pour devenir par la suite une science à soi dans la période couvrant la deuxième guerre mondiale. Cette discipline, croisant les effets aérodynamiques, inertiels et élastiques d’une structure, a donné naissance à des problèmes qui ont une influence primordiale sur la stabilité des structures aéronautiques et par conséquent sur leurs performances et leur longévité. On distingue ainsi l’aéroélasticité statique qui se caractérise par l’étude des efforts et des déformations induites par un écoulement stationnaire sur la structure, et l’aéroélasticité dynamique qui se manifeste par une évolution dans le temps du système aéroélastique. Cette évolution peut être engendrée par une force externe comme dans le cas de la couche limite turbulente atmosphérique qui est susceptible d’exciter les structures surtout lorsqu’elles sont minces et élancées, soit elle est due à une instabilité propre au système. C’est toutefois cette dernière classe de divergence qui constitue l’intérêt de cet ouvrage. L’un des problèmes de l’aéroélasticité dynamique autodéterminé le plus connu est certainement le flottement. Ce phénomène d’instabilité qui a incité les chercheurs durant ces dernières années et qui fait l’objet de la présente recherche. Ce phénomène autodéterminé engendré par un couplage entre l’air et la structure, a été rendu célébré par le spectaculaire écroulement du pont Tacoma en 1940 qui a été effondré sous l’effet d’un mode torsionnel de son tablier. Ce phénomène connu aussi comme le Némésis du vol, a provoqué plusieurs catastrophes aériennes notamment dans l’aviation militaire [1]. La conception des nouveaux aéronefs exige la prise en compte de ce phénomène et considère sa prévention ou sa prédiction comme un critère éliminatoire pour la certification d’un avion notamment pour la conception des véhicules spatiaux à haute vitesse. Mathématiquement, cela correspond au changement de signe de la partie imaginaire de la fréquence du positive (désignant l'amortissement) au négative (désignant l'instabilité). Cela se manifeste par une augmentation exponentielle et rapide de l'amplitude de vibration qui peut conduire à excéder les limites physiques de déformation et mener à la ruine de la structure. Ce sujet a suscité la communauté scientifique pour étudier ce phénomène, d'en comprendre les fondements physiques, de choisir les approches les plus appropriées et d'en trouver les solutions fiables et précises capables de réduire la description du phénomène à ses aspects réels. L'avènement technologique du domaine informatique et le développement continu des ordinateurs numériques ont fait émerger la modélisation mathématique par éléments finis ce qui a permet de traiter des configurations jugées trop complexes incluant des couplages multi-physiques et multi-échelles et a rendu possible la résolution numérique des approches analytiques considérées comme compliqués.

Plusieurs recherches ont été révélées en la matière traitant le flottement supersonique des coques et plaques minces en se basant sur des approches analytiques linéaires. Les prédictions des paramètres caractérisant le flottement restent cependant une approche qui manque de précision du fait de la nature de cette instabilité dynamique qui acquiert un aspect nonlinéaire incité par les grands déplacements d'où la nécessité de se pencher vers une analyse nonlinéaire.

Cette monographie de recherche a recours aux coques cylindriques minces pour désigner la structure, étant donné que cette forme géométrique est très répondue dans le secteur aérospatial. C'est une représentation simplifiée d'un fuselage d'avion.

Les études se sont aiguillées ainsi vers l'approche nonlinéaire pour l'analyse du comportement dynamique des coques cylindriques mince et les formulations développées en la matière se basent principalement sur l'une des quatre théories qui se sont démarquées parmi les différents formulations qui employaient trois paramètres dans leur équations cinématiques à savoir : la théorie nonlinéaire de Donnell, Flügge-Lur'e-Byrne, Sanders-Koiter et celle de Novozhilov.

D'un point de vue numérique, la simulation des phénomènes aéroélastiques en particulier le flottement connait une difficulté majeure du fait de la situation de ce problème multiphysique à la confluence de deux disciplines intrinsèquement complexes et très différentes : la mécanique des solides qui utilise habituellement un formalisme Lagrangien et la mécanique des fluides qui est décrite par une approche Eulérienne. A cela viennent s'ajouter des difficultés spécifiques de type physiques et numériques pour rendre le problème de plus en plus complexe.

1.2. Objectif et Originalité

On est donc devant un problème complexe et pluridisciplinaire, ce qui nous a incités à amener notre étude par étapes afin de l'aborder en lui conférant un aspect "pédagogique".

C'est dans ce cadre que se situe cette thèse qui a donc pour objectif ultime de développer un logiciel maison et un modèle numérique basé sur une approche hybride ralliant à la fois la formulation développée en la matière et basée sur la théorie nonlinéaire de Novozhilov avec la méthode des éléments finis classique. Ce modèle est capable d'analyser linéairement et nonlinéairement le comportement dynamique des structures cylindriques minces à vide et lorsqu'elles sont soumises à un écoulement d'air supersonique et d'examiner en conséquence leur stabilité au moment de flottement et durant les stades d'instabilité dynamique. L'objectif de cette thèse se traduit par une mise en exergue des différents aspects marquant l'originalité de cette recherche et qui réside dans le développement d'une nouvelle formulation basée sur la théorie nonlinéaire de Novozhilov capable de modéliser linéairement et nonlinéairement le comportement dynamique des structures cylindriques fermées et ouvertes, à vide et en présence d'un fluide. Cette formulation est capable de supporter plusieurs formes de discrétisation et ce grâce à la forme de son champ de déplacement que revête une forme générale. Elle tient aussi en compte de l'effet des imperfections géometriques initiales. Subséquemment, la formulation est suivie par le développement d'un modèle numérique qui mise d'une part sur la précision des résultats du faite qu'il emploie les solutions exactes qui découlent de la théorie linéaire des coques comme fonctions de forme et d'autre part sur la rapidité de convergence étant donnée qu'il acquiert un nombre réduit d'éléments finis. Le modèle tient aussi en considération de l'effet des contraintes initiales de raidissement induites par les forces axiales et/ou les pressions radiales et de l'effet du couplage entre les différents modes nonlinéaires. Ce dernier a été négligé dans la plus part des modèles dressés afin d'alléger les calculs. Un tel modèle est destiné à être un outil puissant de conception des véhicules supersoniques qui illustre bien le dilemme temps/précision capable de prédire et d'analyser le flottement dans ces différentes phases de développement en assurant un critère de convergence beaucoup plus rapide que celui des logiciels commerciaux qui exigent un grand nombre d'éléments qui soit utilisé. Ce logiciel pourra aussi servir comme un outil pour l'analyse de fatigue des structures des aéronefs à haute vitesse.

Avant d'entamer les étapes décrivant le modèle développé dans cette thèse il nous est apparu impératif de définir les différents concepts de nonlinéarités que fait intervenir la mécanique des structures ainsi que les différentes approches développées en la matière pour traiter les problèmes géométriquement nonlinéaires.

1.2.1. Différents concepts de nonlinéarité

1.2.1.1. Non linéarité géométrique (Cinématique)

Elle apparaît dans les structures mécaniques minces lorsqu'elles sont sujettes à des sollicitations créant des déplacements nonlinéaires et éventuellement de grandes rotations pouvant être à l'origine des phénomènes d'instabilité par flambement surtout lorsque les pièces sont élancées. Dans ce cas-ci les relations cinématiques (déformation-déplacement) deviennent non linéaires, bien que le matériau reste élastique linéaire et l'hypothèse des petites perturbations considérée lors des problèmes mécaniques linéaires n'est plus valable. Les configurations déformées et initiales ne sont plus confondues et l'équilibre du système dans ce cas de figure ne peut plus être traité dans la configuration initiale mais doit être exprimé dans la configuration déformée. [2]

1.2.1.2. Non linéarité matérielle (Rhéologique)

Cette nonlinéarité est liée à la nature de comportement intrinsèque du matériau. La relation entre les contraintes et les déformations est nonlinéaire. On peut les classer, en générale en deux catégories principales :

- ✓ *Élasticité nonlinéaire*

Elle se caractérise par une non proportionnalité d'accroissement entre les contraintes et les déformations qui en découlent. Ce type de comportement nonlinéaire réversible se manifeste souvent chez les matériaux élastiques "Green" ou hyperélastique pour lesquels l'énergie de déformation élastique n'est plus une fonction quadratique des composantes du tenseur de déformation infinitésimal [2]. Il s'exprime en fonction des invariants des tenseurs de déformations tel que ceux de Green-Lagrange, de Cauchy-Green droit, de Cauchy-Green gauche,…

- ✓ *Plasticité*

Elle est caractérisée par une décroissance irréversible de l'énergie au cours de la déformation. Une partie de l'énergie mécanique est transformée en énergie thermique et la structure ne peut plus restituer sa position d'équilibre stable une fois déchargée [2]. Ce mécanisme place des restrictions sur la direction du processus ainsi que sur les lois constitutives de l'élément étant donné qu'il dépend étroitement du trajet de chargement et donc des effets d'histoire.

1.2.1.3. Non linéarité de contact

Ce type de non linéarité est lié à l'évolution des conditions aux limites et apparaît en particulier à la jonction entre solides. Il se manifeste dans les problèmes de contact, de frottement et de jeu au niveau de liaison entre solides. Ces phénomènes sont décrits généralement, par des inéquations. [2]

L'analyse de ces aspects peut être entreprise en se basant sur ces différentes approches :

- ✓ L'analyse de la nonlinéarité matérielle en considérant les petits déplacements et les petites déformations : la relation contraintes-déformations est nonlinéaire.
- ✓ L'analyse de la nonlinéarité géométrique en considérant les grands déplacements et les petites déformations : La relation déformations-déplacements peut être nonlinéaire.
- ✓ L'analyse de la nonlinéarité géométrique en considérant les grands déplacements et les grandes déformations : Les relations contraintes-déformations et déformations-déplacement sont généralement nonlinéaires. C'est les cas le plus complexe de l'analyse nonlinéaire des structures.

On s'intéresse plus particulièrement au deuxième cas dans cette thèse étant donné qu'on est en présence d'un problème qui se manifeste par des grands déplacements (flottement) tout en admettant que les déformations demeurent petites au voisinage de chaque point de la structure ce qui nous permet d'adopter la loi de Hooke comme loi de comportement.

1.2.2. Différents modèles nonlinéaires

La réduction des coques minces en leurs surfaces moyennes a permis de transformer les problèmes tridimensionnels à des problèmes bidimensionnels ce qui a donné naissance à divers théories développées en la matière dont les écarts reposent sur l'expression du champ de déplacement et les déformations qui en découlent.

Dans ce qui suit, on dresse un aperçu synoptique sur les différentes théories développées traitant les problèmes géométriquement nonlinéaires [3] :

1.2.2.1. Théorie de Donnell

Dans cette section est rappelé le modèle de Donnell pour une coque cylindrique mince et isotrope de rayon R, d'épaisseur h et de longueur L. La théorie repose sur les hypothèses suivantes stipulant : [4]

H1 : la coque est suffisamment mince : $h \ll R,\ h \ll L$ (En pratique, on prend $h/R \leq 1/20$)

H2 : Le déplacement transverse w est de l'ordre de l'épaisseur h : $|w| = o(h)$.

H3 : Les dérivés de w sont considérés petites en revanche, leurs produits et leurs carrés sont de même ordre que les déformations : $|\partial w/\partial x| \ll 1,$ $|\partial w/R\partial\theta| \ll 1,$ $\left\{(\partial w/\partial x)^2, (\partial w/R\partial\theta)^2, |(\partial w/\partial x)\times(\partial w/R\partial\theta)|\right\} = o(\varepsilon)$.

H4 : Les composantes du tenseur de déformation sont considérées comme petites $\varepsilon \ll 1$ de façon à ce que la loi de l'élasticité linéaire (loi de Hooke) peut être appliquée.

H5 : Les hypothèses de Kirchhoff-Love qui stipule que tout segment normal à la surface moyenne non déformée reste droit et normal à la surface moyenne déformée, sont supposées vérifiées ce qui implique que les contraintes de cisaillement transverses $(\tau_{xz}, \tau_{\theta z})$ sont négligées.

H6 : les contraintes normales agissant perpendiculairement à la surface moyenne σ_z sont aussi négligés (hypothèses des contraintes planes)

H7 : Les déplacements tangentiels u et v sont considérés négligeables et par conséquent, seuls les termes nonlinéaires dépendant de w seront retenus dans la partie membranaire du tenseur Green-Lagrange, noté $\tilde{e}$.

H8 : L'inertie de rotation est négligée.

H9 : L'inertie membranaire est négligée.

Les hypothèses *H7* et *H9*, éliminées dans les autres modèles, ont incité les chercheurs à critiquer cette théorie. Toutefois, ce modèle s'avère le plus utilisé parmi toutes les autres théories optant pour l'analyse de l'instabilité des coques en raison de sa simplicité et la précision de ces résultats qui se trouvent tout à fait satisfaisantes d'une façon générale.

1.2.2.2. Théorie de Flügge-Lur'e-Byrne

Lorsque la courbure des coques devient trop grande, l'hypothèse (H7) n'est plus valable ce qui implique que l'inertie membranaire peut être désormais, conservé dans les équations de mouvement. La cinématique en conséquence se complexifie, ce qui peut être illustré dans le cas des coques cylindriques fermées, par une dépendance linéaire du champ de déplacement circonférentiel en fonction de la coordonnée radiale z. [5]

1.2.2.3. Théorie de Novozhilov

Elle se caractérise par une expression plus complexifiée de ces relations cinématiques par rapport aux autres théories. La seule différence entre cette théorie et celle de Flügge-Lur'e-Byrne réside dans l'expression des changements de courbures flexionnelles et torsionnelles de son champ de déformation alors que les déformations membranaires restent les mêmes. Les relations cinématiques de Novozhilov sont considérés comme les équations les plus générales et les plus complètes. [6]

1.2.2.4. Théorie de Sanders-Koiter

La théorie non linéaire de Sanders-koiter est exprimée dans une forme tensorielle. Elle a été développée par Sanders [7], subséquemment, les mêmes résultats ont été trouvés par Koiter [8]. Cette théorie, convenant avec des petites déformations et des rotations modérées, consiste à développer une formulation mathématique qui respecte les exigences mécaniques capable de traiter avec précision les problèmes de stabilité des structures élastiques notamment le comportement critique et post-critique des coques.

Toutes ces théories permettent d'appréhender les phénomènes de stabilité avec des difficultés variables. L'écart entre les prédictions théoriques prend de l'ampleur lorsque les imperfections géométriques initiales ne sont pas tenues en compte d'une manière scrupuleuse.

La majorité des études dressées se sont basées sur les théories nonlinéaires de Donnell et celle de Sander-Koiter pour examiner la stabilité des structures cylindriques fermées en fonction de différents paramètres physiques et thermiques. Peu de travaux qui ont recours à la théorie de Flügge-Lur'e-Byrne et un nombre minime de recherche qui s'est focalisé sur la théorie de Novozhilov à cause de la forme complexifiée de leur champ de déplacement, qui tient compte de plusieurs paramètres tel que l'effet de courbure au niveau du champ de déplacement circonférentiel.

1.3. Décomposition de la thèse

La formulation développée dans cette recherche traite le comportement dynamique géométriquement nonlinéaire des coques cylindriques minces et isotropes en se basant sur la théorie des coques minces de Novozhilov tout en tenant compte de plusieurs aspects tel que l'effet de courbure au niveau du champ de déplacement circonférentiel, l'effet des imperfections géométriques initiales et l'effet du couplage non linéaire entre les différentes cordonnées généralisées.

Ainsi cette thèse s'articule autour de six chapitres répartis comme suit : Le premier chapitre est introductif, il définit plus précisément le cadre de cette recherche et le problème étudié, en mettant en exergue l'approche envisagée pour atteindre les objectifs convoités de cette étude. Le deuxième chapitre contient une recherche bibliographique exhaustive sur le sujet. Cette thèse inclut dans le corps du document le continu de trois articles scientifiques. L'aspect pluridisciplinaire du sujet s'est répercuté sur l'organisation de ces articles en offrant à chacun la flexibilité d'entamer une partie du sujet global de la recherche. Les méthodes employées et les résultats trouvés pour chaque article sont respectivement détaillés dans les chapitres 3,4 et 5.

Le chapitre 3 s'intéresse à l'étude de l'effet des contraintes initiales de raidissement induites par une pression radiale et/ou une force axiale sur le comportement dynamique des structures minces et axisymétriques. L'analyse est fondée sur une approche stipulant l'emploi des éléments finis de type cylindriques et coniques pour assurer la discrétisation des structures sujet d'étude. L'étude a commencé par une analyse de la dynamique linéaire des coques cylindriques et coniques considérées séparées en se basant sur la méthode des éléments finis hybride pour laquelle les fonctions de déplacements sont déduites à partir de la solution exacte des équations d'équilibre de Sanders. Les matrices de masse et de rigidité sont déterminées respectivement à partir de l'expression de l'énergie cinétiques et celle de déformation élastique. La matrice de rigidité inférée par les contraintes initiales de raidissement est déterminée en se basant sur l'expression de l'énergie de déformation due aux flux d'efforts membranaires. Les matrices globales de masse et de rigidité des structures combinées sont ensuite déterminées en assemblant les matrices des éléments cylindriques et coniques. L'influence de la pression radiale et/ou des forces axiales sur le comportement dynamique des coques axisymétriques, est examinée en détail dans ce chapitre.

Le chapitre 4 est consacré à l'étude des vibrations libres nonlinéaires d'une coque cylindrique axisymétrique mince et isotrope à travers le développement d'une théorie se basant sur une approche hybride ralliant la méthode des éléments finis hybride et la théorie des coques minces de Novozhilov. L'approche s'est caractérisée par son aspect général lui offrant la flexibilité de couvrir des différents types de discrétisation grâce l'expression de son champ de déplacement qui se présente par une alliance entre une fonction temporelle (coordonnées généralisées) et une fonction spatiale (fonction de forme). Les coefficients modaux sont déterminés par l'insertion des fonctions de déplacements définies dans les trois axes longitudinal, circonférentiel et radial, dans les relations déformation-déplacement de Novozhilov. Les matrices de masse et de rigidité sont déterminées en se basant sur les équations de Lagrange. La deuxième partie de l'étude consiste à remplacer les fonctions de formes par les fonctions de déplacements trouvées à partir de la théorie développée par Lakis et Paidoussis [9] dans laquelle le champ de déplacement découle de la solution exacte des équations d'équilibre de Sanders. Cette rapproche prend sa légitimité du fait que les valeurs de fréquence linéaires déterminées à partir de la théorie de Sanders sont extrêmement proches à celles induites de la théorie de Novozhilov [10]. Les matrices de rigidité nonlinéaire quadratiques et cubiques sont déterminées par la suite en calculant les coefficients modaux écrites en fonctions des fonctions de forme préalablement déterminées. L'effet des imperfections géométriques initiales est négligé afin de faciliter les calculs. L'équation de mouvement est résolue numériquement par le biais d'une méthode itérative après une transformation modale effectuée et une linéarisation du système.

Le chapitre 5 englobe tous les aspects trouvés dans les articles précédents en dressant une étude aéroélastique traitant le problème de stabilité d'une coque cylindrique mince et isotrope soumise à un écoulement d'air supersonique en tenant compte de l'effet des contraintes initiales de raidissement induite par les pressions radiales et/ou les forces axiales. Les matrices de rigidité et d'amortissement aérodynamiques sont déterminées par le biais de la théorie de Piston. La tendance nonlinéaire du comportement dynamique des structures cylindriques sujet d'étude sont examinées au moment d'apparition de flottement et durant les phases d'instabilité de la coque.

Une discussion générale cernant les résultats obtenus et les contributions apportées dans chaque article sera fournie dans le chapitre 6. Finalement, le chapitre 7 présente les principales conclusions tirées de cette thèse et expose les perspectives des travaux futurs suite à cette recherche.

CHAPITRE 2 REVUE LITTÉRAIRE

L'analyse aéroélastique constitue une étape primordiale dans la conception des aéronefs du fait qu'elle permet de prévenir l'apparition des phénomènes autodéterminés tel que le flottement. Ce phénomène d'instabilité dynamique, connu aussi sous le nom de « Flutter » est considéré comme le « Némésis du vol » vu le potentiel signifiant des défaillances structurelles et des dommages qui peut engendrer à court termes et des problèmes de fatigue qui pourrait générer à long termes. Ceci a incité la communauté scientifique depuis le début du vingtième siècle à mettre l'accent sur son sujet afin de comprendre son origine et de dresser en conséquence les mesures nécessaires afin de l'éviter et assurer l'intégrité de la structure. F.W. Lanchester semble avoir été le pionnier, en 1916, à identifier le flottement comme une vibration auto-excitée. Il a développé avec L.Bairstow et A.Fage les premiers travaux appliqués à la queue du Bombardier *Handley Page 0/400* [11]. Lanchester a proposé de relier les volets de queue avec un arbre de torsion afin de les rigidifier. Quant à Bairsow et Fage, ils ont dressé la première méthode analytique permettant de déterminer la stabilité aéroélastique en se basant sur le critère de Routh. Von Baumhauer et Koning ont aperçu en 1925 que le flottement est induit de l'interaction entre le mode de flexion verticale et le mouvement des ailerons [12]. Expérimentalement, Duncan [11] a conçu un banc d'essai d'une aile suspendue à un système rotatif nommé « moteur de flutter » afin de mettre en exergue le concept d'extraction d'énergie aérodynamique par la structure. Keldysh [13] à son rôle, a présenté des solutions pratiques pour prédire le flottement depuis la phase de conception. Avec le développement des méthodes numériques discrètes dédiées pour l'analyse de flottement en se basant sur la théorie de la surface portante [14], l'aéroélasticité a atteint une phase de maturité pour le traitement de ce phénomène. Les analyses se succèdent après en adoptant l'approche linéaire pour le traitement de ce phénomène et ce pour la simplicité mathématique de la théorie structurale linéaire. Beaucoup de travaux ont été révélées en la matière à savoir celles de Hedgepeth and Widmayer [15], Dugundji [16] et Robinson et al [17]. Dowell [18] signale dans son article que les nonlinéarités structurales ne peuvent pas être prises en compte à travers l'analyse linéaire de flottement d'un panneau qu'il a dressée. Autrement dit, les approches adoptées pour l'étude structurale linéaire se limitent à signaler la transition entre le domaine de stabilité de la structure et la phase de son instabilité à travers la révélation d'une pression aérodynamique critique à partir de laquelle l'amplitude de la structure croit et se développe exponentiellement avec le temps. En conséquence l'analyse structurale linéaire peut servir comme un outil pour prédire les limites de flottement. De ce fait, le besoin est incité pour développer des théories nonlinéaires capables de décrire le comportement de la structure pendant les phases qui suivent le flottement. Plusieurs recherches ont été trouvées dans la littérature, qui se sont concentrées sur l'analyse de flottement des panneaux et des plaques en revanche le nombre des études qui ont analysé l'instabilité des coques cylindrique fermées sous l'effet de flottement supersonique, est minime. Les premiers travaux sont attribués à Librescu [19, 20] qui a analysé la stabilité des panneaux peux profonds et des coques cylindriques circulaires de longueur finie en utilisant la théorie non linéaire des coques surbaissées de Donnell. Il a également associé des termes nonlinéaires à la pression aérodynamique calculée à l'aide de la théorie de piston. La théorie de Librescu convient aussi pour l'étude des coques en composites. Olson et Fung [21] ont utilisé une forme simplifiée de la théorie non linéaire des coques surbaissées de Donnell en employant une expansion à deux modes pour modéliser les coques simplement supportées. Au centre de recherche de NASA, en Californie, Olson et Fung [22] ont effectué une étude expérimentale complète du flottement supersonique des coques cylindriques pressurisées et comprimées axialement. Les chercheurs ont signalé un comportement particulier des coques pressurisées quant aux limites de flottement. Amabili et Pellicano [23] ont analysé la stabilité aéroélastique des coques cylindriques circulaires simplement supportées et soumises à un écoulement supersonique en employant la théorie nonlinéaire de Donnell pour modéliser la nonlinéarité géométrique induite par les grandes amplitudes de vibration. Leur étude tient également compte de l'effet de l'amortissement structurel visqueux. L'interaction fluide-structure est décrite par la théorie de piston linéaire à l'aide de deux formulations différentes. Amabili et Pellicano [24] ont développé dans un autre article une approche multimode impliquant jusqu'à 22 degré de libertés et employant à la fois la théorie de piston linéaire et celle du troisième ordre. Ils ont souligné que les différences entre ces deux théories étaient jugées négligeables relativement à un nombre de Mach égale à trois. Librescu et al. [25] ont étudié le flutter et le post-flutter des panneaux cylindriques à parois minces infiniment longues et soumises à un flux supersonique et hypersonique. Les équations aéroélastiques ont été dérivées à partir de la théorie nonlinéaire des coques conjointement avec la théorie du piston de troisième ordre tout en tenant compte de l'aérodynamique des ondes de choc. Oh et Lee [26] ont appliqué une méthode d'éléments finis non linéaires basée sur la théorie des stratifiés pour étudier l'instabilité dynamique des panneaux cylindriques piézolaminés soumis à des charges thermiques et piézoélectriques. Kurilov et Mikhlin [27] ont étudié le comportement non linéaire des coques cylindriques élastiques en se basant sur la théorie des coques surbaissées. Ils ont analysé l'effet du flux et des déflexions initiales sur les vibrations de la coque. Les auteurs ont constaté que les trajectoires des modes normaux dans le cas des coques présentant des imperfections initiales sont presque rectilignes. Jansen [28] a développé une théorie tenant en compte des effets combinés des amplitudes de vibration, de la déformation statique nonlinéaire et des imperfections géométriques initiales pour étudier la réponse dynamique nonlinéaire des coques cylindriques laminées. Haddadpour et al. [29] ont analysé le déclenchement du flottement supersonique des coques cylindriques fonctionnellement graduées (FGM) pour différentes conditions aux limites en tenant compte du modèle structurale nonlinéaire couplé à la théorie du piston linéarisé. L'étude a mis en évidence l'effet de la température et de la pression interne sur les limites de flottement pour le cas d'une structure cylindrique FG simplement supportée. Kubenko et Koval'chuk [30] ont étudié les vibrations nonlinéaires et la stabilité des coques cylindriques minces interagissant avec le débit de fluide. L'étude a mis en relief l'effet des imperfections géométriques initiales, des conditions limites, des masses concentrées ajoutées et des charges statiques longitudinales et transversales sur les vitesses critiques. Liu et al [31] ont analysé le comportement dynamique nonlinéaire d'une coque cylindrique FGM simplement supportée, soumise à des excitations harmoniques, à des forces de compression membranaires et à des charges thermiques et aérodynamiques en tenant en compte de l'effet des petites imperfections géométriques initiales. Mahmoudkhani et al. [32] ont analysé la stabilité aérothermoélastique des coques cylindriques multicouches avec des cœurs viscoélastiques. Le modèle est développé en se basant sur la théorie de Donnell en combinaison avec la théorie de déformation de cisaillement de premier ordre et en utilisant les relations cinématiques nonlinéaires de Von Karman-Donnell. Les résultats ont montré que la pré-déformation pourrait influencer considérablement les limites de flottement pour des températures élevées. Mahmoudkhani [33] a examiné dans un autre article le flottement supersonique des coques cylindriques fonctionnellement graduées soumises à des charges thermiques, en tenant compte de l'effet des imperfections géométriques. Ses résultats numériques ont montré un changement de la tendance des courbes relatives à la variation de pression de flottement en fonction de la température sous l'effet des imperfections. Chen et Li [34] ont étudié le comportement dynamique nonlinéaire d'une coque cylindrique circulaire en composite sous l'effet d'une compression membranaire et d'une excitation harmonique radiale et soumise à un écoulement d'air supersonique. La nonlinéarité est modélisée en se basant sur la théorie de Donnell et les équations de mouvement sont dérivées à partir du principe variationnel d'Hamilton. Asadi et Wang [35] a examiné l'instabilité nonlinéaire d'une coque cylindrique fonctionnellement graduée en composite, pressurisée, renforcée de nanotubes de carbone (FG-CNTRC) et soumise à un écoulement d'air supersonique. Le modèle structurel est développé en se basant sur la théorie de déformation de cisaillement de premier ordre et sur les relations nonlinéaires de déformation-déplacement de Von-karman-Donnell. La pression aérodynamique est évaluée par le biais de la théorie quasi stable de piston modifiée de Krumhaar en tenant compte de l'effet de courbure. Asadi [36] a poursuivi son étude pour investiguer les instabilités dues au flottement aérothermoélastique et au flambement de la coque cylindrique FG-CNRC. Ses résultats numériques ont montré que l'élévation de la température a un effet significatif sur les caractéristiques de flottement aérothermoélastique de la structure cylindrique et que le nombre circonférentiel critique dépend également de la distribution des nanotubes en carbone (CNTs). Avramov et al. [37] ont mis en point un nouveau modèle de vibration nonlinéaire des coques cylindriques en composite fonctionnellement graduée et renforcées par des nanotubes en carbone, basé sur l'approche de flottement en onde progressive circonférentielle des coques FG-CNRC soumises à un écoulement supersonique. Fazilati et al. [38] ont étudié le comportement aéro-thermo-élastique d'un panneau cylindrique courbé soumis à un flux d'air supersonique en prenant en considération l'effet de la nonlinéarité structurale basée sur les relations déformation-déplacement de Von Karman-Donnell et l'effet aéroélastique nonlinéaire qui découle de la théorie de piston de troisième ordre et ce dans le but d'évaluer la stabilité de la structure. Khudayarov et Turaev [39] ont investigué la réponse dynamique des coques cylindriques orthotropes soumises à un écoulement supersonique en tenant compte des propriétés viscoélastiques du matériau et l'effet des nonlinéarités géométriques. La charge aérodynamique est déterminée à en se basant sur la théorie de piston de AA.ilyushin. Les résultats numériques ont révélé que la diminution de la vitesse critique de flottement est due à la prise en compte des propriétés viscoélastiques du matériau de la coque. Baghdasaryan et al. [40] ont examiné la réponse aéroélastique non linéaire et la stabilité des coquilles cylindriques fermées soumises à un flux supersonique et placées dans un champ de température non homogène. Leurs résultats numériques ont montré que la vitesse critique est inversement proportionnelle à l'épaisseur relative de la coque et se manifeste par une fonction décroissante ayant un point minimum qui dépend de la valeur du champ de température. Dans un autre article, Baghdasaryan et al. [41] ont étudié les vibrations nonlinéaires d'une coque cylindrique surbaissée, isotrope soumise à un écoulement d'air supersonique en tenant compte des nonlinéarités géométriques structurales et celles aérodynamiques.

CHAPITRE 3 ARTICLE 1: NUMERICAL MODELING OF INITIAL STRESS STIFFENING EFFECT ON THE DYNAMIC BEHAVIOUR OF AXISYMMETRIC SHELLS

(Published in Journal of Pressure Vessel Technology (ASME), DOI: 10.1115/1.4050092)

Yacine Ben-Youssef, Youcef Kerboua, Aouni A. Lakis

3.1. Abstract

This paper presents a numerical model to simulate the initial stress stiffening effect, induced by radial pressure and/or axial load on the dynamic behaviour of axisymmetric shells. This effect is particularly important for thin shells since their bending stiffness is very small compared to membrane stiffness. The theoretical formulation is based on a combination of the finite element method and classical shell theory. For a perfect geometrical consistency, two semi-analytical finite elements, conical and cylindrical, are used to model axisymmetric shells. The displacement functions are derived from exact solutions of Sanders' shell equilibrium equations. The results obtained using this approach are remarkably accurate. The potential energy is calculated to estimate the initial stiffening effect using direct membrane forces per unit width and rotations about the orthogonal axes. The final stiffness matrix of each finite element is composed of the regular stiffness matrix and the added stiffness matrix generated by membrane loads. The frequencies of vibration are compared with those obtained in other experimental and theoretical research works and very good agreement is observed.

Keywords

Thin shell, stiffening effect, frequency, axial load, radial pressure, finite element.

3.2. Introduction

An initial stress stiffening effect occurs in shell-type structures when they are subjected to membrane loads. This phenomenon significantly affects the dynamic behaviour of thin-walled axisymmetric shells widely used in aerospace, aeronautical, submarine and submersible structures and can bring them to dynamic collapse at an early stage. This issue has been studied in many works. In order to clarify the significant effects of internal pressure on thin cylindrical shells, Fung et al. [42] derived the vibration modes associated with the lowest frequency using conventional shell theory. The frequency spectra were calculated and compared with experimental results performed in the same work. Miserentino and Vosteen [43] experimentally determined the vibration modes and frequencies of thin cylindrical shells subjected to various values of internal pressure. His results compared reasonably well with those of Reissner [44] based on Donnell's equation. Weingarten [45] developed an analytical model and carried out an experimental investigation to determinate the effect of internal and external radial pressure on the natural frequencies of simply supported conical shells. He realized that the test data were generally slightly higher than the theoretical prediction, since the clamping mechanism for the tests was more restraining than a simply supported end. Dixon and Hudson [46] investigated the flutter, vibration and buckling characteristics of orthotropic conical shells and their sensitivity to fluctuation of hydrostatic pressure and axial loads. They remark that blunt cones are more susceptible to flutter than cylinders. The experimental work of Dixon and Miserentino [47] presents the fundamental frequencies of simply supported and clamped conical shells subjected to internal pressure. Their results were compared with those calculated theoretically in Ref. [46]. Generally, good agreement was found, although the theoretical model overestimated the increase in frequency resulting from an increase in internal pressure. The analysis of supersonic panel flutter of conical shells by Ueda et al. [48] included the effect of radial pressure. Their results were compared with those of Ref. [45] and good agreement was found. They revealed that flutter is very sensitive to the critical pressure. They also observed that, once the value of buckling is exceeded, the shell continues fluttering locally around the buckling configuration in rather small amplitudes. An analytical solution in the form of a power series was used by Tong [49] to investigate the effect of axial load on the dynamic behaviour of orthotropic conical shells. Numerical results showed that the frequency parameters are decreased by the axial compressive load and increased by axial tension. Lam and Hua [50] used the generalized differential quadrature method to study the influence of initial uniform pressure on the frequency characteristics of a rotating thin truncated isotropic conical shell. It was shown that this influence becomes more significant for large cone angles and/or high circumferential wave number. Their approach was validated and may be used accurately for vibration analysis of rotating conical shells under initial uniform pressure load. Zhang et al. [51] developed a finite element model to investigate the dynamic behaviour of prestressed thin cylindrical shells conveying a steady fluid flow. Their theoretical approach is based on Sanders' nonlinear theory of thin shells and classical potential flow theory. Their empty shell model was validated using Lindohlm's experimental results [52]. Sofiyev et al. [53] analyzed the vibration and stability of an orthotropic conical shell with nonhomogeneous material properties under hydrostatic pressure. The effects of nonhomogeneity and orthotropy on the critical hydrostatic pressure and frequency parameter were investigated for different mode numbers, when Young's moduli and density vary together or separately. Heydarpour et al. [54] surveyed the influence of internal pressure on the free vibration behavior of functionally graded truncated conical shells based on first-order shear deformation theory. They pointed out that the minimum value of the asymmetric frequency parameter can occur for a circumferential wave number other than (n=1) depending on the boundary conditions of the shell and the internal pressure. Chiba et al [55-57] studied the linear free vibration of a clamped-free cylindrical shell partially filled with an incompressible, inviscid liquid using the Donnell shell theory and taking into account the effect of the axisymmetric deformation due to the static liquid pressure. They reinforced their theoretical analyses by a numerical study, in which calculations are carried out for two test cylinders partially filled with liquid highlighting the whole aspect of the free vibration characteristics of the shell-liquid system. The authors took then their research one step farther by comparing their results predicted theoretically with those issues from an experimental study and an excellent agreement was found. Yamaki et al. [58] developed an analytical method for free vibration of a clamped cylindrical shell partially filled with an incompressible, inviscid liquid using the Galerkin procedure. Chiba and Osumi [59] analyzed theoretically and experimentally the free vibration and buckling under axial compression of a clamped cylindrical shell on both sides, which partially contains liquid and is partially submerged in a liquid. Tani et al [60] performed a theoretical analysis on the linear free vibration of the free-clamped coaxial cylinders with the liquid-filled annular gap. The authors found that the interactive effect of the coaxial cylinders becomes small and the mode shape changes with an increase in the wave number and the annular gap size. They also reported that an increase in liquid filled rate leads to a decrease in the natural frequencies. Chiba [61] conducted also a theoretical analysis to investigate the influence of the liquids inside and outside the shell on the free-vibration characteristics of a thin cantilever cylindrical shell partially submerged in a liquid.

Most of works cited above are devoted to studying the initial stiffening effect on the dynamic behavior of either cylindrical or conical shells separately. However, in practice, axisymmetric shells are often made up of joined conical and cylindrical shells (see Fig.3.1) or axisymmetric shells with variable radius. The aim of our paper is to develop a numerical model able to investigate the initial stiffening effect of axisymmetric thin-walled shells. To ensure better geometrical consistency, two finite elements of cylindrical and conical shape based on the hybrid finite element method are used. This hybrid method is based on Sanders' thin shell theory and the finite element method. It stood out for its accuracy and its speed of convergence for the treatment of axisymmetric shells using a small number of finite elements. This is due to the fact that the displacement functions are derived from exact solutions of Sanders' shell equilibrium equations rather than an approximation with polynomial functions [9]**.** Moreover, this method has also shown its ability to detect low as well as high frequencies with excellent precision. The middle surface of each finite element is matched with the middle surface of the axisymmetric shell. The strain and the displacement functions are continuous between two overlapping nodes in the interface between the conical and cylindrical finite elements of the axisymmetric shell. Our approach is based on the idea that the characterization of the combined structures (cylindrical and conical) passes through the modeling of its components behavior since the combined shell manifests itself by an assembly of cylindrical and conical segments based on standard techniques of finite elements. Hence, the combined structure can benefit from the advantages of the conical and cylindrical models taken separately. One can thus conclude that the field of displacement in the combined model is derived from the exact solution of the equilibrium equations of the Sanders's linear theory instead of the polynomial approximation. The initial stiffening effect is considered by calculating the potential energy using direct membrane forces per unit width and rotations about the orthogonal axes. It is accounted for by generating, for each finite element, an additional stiffness matrix that should be added to the regular stiffness matrix.

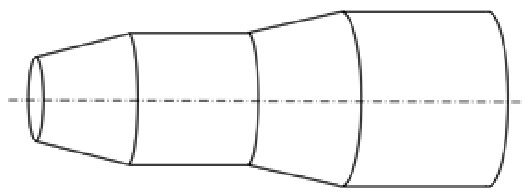

Figure 3.1: Combined cylindrical-conical shell

3.3. Structural modeling of axisymmetric shells

In order to accurately determine the initial stress stiffening effect on the dynamic behavior of an axisymmetric shell, two finite elements are used. The geometry and nodal displacements of the two finite elements are depicted in Figs 3.2 and 3.3. Detailed formulation is given in Sections 3.3.1 and 3.3.2.

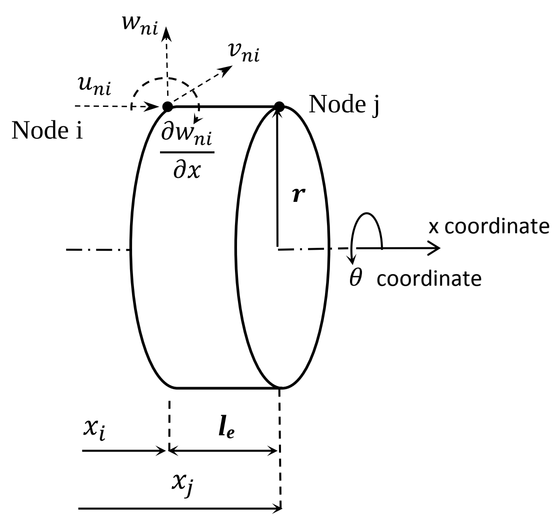

Figure 3.2: Geometry and nodal displacements of a cylindrical F.E [69]

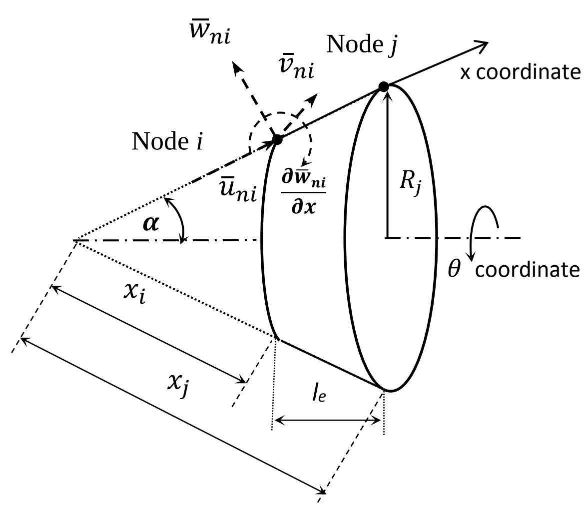

Figure 3.3: Geometry and nodal displacements of a conical F.E [69]

3.3.1. Cylindrical shell model

The linear strain vector according to Sanders theory [62] in the cylindrical coordinate system is expressed in terms of axial U, radial W, and circumferential V mid-surface displacements as follows:

$$\begin{Bmatrix} \varepsilon_x \\ \varepsilon_\theta \\ 2\varepsilon_{x\theta} \\ k_x \\ k_\theta \\ 2k_{x\theta} \end{Bmatrix} = \begin{Bmatrix} \dfrac{\partial U}{\partial x} \\ \dfrac{1}{r}\dfrac{\partial V}{\partial \theta} + \dfrac{W}{r} \\ \dfrac{\partial V}{\partial x} + \dfrac{1}{r}\dfrac{\partial U}{\partial \theta} \\ -\dfrac{\partial^2 W}{\partial x^2} \\ -\dfrac{1}{r^2}\dfrac{\partial^2 W}{\partial \theta^2} + \dfrac{1}{r^2}\dfrac{\partial V}{\partial \theta} \\ -\dfrac{2}{r}\dfrac{\partial^2 W}{\partial x \partial \theta} + \dfrac{3}{2r}\dfrac{\partial V}{\partial x} - \dfrac{1}{2r^2}\dfrac{\partial U}{\partial \theta} \end{Bmatrix} \tag{1}$$

Where r is the mean radius of the solid shell.

In Eq. (1), ε_x and ε_θ represent strain components in the axial and circumferential directions, respectively. $\varepsilon_{x\theta}$ represents the shear strain in the $x\theta$ plane. k_x and k_θ are the change of curvature of the normal midsurface and $k_{x\theta}$ is the modified twisting strain. The stress-strain relation is given by:

$$\{\sigma\} = [P]\{\varepsilon\} \tag{2}$$

where $[P]$ is the elasticity matrix for an anisotropic shell [63]. Its components for an isotropic shell are given in appendix A.

The equilibrium equations of cylindrical shells are expressed in terms of axial, tangential and radial displacements of the mean surface [9, 62]. They are given below using three linear differential operators $L_k\left(k = 1,\ 2,\ 3\right)$

$$L_k\left(U, W, V, P_{ij}\right) = 0 \tag{3}$$

Where $L_k\left(U, W, V, P_{ij}\right)_{k=1,2,3}$ are the linear partial differential equations of an anisotropic cylindrical shell given in Appendix A. P_{ij} are the components of an elasticity matrix $\left[P\right]$ of order $\left(6\times6\right)$ for an anisotropic material (see appendix A).

The displacements of Eq. (3) are considered as periodic functions and can be expressed in Fourier series as (see Ref. [9]):

$$U\left(x,\theta\right)=\sum_{n=0}^{\infty}u_n\left(x\right)\cos\left(n\theta\right) \qquad (4.a)$$

$$W\left(x,\theta\right)=\sum_{n=0}^{\infty}w_n\left(x\right)\cos\left(n\theta\right) \qquad (4.b)$$

$$V\left(x,\theta\right)=\sum_{n=0}^{\infty}v_n\left(x\right)\sin\left(n\theta\right) \qquad (4.c)$$

Where n is the circumferential wave number, and u_n, v_n and w_n are the magnitudes of displacements that depend only on the x coordinate, as follows:

$$u_n\left(x\right)=Ae^{\lambda x/r} \qquad (5.a)$$

$$v_n\left(x\right)=Be^{\lambda x/r} \qquad (5.b)$$

$$w_n\left(x\right)=Ce^{\lambda x/r} \qquad (5.c)$$

By introducing Eqs. (4) and (5) into the Sanders equilibrium Eq. (3), the following system of equations in terms of displacement parameters is obtained:

$$\begin{bmatrix} H_{11} & H_{12} & H_{13} \\ H_{21} & H_{22} & H_{23} \\ H_{31} & H_{32} & H_{33} \end{bmatrix} \begin{Bmatrix} A \\ B \\ C \end{Bmatrix} = \begin{Bmatrix} 0 \\ 0 \\ 0 \end{Bmatrix} \qquad (6)$$

For the nontrivial solution of Eq. (6), the determinant of $\left[H_{ij}\right]$ must vanish yielding the following characteristic equation:

$$a\lambda^8+b\lambda^6+c\lambda^4+d\lambda^2+e=0 \qquad (7)$$

Coefficients (a, b, c, d and e) are given in Appendix A. Each root λ_i of the characteristic equation represents a solution of Eq. (3). Complete solution of the spatial displacement function is obtained by summation of the eight roots of the characteristic equation and constants A_i, B_i and C_i $(i=1,2,\ldots..,8)$ as follows:

$$u_n(x)=\sum_{i=1}^{8}A_i e^{\lambda_i x/r} \tag{8.a}$$

$$v_n(x)=\sum_{i=1}^{8}B_i e^{\lambda_i x/r} \tag{8.b}$$

$$w_n(x)=\sum_{i=1}^{8}C_i e^{\lambda_i x/r} \tag{8.c}$$

Since the solution of Eq. (6) is nontrivial, A_i, B_i and C_i are not independent. We can express A_i, B_i in terms of C_i as follows: $A_i=\alpha_i C_i$ and $B_i=\beta_i C_i$. Where α_i and β_i are complex numbers. Details of the procedure are given in Ref.[9]. The displacement functions may be written as:

$$\begin{Bmatrix} U(x,\theta) \\ W(x,\theta) \\ V(x,\theta) \end{Bmatrix}=[T][R]\{C\} \tag{9}$$

where matrices $[T]$ of order (3×3), $[R]$ of order (3×8) and vector $\{C\}$ of order (8) are given in Appendix A.

Each cylindrical finite element has two nodes (*i* and *j*), each with four degrees-of-freedom: axial, radial, circumferential displacements and a rotation, (see Fig.3.2). Therefore, the nodal displacement vector can be defined by

$$\begin{Bmatrix} \delta_i \\ \delta_j \end{Bmatrix}=\left\{u_{ni}\ ,w_{ni},\partial w_{ni}/\partial x,v_{ni},u_{nj},w_{nj},\partial w_{nj}/\partial x,v_{nj}\right\}^T=[A]\{C\} \tag{10}$$

Since the cylindrical frustum is defined by two line nodes, *i* and *j*, the terms of matrix $[A]$ are obtained using Eq. (8), where *x* in matrix $[R]$ is replaced by definite coordinate values x_i and x_j corresponding, respectively, to nodes *i* and *j*, (see Fig.3.2). The components of matrix $[A]_{8\times8}$ are defined in Ref. [9].

Multiplying Eq. (10) by $[A]^{-1}$, the constant vector $\{C\}$ will be expressed as

$$\{C\} = [A]^{-1} \begin{Bmatrix} \delta_i \\ \delta_j \end{Bmatrix} \tag{11}$$

Substituting Eq. (11) into Eq. (9), one obtains the displacement functions expressed in terms of nodal displacements as follows:

$$\begin{Bmatrix} U(x,\theta) \\ W(x,\theta) \\ V(x,\theta) \end{Bmatrix} = [T][R][A]^{-1} \begin{Bmatrix} \delta_i \\ \delta_j \end{Bmatrix} = [N] \begin{Bmatrix} \delta_i \\ \delta_j \end{Bmatrix} \tag{12}$$

By introducing Eqs. (4) and (8) into Eq. (1) and using Eq. (11), the strain vector expression becomes

$$\{\varepsilon\} = \begin{bmatrix} [T] & [0] \\ [0] & [T] \end{bmatrix} [Q][A]^{-1} \begin{Bmatrix} \delta_i \\ \delta_j \end{Bmatrix} = [B] \begin{Bmatrix} \delta_i \\ \delta_j \end{Bmatrix} \tag{13}$$

where the components of matrix $[Q]$ are given in Ref.[9]. Now, the components of the stress vector may be written in terms of nodal displacements using Eqs (2) and (13) as

$$\{\sigma\} = [P][B] \begin{Bmatrix} \delta_i \\ \delta_j \end{Bmatrix} \tag{14}$$

Based on the standard finite element approach, the elementary mass $[m]_s^e$ and stiffness $[k]_s^e$ matrices of the cylindrical finite element are calculated using the following relations:

$$[k]_s^e = \int_0^l \int_0^{2\pi} [B]^T [P][B] r dx d\theta \tag{15}$$

$$[m]_s^e = \rho h \int_0^l \int_0^{2\pi} [N]^T [N] r dx d\theta \tag{16}$$

Where ρ is the density of the solid shell, h is its wall thickness, l is the length of the finite element and r is the mean radius of the cylindrical shell.

Using Eqs. (12) and (13) in Eqs. (15) and (16) and integrating over θ, one obtains

$$[k]_s^e = \left[[A]^{-1}\right]^T \left[\pi r \int_0^l [Q]^T [P][Q] dx\right][A]^{-1} \tag{17}$$

$$[m]_s^e = \rho h \left[[A]^{-1}\right]^T \left[\pi r \int_0^l [R]^T [R] dx\right][A]^{-1} \tag{18}$$

3.3.2. Conical shell model

Overline accentuation is used for conical parameters to differentiate them from those of the cylindrical model. According to Sanders' linear thin shell theory, the equilibrium equations of truncated conical shells (see Fig.3.4) are expressed in terms of their middle surface displacements and mechanical properties [62] by:

$$S_k = \left(\bar{U}, \bar{W}, \bar{V}, \bar{B}_{ij}\right) = 0 \tag{19}$$

where $S_k\left(k = 1,2,3\right)$ are three linear differential equations written in terms of displacements whose form is given fully in Appendix B. $\bar{U}, \bar{W}, \bar{V}$ are, respectively, meridional, radial and circumferential displacements. $\bar{B}_{ij}$ terms are the components of an anisotropic matrix of elasticity $\left[\bar{P}\right]$ of order $\left(6 \times 6\right)$, see Appendix B.

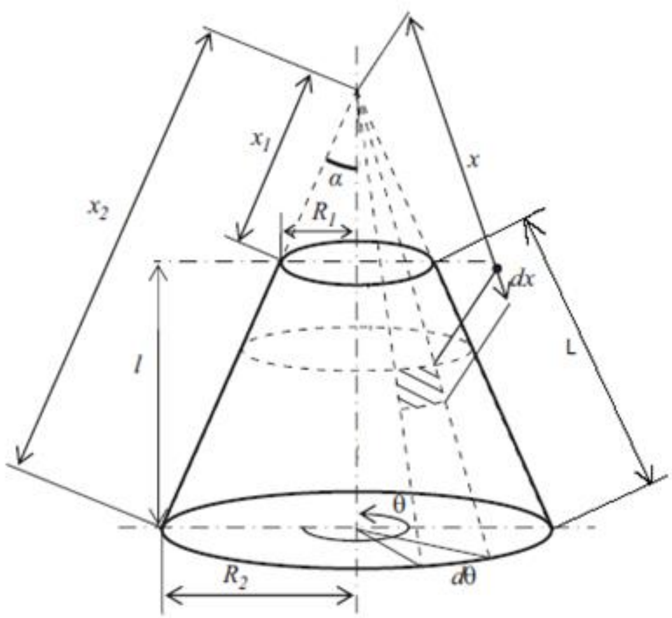

Figure 3.4: Geometry of a truncated conical shell [66]

The shell theory used here corresponds to the case of a conical shell with linearly variable thickness. This latter condition permits exact solution of the equilibrium equations. It is possible, however, to study the case of truncated conical shells with a constant thickness by using a thickness proportionality coefficient, defined as follows:

$$\zeta = h / x \tag{20}$$

The strain-displacement equations of conical shells in a conical coordinate system $(x,\ r,\ \theta)$ are expressed in terms of meridional $\bar{U}$, radial $\bar{W}$ and circumferential $\bar{V}$ mid-surface displacements, see Appendix B. The components of the strain vector are

$$\{\bar{\varepsilon}\} = \{\bar{\varepsilon}_x \quad \bar{\varepsilon}_\theta \quad 2\bar{\varepsilon}_{x\theta} \quad \bar{k}_x \quad \bar{k}_\theta \quad 2\bar{k}_{x\theta}\}^T \tag{21}$$

The conical finite element illustrated in Fig.3.3 is bounded by two circular nodes *i* and *j*. Each node has four degrees-of-freedom, three displacements $(\bar{u}_{ni}, \bar{v}_{ni}, \bar{w}_{ni})$ and one rotation $(\partial \bar{w}_{ni} / \partial x)$. The geometry of this finite element allows us to find the displacement functions in terms of nodal displacements based on Sanders' shell theory.

This approach is more accurate than the use of polynomial functions. The stress-strain relation for an anisotropic shell may be expressed by

$$\{\bar{\sigma}\} = [\bar{P}]\{\bar{\varepsilon}\} \tag{22}$$

Where $[\bar{P}]$ is the elasticity matrix for an anisotropic shell of order (6×6), see Appendix B.

The displacement functions associated with the n^{th} circumferential wave number may be developed into a Fourier series as follows:

$$\begin{Bmatrix} \bar{U}(x,\theta) \\ \bar{W}(x,\theta) \\ \bar{V}(x,\theta) \end{Bmatrix} = \sum_{n=0}^{\infty} [T] \begin{Bmatrix} \bar{u}_n(x) \\ \bar{w}_n(x) \\ \bar{v}_n(x) \end{Bmatrix} \tag{23}$$

Where $[T]$ is a matrix of order (3×3) given in Appendix A. $\bar{u}_n(x)$, $\bar{w}_n(x)$ and $\bar{v}_n(x)$ depend only on the *x* coordinate: By introducing the displacement functions of Eq.(23) into Eq.(19) and working out derivatives with respect to θ, one obtains three ordinary differential equations. The solutions of these equations have the following general form (see Refs [64] and [65] for more details):

$$\begin{Bmatrix} \bar{u}_n(x) \\ \bar{w}_n(x) \\ \bar{v}_n(x) \end{Bmatrix} = \left(\frac{x}{L}\right)^{\frac{\bar{\lambda}-1}{2}} \begin{Bmatrix} \bar{A} \\ \bar{C} \\ \bar{B} \end{Bmatrix} \tag{24}$$

where $\bar{\lambda}$, $\bar{A}$, $\bar{B}$ and $\bar{C}$ are unknown complex numbers and L is a reference slant length. By introducing Eq. (24) into equilibrium equations given in Appendix B, we obtain the following algebraic system:

$$\begin{bmatrix} \bar{H}_{11} & \bar{H}_{12} & \bar{H}_{13} \\ \bar{H}_{21} & \bar{H}_{22} & \bar{H}_{23} \\ \bar{H}_{31} & \bar{H}_{31} & \bar{H}_{32} \end{bmatrix} \begin{Bmatrix} \bar{A} \\ \bar{B} \\ \bar{C} \end{Bmatrix} = \left[\bar{H}\right] \begin{Bmatrix} \bar{A} \\ \bar{B} \\ \bar{C} \end{Bmatrix} = \begin{Bmatrix} 0 \\ 0 \\ 0 \end{Bmatrix} \tag{25}$$

Matrix $\left[\bar{H}\right]$ is a square matrix (3×3), the terms of which are functions of $\bar{\lambda}$, see Ref. [66]. For nontrivial solution, the determinant of matrix $\left[\bar{H}\right]$ must be zero. Application of this condition brings us to the following characteristic equation in terms of $\bar{\lambda}$:

$$\bar{a}\bar{\lambda}^8 + \bar{b}\bar{\lambda}^6 + \bar{c}\bar{\lambda}^4 + \bar{d}\bar{\lambda}^2 + \bar{e} = 0 \tag{26}$$

The coefficients $\left(\bar{a}, \bar{b}, \bar{c}, \bar{d} \text{ and } \bar{e}\right)$ of the characteristic equation are given in Ref. [66]. Each root $\overline{\lambda_i}$ solution of the equation above yields a solution to the equilibrium equations according to Sanders' thin shell theory. The complete solution is obtained by summation of these eight solutions independently with the constants $\bar{A}_i$, $\bar{B}_i$ and $\bar{C}_i$ $(i = 1,..,8)$ as follows:

$$\bar{u}_n(x) = \sum_{i=1}^{8} \bar{A}_i y^{\bar{\lambda}_i - 1} \tag{27.a}$$

$$\bar{v}_n(x) = \sum_{i=1}^{8} \bar{B}_i y^{\bar{\lambda}_i - 1} \tag{27.b}$$

$$\bar{w}_n(x) = \sum_{i=1}^{8} \bar{C}_i y^{\bar{\lambda}_i - 1} \tag{27.c}$$

Where y is the variable replacing the dimensionless ratio $(x/L)^{1/2}$ given in Eq. (24).

The dependent constants A_i and B_i are expressed in terms of constants C_i, see Ref.[66]. The displacement functions are written as

$$\begin{Bmatrix} \bar{u}_n(x) \\ \bar{w}_n(x) \\ \bar{v}_n(x) \end{Bmatrix} = \left[\bar{R}\right]\left\{\bar{C}\right\} \tag{28}$$

Where $\left[\bar{R}\right]$ is a (3×8) matrix given in Ref. [66]. The displacement vector corresponding to the circumferential mode n, at any point (x,θ), is then given by

$$\begin{Bmatrix} \bar{U}(x,\theta) \\ \bar{W}(x,\theta) \\ \bar{V}(x,\theta) \end{Bmatrix} = [T]\left[\bar{R}\right]\left\{\bar{C}\right\} \tag{29}$$

The nodal displacement vector of a conical finite element is

$$\begin{Bmatrix} \bar{\delta}_i \\ \overline{} \\ \bar{\delta}_j \end{Bmatrix} = \left\{\bar{u}_{ni}\ ,\bar{w}_{ni}, \partial\bar{w}_{ni}/\partial x, \bar{v}_{ni}, \bar{u}_{nj}, \bar{w}_{nj}, \partial\bar{w}_{nj}/\partial x, \bar{v}_{nj}\right\}^T = \left[\bar{A}\right]\left\{\bar{C}\right\} \tag{30}$$

where matrix $\left[\bar{A}\right]$ is obtained from the terms of the nodal displacements by replacing x by the nodal coordinates x_i and x_j corresponding, respectively, to nodes i and j (see Ref. [67]). The vector $\left\{\bar{C}\right\} = \left\{\bar{C}_1,\ldots,\bar{C}_8\right\}^T$ is a set of constants that may be determined from the eight nodal displacements of the conical finite element.

Premultiplying Eq. (30) by $\left[\bar{A}\right]^{-1}$, we obtain

$$\left\{\bar{C}\right\} = \left[\bar{A}\right]^{-1} \begin{Bmatrix} \bar{\delta}_i \\ \bar{\delta}_j \end{Bmatrix} \tag{31}$$

Substituting Eq. (31) into Eq. (29), one finds the displacement functions in term of the nodal displacements as follows:

$$\begin{Bmatrix} \bar{U}(x,\theta) \\ \bar{W}(x,\theta) \\ \bar{V}(x,\theta) \end{Bmatrix} = [T]\left[\bar{R}\right]\left[\bar{A}\right]^{-1} \begin{Bmatrix} \bar{\delta}_i \\ \bar{\delta}_j \end{Bmatrix} = \left[\bar{N}\right] \begin{Bmatrix} \bar{\delta}_i \\ \bar{\delta}_j \end{Bmatrix} \tag{32}$$

By introducing Eqs. (23) and (27) into Eq. (21) and using Eq. (31), the relationship between the strain and the displacements for conical shell can be rewritten as

$$\{\bar{\varepsilon}\} = \begin{bmatrix} [T] & [0] \\ [0] & [T] \end{bmatrix} \left[\bar{Q}\right]\left[\bar{A}\right]^{-1} \begin{Bmatrix} \bar{\delta}_i \\ \bar{\delta}_j \end{Bmatrix} = \left[\bar{B}\right] \begin{Bmatrix} \bar{\delta}_i \\ \bar{\delta}_j \end{Bmatrix} \tag{33}$$

Where $\left[\bar{Q}\right]$ is a (6×8) matrix given in Ref. [67].

The stress resultant vector may be found in terms of nodal displacements by inserting Eq. (33) into Eq. (22) as

$$\{\bar{\sigma}\} = \left[\bar{P}\right]\left[\bar{B}\right] \begin{Bmatrix} \bar{\delta}_i \\ \bar{\delta}_j \end{Bmatrix} \tag{34}$$

Following the framework of the finite element approach, the elementary mass and stiffness matrices defined in the conical coordinate system can be expressed as follows:

$$[\bar{m}]_s^e = \rho h \iint \left[\bar{N}\right]^T \left[\bar{N}\right] dA \tag{35}$$

$$\left[\bar{k}\right]_s^e = \iint \left[\bar{B}\right]^T \left[\bar{P}\right]\left[\bar{B}\right] dA \tag{36}$$

Where ρ is the material density, h is the shell thickness and dA is the differential area of the conical finite element expressed by

$$dA = x\sin(\alpha)\,dx\,d\theta \tag{37}$$

Using Eqs. (32) and (33) in Eqs. (35) and (36), respectively, one obtains

$$[\bar{m}]_s^e = \rho h \left[\left[\bar{A}\right]^{-1}\right]^T \left[\int_{x_1}^{x_2}\int_0^{2\pi} \left[\bar{R}\right]^T [T]^T [T]\left[\bar{R}\right] dA\right]\left[\bar{A}\right]^{-1} \tag{38}$$

$$\left[\bar{k}\right]_s^e = \left[\left[\bar{A}\right]^{-1}\right]^T \left[\int_{x_1}^{x_2}\int_0^{2\pi} \left[\bar{Q}\right]^T \begin{bmatrix} [T] & [0] \\ [0] & [T] \end{bmatrix}^T \left[\bar{P}\right] \begin{bmatrix} [T] & [0] \\ [0] & [T] \end{bmatrix} \left[\bar{Q}\right] dA\right]\left[\bar{A}\right]^{-1} \tag{39}$$

3.4. Modeling of initial stress stiffening

The initial stiffening stresses in axisymmetric shells result from radial pressure and axial load. Their effect is estimated here by calculating the potential energy using direct membrane forces per unit width and rotations about the orthogonal axes. We assume that the shell is under equilibrium conditions without deforming excessively, which makes the model appropriate for small vibrations and cannot examine the effect of nonlinearity on the dynamic behaviour. Also, the initial in-plane shear, static bending and transverse shear are ignored [68].

We first introduce the general formulation of the initial stiffening effect and then apply it to the conical and cylindrical finite elements including their kinematic equations. The resultant membrane forces per unit width $\bar{N}_x$ and $\bar{N}_\theta$ are expressed in terms of axial load P_x and radial pressure P_m. The strain energy associated with these loads is [68]:

$$U_e = \frac{1}{2}\iint\left[\bar{N}_x\varphi_{xx}^2 + \bar{N}_\theta\varphi_{\theta\theta}^2 + \left(\bar{N}_x + \bar{N}_\theta\right)\varphi_{nn}^2\right]dA \qquad (40)$$

φ_{xx}, $\varphi_{\theta\theta}$ and φ_{nn} are the elastic rotations and are defined according to Sanders' shell theory as follows:

$$\varphi_{xx} = \frac{U_1}{R_1} - \frac{1}{\alpha_1}\frac{\partial W}{\partial \xi_1} \qquad (41.a)$$

$$\varphi_{\theta\theta} = \frac{U_2}{R_2} - \frac{1}{\alpha_2}\frac{\partial W}{\partial \xi_2} \qquad (41.b)$$

$$\varphi_{nn} = \frac{1}{2\alpha_1\alpha_2}\left(\frac{\partial\left(\alpha_2 U_2\right)}{\partial \xi_1} - \frac{\partial\left(\alpha_1 U_1\right)}{\partial \xi_2}\right) \qquad (41.c)$$

Where α_i and ξ_i $\left(i = 1, 2\right)$ are, respectively, the coefficient in metric form and the generalized coordinates on the middle surface associated with Sanders' shell theory [62]. U_1 and U_2 are the displacements tangential to the middle surface and W is the displacement normal to middle surface. R_1 and R_2 are the principal radii of a doubly curved shell.

Equations (40) and (41) may be rewritten in matrix form as

$$U_e = \frac{1}{2}\iint\begin{Bmatrix}\varphi_{xx}\\ \varphi_{\theta\theta}\\ \varphi_{nn}\end{Bmatrix}^T \left[Z\right]\begin{Bmatrix}\varphi_{xx}\\ \varphi_{\theta\theta}\\ \varphi_{nn}\end{Bmatrix}\alpha_1\alpha_2 d\xi_1 d\xi_2 \qquad (42)$$

$$\begin{Bmatrix}\varphi_{xx}\\ \varphi_{\theta\theta}\\ \varphi_{nn}\end{Bmatrix} = \left[G\right]\begin{Bmatrix}U_1\\ W\\ U_2\end{Bmatrix} \qquad (43)$$

With

$$[Z] = \begin{bmatrix} \bar{N}_x & 0 & 0 \\ 0 & \bar{N}_\theta & 0 \\ 0 & 0 & \bar{N}_x + \bar{N}_\theta \end{bmatrix}$$

And

$$[G] = \begin{bmatrix} \dfrac{1}{R_1} & -\dfrac{1}{\alpha_1}\dfrac{\partial}{\partial \xi_1} & 0 \\ 0 & -\dfrac{1}{\alpha_2}\dfrac{\partial}{\partial \xi_2} & \dfrac{1}{R_2} \\ -\dfrac{1}{2\alpha_1\alpha_2}\left(\dfrac{\partial \alpha_1}{\partial \xi_2} + \alpha_1 \dfrac{\partial}{\partial \xi_2}\right) & 0 & \dfrac{1}{2\alpha_1\alpha_2}\left(\dfrac{\partial \alpha_2}{\partial \xi_1} + \alpha_2 \dfrac{\partial}{\partial \xi_1}\right) \end{bmatrix}$$

Expressing the displacement functions in Eq. (43) by those obtained above in Eqs. (12) and (32), either for conical or cylindrical finite elements, one obtains:

$$\begin{Bmatrix} \varphi_{xx} \\ \varphi_{\theta\theta} \\ \varphi_{nn} \end{Bmatrix} = [G]\left[\hat{N}\right]\begin{Bmatrix} \delta_i \\ \delta_j \end{Bmatrix} \tag{44}$$

Where $\left[\hat{N}\right]$ is the shape function matrix in local coordinates and $\{\delta_i\}$ is the nodal displacement vector. Now, introducing Eq. (44) into Eq. (42), the expression of the elastic strain energy may be rewritten as

$$U_e = \frac{1}{2}\iint \begin{Bmatrix} \delta_i \\ \delta_j \end{Bmatrix}^T \left[\hat{N}\right]^T [G]^T [Z][G]\left[\hat{N}\right]\begin{Bmatrix} \delta_i \\ \delta_j \end{Bmatrix} \alpha_1\alpha_2 d\xi_1 d\xi_2 \tag{45}$$

The initial stiffness matrix for each element can be deduced from Eq. (45) as

$$[k_I]^e = \iint \left[\hat{N}\right]^T [G]^T [Z][G]\left[\hat{N}\right]\alpha_1\alpha_2 d\xi_1 d\xi_2 \tag{46}$$

The general formulation of the initial stiffening effect presented above will be applied below for conical and cylindrical shells by considering the proper resultant loads and elastic middle surface rotations.

3.4.1. Initial stress stiffening for a cylindrical finite element

The resultant membrane loads due to a differential radial pressure P_m and axial load P_x shown in Fig.3.5, may be expressed, respectively, by:

$$\bar{N}_\theta = P_m r \quad \text{and} \quad \bar{N}_x = -\frac{P_x}{2\pi r} \tag{47}$$

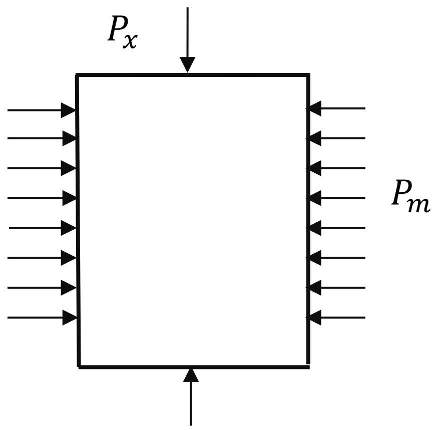

Figure 3.5: Configuration of the axial loads and radial pressure applied on the cylindrical shell

The Sanders' theory parameters α_i and ξ_i and the elastic rotations for a cylindrical shell are:

$$\xi_1 = x, \qquad U_1 = U, \qquad R_1 = \infty\,, \qquad \alpha_1 = 1 \tag{48.a}$$

$$\xi_2 = \theta, \qquad U_2 = V, \qquad R_2 = r\,, \qquad \alpha_2 = r \tag{48.b}$$

Elastic rotations for the present geometry are:

$$\begin{Bmatrix} \varphi_{xx} \\ \varphi_{\theta\theta} \\ \varphi_{nn} \end{Bmatrix} = \begin{bmatrix} 0 & -\dfrac{\partial}{\partial x} & 0 \\ 0 & -\dfrac{1}{r}\dfrac{\partial}{\partial \theta} & \dfrac{1}{r} \\ -\dfrac{1}{2r}\dfrac{\partial}{\partial \theta} & 0 & \dfrac{1}{2}\dfrac{\partial}{\partial x} \end{bmatrix} \begin{Bmatrix} U \\ W \\ V \end{Bmatrix} = [G] \begin{Bmatrix} U \\ W \\ V \end{Bmatrix} \tag{49}$$

By inserting Eq. (12) into Eq. (49), one obtains the elastic rotations in terms of nodal displacement as follows

$$\begin{Bmatrix} \varphi_{xx} \\ \varphi_{\theta\theta} \\ \varphi_{nn} \end{Bmatrix} = [G][N]\begin{Bmatrix} \delta_i \\ \delta_j \end{Bmatrix} \tag{50}$$

Using Eq. (46), the initial stress stiffness matrix for each cylindrical finite element is

$$[k_I]^e = \int_0^l \int_0^{2\pi} [N]^T [G]^T [Z][G][N] r dx d\theta \tag{51}$$

Rearranging Eq. (51), we obtain

$$[k_I]^e = \left[A^{-1}\right]^T \int_0^l \int_0^{2\pi} [R]^T [T]^T [G]^T [Z][G][T][R] r dx d\theta \left[A^{-1}\right] \tag{52}$$

Finally, the stress stiffness matrix can be written as

$$[k_I]^e = \left[A^{-1}\right]^T [D]\left[A^{-1}\right] \tag{53}$$

where

$$[D] = \int_0^l \int_0^{2\pi} [R]^T [T]^T [G]^T [Z][G][T][R] r dx d\theta = \int_0^l \int_0^{2\pi} [D_a] r dx d\theta \tag{54}$$

The analytical form of matrix $\left[D_a\right]$ is

$$D_a(i,j) = \frac{e^{(\lambda_i+\lambda_j)x/r}}{r^2}\left\{ \bar{N}_x \lambda_i \lambda_j (\cos n\theta)^2 + \left[\bar{N}_\theta (n+\beta_i)(n+\beta_j) + \frac{(\bar{N}_x + \bar{N}_\theta)}{4}(\alpha_i n + \beta_i \lambda_i)(\alpha_j n + \beta_j \lambda_j) \right](\sin n\theta)^2 \right\}$$

$$i = 1,..,8 \text{ and } j = 1,..,8 \tag{55}$$

By integrating Eq. (55) over x and θ, we obtain the analytical expression of the $D(i,j)$ matrix depending on the sum $(\lambda_i + \lambda_j)$

For $(\lambda_i + \lambda_j) \neq 0$

$$D(i,j) = \frac{\pi}{\lambda_i + \lambda_j}\left(e^{(\lambda_i+\lambda_j)l/r} - 1\right)\left\{ \lambda_i \lambda_j \bar{N}_x + \bar{N}_\theta (n+\beta_i)(n+\beta_j) + \frac{(\bar{N}_x + \bar{N}_\theta)}{4}(\alpha_i n + \beta_i \lambda_i)(\alpha_j n + \beta_j \lambda_j) \right\} \tag{56}$$

For $(\lambda_i + \lambda_j) = 0$

$$D(i,j)=\frac{\pi l}{r}\left\{\lambda_i\lambda_j\bar{N}_x+\bar{N}_\theta(n+\beta_i)(n+\beta_j)+\frac{(\bar{N}_x+\bar{N}_\theta)}{4}(\alpha_i n+\beta_i\lambda_i)(\alpha_j n+\beta_j\lambda_j)\right\} \tag{57}$$

3.4.2. Initial stress stiffening for a conical finite element

The linear membrane stress resultant $\bar{N}_\theta$ and $\bar{N}_x$ in terms of the external radial static pressure P_m and compressive axial load P_x shown in Fig.3.6, are given by [46]:

$$\bar{N}_\theta=-x\tan(\alpha)P_m \tag{58.a}$$

$$\bar{N}_x=-\frac{x}{2}\tan(\alpha)P_m-\frac{P_x}{2\pi\sin\alpha\cos\alpha} \tag{58.b}$$

The Sanders' theory parameters α_i, ξ_i and the elastic rotations for this geometry are:

$$\xi_1=x,\qquad U_1=\bar{U},\qquad R_1=\infty\,,\qquad \alpha_1=1 \tag{59.a}$$

$$\xi_2=\theta,\qquad U_2=\bar{V},\qquad R_2=x\tan\alpha\,,\qquad \alpha_2=x\sin\alpha \tag{59.b}$$

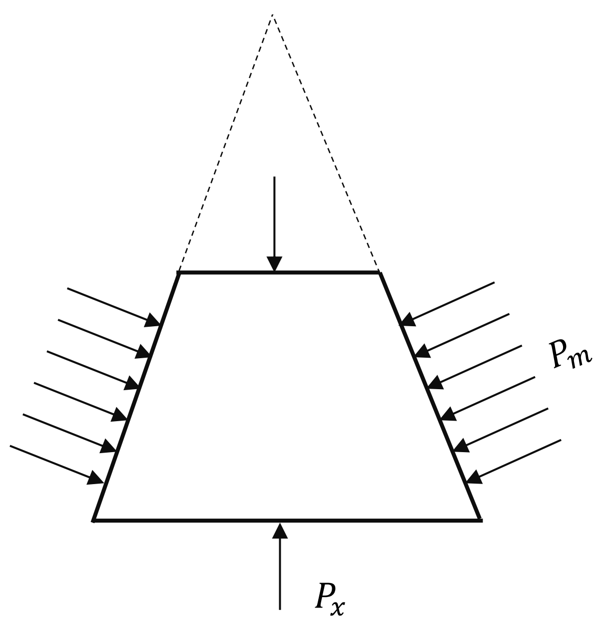

Figure 3.6: Configuration of the axial loads and radial pressure applied on the conical shell

Elastic rotations for the present geometry may be written in their matrix form as:

$$\begin{Bmatrix} \bar{\varphi}_{xx} \\ \bar{\varphi}_{\theta\theta} \\ \bar{\varphi}_{nn} \end{Bmatrix} = \begin{bmatrix} 0 & -\frac{\partial}{\partial x} & 0 \\ 0 & -\frac{1}{(x\sin\alpha)}\frac{\partial}{\partial\theta} & \frac{1}{x\tan\alpha} \\ -\frac{1}{(2x\sin\alpha)}\frac{\partial}{\partial\theta} & 0 & \frac{1}{2x}+\frac{1}{2}\frac{\partial}{\partial x} \end{bmatrix} \begin{Bmatrix} \bar{U} \\ \bar{W} \\ \bar{V} \end{Bmatrix} = \left[\bar{G}\right] \begin{Bmatrix} \bar{U} \\ \bar{W} \\ \bar{V} \end{Bmatrix} \tag{60}$$

By inserting Eq. (32) into Eq. (60), the latter is written in terms of nodal displacement:

$$\begin{Bmatrix} \bar{\varphi}_{xx} \\ \bar{\varphi}_{\theta\theta} \\ \bar{\varphi}_{nn} \end{Bmatrix} = \left[\bar{G}\right]\left[\bar{N}\right] \begin{Bmatrix} \bar{\delta}_i \\ \bar{\delta}_j \end{Bmatrix} \tag{61}$$

Using Eq. (46), the initial stiffness matrix for each conical finite element is

$$\left[\bar{k}_I\right]^e = \int_{x_i}^{x_j}\int_0^{2\pi} \left[\bar{N}\right]^T \left[\bar{G}\right]^T [Z]\left[\bar{G}\right]\left[\bar{N}\right] x\sin\alpha\, dxd\theta \tag{62}$$

By inserting Eq. (32) into Eq. (62), the stiffness matrix can be written as follows:

$$\left[\bar{k}_I\right]^e = \left[\left[\bar{A}\right]^{-1}\right]^T \int_{x_i}^{x_j}\int_0^{2\pi} \left[\bar{R}\right]^T [T]^T \left[\bar{G}\right]^T [Z]\left[\bar{G}\right][T]\left[\bar{R}\right] x\sin\alpha\, dxd\theta \left[\bar{A}\right]^{-1} \tag{63}$$

Finally, the initial stiffness matrix is written as

$$\left[\bar{k}_I\right]^e = \left[\left[\bar{A}\right]^{-1}\right]^T \left[\bar{D}\right]\left[\bar{A}\right]^{-1} \tag{64}$$

where

$$\left[\bar{D}\right] = \int_{x_i}^{x_j}\int_0^{2\pi} \left[\bar{R}\right]^T [T]^T \left[\bar{G}\right]^T [Z]\left[\bar{G}\right][T]\left[\bar{R}\right] x\sin\alpha\, dxd\theta = \int_{x_i}^{x_j}\int_0^{2\pi} \left[\bar{D}_a\right] x\sin\alpha\, dxd\theta \tag{65}$$

The analytical form of matrix $\left[\bar{D}_a\right]$ is

$$\bar{D}_a(i,j) = \left[-\frac{x}{2}\tan\alpha\, P_m - \frac{P_x}{\pi\sin(2\alpha)}\right]F_1 - x\tan\alpha\, P_m \frac{\sin^2(n\theta)}{x^2\sin^2\alpha}F_2 + \left[-\frac{3x}{2}\tan\alpha\, P_m - \frac{P_x}{\pi\sin(2\alpha)}\right]\frac{\sin^2(n\theta)}{4x^2}F_3$$
$$\text{avec } i = 1,..,8 \text{ and } j = 1,..,8 \tag{66}$$

where

$$F_1 = \cos^2(n\theta)\left(\frac{\lambda_i - 1}{2L}\right)\left(\frac{x}{L}\right)^{\frac{\lambda_i - 3}{2}}\left(\frac{\lambda_j - 1}{2L}\right)\left(\frac{x}{L}\right)^{\frac{\lambda_j - 3}{2}}$$

$$F_2 = \left(\frac{x}{L}\right)^{\frac{\lambda_i - 1}{2}}\left(\frac{x}{L}\right)^{\frac{\lambda_j - 1}{2}}\left(n + \beta_i \cos\alpha\right)\left(n + \beta_j \cos\alpha\right)$$

$$F_3 = \left(\frac{x}{L}\right)^{\frac{\lambda_i - 1}{2}}\left(\frac{x}{L}\right)^{\frac{\lambda_j - 1}{2}}\left(\frac{n\alpha_i}{\sin\alpha} + \beta_i\left(\frac{1+\lambda_i}{2}\right)\right)\left(\frac{n\alpha_j}{\sin\alpha} + \beta_j\left(\frac{1+\lambda_j}{2}\right)\right)$$

After integrating Eq. (66) over x and θ, we can express Eq. (65) for the k^{th} element, as follows

For $\left(\lambda_i + \lambda_j\right) \neq 0$ and $\left(\lambda_i + \lambda_j - 2\right) \neq 0$

$$\bar{D}(i,j) = Aux_1 + Aux_2 + Aux_3 \qquad (67)$$

For $\left(\lambda_i + \lambda_j\right) = 0$

$$\bar{D}(i,j) = Aux_4 + Aux_5 + Aux_6 \qquad (68)$$

For $\left(\lambda_i + \lambda_j - 2\right) = 0$

$$\bar{D}(i,j) = Aux_7 + Aux_8 + Aux_9 \qquad (69)$$

Where Aux_p $(p = 1,..,9)$ are given in Appendix B.

3.5. Geometrical transformation

The elementary matrices of the conical finite elements should be transformed to a common global system, (see Fig.3.7). The nodal displacement vector is related to its counterpart in the global coordinate system by:

$$\begin{Bmatrix} u_{ni} \\ w_{ni} \\ \dfrac{\partial w_{ni}}{\partial x} \\ v_{ni} \end{Bmatrix} = \begin{bmatrix} \cos\alpha & -\sin\alpha & 0 & 0 \\ \sin\alpha & \cos\alpha & 0 & 0 \\ 0 & 0 & 1 & 0 \\ 0 & 0 & 0 & 1 \end{bmatrix} \begin{Bmatrix} \bar{u}_{ni} \\ \bar{w}_{ni} \\ \dfrac{\partial \bar{w}_{ni}}{\partial x} \\ \bar{v}_{ni} \end{Bmatrix} = [TR] \begin{Bmatrix} \bar{u}_{ni} \\ \bar{w}_{ni} \\ \dfrac{\partial \bar{w}_{ni}}{\partial x} \\ \bar{v}_{ni} \end{Bmatrix} \qquad (70)$$

The mass and stiffness elementary matrices are then transformed to the global coordinate system as follows:

$$[k]_s^e = \begin{bmatrix} [TR] & [0] \\ [0] & [TR] \end{bmatrix} \left[\bar{k}\right]_s^e \begin{bmatrix} [TR] & [0] \\ [0] & [TR] \end{bmatrix}^T \qquad (71)$$

$$[m]_s^e = \begin{bmatrix} [TR] & [0] \\ [0] & [TR] \end{bmatrix} [\bar{m}]_s^e \begin{bmatrix} [TR] & [0] \\ [0] & [TR] \end{bmatrix}^T \quad (72)$$

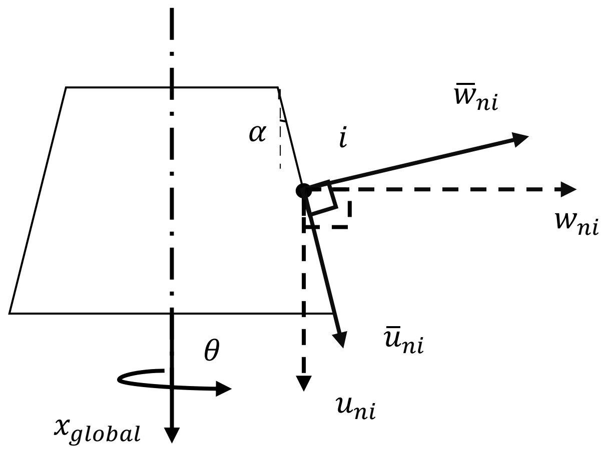

Figure 3.7: Geometrical transformation from local to global coordinates

Where $[k]_s^e$ and $[m]_s^e$ are, respectively, the elementary stiffness and mass matrices defined in the global coordinate system.

Once all the elementary matrices relative to each structural geometry are defined, we proceed to determine the equivalent stiffness matrix by adding the structural stiffness matrix to that attributed to the initial stiffening effect.

3.6. Equations of motion

After superimposing the elementary matrices of the structure and introducing the boundary conditions, the dynamic behaviour of a combined axisymmetric shell subjected to membrane loads can be represented by the following system:

$$[M_s]\{\ddot{\Delta}\} + [[K_s] + [K_I]]\{\Delta\} = \{0\} \quad (73)$$

where $\{\Delta\}$ is the global displacement vector, and $[M_s]$ and $[K_s]$ are, respectively, the global mass and stiffness matrices of the whole structure. $[K_I]$ represents the global matrix of the initial stress stiffening effect. The vibration frequencies of the system above may be calculated by solving the standard eigenvalue problem.

3.7. Results and discussions

The hybrid approach, presented above to model the elastic behavior of conical and cylindrical frustums, enables very accurate results using a small number of finite elements [9, 69]. Before performing numerical calculations to determine the initial stress stiffening effect, it is important to conduct a convergence study of the solution as a function of the number of finite elements and to confirm the validity of the solid model. In our work, numerical calculations were carried out beforehand separately for conical and cylindrical shells. Later, both models were used to analyze combined structures.

3.7.1. Cylindrical model

3.7.1.1. Convergence test and free vibration

The first set of calculations was performed for a clamped-free cylindrical shell with an axial length $L = 0.231\,\mathrm{m}$, radius $r = 7.725\ \mathrm{cm}$, and thickness $h = 1.5\,\mathrm{mm}$. Its mechanical properties are: Young's modulus $E = 206\ \mathrm{GPa}$, Poisson's ratio $\nu = 0.3$ and density $\rho_s = 7800\ \mathrm{kg/m^3}$. Variation of the percentage error of natural frequencies relative to the requisite mesh size (30 F.E.) $(\omega_{\mathrm{NFE}} - \omega_{\mathrm{30FE.}}) \times 100 / \omega_{\mathrm{NFE}}$ is given in Fig.3.8 versus the number of cylindrical finite elements. The results were calculated using a regular mesh for two fundamental circumferential modes $n = 2$ and 3, and for four axial modes from $m = 1$ to 4. The fundamental mode requires a very small number of finite elements while the higher modes require a more refined mesh. Based on these results, we can conclude that only twenty finite elements are sufficient to ensure convergence for the case of cylindrical shells.

Table 3.1 lists the natural frequencies of the same clamped-free shell calculated above using thirty cylindrical finite elements for various axial and circumferential modes. The obtained results are compared to those of Refs [51] and [70]. Very good agreement is found between our results and those of Ref. [51]. It can also be seen that numerical results obtained using our theory are closer to experimental results than those based on Zhang's theory. The small margin of error in frequency between our model and the experimental results in Ref. [70] may be due to experimental difficulties encountered to reproduce the boundary conditions of the clamped side of the shell.

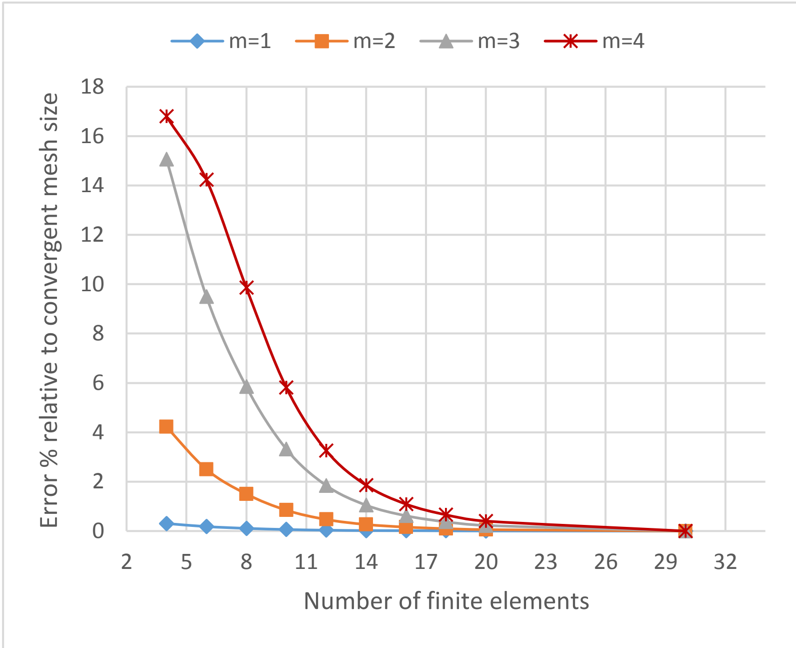

(a)

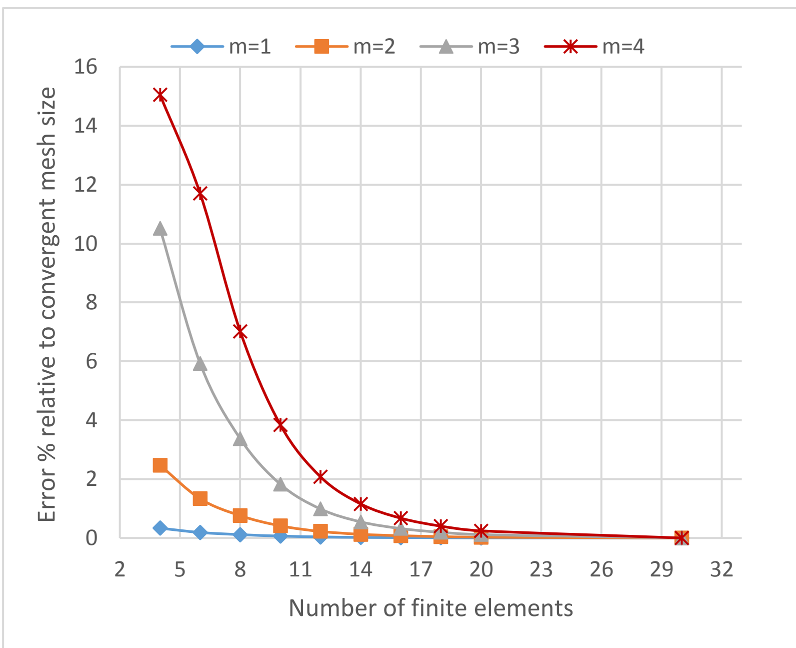

(b)

Figure 3.8: Variation of the percentage error of natural frequencies of a cylindrical shell relative to the requisite mesh size (a) $n=2$ and (b) $n=3$ $(100\times(\omega_{\text{N F.E.}}-\omega_{\text{30 F.E.}})/\omega_{\text{N. F.E.}})$

Table 3.1: Natural frequencies of a clamped-free cylindrical shell compared to numerical and experimental results of Refs. [51] and [70], respectively.

m	n	Present	Experimental of Ref. [70]	Finite element model of Ref. [51]
1	2	816.69	708	816
	3	635.3	616	637.9
	4	950.04	945	952.8
	5	1483.76	1479	1487.6
	6	2158.93	2151	2164.2
2	2	3166.81	N.A.	N.A.
	3	2033.43	1969	2049
	4	1652.18	1628	1665.3
	5	1842.82	1851	1853.3
	6	2389.48	N.A.	N.A.

3.7.1.2. Axial load

The influence of axial load on the dynamic behaviour of the structure was investigated by calculating the natural frequencies of cylindrical shells clamped at opposing sides and having an axial length $L = 0.9144\,\mathrm{m}$, radius $r = 0.1527\,\mathrm{m}$, shell thickness $h = 0.47\,\mathrm{mm}$, Young's modulus $E = 200$ GPa, Poisson's ratio $\nu = 0.3$ and density $\rho_s = 7639\ \mathrm{kg/m^3}$. This case was calculated to validate our initial stiffening effect model. Table 3.2 shows that a tensile membrane load increases the shell frequencies. Our results were compared with those measured in Ref. [43] and calculated in Ref. [51]. Excellent agreement of our results may be noted, particularly with the numerical results of Ref. [51]. The maximum relative error for the worst case of the calculated frequencies is limited to 4%.

The axial force can be applied as tension or compression. The compressive axial load should be validated as it enables determination of the critical compressive load. The frequencies calculated using our model were validated by comparing them to those obtained using the ANSYS finite element 'SHELL281'. This finite element is able to take the stiffening effect into account by activating the 'PSTRES' command [71]. The physical properties of the studied clamped-free structure are: shell density $\rho_s = 7916\ \mathrm{kg/m^3}$, Young's modulus $E = 200$ GPa, Poisson's ratio $\nu = 0.32$, axial length $L = 0.6096\,\mathrm{m}$, radius $r = 0.1016\,\mathrm{m}$ and shell thickness $h = 0.152\,\mathrm{mm}$.

Table 3.2: Natural frequencies of a clamped-clamped cylindrical shell under axial load F_x compared to those of Refs. [51] and [43].

Axial load $F_x\,(\mathrm{N})$	Circumferential mode n	Present model	Experimental results of Ref. [43]	Numerical model of Zhang [51]
1.198×10^4	5	173.65	162	175.48
	6	196.12	191	196.49
	7	247.62	243	247.07
	8	316.58	320	315.34
2.397×10^4	5	177.11	165	176.44
	6	199.22	194	197.37
	7	250.07	246	247.00
	8	318.49	321	315.90
3.597×10^4	5	185.94	167	177.40
	6	207.13	196	198.24
	7	256.37	247	248.47
	8	323.41	323	316.45

Figure 3.9 compares our frequencies to those calculated by the ANSYS software. Compressive membrane forces decrease the natural frequencies until dynamic instability occurs. Perfect concordance is found between our results and those of the ANSYS software. It is important to note that the ANSYS software requires an excessive bidimensional finite element (350 F.E) number and a two-step solution using a nonlinear model. In comparison, the same results are obtained by our model using only 20 finite elements and a single calculation step.

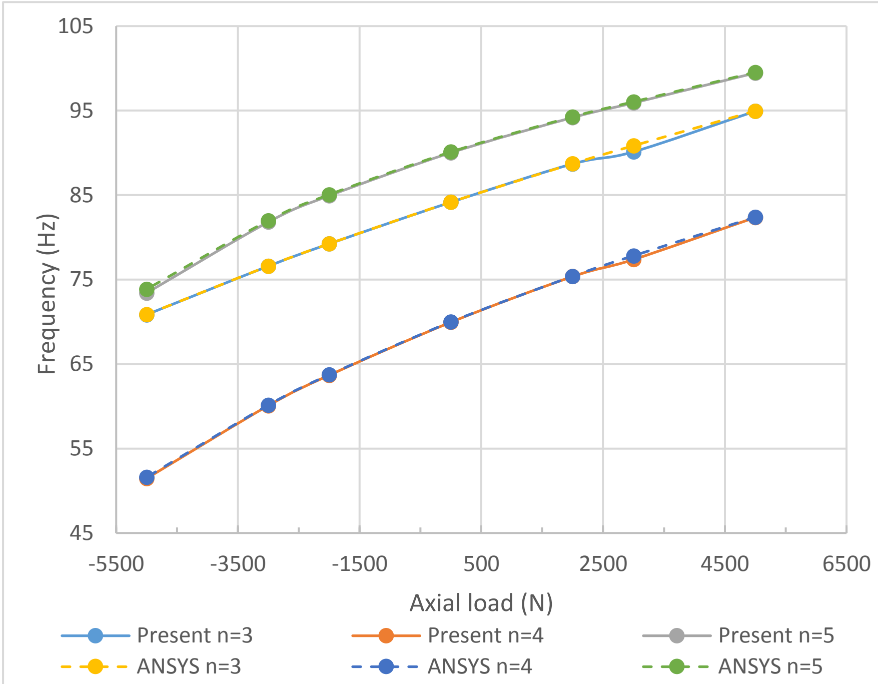

Figure 3.9: Frequencies of a clamped-free cylindrical shell as a function of axial compressive load (N) compared to ANSYS finite element model (SHELL281)

3.7.1.3. Internal pressure

The effect of hydrostatic pressure on a clamped-clamped stainless steel cylindrical shell was investigated. The physical properties of the cylindrical shell are the same as the case described just above. By examining the results presented in Table 3.3, we find that the frequencies increase with internal pressure for all circumferential modes considered.

This increase is related to the fact that the elastic deformation energy associated with the membrane forces is added to the preliminary deformation energy calculated without any initial stiffening effect. Excellent agreement may be noted between our results, using a small number of finite elements, and those of Refs. [51] and [43].

Table 3.3: Frequencies of a clamped-clamped stainless steel cylindrical shell under internal static pressure compared to those of Refs. [51] and [43].

Mode n	Internal pressure P_m (kPa)	Present	Experiment [43]	Zhang [51]
5	29.65	418.997	402	423.13
	32.41	433.807	424	437.79
	32.75	435.597	428	439.59
	39.65	470.446	466	474.12
	46.69	503.523	492	507.86
	51.02	522.828	507-508	526.17
	59.99	560.711	544-556	563.8
	66.88	588.154	567	591.12
	69.64	598.795	590	601.7
	87.94	665.054	651	667.58
6	20.68	416.732	402	419.84
	27.58	469.96	458	472.68
	42.75	569.762	548	572
	55.16	639.934	619-620	641.93
	62.74	679.238	645	681.14
	68.95	709.818	675-685	711.62
7	27.58	549.024	579	550.83
	30.34	572.456	597	574.17
	38.61	637.531	656	639.1
	46.19	691.821	709	693.3
	59.98	780.969	761	782.27
	67.57	825.941	826	827.14
8	19.99	555.786	568	557.27
	26.89	629.252	631	630.51
	33.09	688.611	684	689.81
	45.51	794.288	777	795.26
	55.85	872.557	848	873.46
	62.05	916.288	884	917.18
	68.95	962.623	937	963.44

3.7.1.4. Effect of geometric properties

The initial stiffening effect, resulting from radial pressure and axial load, influences the dynamic behaviour of the structure and can lead to instability by exceeding certain critical compressive loads and/or certain external radial pressures. We focus our study in this section on investigating the influence of some geometric properties on the dynamic stability of the structure, highlighting the fluctuation of the critical buckling loads and the critical pressures. Numerical computations were carried out for clamped-clamped cylindrical shells with various geometrical ratios (r/h) and (L/r) [43].

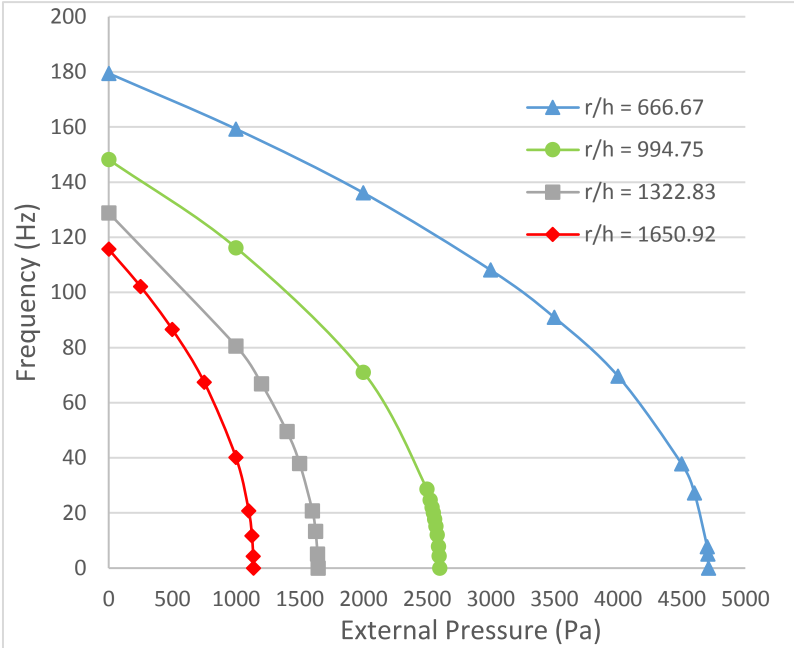

Figure 3.10: Fluctuation of frequencies of a clamped-clamped cylindrical shell as a function of external pressure for various radius-thickness ratios $\left(L = 0.6096 \text{ m},\ h = 1.52\times10^{-4} \text{ m}\right)$ [43]

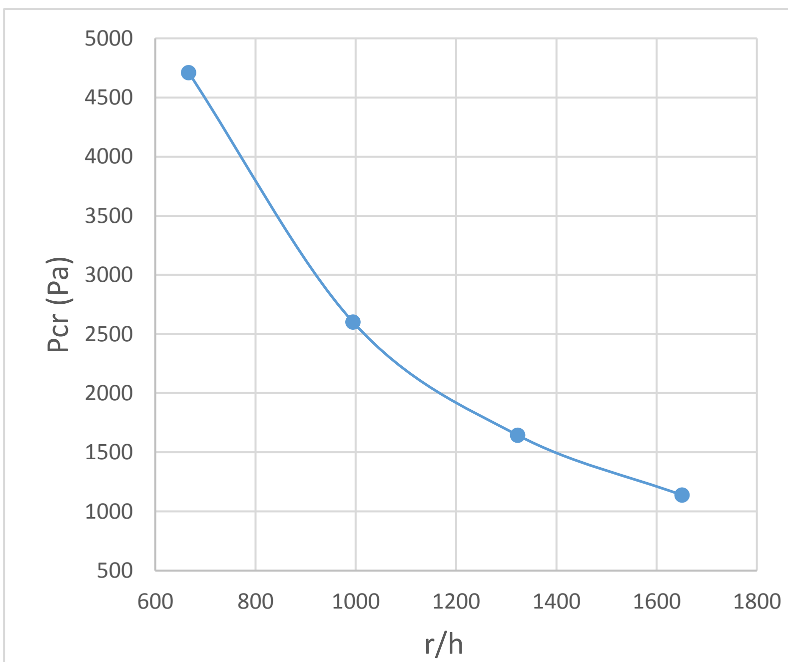

Figure 3.11: Variation of the critical pressure P_{cr} of a clamped-clamped cylindrical shell as a function of the radius-thickness ratios

The structure is subjected to variable external pressure and compressive axial loads, applied separately.

It is observed from Fig.3.10 that frequencies reduce nonlinearly as the external pressure increases, for different radius-thickness ratios. The thickness is maintained fixed here and the radius is varied. When the frequency reaches zero, the structure loses its stability and converts membrane strain energy into bending strain energy. The dynamic critical pressure P_{cr} is determined from the intersection of the curve with the x-axis. By setting a fixed value of external pressure, Fig.3.10 exhibits a decrease of frequencies with an increasing radius-thickness ratio. It can also be seen that the frequency drop corresponding to different r/h ratios is more significant as the external pressure increases. Figure 3.11 depicts the variation of the critical buckling pressure versus the radius-thickness ratio for the same shell defined above.

The critical pressure is inversely proportional to the radius-thickness ratio. The slope of the curve is more accentuated for small ratios r/h. It can be concluded that thinner and/or wider shells become more vulnerable to dynamic instability.

Numerical calculations were carried out for clamped-clamped cylindrical shells with various geometrical ratios r/h.

The second geometrical parameter investigated here is the length/radius ratio. The latter was varied from 6 to 13.78 by keeping the shell radius fixed $\left(r = 0.1016\,\mathrm{m}\right)$ and varying its length. The variation of frequency versus external pressure for different values of length/radius ratio is plotted in Fig.3.12. It can be noticed that the frequency drop is more remarkable for slender shells as the external pressure increases $\left(L/r = 11.81 \text{ and } L/r = 13.78\right)$.

Figure 3.13 exhibits a decreasing trend of the critical load while the slenderness of the structure is still increasing. Beyond $L/r = 11.81$, the slope of the curve becomes more pronounced.

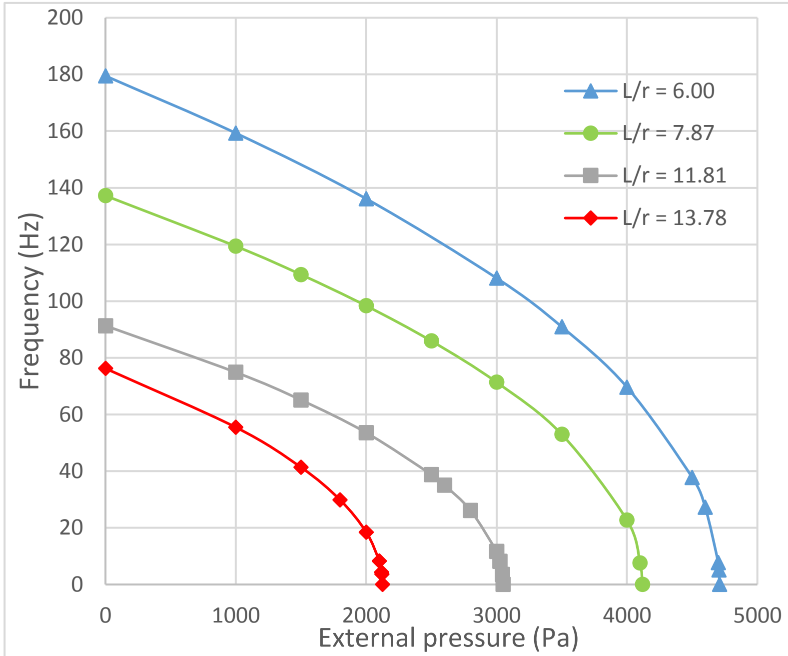

Figure 3.12: Fluctuation of frequencies of a clamped-clamped cylindrical shell as a function of external pressure for various length-radius ratios

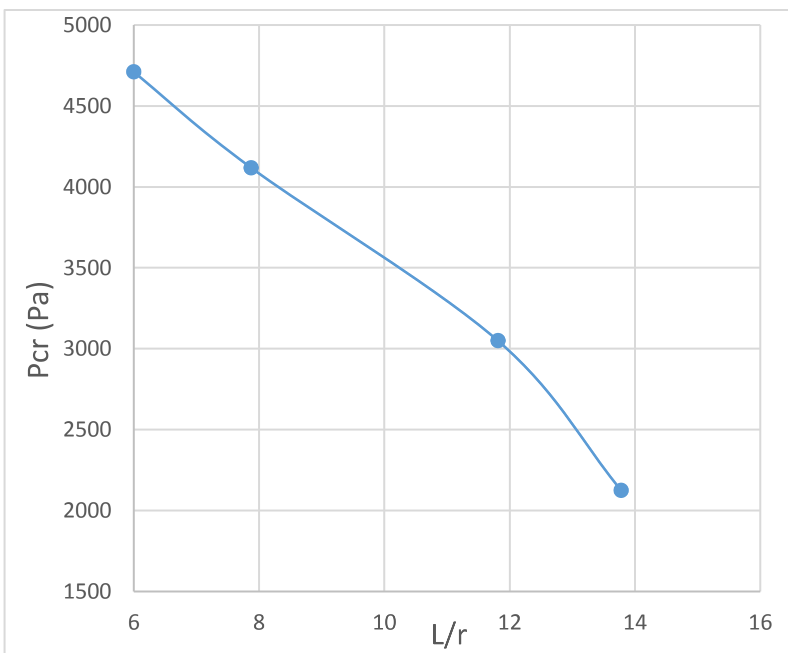

Figure 3.13: Variation of the critical pressure P_{cr} of a clamped-clamped cylindrical shell as a function of the length-radius ratios

Figures 3.14 and 3.15 investigate the effect of axial compressive load on the dynamic stability of the aforementioned shell using the same geometrical parameters r/h and L/r. It is obvious from Fig.3.14 that the frequencies are inversely related to the dimensionless parameter r/h. The frequency drop for the different r/h ratios depicted in the same figure, decreases as the axial force increases, which represents an opposite effect to that observed above for a cylindrical shell subjected to external pressures. In the neighbourhood of the critical force, the effect of r/h becomes minimal. The three curves converge almost to the same value of the critical buckling load $\left(F_{cr} \cong 27.8\,\mathrm{kN}\right)$. Figure 3.15 shows the variation of the natural frequency of the cylindrical shell versus the axial compression load for the different L/r ratios. According to this figure, the frequency of the system is enhanced as the L/r ratio decreases.

As the axial compression load increases, the structure loses its stability and the critical buckling load can be predicted at the point of intersection of the natural frequencies curve with the abscissa $\left(F_{cr} \cong 27.8\,\mathrm{kN}\right)$. According to Figure 3.15, the three curves converge almost to the same value of the critical buckling load.

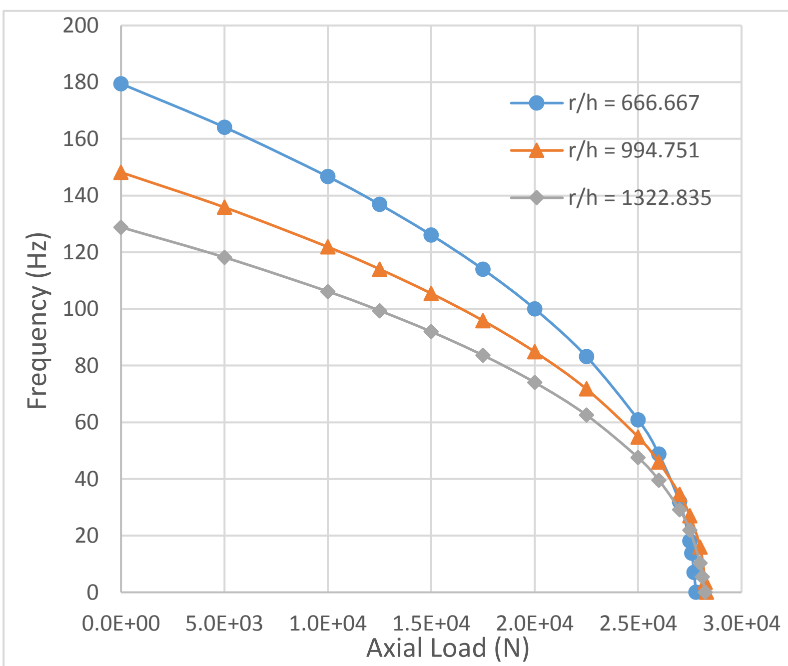

Figure 3.14: Fluctuation of frequencies of a clamped-clamped cylindrical shell as a function of axial load for various radius-thickness ratios

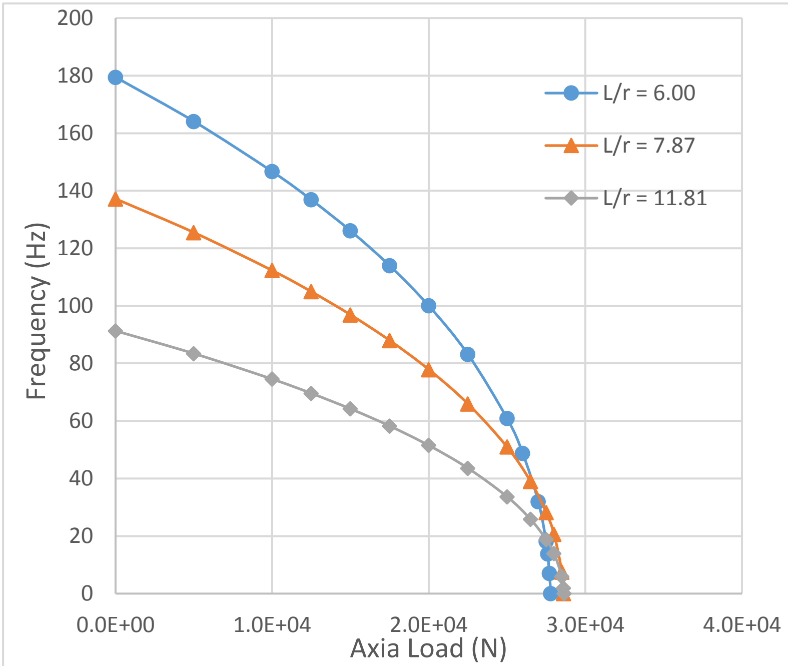

Figure 3.15: Fluctuation of frequencies of a clamped-clamped cylindrical shell as a function of axial load for various length-radius ratios

3.7.1.5. Effect of boundary conditions

The effect of boundary conditions on the dynamic behaviour of the cylindrical shell, with the same geometric properties cited above, is studied in the Figs.3.16 and 3.17 by varying separately the external radial pressure and the axial compression load.

It is observed from the two curves that the clamped-free cylindrical shells are more vulnerable to instability than those clamped-clamped and simply supported at both opposite sides. In Figure 3.17, the critical buckling load for the structures clamped at both opposite sides is more than 1.5 times larger than simply supported at both opposite sides.

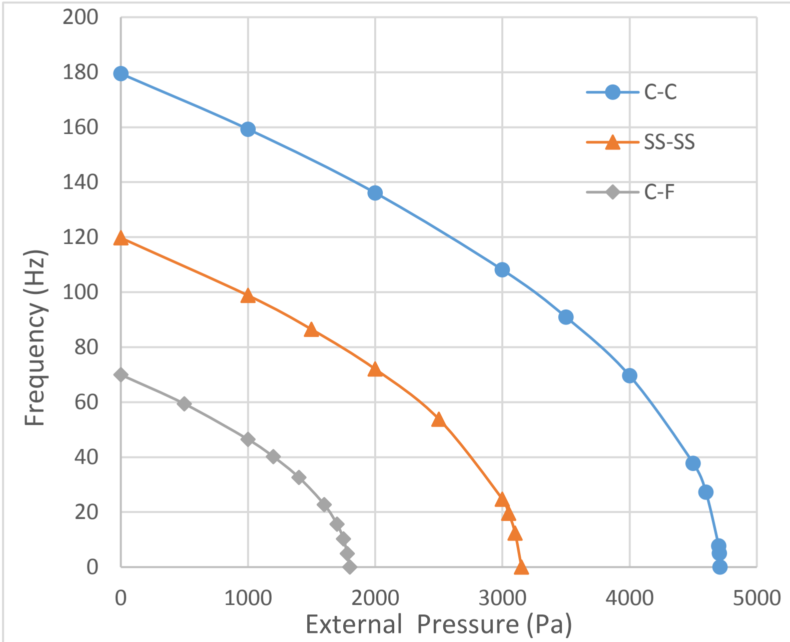

Figure 3.16: Fluctuation of frequencies of a cylindrical shell as a function of external pressure for different boundary conditions $\left(L = 0.6096\text{ m},\ h = 1.52\times10^{-4}\text{ m},\ r/h = 666.67\right)$

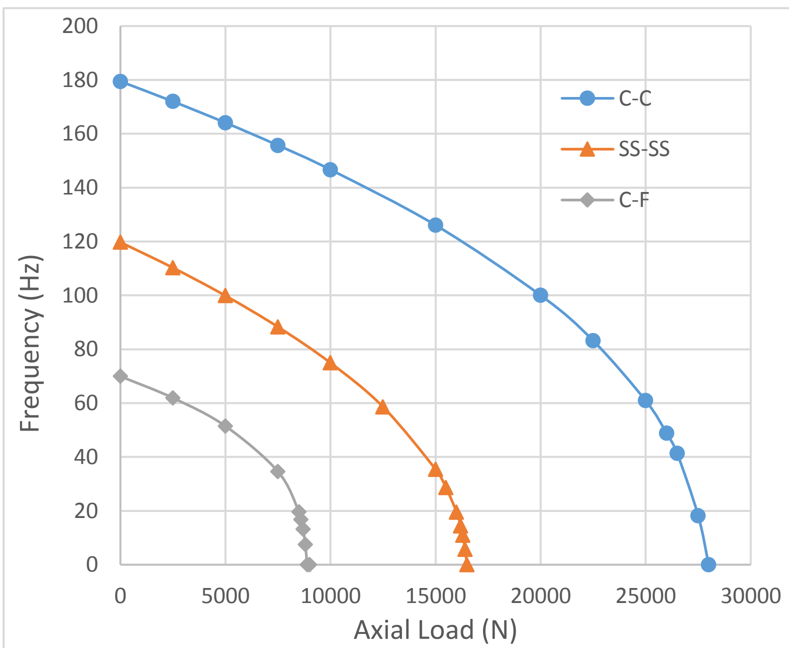

Figure 3.17: Fluctuation of frequencies of a cylindrical shell as a function of axial load for different boundary conditions $\left(L = 0.6096\text{ m},\ h = 1.52\times10^{-4}\text{ m},\ r/h = 666.67\right)$

3.7.2. Conical model

According to the mathematical development presented above, positive values correspond to external pressure and externally applied axial load.

3.7.2.1. Convergence Test

Focusing here on the conical model and in order to investigate how the geometry of the shell and the number of finite elements could affect the requisite mesh size, two semivertex angles of conical shells are considered $\left(\alpha = 15^\circ \text{ and } \alpha = 45^\circ\right)$. The percentage error of natural frequencies relative to the requisite mesh size elements is plotted in Fig.3.18 versus the number of conical finite elements. Only ten finite elements are sufficient to keep the relative error less than 0.6% for both $\alpha = 15^\circ$ and $\alpha = 45^\circ$. On this same figure, a gap can be seen in the relative error between the two semivertex angles for this small number of finite elements. The relative error is more significant for a large semivertex angle. This gap fades as the number of finite elements increases. Twenty finite elements allow us to reach mesh independency. In the following calculations, a larger mesh size is considered.

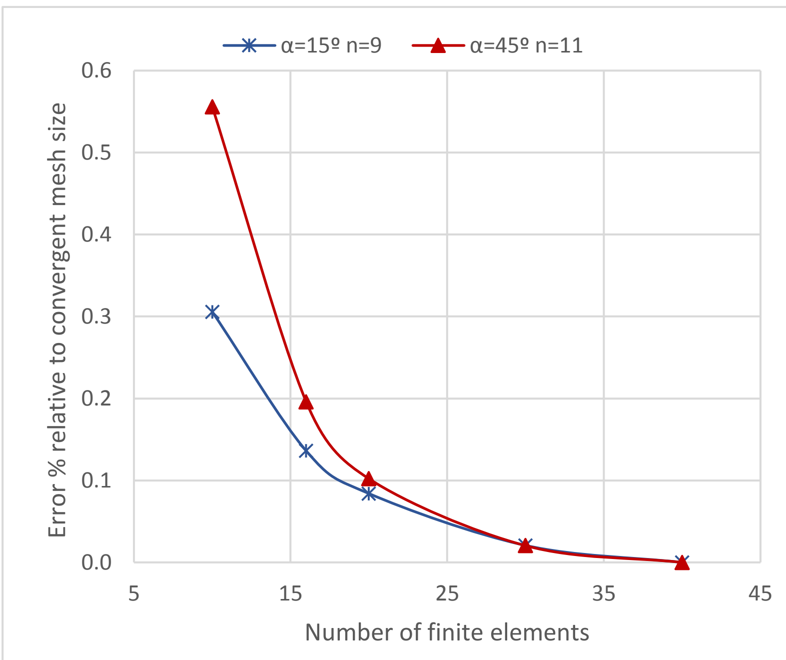

Figure 3.18: Variation of the percentage error of fundamental frequencies of a conical shell relatively to the requisite mesh size $(100\times\left(\omega_{\text{N F.E.}} - \omega_{\text{45 F.E.}}\right)/\omega_{\text{N F.E.}})$ $\left(E = 69 \text{ GPa},\ \nu = 0.32,\ \rho = 2750 \text{ kg}/\text{m}^3,\ h = 0.5\text{mm},\ l = 0.5 \text{ m}\right)$

3.7.2.2. Radial pressure

A truncated conical shell made of 2024 aluminum, simply supported on both sides and subjected to uniform external radial pressure, was analyzed. The obtained results are presented in Fig.3.19 along with experimental data measured by Weingarten [45] and his theoretical outcomes. The physical properties of the truncated conical shell are: semi-vertex angle $\alpha = 20°$, small radius $R_1 = 5.45\,\text{cm}$, Slant length of the shell $L = 21.62$ cm and thickness $h = 0.508$ mm. The dimensionless internal pressure applied is given by $P_m/P_{cr} = 0.446$. The critical pressure P_{cr} is defined in Ref. [72] by the following expression:

$$P_{cr} = \frac{0.87(h \times cos\alpha\ /D_2)^{2.5}}{L \times cos\alpha\ / D_2} \times \frac{2E}{\left(1 + D_1 / D_2\right)} \tag{74}$$

where D_1 and D_2 are the base diameters, respectively, at small and large ends of the cone. Even though a small number of finite elements was used, very good agreement was found between our results and those quoted in the experimental measurements of Weingarten [45] for all of the considered circumferential modes. Compared to the numerical model performed by Lam and Hua [50] using the generalized differential quadratic method, the deviation is considerable for low circumferential modes while the concordance is better for higher modes. As stated in Ref. [50], the theoretical approach used in Refs. [45] and [73] assumes that the meridional and circumferential displacements *u* and *v* are a function of the normal displacement *w*, which considerably simplifies the governing equations of motion. This explains the discrepancy between this approach and the other methods.

Figure 3.19 also shows that the minimum frequency is found at the same circumferential mode $(n = 6)$ except for Lam and Hua’s curve, which is slightly offset.

The case of external and internal pressure is validated by comparing our results to those of Ueda et al. [48] (see Fig.3.20). A truncated conical shell, clamped on both sides is made of super-invar with Young’s modulus $E = 12.8$ GPa, Poisson’s ratio $\nu = 0.25$ and density $\rho_s = 813\ \text{kg}/\text{m}^3$. The ratio of slant length to small radius is 1.61. The semivertex angle $\alpha = 14°$ and the shell thickness $h = 0.05\,\text{mm}$. Figure 3.20 shows the variation of frequencies as a function of the circumferential modes for static pressures $P_m = -200$ kPa and 200 kPa. The concordance among the results is generally very good.

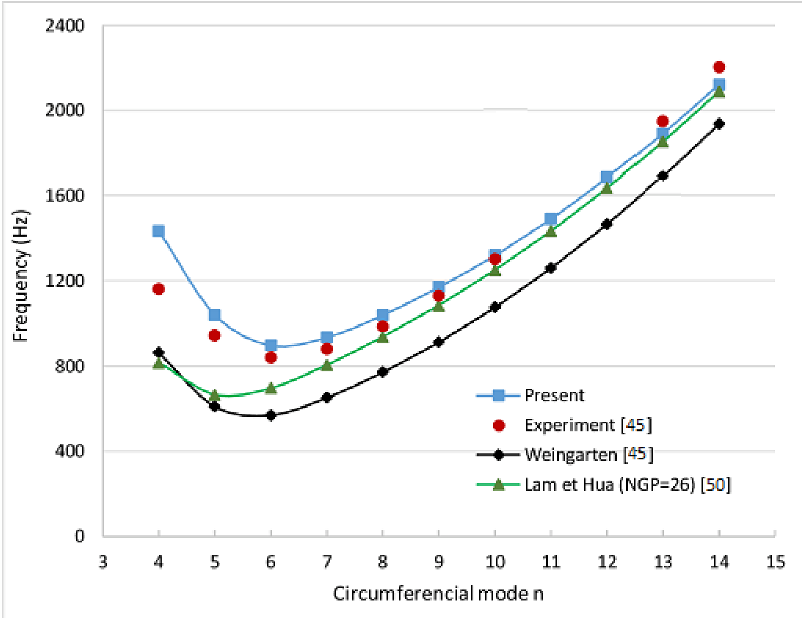

Figure 3.19: Frequencies corresponding to the axial mode $m=1$ of a conical shell simply supported at both opposite sides subjected to external pressure $P_m = 7488\,\mathrm{Pa}$ as a function of circumferential modes

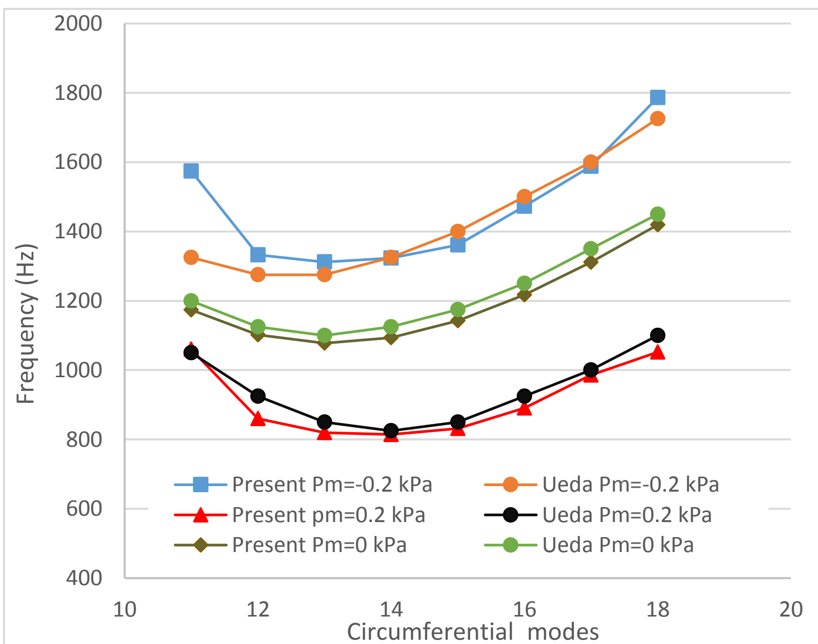

Figure 3.20: Frequencies corresponding to the axial mode $m=1$ of a clamped-clamped conical shell as a function of circumferential modes for various radial static pressures

3.7.2.3. Axial load

The last set of validation concerns the vibration of axially loaded conical shells. The considered shell is clamped-clamped with Young's modulus $E = 210$ GPa, Poisson's ratio $\nu = 0.3$, and

$R_2/h = 100$, $(1 - R_1/R_2) = 0.25$ and the semi vertex angle $\alpha = 30°$. Calculations are performed for many circumferential wave numbers n using load and frequency parameters ρ_p and ω_p, respectively, defined by [49]:

$$\rho_p = P/P_{cl} \text{ and } \omega_P = \omega R_2 \sqrt{\frac{(1-\nu^2)\rho}{E}} \tag{75}$$

where P is the axial applied load and P_{cl} is the critical buckling load for simply supported, moderately long isotropic conical shells [74], expressed by:

$$P_{cl} = \frac{2\pi E h^2 cos^2\alpha}{\sqrt{3(1-\nu^2)}} \tag{76}$$

Figure 3.21 shows that an increase of axial load induces a linear augmentation of the frequency. However, the same figure exhibits a nonlinear frequency decrease versus an increase in compressive axial load, particularly when the parameter ρ_p is in the range of -0.5 to -1. The results are in very good agreement with those of Ref. [49].

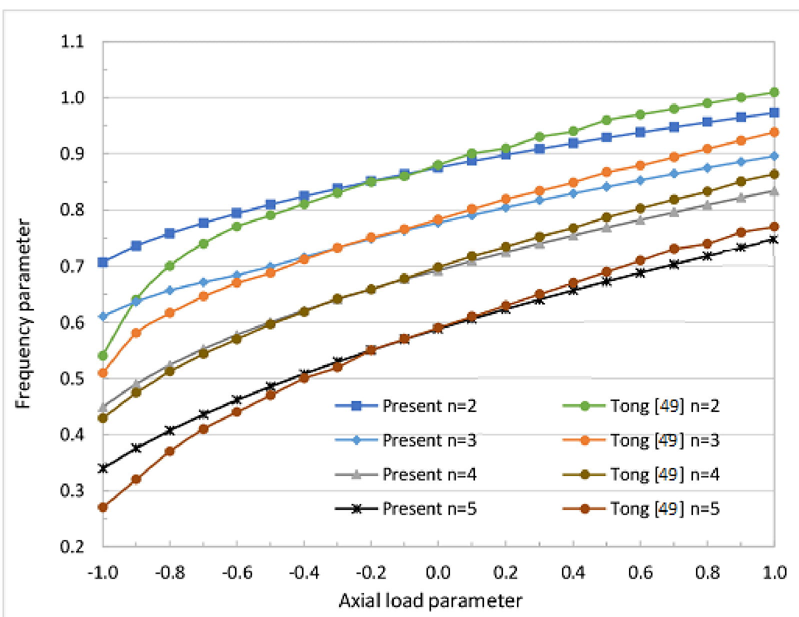

Figure 3.21: Variation of the frequency parameter of a clamped-clamped conical shell $(m = 1)$ as a function of the ratio of the applied axial force by the critical buckling load P_{cl} for different values of circumferential wave number

3.7.2.4. Effect of geometric properties

Numerical computations were carried out to assess the effect of the semivertex angle variation on the dynamic behavior of a clamped-clamped isotropic conical shell with increasing applied axial load.

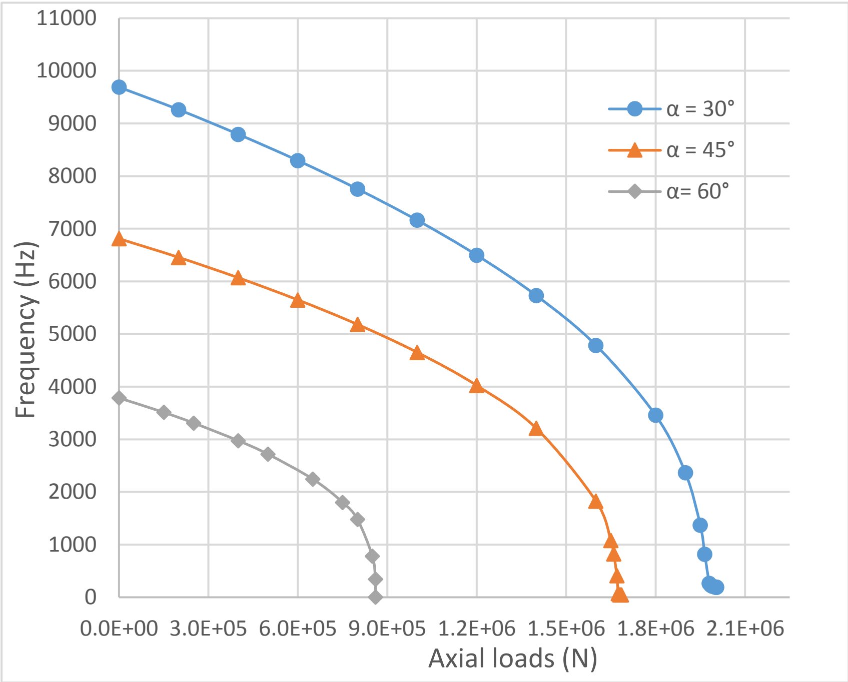

Figure 3.22: Variation of frequencies of a clamped-clamped truncated conical shell as a function of compression axial load for various semivertex angle

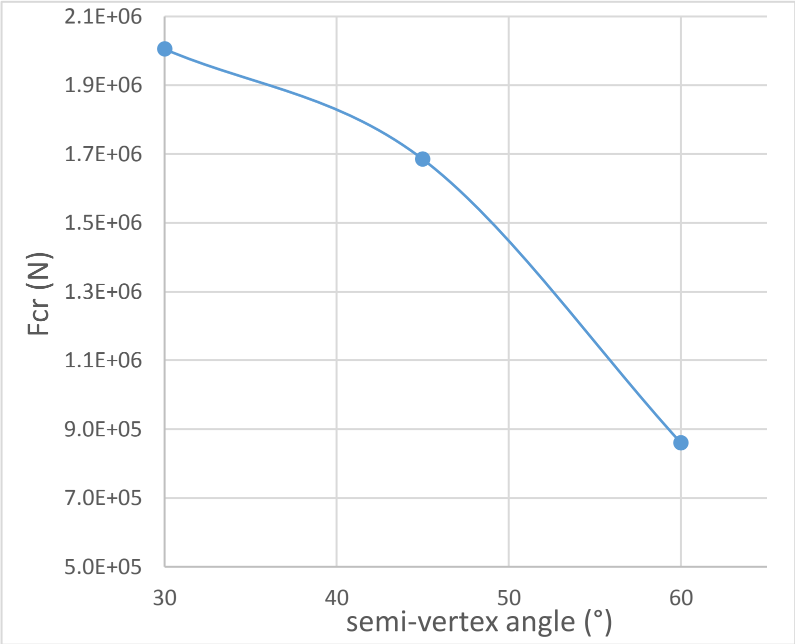

Figure 3.23: Variation of the critical buckling load of a clamped-clamped truncated conical shell as a function of the semivertex angle

The mechanical properties of the shell are the same as those provided in Sec. 3.7.2.3. Figure 3.22 depicts a decrease of the frequencies as axial compression load and semivertex angle increase. The critical loads corresponding to various semivertex angles are investigated here. Once these critical points are reached, the structure loses its bearing capacity and a significant drop of its total rigidity can be noticed. Since conical shell structures are known to be more resistant to membrane stresses, their critical loads are relatively higher than those of cylindrical shells. By examining Fig.3.23, it can be observed that the slope of the tangent to the curve becomes more pronounced by exceeding the semivertex angle $\alpha = 45°$. We can therefore conclude that, as the semivertex angle of a conical shell increases, the structure becomes more prone to instability.

3.7.2.5. Effect of boundary conditions

Figure 3.24 shows the effect of boundary conditions on the critical axial load of the conical shell studied above. Three cases are considered: clamped-clamped, simply supported-simply supported and clamped-free. It is obvious that frequency has an inverse proportionality to axial load for these three boundary conditions. Moreover, the critical load of the clamped-clamped shell is the largest compared to those of the other two boundary conditions. Its value is almost three times larger than that of the clamped-free shell.

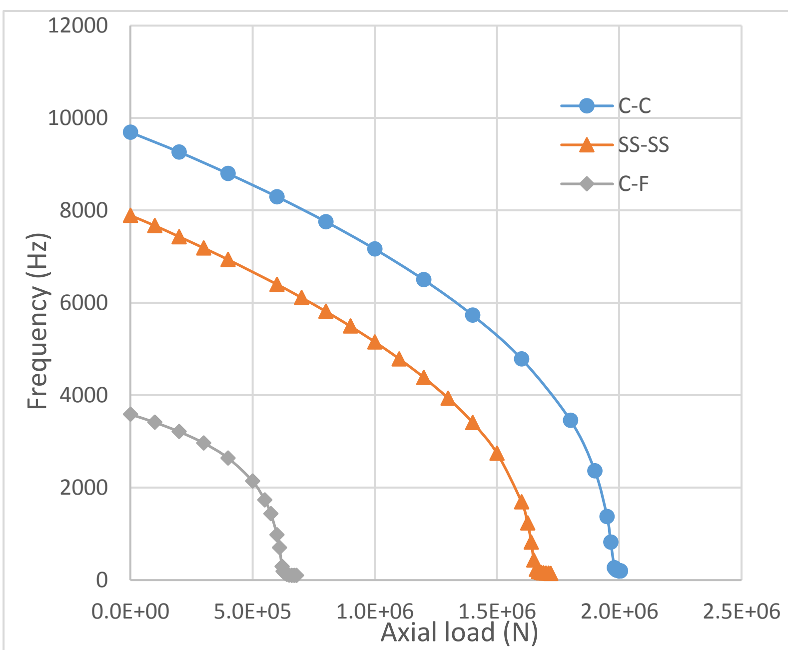

Figure 3.24: Fluctuation of frequencies of a truncated conical shell as a function of axial load for different boundary conditions

3.7.3. Combined conical-cylindrical model

The case of a combined shell is calculated in order to check results correctness when the two models are joined together. The structure shown in Fig.3.25 is a shell which is clamped on both opposite sides, made of aluminium with Young's modulus $E = 69$ GPa. The shell thickness $h = 0.5$ mm. The remaining geometrical properties of this structure are denoted in the same figure. The validity is established by comparing the natural frequencies calculated by our model for the combined structure cited above versus those found using a numerical study based on the ANSYS software within shell 281 finite element model.

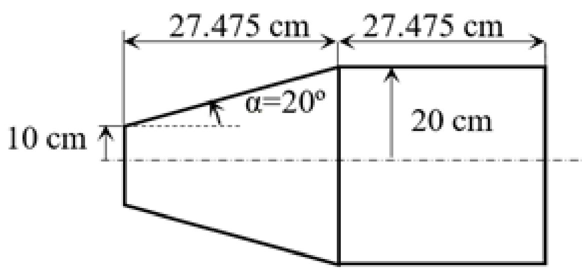

Figure 3.25: Geometrical characteristics of a combined shell [69]

Table 3.4: Comparison of natural frequencies of a combined conical-cylindrical shell under clamped-clamped boundary conditions

n	Present	Ansys	Relative error $(\%)$
3	841.33	838.91	-0.29
4	645.52	642.54	-0.46
5	510.02	512.94	0.57
6	430.19	431.73	0.36
7	403.75	404.4	0.16
8	419.44	420.22	0.19
9	418.44	420.04	0.38
10	422.63	424.6	0.46
11	450.71	453.41	0.60
12	497.92	502.04	0.82
13	559.81	566.12	1.12
14	633.18	615.17	-2.93
15	716.01	729.38	1.83
16	807.04	813.68	0.82

Excellent agreement between our results and those generated from the finite element program ANSYS has been achieved for not only the lower order natural frequencies but also the higher order frequencies. (See Table 3.4).

A series of radial pressures and axial loads were applied then on the studied structure in order to detect the initial stiffening effect on the dynamic behavior of the combined shell. By analyzing the frequency curves of Fig.3.26, we observe two minimum values. One corresponds to the cylindrical frustum and the other to the conical part of the combined structure. External pressure decreases the frequencies, whereas internal pressure reinforces the dynamic behavior of the structure.

The case of axial loads applied at opposite sides of the combined shell shown in Fig.3.25 was investigated by considering the effects of tension and compression loads. The obtained results are shown in Fig.3.27. By examining the last figure, we find that for low values of circumferential modes *n*, the frequency difference is narrower than in the case of high order circumferential modes.

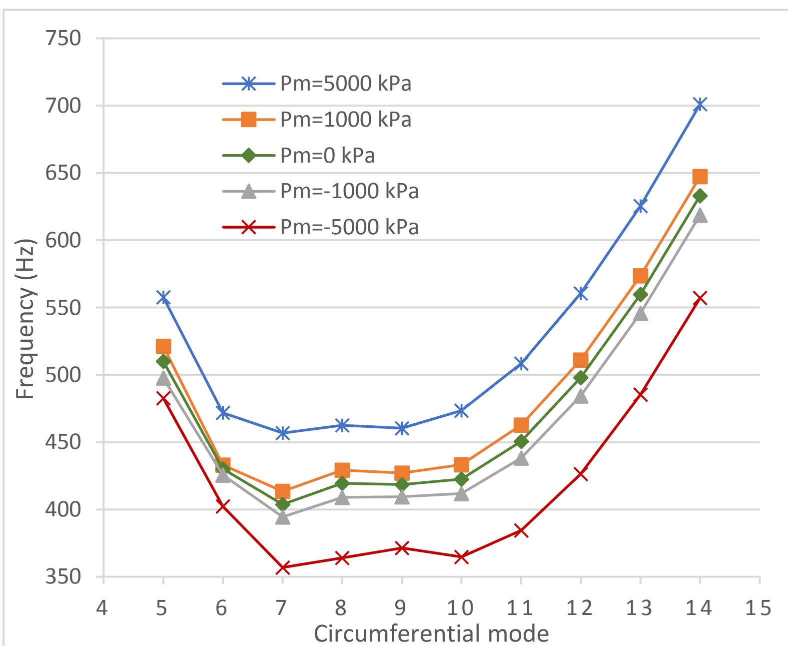

Figure 3.26: Frequencies of a clamped at both opposite sides combined conical-cylindrical shell subjected to radial pressures

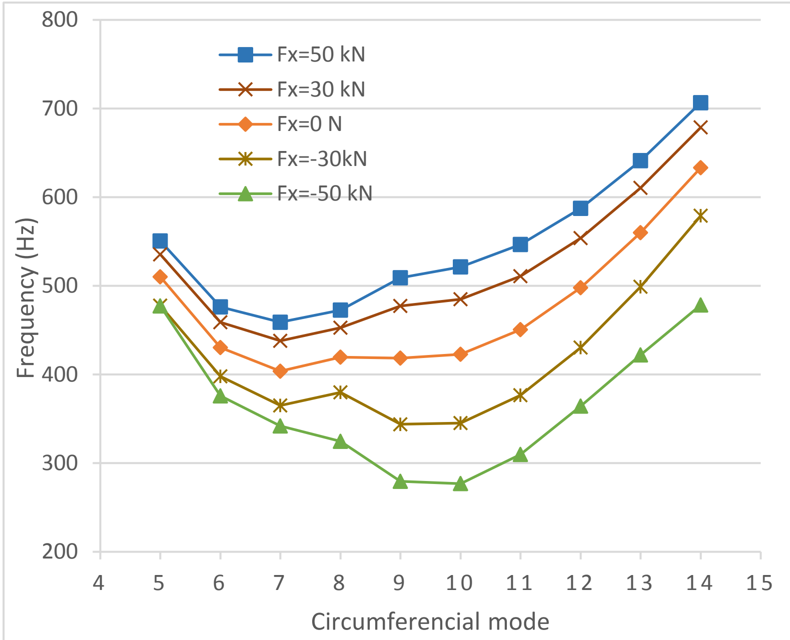

Figure 3.27: Frequencies of a clamped-clamped combined conical-cylindrical shell subjected to axial loads

We can conclude that the initial stiffening effect is remarkable for large values of the number of circumferential waves. However, it is minimal when the structure membrane behaviour governs. The theory developed in this document does not support post-buckling study. It is mainly based on the hypothesis of small displacements within a framework of linear elasticity. Exceeding a certain compression membrane force (critical load) and for low frequency values tending towards their nullity, the structure loses its bearing capacity and a large flexural deformation is therefore needed to absorb the released membrane strain energy.

3.8. Conclusions

This paper presents a numerical approach based on a hybrid finite element method to predict the dynamic behaviour of axisymmetric shells under the initial stiffening effect induced by membrane loads. The axisymmetric shell is a class of structure, which is of great interest and is found in a variety of sectors of engineering and industry. Two axisymmetric conical and cylindrical finite elements are used to perfectly match the geometry of the studied axisymmetric shells. The displacement functions of each finite element are derived from exact solution of Sanders' shell equilibrium equations. Due to its high accuracy, this approach motivated us to model combined conical-cylindrical shells subjected to initial stiffening stresses induced by radial pressure and/or axial loads.

We validated conical and cylindrical models separately under the effects of axial force and radial pressure to check the accuracy of our results. The obtained results were compared with those found in other theoretical and experimental works. Very good agreement was generally found. Several example calculations show that external pressure and compression axial load degrade the frequencies and can lead to instability of the structure.

The natural frequencies decrease as the radius and/or the length of the cylindrical shells increases. This frequency drop is accentuated when the cylindrical shell is subjected to an increasing external pressure and diminishes when it is exposed to an increasing axial load. The effect of augmentation of the external pressure is preponderant, especially for slender cylindrical structures and those with small radius. Numerical analyses also showed that the critical buckling load is independent of the variation of the radius and the length of a cylindrical shell. According to the abovementioned numerical results for conical shells, the critical buckling load has an inverse proportionality with the semivertex angle variation. Consequently, we can say that variation of the semivertex angle in thin conical shells represents a decisive criterion for judging the stability of these structures.

Another conclusion that can be inspired from our numerical study is, when the boundary conditions are more restrictive, the structure becomes less sensitive to instability.

Concerning the variation of frequencies as a function of circumferential wave number, the curves of the combined conical-cylindrical shell show two minimums instead of one due to a combination effect. The theory developed in this paper presents a powerful model that converges within a minimum number of finite elements with great accuracy. It may be used to solve complicated problems commonly encountered in the design of aerospace, aeronautical and submarine structures. The theory developed in this paper serves as a tool for other complex studies highlighting the hydrodynamic and aerodynamic effects on the dynamic behaviour of structures.

3.9. Appendix

3.9.1. Appendix A

This Appendix contains some matrices and relations cited in the text of this paper.

Equilibrium equations for thin anisotropic cylindrical shell

$$L_1\left(U,V,W,P_{ij}\right)=P_{11}\frac{\partial^2 U}{\partial x^2}+\frac{P_{12}}{r}\frac{\partial^2 U}{\partial x^2}\left(\frac{\partial^2 V}{\partial x\partial\theta}+\frac{\partial W}{\partial x}\right)-P_{14}\frac{\partial^3 W}{\partial x^3}+\frac{P_{15}}{r^2}\left(\frac{\partial^3 W}{\partial x\partial\theta^2}+\frac{\partial^2 V}{\partial x\partial\theta}\right)$$
$$+\left(\frac{P_{33}}{r}-\frac{P_{63}}{2r^2}\right)\left(\frac{\partial^2 V}{\partial x\partial\theta}+\frac{1}{r}\frac{\partial^2 U}{\partial\theta^2}\right)+\left(\frac{P_{36}}{r^2}-\frac{P_{66}}{2r^3}\right)\left(-2\frac{\partial^3 W}{\partial x\partial\theta^2}+\frac{3}{2}\frac{\partial^2 V}{\partial x\partial\theta}-\frac{1}{2r}\frac{\partial^2 U}{\partial\theta^2}\right) \qquad (A.1)$$

$$L_2\left(U,V,W,P_{ij}\right)=\left(\frac{P_{21}}{r}-\frac{P_{51}}{r^2}\right)\frac{\partial^2 U}{\partial x\partial\theta}+\frac{1}{r}\left(\frac{P_{22}}{r}+\frac{P_{52}}{r^2}\right)\left(\frac{\partial^2 V}{\partial\theta^2}+\frac{\partial W}{\partial\theta}\right)-\left(\frac{P_{24}}{r}+\frac{P_{54}}{r^2}\right)\frac{\partial^3 W}{\partial x^2\partial\theta}$$
$$+\frac{1}{r^2}\left(\frac{P_{25}}{r}+\frac{P_{55}}{r^2}\right)\left(-\frac{\partial^3 W}{\partial\theta^3}+\frac{\partial^2 V}{\partial\theta^2}\right)+\left(P_{33}+\frac{3P_{63}}{2r}\right)\left(\frac{\partial^2 V}{\partial x^2}+\frac{\partial^2 U}{r\partial x\partial\theta}\right)$$
$$+\frac{1}{r}\left(P_{36}+\frac{3P_{66}}{2r}\right)\left(-2\frac{\partial^3 W}{\partial x^2\partial\theta}+\frac{3}{2}\frac{\partial^2 V}{\partial x^2}-\frac{1}{2r}\frac{\partial^2 U}{\partial x\partial\theta}\right) \qquad (A.2)$$

$$L_3\left(U,V,W,P_{ij}\right)=P_{41}\frac{\partial^3 U}{\partial x^3}+\frac{P_{42}}{r}\left(\frac{\partial^3 V}{\partial x^2\partial\theta}+\frac{\partial^2 W}{\partial x^2}\right)-P_{44}\frac{\partial^4 W}{\partial x^4}+\frac{P_{45}}{r^2}\left(-\frac{\partial^4 W}{\partial x^2\partial\theta^2}+\frac{\partial^3 V}{\partial x^2\partial\theta}\right)$$
$$+\frac{2P_{63}}{r}\left(\frac{1}{r}\frac{\partial^3 U}{\partial x\partial\theta^2}+\frac{\partial^3 V}{\partial x^2\partial\theta}\right)+\frac{2P_{66}}{r^2}\left(-2\frac{\partial^4 W}{\partial x^2\partial\theta^2}+\frac{3}{2}\frac{\partial^3 V}{\partial x^2\partial\theta}-\frac{1}{2r}\frac{\partial^3 U}{\partial x\partial\theta^2}\right)+\frac{P_{51}}{r^2}\frac{\partial^3 U}{\partial x\partial\theta^2}+\frac{P_{52}}{r^3}\left(\frac{\partial^3 V}{\partial\theta^3}+\frac{\partial^2 W}{\partial\theta^2}\right)$$
$$+\frac{P_{55}}{r^4}\left(-\frac{\partial^4 W}{\partial\theta^4}+\frac{\partial^3 V}{\partial\theta^3}\right)-\frac{P_{21}}{r}\frac{\partial U}{\partial x}-\frac{P_{54}}{r^2}\frac{\partial^4 W}{\partial x^2\partial\theta^2}+\frac{P_{22}}{r^2}\left(\frac{\partial V}{\partial\theta}+W\right)+\frac{P_{24}}{r^2}\frac{\partial^2 W}{\partial\theta^2}-\frac{P_{25}}{r^3}\left(-\frac{\partial^2 W}{\partial\theta^2}+\frac{\partial V}{\partial\theta}\right) \quad (A.3)$$

Matrix $\left[P\right]$

The elasticity matrix $\left[P\right]$ of order $\left(6\times 6\right)$ for an anisotropic material is expressed as

$$\left[P\right]=\begin{bmatrix} P_{11} & P_{12} & 0 & P_{14} & P_{15} & 0 \\ P_{21} & P_{22} & 0 & P_{24} & P_{25} & 0 \\ 0 & 0 & P_{33} & 0 & 0 & P_{36} \\ P_{41} & P_{42} & 0 & P_{44} & P_{45} & 0 \\ P_{51} & P_{52} & 0 & P_{54} & P_{55} & 0 \\ 0 & 0 & P_{63} & 0 & 0 & P_{66} \end{bmatrix} \qquad (A.4)$$

In the case of isotropic material, the matrix of elasticity becomes

$$[P]=\begin{bmatrix} D & \nu D & 0 & 0 & 0 & 0 \\ \nu D & D & 0 & 0 & 0 & 0 \\ 0 & 0 & D(1-\nu)/2 & 0 & 0 & 0 \\ 0 & 0 & 0 & K & \nu K & 0 \\ 0 & 0 & 0 & \nu K & K & 0 \\ 0 & 0 & 0 & 0 & 0 & K(1-\nu)/2 \end{bmatrix} \qquad (A.5)$$

where $K=\dfrac{Eh^3}{12\left(1-\nu^2\right)}$ and $D=\dfrac{Eh}{1-\nu^2}$

E is Young's modulus, ν is Poisson's ratio and h is the shell thickness.
After integrating each component of the stress vector over the thickness of the shell, the normal stress resultant and moment resultant for an isotropic cylindrical shell can be written as

$$\{\sigma\}=\begin{Bmatrix} N_x \\ N_\theta \\ N_{x\theta} \\ M_x \\ M_\theta \\ M_{x\theta} \end{Bmatrix}=[P]\begin{Bmatrix} \varepsilon_x \\ \varepsilon_\theta \\ 2\varepsilon_{x\theta} \\ k_x \\ k_\theta \\ 2k_{x\theta} \end{Bmatrix} \qquad (A.6)$$

Matrix $[T]$

$$[T]=\begin{bmatrix} \cos n\theta & 0 & 0 \\ 0 & \cos n\theta & 0 \\ 0 & 0 & \sin n\theta \end{bmatrix} \qquad (A.7)$$

Coefficients of the characteristic equation for an isotropic material

$$a=1,\;\; b=-4n^2,\;\; c=\left[\frac{1-\nu^2}{\kappa}+6n^2\left(n^2-1\right)\right],\;\; d=-4n^2\left(n^2-1\right)^2,\;\; e=n^4\left(n^2-1\right)^2 \qquad (A.8)$$

Where $\kappa=\left(\dfrac{1}{12}\right)\left(\dfrac{h}{r}\right)^2$

Matrix $[R]$

$$\begin{bmatrix} \alpha_1 e^{(\lambda_1 x/r)} & \alpha_2 e^{(\lambda_2 x/r)} & \alpha_3 e^{(\lambda_3 x/r)} & \alpha_4 e^{(\lambda_4 x/r)} & \alpha_5 e^{(\lambda_5 x/r)} & \alpha_6 e^{(\lambda_6 x/r)} & \alpha_7 e^{(\lambda_7 x/r)} & \alpha_8 e^{(\lambda_8 x/r)} \\ e^{(\lambda_1 x/r)} & e^{(\lambda_2 x/r)} & e^{(\lambda_3 x/r)} & e^{(\lambda_4 x/r)} & e^{(\lambda_5 x/r)} & e^{(\lambda_6 x/r)} & e^{(\lambda_7 x/r)} & e^{(\lambda_8 x/r)} \\ \beta_1 e^{(\lambda_1 x/r)} & \beta_2 e^{(\lambda_2 x/r)} & \beta_3 e^{(\lambda_3 x/r)} & \beta_4 e^{(\lambda_4 x/r)} & \beta_5 e^{(\lambda_5 x/r)} & \beta_6 e^{(\lambda_6 x/r)} & \beta_7 e^{(\lambda_7 x/r)} & \beta_8 e^{(\lambda_8 x/r)} \end{bmatrix} \qquad (A.9)$$

Vector $\{C\}$

$$\{C\}=\{C_1\ C_2\ C_3\ C_4\ C_5\ C_6\ C_7\ C_8\}^T \tag{A.10}$$

3.9.2. Appendix B

Equilibrium equations of a multilayer anisotropic truncated conical shell with variable thickness

$$\begin{aligned}
S_1\left(\bar{U},\bar{V},\bar{W},\bar{B}_{ij}\right) &= \bar{B}_{11}\left[2x\sin\alpha\frac{\partial\bar{U}}{\partial x}+x^2\sin\alpha\frac{\partial^2\bar{U}}{\partial x^2}\right]+\bar{B}_{12}\left[x\frac{\partial^2\bar{V}}{\partial x\partial\theta}+x\cos\alpha\frac{\partial\bar{W}}{\partial x}+\bar{U}\sin\alpha+\bar{W}\cos\alpha\right]\\
&-\bar{B}_{14}\left[3x^2\sin\alpha\frac{\partial^2\bar{W}}{\partial x^2}+x^3\sin\alpha\frac{\partial^3\bar{W}}{\partial x^3}\right]\\
&+\bar{B}_{15}\left[x\cot\alpha\frac{\partial^2\bar{V}}{\partial x\partial\theta}-\frac{x}{\sin\alpha}\frac{\partial^3\bar{W}}{\partial\theta^2\partial x}-2x\sin\alpha\frac{\partial\bar{W}}{\partial x}-x^2\sin\alpha\frac{\partial^2\bar{W}}{\partial x^2}+\cot\alpha\frac{\partial\bar{V}}{\partial\theta}-\frac{1}{\sin\alpha}\frac{\partial^2\bar{W}}{\partial\theta^2}\right]\\
&-\bar{B}_{22}\left[\frac{\partial\bar{V}}{\partial\theta}+\sin\alpha\,\bar{U}+\cos\alpha\,\bar{W}\right]+\bar{B}_{24}\left[x^2\sin\alpha\frac{\partial^2\bar{W}}{\partial x^2}\right]+\bar{B}_{25}\left[-\cot\alpha\frac{\partial\bar{V}}{\partial\theta}+\frac{1}{\sin\alpha}\frac{\partial^2\bar{W}}{\partial\theta^2}+x\sin\alpha\frac{\partial\bar{W}}{\partial x}\right]\\
&+\bar{B}_{33}\left[x\frac{\partial^2\bar{V}}{\partial x\partial\theta}+\frac{1}{\sin\alpha}\frac{\partial^2\bar{U}}{\partial\theta^2}-\frac{\partial\bar{V}}{\partial\theta}\right]+\bar{B}_{36}\left[-\frac{2x}{\sin\alpha}\frac{\partial^3\bar{W}}{\partial\theta^2\partial x}+x\cot\alpha\frac{\partial^2\bar{V}}{\partial x\partial\theta}-\frac{\cot\alpha}{\sin\alpha}\frac{\partial^2\bar{U}}{\partial\theta^2}+\frac{2}{\sin\alpha}\frac{\partial^2\bar{W}}{\partial\theta^2}-\cot\alpha\frac{\partial\bar{V}}{\partial\theta}\right]\\
&+\bar{B}_{66}\left[\frac{x\cot\alpha}{\sin\alpha}\frac{\partial^3\bar{W}}{\partial\theta^2\partial x}-\frac{3x}{4}\cot^2\alpha\frac{\partial^2\bar{V}}{\partial x\partial\theta}+\frac{\cot^2\alpha}{4\sin\alpha}\frac{\partial^2\bar{U}}{\partial\theta^2}-\frac{\cot\alpha}{\sin\alpha}\frac{\partial^2\bar{W}}{\partial\theta^2}+\frac{3\cot^2\alpha}{4}\frac{\partial\bar{V}}{\partial\theta}\right]
\end{aligned}\tag{B.1}$$

$$\begin{aligned}
S_2\left(\bar{U},\bar{V},\bar{W},\bar{B}_{ij}\right) &= \bar{B}_{12}x\frac{\partial^2\bar{U}}{\partial x\partial\theta}+\bar{B}_{15}x\cot\alpha\frac{\partial^2\bar{U}}{\partial x\partial\theta}+\bar{B}_{22}\left[\frac{1}{\sin\alpha}\frac{\partial^2\bar{V}}{\partial\theta^2}+\frac{\partial\bar{U}}{\partial\theta}+\cot\alpha\frac{\partial\bar{W}}{\partial\theta}\right]-\bar{B}_{24}x^2\frac{\partial^3\bar{W}}{\partial x^2\partial\theta}\\
&+\bar{B}_{25}\left[\frac{2\cot\alpha}{\sin\alpha}\frac{\partial^2\bar{V}}{\partial\theta^2}-\frac{1}{\sin^2\alpha}\frac{\partial^3\bar{W}}{\partial\theta^3}-x\frac{\partial^2\bar{W}}{\partial x\partial\theta}+\cot^2\alpha\frac{\partial\bar{W}}{\partial\theta}+\cot\alpha\frac{\partial\bar{U}}{\partial\theta}\right]\\
&+\bar{B}_{33}\left[x^2\sin\alpha\frac{\partial^2\bar{V}}{\partial x^2}+x\frac{\partial^2\bar{U}}{\partial x\partial\theta}+2x\sin\alpha\frac{\partial\bar{V}}{\partial x}+2\frac{\partial\bar{U}}{\partial\theta}-2\sin\alpha\bar{V}\right]\\
&+\bar{B}_{36}\left[-2x^2\frac{\partial^3\bar{W}}{\partial x^2\partial\theta}+3x^2\cos\alpha\frac{\partial^2\bar{V}}{\partial x^2}+x\cot\alpha\frac{\partial^2\bar{U}}{\partial x\partial\theta}-4x\frac{\partial^2\bar{W}}{\partial x\partial\theta}+6x\cos\alpha\frac{\partial\bar{V}}{\partial x}+2\cot\alpha\frac{\partial\bar{U}}{\partial\theta}+4\frac{\partial\bar{W}}{\partial\theta}-6\cos\alpha\bar{V}\right]\\
&-\bar{B}_{45}x^2\cot\alpha\frac{\partial^3\bar{W}}{\partial x^2\partial\theta}+\bar{B}_{55}\left[\frac{\cot^2\alpha}{\sin\alpha}\frac{\partial^2\bar{V}}{\partial\theta^2}-\frac{\cot\alpha}{\sin^2\alpha}\frac{\partial^3\bar{W}}{\partial\theta^3}-x\cot\alpha\frac{\partial^2\bar{W}}{\partial x\partial\theta}\right]\\
&+\bar{B}_{66}\left[-6x\cot\alpha\frac{\partial^2\bar{W}}{\partial x\partial\theta}-3x^2\cot\alpha\frac{\partial^3\bar{W}}{\partial x^2\partial\theta}+\frac{9x}{2}\cos\alpha\cot\alpha\frac{\partial\bar{V}}{\partial x}+\frac{9x^2}{4}\cos\alpha\cot\alpha\frac{\partial^2\bar{V}}{\partial x^2}-\frac{3}{2}\cot^2\alpha\frac{\partial\bar{U}}{\partial\theta}\right.\\
&\left.-\frac{3x}{4}\cot^2\alpha\frac{\partial^2\bar{U}}{\partial x\partial\theta}+6\cot\alpha\frac{\partial\bar{W}}{\partial\theta}-\frac{9}{2}\cos\alpha\cot\alpha\bar{V}\right]
\end{aligned}\tag{B.2}$$

$$S_3\left(\bar U,\bar V,\bar W,\bar B_{ij}\right)=-\bar B_{12}x\cos\alpha\frac{\partial\bar U}{\partial x}+\bar B_{14}\left[6x\sin\alpha\frac{\partial\bar U}{\partial x}+6x^2\sin\alpha\frac{\partial^2\bar U}{\partial x^2}+x^3\sin\alpha\frac{\partial^3\bar U}{\partial x^3}\right]$$
$$+\bar B_{15}\left[\frac{x}{\sin\alpha}\frac{\partial^3\bar U}{\partial\theta^2\partial x}-2x\sin\alpha\frac{\partial\bar U}{\partial x}-x^2\sin\alpha\frac{\partial^2\bar U}{\partial x^2}\right]-\bar B_{22}\left[\cot\alpha\frac{\partial\bar V}{\partial\theta}+\cos\alpha\bar U+\cos\alpha\cot\alpha\bar W\right]$$
$$+\bar B_{24}\left[4x\frac{\partial^2\bar V}{\partial x\partial\theta}+x^2\frac{\partial^3\bar V}{\partial x^2\partial\theta}+4x\sin\alpha\frac{\partial\bar U}{\partial x}+x^2\sin\alpha\frac{\partial^2\bar U}{\partial x^2}+4x\cos\alpha\frac{\partial\bar W}{\partial x}+2x^2\cos\alpha\frac{\partial^2\bar W}{\partial x^2}\right.$$
$$\left.+2\frac{\partial\bar V}{\partial\theta}+2\sin\alpha\bar U+2\cos\alpha\bar W\right]+\bar B_{25}\left[-\cot^2\alpha\frac{\partial\bar V}{\partial\theta}+\frac{1}{\sin^2\alpha}\frac{\partial^3\bar V}{\partial\theta^3}+\frac{1}{\sin\alpha}\frac{\partial^2\bar U}{\partial\theta^2}+2\frac{\cot\alpha}{\sin\alpha}\frac{\partial^2\bar W}{\partial\theta^2}\right.$$
$$\left.-\frac{\partial\bar V}{\partial\theta}-x\frac{\partial^2\bar V}{\partial x\partial\theta}-\sin\alpha\bar U-x\sin\alpha\frac{\partial\bar U}{\partial x}-\cos\alpha\bar W\right]+\bar B_{36}\left[6x\frac{\partial^2\bar V}{\partial x\partial\theta}+2x^2\frac{\partial^3\bar V}{\partial x^2\partial\theta}+\frac{4}{\sin\alpha}\frac{\partial^2\bar U}{\partial\theta^2}\right.$$
$$\left.+\frac{2x}{\sin\alpha}\frac{\partial^3\bar U}{\partial\theta^2\partial x}-4\frac{\partial\bar V}{\partial\theta}-2x\frac{\partial^2\bar V}{\partial x\partial\theta}\right]-\bar B_{44}\left[12x^2\sin\alpha\frac{\partial^2\bar W}{\partial x^2}+8x^3\sin\alpha\frac{\partial^3\bar W}{\partial x^3}+x^4\sin\alpha\frac{\partial^4\bar W}{\partial x^4}\right]$$
$$+\bar B_{45}\left[4x\cot\alpha\frac{\partial^2\bar V}{\partial x\partial\theta}+x^2\cot\alpha\frac{\partial^3\bar V}{\partial x^2\partial\theta}-\frac{4x}{\sin\alpha}\frac{\partial^3\bar W}{\partial x\partial\theta^2}-\frac{2x^2}{\sin\alpha}\frac{\partial^4\bar W}{\partial\theta^2\partial x^2}-6x\sin\alpha\frac{\partial\bar W}{\partial x}\right.$$
$$\left.+2\cot\alpha\frac{\partial\bar V}{\partial\theta}-\frac{2}{\sin\alpha}\frac{\partial^2\bar W}{\partial\theta^2}-3x^2\sin\alpha\frac{\partial^2\bar W}{\partial x^2}\right]-\bar B_{55}\left[\cot\alpha\frac{\partial\bar V}{\partial\theta}+x\cot\alpha\frac{\partial^2\bar V}{\partial x\partial\theta}-\frac{1}{\sin\alpha}\frac{\partial^2\bar W}{\partial\theta^2}-2x\sin\alpha\frac{\partial\bar W}{\partial x}\right.$$
$$\left.-x^2\sin\alpha\frac{\partial^2\bar W}{\partial x^2}-\frac{\cot\alpha}{\sin^2\alpha}\frac{\partial^3\bar V}{\partial\theta^3}+\frac{1}{\sin^3\alpha}\frac{\partial^4\bar W}{\partial\theta^4}\right]+\bar B_{66}\left[-\frac{8x}{\sin\alpha}\frac{\partial^3\bar W}{\partial\theta^2\partial x}-\frac{4x^2}{\sin\alpha}\frac{\partial^4\bar W}{\partial\theta^2\partial x^2}+6x\cot\alpha\frac{\partial^2\bar V}{\partial x\partial\theta}\right.$$
$$\left.+3x^2\cot\alpha\frac{\partial^3\bar V}{\partial x^2\partial\theta}-\frac{2\cot\alpha}{\sin\alpha}\frac{\partial^2\bar U}{\partial\theta^2}-\frac{x\cot\alpha}{\sin\alpha}\frac{\partial^3\bar U}{\partial\theta^2\partial x}+\frac{8}{\sin\alpha}\frac{\partial^2\bar W}{\partial\theta^2}-6\cot\alpha\frac{\partial\bar V}{\partial\theta}\right] \qquad (B.3)$$

Matrix $\left[\bar P\right]$

The elasticity matrix $\left[\bar P\right]$ depends only upon the mechanical characteristics of the material of the shell. When dealing with anisotropic material, it will have the same shape as Eq. (A.4). For shells of variable thickness, $\left[\bar P\right]$ can be written as

$$\left[\bar P\right]=\begin{bmatrix} xB_{11} & xB_{12} & 0 & x^2B_{14} & x^2B_{15} & 0\\ xB_{21} & xB_{22} & 0 & x^2B_{24} & x^2B_{25} & 0\\ 0 & 0 & xB_{33} & 0 & 0 & x^2B_{36}\\ x^2B_{41} & x^2B_{42} & 0 & x^3B_{44} & x^3B_{45} & 0\\ x^2B_{51} & x^2B_{52} & 0 & x^3B_{54} & x^3B_{55} & 0\\ 0 & 0 & x^2B_{63} & 0 & 0 & x^3B_{66}\end{bmatrix} \qquad (B.4)$$

where x is the conical coordinate, (see Fig.3.3).

The expressions of B_{ij} are given below for a shell composed of number of symmetric isotropic or orthotropic layers:

(a) *For even number of layers 2n, we have*

$$B_{ij} = 2\sum_{s=1}^{n} Z_{ij}^{s}\left(\zeta_s - \zeta_{s+1}\right) \quad \text{for } i = 1..3 \text{ and } j = 1..3 \tag{B.5}$$

$$B_{ij} = \frac{2}{3}\sum_{s=1}^{n} Z_{i-3,j-3}^{s}\left(\zeta_s^3 - \zeta_{s+1}^3\right) \quad \text{for } i = 4..6 \text{ and } j = 4..6 \tag{B.6}$$

$$B_{ij} = 0 \text{ for } \left(i = 1..3 \text{ and } j = 4..6\right) \text{ or } \left(i = 4..6 \text{ and } j = 1..3\right) \tag{B.7}$$

(b) *For odd number of layers 2n+1, we have*

$$B_{ij} = 2Z_{ij}^{n+1}\zeta_{n+1} + 2\sum_{s=1}^{n} Z_{ij}^{s}\left(\zeta_s - \zeta_{s+1}\right) \quad \text{for } i = 1..3 \text{ and } j = 1..3 \tag{B.8}$$

$$B_{ij} = \frac{2}{3} Z_{i-3,j-3}^{n+1}\, \zeta_{n+1}^3 + \frac{2}{3}\sum_{s=1}^{n} Z_{i-3,j-3}^{s}\left(\zeta_s^3 - \zeta_{s+1}^3\right) \text{ for } i = 4..6 \text{ and } j = 4..6 \tag{B.9}$$

$$B_{ij} = 0 \text{ for } \left(i = 1..3 \text{ and } j = 4..6\right) \text{ or } \left(i = 4..6 \text{ and } j = 1..3\right) \tag{B.10}$$

With

$$Z_{11}^{s} = E_1^{s} / \left(1 - \nu_1^{s}\nu_2^{s}\right),\ Z_{22}^{s} = E_2^{s} / \left(1 - \nu_1^{s}\nu_2^{s}\right),\ Z_{12}^{s} = Z_{21}^{s} = E_1^{s}\nu_2^{s} / \left(1 - \nu_1^{s}\nu_2^{s}\right),\ Z_{33}^{s} = \frac{1}{2} G_{12}^{s}$$

$$Z_{11}^{s} = E_1^{s} / \left(1 - \nu_1^{s}\nu_2^{s}\right),\ Z_{22}^{s} = E_2^{s} / \left(1 - \nu_1^{s}\nu_2^{s}\right),\ Z_{12}^{s} = Z_{21}^{s} = E_1^{s}\nu_2^{s} / \left(1 - \nu_1^{s}\nu_2^{s}\right),\ Z_{33}^{s} = \frac{1}{2} G_{12}^{s}.$$

$\left(E_1^{s}, \nu_1^{s}\right)$ and $\left(E_2^{s}, \nu_2^{s}\right)$ are Young's modulus and Poisson's ratio with respect to axis $x\left(\theta\right)$; G_{12}^{s} is the shear modulus of elasticity, ζ_s is the coefficient of proportionality of thickness corresponding to the s^{th} layer.

In the case of an isotropic conical shell with a constant thickness, the elasticity matrix $\left[\bar{P}\right]$ will correspond to that found in Appendix (A.5).

Strain vector of conical shell

$$\{\bar{\varepsilon}\}=\begin{Bmatrix}\bar{\varepsilon}_x\\ \bar{\varepsilon}_\theta\\ 2\bar{\varepsilon}_{x\theta}\\ \bar{k}_x\\ \bar{k}_\theta\\ 2\bar{k}_{x\theta}\end{Bmatrix}=\begin{Bmatrix}\dfrac{\partial\bar{U}}{\partial x}\\ \dfrac{1}{x\sin\alpha}\dfrac{\partial\bar{V}}{\partial\theta}+\dfrac{\bar{U}}{x}+\dfrac{\bar{W}\cot\alpha}{x}\\ \dfrac{\partial\bar{V}}{\partial x}+\dfrac{1}{x\sin\alpha}\dfrac{\partial\bar{U}}{\partial\theta}-\dfrac{\bar{V}}{x}\\ -\dfrac{\partial^2\bar{W}}{\partial x^2}\\ \dfrac{\partial\bar{V}}{\partial\theta}\dfrac{\cos\alpha}{x^2\sin^2\alpha}-\dfrac{1}{x^2\sin^2\alpha}\dfrac{\partial^2\bar{W}}{\partial\theta^2}-\dfrac{\partial\bar{W}}{\partial x}\dfrac{1}{x}\\ -\dfrac{2}{x\sin\alpha}\dfrac{\partial^2\bar{W}}{\partial x\partial\theta}+\dfrac{3}{2}\dfrac{\cot\alpha}{x}\dfrac{\partial\bar{V}}{\partial x}-\dfrac{\partial\bar{U}}{\partial\theta}\dfrac{\cos\alpha}{2x^2\sin^2\alpha}+\dfrac{2}{x^2\sin\alpha}\dfrac{\partial\bar{W}}{\partial\theta}-\dfrac{3}{2}\dfrac{\cot\alpha}{x^2}\bar{V}\end{Bmatrix}\qquad(B.11)$$

where α is the semivertex angle of the cone, (see Fig.3.4).

Terms $\boldsymbol{Aux_p}$ *for the* k^{th} *element are given as follows (i=1,..,8 and j=1,..,8)*

$$\boldsymbol{Aux}_1=\left[-\frac{P_m}{\lambda_i+\lambda_j}\sin\alpha\tan\alpha\left(x_{k+1}^{\frac{\lambda_i+\lambda_j}{2}}-x_k^{\frac{\lambda_i+\lambda_j}{2}}\right)-\frac{P_x}{\pi\cos\alpha\left(\lambda_i+\lambda_j-2\right)}\left(x_{k+1}^{\frac{\lambda_i+\lambda_j-2}{2}}-x_k^{\frac{\lambda_i+\lambda_j-2}{2}}\right)\right]\frac{\pi}{4}\frac{\left(\lambda_i-1\right)\left(\lambda_j-1\right)}{L^{\frac{\lambda_i+\lambda_j-2}{2}}}\qquad(B.12)$$

$$\boldsymbol{Aux}_2=-\frac{2P_m\pi}{\cos\alpha\left(\lambda_i+\lambda_j\right)L^{\frac{\lambda_i+\lambda_j-2}{2}}}\left(x_{k+1}^{\frac{\lambda_i+\lambda_j}{2}}-x_k^{\frac{\lambda_i+\lambda_j}{2}}\right)\left(n+\beta_i\cos\alpha\right)\left(n+\beta_j\cos\alpha\right)\qquad(B.13)$$

$$\boldsymbol{Aux}_3=\left[-\frac{3P_m\tan\alpha\sin\alpha}{\lambda_i+\lambda_j}\left(x_{k+1}^{\frac{\lambda_i+\lambda_j}{2}}-x_k^{\frac{\lambda_i+\lambda_j}{2}}\right)-\frac{P_x}{\pi\cos\alpha\left(\lambda_i+\lambda_j-2\right)}\left(x_{k+1}^{\frac{\lambda_i+\lambda_j-2}{2}}-x_k^{\frac{\lambda_i+\lambda_j-2}{2}}\right)\right]\times$$
$$\frac{\pi}{4L^{\frac{\lambda_i+\lambda_j-2}{2}}}\left(\frac{n\alpha_i}{\sin\alpha}+\beta_i\left(\frac{1+\lambda_i}{2}\right)\right)\left(\frac{n\alpha_j}{\sin\alpha}+\beta_j\left(\frac{1+\lambda_j}{2}\right)\right)\qquad(B.14)$$

$$\boldsymbol{Aux}_4=\left[-\frac{P_m}{2}\sin\alpha\tan\alpha\ \ln\left(\frac{x_{k+1}}{x_k}\right)+\frac{P_x}{2\pi\cos\alpha}\left(\frac{x_k-x_{k+1}}{x_kx_{k+1}}\right)\right]\frac{\pi L}{4}\left(\lambda_i-1\right)\left(\lambda_j-1\right)\qquad(B.15)$$

$$\boldsymbol{Aux}_5=-\frac{P_m\pi L}{\cos\alpha}\ln\left(\frac{x_{k+1}}{x_k}\right)\left(n+\beta_i\cos\alpha\right)\left(n+\beta_j\cos\alpha\right)\qquad(B.16)$$

$$\boldsymbol{Aux}_6=\left[-\frac{3}{2}P_m\tan\alpha\sin\alpha\ \ln\left(\frac{x_{k+1}}{x_k}\right)+\frac{P_x}{2\pi\cos\alpha}\left(\frac{x_k-x_{k+1}}{x_kx_{k+1}}\right)\right]\frac{\pi L}{4}\left(\frac{n\alpha_i}{\sin\alpha}+\beta_i\left(\frac{1+\lambda_i}{2}\right)\right)\left(\frac{n\alpha_j}{\sin\alpha}+\beta_j\left(\frac{1+\lambda_j}{2}\right)\right)\qquad(B.17)$$

$$\boldsymbol{Aux}_7=\left[-\frac{\tan\alpha\sin\alpha}{2}P_m\left(x_{k+1}-x_k\right)-\frac{P_x}{2\pi\cos\alpha}\ln\left(\frac{x_{k+1}}{x_k}\right)\right]\frac{\pi}{4}\left(\lambda_i-1\right)\left(\lambda_j-1\right)\qquad(B.18)$$

$$\boldsymbol{Aux}_8 = -\frac{P_m \pi}{\cos\alpha}\left(n+\beta_i \cos\alpha\right)\left(n+\beta_j \cos\alpha\right)\left(x_{k+1}-x_k\right) \qquad (B.19)$$

$$\boldsymbol{Aux}_9 = \left[-\frac{3}{2}P_m \tan\alpha \sin\alpha\left(x_{k+1}-x_k\right)-\frac{P_x}{2\pi\cos\alpha}\ln\left(\frac{x_{k+1}}{x_k}\right)\right]\frac{\pi}{4}\left(\frac{n\alpha_i}{\sin\alpha}+\beta_i\left(\frac{1+\lambda_i}{2}\right)\right)\left(\frac{n\alpha_j}{\sin\alpha}+\beta_j\left(\frac{1+\lambda_j}{2}\right)\right) \qquad (B.20)$$

After integrating each component of the stress vector over the thickness of the shell, the normal stress resultant and moment resultant for an isotropic conical shell can be written as

$$\{\bar{\sigma}\} = \begin{Bmatrix} \bar{N}_x \\ \bar{N}_\theta \\ \bar{N}_{x\theta} \\ \bar{M}_x \\ \bar{M}_\theta \\ \bar{M}_{x\theta} \end{Bmatrix} = \left[\bar{P}\right]\begin{Bmatrix} \bar{\varepsilon}_x \\ \bar{\varepsilon}_\theta \\ 2\bar{\varepsilon}_{x\theta} \\ \bar{k}_x \\ \bar{k}_\theta \\ 2\bar{k}_{x\theta} \end{Bmatrix} \qquad (B.21)$$

CHAPITRE 4 ARTICLE 2: AN ANALYTICAL APPROACH FOR THE NONLINEAR FREE VIBRATION ANALYSIS OF THIN-WALLED CIRCULAR CYLINDRICAL SHELLS

(Published in International Journal of Structural Stability and Dynamics (IJSSD), DOI: 10.1142/S0219455421501728)

Yacine Ben-Youssef, Youcef Kerboua, Aouni A. Lakis

4.1. Abstract

This paper presents a new formulation combining the nonlinear theory of Novozhilov with the classical finite element method for the purpose of evaluating the vibratory characteristics of thin, closed and isotropic cylindrical shells. The theory developed in this paper is able to include the shell curvature effect in the circumferential direction of the orthogonal displacements and considers the impact of initial geometric imperfections on the dynamic response of the system. The formulation first takes a general form by expressing the shell displacements as an alliance between the generalized coordinates and spatial functions. Nonlinear kinematic relationships are inferred from Novozhilov's theory. The equations of motion as well as the expressions of the mass, linear and nonlinear stiffness matrices are derived through the Lagrange method by considering the coupling between the different modes. An application of this model is illustrated in a further step, by adopting the displacement functions derived from exact solutions of linear Sander's theory equilibrium equations for thin cylindrical shells. The governing equations of motion are solved with the help of a direct iterative method. Linear and nonlinear frequencies are validated by comparison with the results in the literature. The relative nonlinear frequencies are determined as a function of vibration amplitudes and then compared with published results for several cases of shells. Excellent agreement is observed between the results derived from this theory and those found in the literature. The effect of different parameters including axial and circumferential wave number, length-to-radius ratio, thickness-to-radius ratio and various boundary conditions, on the nonlinear frequencies of cylindrical shells is investigated.

Keywords: Thin cylindrical shells; geometry nonlinearities; finite element; hybrid method; nonlinear free vibration; nonlinear Novozhilov theory.

4.2. Introduction

Cylindrical thin shells are important structural elements and are widely employed in a variety of fields. Examples of their use in modern construction engineering include missiles, hydrospace, rockets, aircraft and other industrial applications such as civil engineering, nuclear, shipbuilding, petroleum and petrochemical. The study of the dynamic behavior of these structures has attracted the attention of the scientific community during recent decades as they seek to use them safely and achieve the desired performance in different conditions. The results of numerous studies focusing on linear free vibration analysis however seem to be inaccurate. This has prompted researchers to lean towards nonlinear analysis of these structures in order to design a model that faithfully translates reality. The geometrical nonlinearity generated by large vibration amplitudes influences the vibratory properties of cylindrical shells, which exhibit significant qualitative and quantitative changes in their dynamic characteristics.

Several analytical and experimental research studies have been performed on this subject. The pioneer who studied the vibration of circular cylindrical shells without geometric imperfections was Reissner [44]. He isolated a single half-wave (lobe) from the vibration mode and analyzed it for simply-supported shells. Based on Donnell's nonlinear shallow-shell theory for thin-walled `^shells, Reissner discovered that the trend of nonlinearity may vary depending on lobe geometry. It could be either of the hardening or softening types. Grigolyuk [75] adopted the same shell theory as Reissner [44] and employed the first and third longitudinal modes for the flexural displacement in order to study the nonlinear free vibration of circular cylindrical panels simply-supported at all four edges. The trend of nonlinearity found is of a hardening type. Chu [76] extended Reissner's analysis to closed cylindrical shells. By plotting his results and comparing them with a previous study carried out on flat plates, he found that nonlinear effects are considerably more manifest in flat plates than in the corresponding cylinders. Cummings [77] confirmed Reissner's analysis for circular cylindrical panels simply-supported at four edges. He also examined the response to delta function, step function and harmonic function loadings and predicted the dynamic buckling using the shock response method. Nowinski [78] confirmed Chu's results for closed circular shells. However, Evensen [79] revealed the lack of precision of Nowinski's analysis because it did not maintain a zero transverse deflection at the ends of the shell. Evensen indicated in his experimental studies that the nonlinearity in closed shells is of the softening type and weak. Matsuzaki [80] studied theoretically the nonlinear flexural vibration of thin, simply-supported circular cylindrical shells based on Donnell’s nonlinear shallow-shell theory. He also investigated the effect of structural damping and presented a detailed analysis of travelling wave oscillations. In another paper, Matsuzaki and Kobayashi [81] studied theoretically and experimentally clamped circular cylindrical shells. Their stress function takes into consideration both the particular and homogenous solutions and the mode expansion was modified in order to satisfy the different boundary conditions. The study revealed a nonlinearity of the softening type. Dowell and Ventres [82] used modal approximations in deriving the equations of motion for the nonlinear flexural vibrations of a cylindrical shell. They propose a method that satisfies boundary conditions more exactly. Their approach was followed by Atluri [83], who found that some terms were missing in one of the equations used by the authors. Recently, Dowell *et al.* [84] corrected their omissions. The boundary conditions assumed both by Dowell *et al.* and by Atluri consider the nullity of the axial displacement at the shell extremities and the nonlinearity found in their study is of the hardening type. Varadan *et al* [85] revealed that the choice of the axisymmetric term is the cause of the hardening-type results based on the theory of Dowell and Ventres and Atluri. Prathap [86] commented on the nonlinear asymmetric vibrations of some thin shells of revolution. He revealed the existence of some inconsistencies in the mathematical formulation of Evensen. El-Zaouk and Dym [87] evaluated the effects of curvature, material orthotropy and internal pressure on the nonlinear vibrations of shallow shells. Their study exhibited a change in the type of nonlinearity observed, which transforms from a softening trend to a hardening tendency for very large displacements. Ginsberg used a different approach to solve the problem of asymmetric [5] and axisymmetric [88] nonlinear vibrations of circular cylindrical shells. He adopted an asymptotic analysis instead of the assumptions of mode shapes to solve the nonlinear boundary conditions for a simply-supported shell. The equations of motion were obtained from the Lagrange equations based on an energy approach and subsequently solved using a perturbation technique. The nonlinearities revealed are either softening or hardening depending on some system parameters. Furthermore, Ginsberg [5] utilized the Flügge–Lur'e–Byrne shell theory, which neglects transverse shear, instead of Donnell’s nonlinear shallow-shell theory and studied the damped response to an excitation and its stability considering both the driven and companion modes. Radwen and Genin [89] derived nonlinear modal equations for thin elastic shells of an arbitrary geometry based on the Lagrange method. They used the strain-displacement relations of the Sanders–Koiter nonlinear shell theory, and imperfections were taken into account. The nonlinear coupling between the linear modes was neglected. Radwen and Genin [90] subsequently extended their study to integrate nonlinear coupling with axisymmetric modes. Most of their results illustrate a hardening type nonlinearity. Raju and Rao [91] analyzed large-amplitude asymmetric vibrations of shells of revolution by developing a finite element formulation. They determined the stiffness matrix based on Sanders' nonlinear strain–displacement relations and found the mass matrix by including the effect of in-plane inertia in their analysis. Their numerical results showed a nonlinear trend of the hardening type. Chiba [92] carried out experimental studies on the nonlinear vibrations of two polyester cantilevered circular cylindrical shells. He noted that almost all responses have a softening nonlinearity. The softening trend of the nonlinearity turns out to be more accentuated for shorter shells. He also found that between all modes presenting the same axial wave number, those with the minimum natural frequency present the weakest degree of softening nonlinearity. Travelling wave modes were also observed. Ganapathi and Varadan [93] developed a formulation to investigate the nonlinear free flexural vibration of circular cylindrical shells using a C_0 continuous QUAD-4 shear flexible doubly-curved shell element, based on the field consistency principle. The anisotropy, transverse shear deformation, in-plane and rotary inertia effects were considered in their formulation. A four-node finite element was developed with five degrees of freedom for each node. Only free vibrations were investigated in the paper using Novozhilov's theory of shells. The Wilson-θ numerical integration technique coupled with a modified Newton–Raphson iteration scheme was used. The study also brings out the participation of the axisymmetric contraction mode with the asymmetric mode. Selmane and Lakis [94] propose a general approach to investigate the geometric nonlinearity effect on the free vibration of freely simply-supported thin, orthotropic open cylindrical shells. The method used in this paper is a hybrid method based on a combination of thin shell theory and the finite element method (FEM). The linear solution is derived based on the displacement functions that arise from Sander's linear shell theory. The mass and linear stiffness matrices are subsequently determined using the finite element procedure. The expressions of the second- and third-order nonlinear stiffness matrices are obtained based on the Sanders–Koiter nonlinear theory. The nonlinear equations of motion are solved using the fourth-order Runge–Kutta numerical method. The trend of nonlinearity revealed is of a hardening type. In another paper, Lakis *et al.* [95] used the hybrid method they developed to analyze the effect of nonlinearities on the free vibration of laminated orthotropic cylindrical shells. The strain–displacement relations were obtained from Sanders–Koiter nonlinear theory. The displacement functions were derived from linear thin shell theory. Expressions of the mass, linear and nonlinear stiffness matrices were calculated using the FEM. The uncoupled equations of motion were solved through the elliptic functions and the numerical results derived from this study exhibit a nonlinear trend of the hardening type. Amabili *et al.* [96] investigated the nonlinear free and forced vibrations of a simply-supported circular cylindrical shell empty or in contact with an incompressible and inviscid fluid. The study is based on Donnell's shallow shell theory. The Galerkin method is employed to reduce the problem to a system of ordinary differential equations. Effects of both internal and external dense fluid are studied. The authors found that nonlinear analysis is more important for fluid-filled shells than for empty ones. Indeed, they revealed that the effect of the fluid is to enhance the nonlinear character of shell vibration. Solution of the problem was obtained both numerically and by the method of normal forms. The results obtained in this analysis exhibited a nonlinear behavior of the softening type. Amabili [97] analyzed the geometrically nonlinear vibrations of simply-supported circular cylindrical shells subjected to harmonic excitation in the spectral neighbourhood of the fundamental frequency with the help of four nonlinear thin shell theories. Namely Donnell's, Sanders–Koiter, Flügge–Lur'e–Byrne and Novozhilov's theories. The author used a potential fluid model to examine empty and fluid-filled shells. The nonlinear equations of motion were solved using a code based on an arclength continuation method allowing bifurcation analysis. Liu and Chu [98] examined the nonlinear vibrations of rotating thin circular cylindrical shells. The equations of motion were derived based on the Hamilton principle by considering clamped-free boundary conditions. The system of equations was truncated with the help of the Galerkin method. The numerical results highlighted the effects of certain parameters including axial half wave number, temperature, circumferential wave number, geometrical parameters, rotating speed, excitation frequency, damping and nonlinearity on the frequency responses and dynamic characteristics. Due to the factor of nonlinearity, Liu and Chiu determined whether the system stiffness had become hardening or softening by comparing it to hard or soft spring characteristics. They also revealed the existence of a jumping phenomenon in the nonlinear vibrations of the rotating circular cylindrical shell. Ramzi and Lakis [99] investigated geometrically nonlinear free vibrations of closed isotropic cylindrical shells through an analytical numerical model. The method developed was a combination of Sanders–Koiter nonlinear shell theory and the FEM. Nonlinear responses were evaluated using the Runge–Kutta numerical method. The numerical results that ensued from this study indicated either hardening or softening types of nonlinear behaviors depending on the structure data. Sofiyev [100] developed a formulation based on the shear deformation theory (SDT) and Von Kármán-type strain– displacement relationships in order to analyze the nonlinear free vibration of functionally graded (FG) orthotropic cylindrical shells. The equations of motion of these shells were derived from Donnell's nonlinear shell theory. The expressions of the relative nonlinear frequency depending on the amplitude as well as the nonlinear frequency parameters were obtained in the form of a Jacobian elliptic function. The effects of the nonlinearity, shear stresses, material gradient, material orthotropy and cylindrical shell characteristics on the values of the nonlinear frequency parameters were investigated in detail. Sofiyev *et al.* [101] studied the nonlinear vibration of orthotropic cylindrical shells by considering large deformations. The formulation included the Von Kármán type of geometrical nonlinearity and used the SDT to obtain the basic equations of orthotropic cylindrical shells on the nonlinear elastic foundations within Donnell's shell theory. Dey and Ramachandra [102] investigated the nonlinear transverse vibration of cross-ply laminated circular cylindrical shells subjected to static axial and periodic radial loading. The simply-supported cylindrical shell was modeled using Donnell's shell theory integrating in-plane and rotary inertia as well as first-order shear deformation. The equations of motion were first reduced using the Galerkin method and then solved using the incremental harmonic balance method to obtain frequency–amplitude responses for free and forced vibration. The analysis contains both asymmetric and axisymmetric terms and the forced vibration responses show a softening trend of nonlinear behavior. Hasrati *et al.* [103] developed a numerical solution method to analyze the nonlinear free vibrations of shells based on the six-parameter shell theory. Their approach was based on Hamilton's principle and used the idea of the variational differential quadrature method, which allows the energy functional to be accurately discretized in a direct way. The authors focused their study on cylindrical and spherical shells subjected to various types of boundary conditions. Solution of the problem was obtained using time-periodic discretization and pseudo arc-length continuation techniques. After making a comparison between the results of the six-parameter shell theory and first-order SDT, the authors concluded that the nonlinear hardening effects are more pronounced when the former theory is used. Kurylov and Amabilli [104] calculated the elastic strain energy based on the Sanders–Koiter nonlinear shell theory during their investigation of the nonlinear dynamic behaviour of clamped and simply-supported circular cylindrical shells. The shell displacements were developed in the form of a double mixed series. The equations of motion were expanded using the Lagrangian approach and resolved by employing the arclength continuation method and bifurcation analysis. Kamaloo *et al.* [105] studied the nonlinear dynamic behaviour of simply-supported laminated composite circular cylindrical shells. The equations of motion were expanded using an energy approach and reduced using the Galerkin method. Numerical results show that a decrease in the delamination effect can be caused by an increase in the circumferential wave number and an increase in orthotropy of the layers leads to a decrease in nonlinearity. Nguyen *et al.* [106] analyzed the nonlinear free and forced vibration of corrugated sandwich FG cylindrical shells by introducing a semi-analytical approach based on the Donnell shell theory and using the geometrical nonlinearity of von Kármán. The equations of motion were reduced using the Galerkin procedure and resolved by adopting the fourth-order Runge–Kutta method. Khuc *et al.* [107] investigated the nonlinear vibrations of sandwich Functionally Graded Material (FGM) cylindrical shells containing fluid under mechanical and thermal loads. The equations of motion were derived based on classical shell theory and the nonlinear geometry of von Kármán–Donnell and reduced using the Galerkin procedure. Zhu *et al.* [108] examined the effect of surface energy on the nonlinear dynamic behaviour of orthotropic piezoelectric cylindrical nanoshells. The total energy of the shell was obtained based on the von Kármán–Donnell-type geometric nonlinearity. The equations of motion were derived using the Hamilton's principle and solved by employing the homotopy perturbation method. Van Dung and Nam [109] developed a semi-analytical approach based on classical shell theory with the von Kármán–Donnell's nonlinear model to study the nonlinear vibration of eccentrically stiffened cylindrical shells surrounded by an elastic medium subjected to external pressure. The system was resolved using the fourth-order Runge–Kutta method and the numerical results revealed the effect of the input factors on the dynamic behaviour of the FG cylindrical shells. Foroutan and Ahmadi [110] presented semi-analytical and analytical methods to study the nonlinear static and dynamic buckling of imperfect FG porous cylindrical shells subjected to axial compression. Xu *et al.* [111] examined the nonlinear dynamic behavior of a hyperelastic moderately thick cylindrical shell with 2:1 internal resonance in a temperature field using the third-order SDT. The graphical results showed have emphasized the significant impact of the temperature on the nonlinear vibration of the shell. Wang *et al.* [112] analyzed the thermo-electro-mechanical nonlinear vibration of circular cylindrical nanoshells on the Winkler–Pasternak foundation using the nonlocal elasticity theory and Donnell's nonlinear shell theory. The nonlinear governing equations are derived based on the Hamilton's principle. Numerical results exhibit hardening spring behavior. Phuong *et al.* [113] examined the geometrically nonlinear response of sandwich FG cylindrical shells reinforced by orthogonal and/or spiral stiffeners and subjected to axial compressive loads. The results reveal that the spiral stiffeners have significant influences on the nonlinear buckling behavior of shells compared to orthogonal stiffeners.

In this paper, we derive general nonlinear modal equations in order to calculate the free nonlinear response of cylindrical shells. The dynamic behaviour of these elastic shells can thus be found using the method of assumed mode shape by representing the structure response in terms of suitably chosen spatial functions. The developed model can also support the calculation of the nonlinear response of thin-walled cylindrical shells under any static or dynamic loading. The linear mass and stiffness matrices are derived from linear analysis based on Sanders' shell theory. The second and third-order nonlinear stiffness matrices are determined based on Novozhilov's nonlinear theory. The equations of motion are derived using Lagrange equations, which are based on an energetic approach. The choice of a general shape for the displacement field allows the developed formulation to have some flexibility pertaining to the choice of discretization. This leads us to first choose the type of the finite element, which manifests in this study in a cylindrical form, and second, proceed to the determination of the linear and nonlinear mass and stiffness elementary matrices.

The formulation involves three steps as follows:

(i) Develop the expression of the second- and third-order nonlinear stiffness matrices based on the Lagrange method using the strain–displacement relations of Novozhilov’s nonlinear shell theory.

(ii) Determine the linear mass and stiffness matrices based on Sander’s thin shell theory.

(iii) Evaluate the modal coefficients using the displacement functions resulting from linear analysis, and subsequently determine the second- and third-order nonlinear stiffness matrices.

The linear and nonlinear global mass and stiffness matrices are determined by applying the finite element assembly procedure and considering the boundary conditions. The dynamic behaviour of an empty cylindrical shell, in the absence of external loads, is investigated by resolution of the equation of motion.

4.2.1. Hypothesis

A circular cylindrical shell of mean radius R, thickness h and length L is considered in this paper. The orthogonal displacements of a generic point P of the shell at coordinates $\left(x,\ \theta,\ \rho = R + z\right)$ are denoted by $u_1,\ u_2,\ u_3$ in the axial, circumferential and radial directions respectively. $u,\ v,\ w$ are the displacements of points on the middle surface of the shell (the middle surface corresponds to $z = 0$, where z is the coordinate along the shell thickness). Radial displacements u_3 and w are positive in the outward direction as shown in Fig.4.1, and therefore a formulation for nonlinear vibration of circular cylindrical shells was developed in cylindrical coordinates. The theory is based on the following assumptions [3] (see Fig.4.1):

(**H1**) *The shell is thin:* $h \ll R,\ h \ll L$ (*in practical applications* $h/R \le 1/20$).

(**H2**) *The magnitude of deflection* w *is of the same order as the thickness* h *of the shell.*

(**H3**) *The slope is small at each point:* $\left|\partial w/\partial x\right| \ll 1,\ \left|\partial w/\left(R\partial\theta\right)\right| \ll 1$.

(**H4**) *All strain components are small, which enables adoption of Hooke's stress–strain relations.*

(**H5**) *The Kirchhoff–Love kinematic hypothesis is valid, in which it is assumed that the normal to the undeformed middle surface remains straight and normal to the mid-surface after deformation, and undergoes no thickness stretching. The transverse normal stresses are negligible and shear deformations are neglected.*

(**H6**) *Rotary inertia is neglected.*

(**H7**) *Initial geometric imperfections of circular cylindrical shells are denoted by radial displacement* w_0, *and in-plane initial imperfections are neglected.*

(**H8**) *The circumferential displacement field of a generic point* P *of the shell is related to that of its counterpart located in the middle plane by taking into consideration the curvature effect of the shell in* u_2 *direction.*

4.2.2. Method

In this section we describe the approach followed for each of the three steps listed above. The first step stipulates the theory developed in this paper, which involves determining the linear and nonlinear mass and stiffness matrices based on Lagrange's equations of motion, resulting from Hamilton's variational principle. The second- and third-order nonlinear stiffness matrices are developed by calculating all the coefficients of the nonlinear modal equations. These coefficients are derived from the nonlinear strain–displacement relationships of Novozhilov. Kinematic relationships are presented as a product summation of generalized coordinates and spatial modal functions. The initial geometric imperfections as well as the shell curvature effect in the circumferential direction of the orthogonal displacements are also taken into consideration in this research. So that the middle surface tangential displacement v gives a contribution linearly increasing with z to u_2. The phenomenon of coupling between different modes is also accounted for in this study. The second step deals with linear behaviour for which the linear strain–displacement and stress–strain relationships are inserted into Sander's equations of equilibrium. Resolution of the linear equation system leads to determination of the real displacement functions, which satisfy the geometric boundary conditions. The mass and linear stiffness matrices are then developed for each element. The third step involves determination of the modal coefficients, which are presented in a general form, by replacing the displacement functions with those resulting from the linear analysis. The nonlinear stiffness matrices for an empty finite element are subsequently calculated using analytical integration with respect to modal coefficients. The second- and third-order nonlinear stiffness matrices, once calculated, are overlaid onto the linear system. The equations of motion are then solved with the help of a direct iterative method, leading to the determination of the linear and nonlinear frequencies. Green's strain tensor in cylindrical coordinates is defined as follows [3, 2]:

$$e_{11}=\varepsilon_{xx}=\frac{\partial u_1}{\partial x}+\frac{1}{2}\left[\left(\frac{\partial u_1}{\partial x}\right)^2+\left(\frac{\partial u_2}{\partial x}\right)^2+\left(\frac{\partial u_3}{\partial x}\right)^2\right] \tag{1a}$$

$$e_{22}=\varepsilon_{\theta\theta}=\frac{1}{\rho}\left(\frac{\partial u_2}{\partial\theta}+u_3\right)+\frac{1}{2\rho^2}\left[\left(\frac{\partial u_1}{\partial\theta}\right)^2+\left(\frac{\partial u_3}{\partial\theta}-u_2\right)^2+\left(\frac{\partial u_2}{\partial\theta}+u_3\right)^2\right] \tag{1b}$$

$$2e_{12}=\gamma_{x\theta}=\left(\frac{\partial u_1}{\rho\partial\theta}+\frac{\partial u_2}{\partial x}\right)+\frac{1}{\rho}\left[\left(\frac{\partial u_1}{\partial x}\frac{\partial u_1}{\partial\theta}\right)+\frac{\partial u_2}{\partial x}\left(\frac{\partial u_2}{\partial\theta}+u_3\right)+\frac{\partial u_3}{\partial x}\left(\frac{\partial u_3}{\partial\theta}-u_2\right)\right] \tag{1c}$$

According to the Novozhilov nonlinear shell theory, the nonlinear kinematic relationships are represented by the following equations [3]:

$$u_1=u+z.\beta \tag{2a}$$

$$u_2=v+z.\psi \tag{2b}$$

$$u_3=w+w_0+z.\chi \tag{2c}$$

Where β, ψ and χ are given in Appendix A, and w_0 designates the radial displacement due to the initial geometric imperfections of circular cylindrical shells associated with zero initial stress.

We can now introduce the following thinness approximations [3]:

$$\frac{1}{R+z} = \frac{1}{R}\left[1 - \frac{z}{R} + o\left(z/R\right)^2\right] \tag{3a}$$

$$\frac{1}{\left(R+z\right)^2} = \frac{1}{R^2}\left[1 - \frac{2 \cdot z}{R} + o\left(z/R\right)^2\right] \tag{3b}$$

where $o\left(z/R\right)^2$ is a small quantity of order $\left(z/R\right)^2$, which is negligible.

By introducing Eqs. (2a)–(2c) into Eqs. (1a)–(1c) and using approximations (3a) and (3b), the middle surface strain–displacement relationships are obtained for the Novozhilov nonlinear shell theory of circular shells and can be found in Appendix A.

The shell material is assumed to be elastic, homogenous and isotropic. The shell thickness h is allowed to vary arbitrarily within the limits of thin shell theory [2].

The displacement vector of an arbitrary point $\left(x, \theta\right)$ on the middle surface along x, θ and z respectively can be approximated in the form:

$$u = \sum_i q_i\left(t\right).f_i\left(x, \theta\right) \tag{4a}$$

$$v = \sum_i q_i\left(t\right).g_i\left(x, \theta\right) \tag{4b}$$

$$w = \sum_i q_i\left(t\right).h_i\left(x, \theta\right) \tag{4c}$$

Where functions $q_i\left(t\right)$ are the generalized coordinates to be determined and f_i, g_i, h_i represent the spatial functions, which should at least satisfy the geometric boundary conditions of the shell. Let us now represent the initial imperfections $w_0(x, \theta)$ in the form of a series. $w_0 = \sum_i \delta_i h_i\left(x, \theta\right)$.

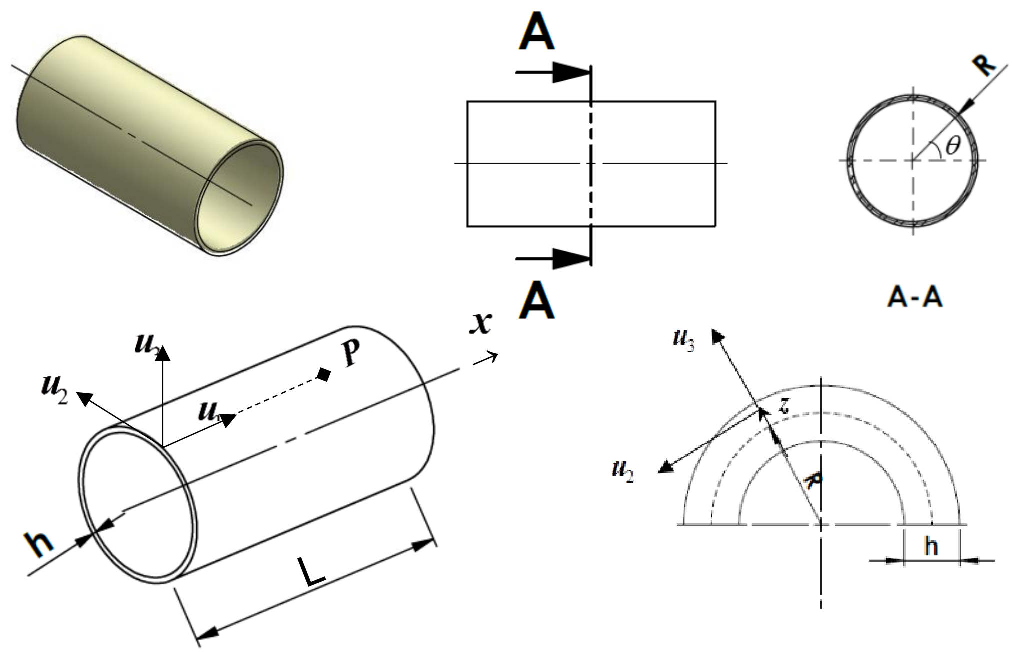

Figure 4.1: Geometry and displacement function of a generic point of a circular cylindrical shell; longitudinal and cross-section

The Lagrange equations, which follow from Hamilton's variational principle, are used to determine the equations of motion as follows:

$$\frac{d}{dt}\left(\frac{\partial T}{\partial \dot{q}_i}\right)-\frac{\partial T}{\partial q_i}+\frac{\partial V}{\partial q_i}=Q_i\,, \qquad i=1,2,..,N. \tag{5}$$

Here, N is the number of degrees of freedom, and can be chosen according to the desired accuracy, T is the total kinetic energy, V represents the total elastic strain energy of deformation and the Q's are the generalized forces.

Referring to Eq. (5) and using Eqs. (4a)–(4c), we proceed to evaluate each term of this equation separately in terms of the generalized coordinates q_i and the assumed mode shapes f_i, g_i, h_i. Thus, the kinetic energy T of the shell defined in cylindrical coordinates is given by [2]:

$$T=\frac{\bar{m}}{2}\int_0^L\int_0^{2\pi}\left(\dot{u}^2+\dot{v}^2+\dot{w}^2\right)R\,dx\,d\theta \tag{6}$$

Where $\bar{m}$ is the mass per unit area of the undeformed middle surface of the shell.

By evaluating the second term of the Lagrange equations, one can obtain:

$$\frac{\partial T}{\partial q_i}=0 \tag{7}$$

To evaluate the expression of the first term of the Lagrange equations, it suffices to write

$$\frac{\partial T}{\partial \dot{q}_i}=\frac{1}{2}\int_0^L\int_0^{2\pi} 2\,\bar{m}\left(\dot{u}\frac{\partial \dot{u}}{\partial \dot{q}_i}+\dot{v}\frac{\partial \dot{v}}{\partial \dot{q}_i}+\dot{w}\frac{\partial \dot{w}}{\partial \dot{q}_i}\right)R\,dx\,d\theta \tag{8}$$

By introducing the Eqs. (4a)–(4c) into Eq. (8), we obtain [2]:

$$\frac{\partial T}{\partial \dot{q}_i}=\int_0^L\int_0^{2\pi}\bar{m}\left(f_i\sum_i f_i\,\dot{q}_i+g_i\sum_i g_i\,\dot{q}_i+h_i\sum_i h_i\,\dot{q}_i\right)R\,dx\,d\theta \tag{9}$$

Where,

$$\frac{\partial T}{\partial \dot{q}_i}=\sum_j m_{ij}\,\dot{q}_j \tag{10}$$

Therefore,

$$m_{ij}=\int_0^L\int_0^{2\pi}\bar{m}\left(f_i\ f_j+g_i\ g_j+h_i\ h_j\right)R\,dx\,d\theta \tag{11}$$

It follows that:

$$\frac{d}{dt}\left(\frac{\partial T}{\partial \dot{q}_i}\right)=\sum_j m_{ij}\,\ddot{q}_j\ ,\ i=1,2,\ldots,N \tag{12}$$

We note that if $f_i,\ g_i,\ h_i$ are the normal modes of the linearized system, then orthogonality of these modes ensures that $m_{ij}=0$ when $i\neq j$.

Turning now to elastic strain energy V, we know that [2]:

$$V=\frac{1}{2}\int_0^L\int_0^{2\pi}C\left[\varepsilon_{11}^2+\varepsilon_{22}^2+2\nu\,\varepsilon_{11}\,\varepsilon_{22}+2\left(1-\nu\right)\varepsilon_{12}^2\right]R\,dx\,d\theta$$
$$+\frac{1}{2}\int_0^L\int_0^{2\pi}D\left[k_{11}^2+k_{22}^2+2\nu\,k_{11}\,k_{22}+2\left(1-\nu\right)k_{12}^2\right]R\,dx\,d\theta \tag{13}$$

Where $\varepsilon_{11},\,\varepsilon_{12},\,\varepsilon_{22}$ are the middle surface strain components, $k_{11},\,k_{12},\,k_{22}$ are the changes in curvature and torsion of the middle surface and $C=Eh\big/\left(1-\nu^2\right)$, $D=Eh^3\big/\left[12\left(1-\nu^2\right)\right]$, where E is the Young’s modulus of the shell and ν is its Poison’s ratio.

From the expression of the elastic strain energy (13), we proceed to evaluate the third term of the Lagrange equations (5). One can write [2]:

$$\begin{aligned}\frac{\partial V}{\partial q_i} &= \int_0^L \int_0^{2\pi} C\left[\varepsilon_{11}\frac{\partial \varepsilon_{11}}{\partial q_i} + \varepsilon_{22}\frac{\partial \varepsilon_{22}}{\partial q_i} + \nu\varepsilon_{11}\frac{\partial \varepsilon_{22}}{\partial q_i} + \nu\varepsilon_{22}\frac{\partial \varepsilon_{11}}{\partial q_i} + 2(1-\nu)\,\varepsilon_{12}\frac{\partial \varepsilon_{12}}{\partial q_i}\right] R\,dx\,d\theta \\ &+ \int_0^L \int_0^{2\pi} D\left[k_{11}\frac{\partial k_{11}}{\partial q_i} + k_{22}\frac{\partial k_{22}}{\partial q_i} + \nu k_{11}\frac{\partial k_{22}}{\partial q_i} + \nu k_{22}\frac{\partial k_{11}}{\partial q_i} + 2(1-\nu)\,k_{12}\frac{\partial k_{12}}{\partial q_i}\right] R\,dx\,d\theta \end{aligned} \tag{14}$$

In general, the deformation field of an arbitrary point belonging to the mean surface can be expressed in the following form [2] (see Appendix A):

$$\varepsilon_{x,0} = \varepsilon_{11} = \sum_j a_j q_j + \sum_j \sum_k A_{jk} q_j q_k \tag{15}$$

By taking the derivation of Eqs. (15) and (A.13)–(A.23) with respect to the generalized coordinates q_i, we obtain [2]

$$\frac{\partial \varepsilon_{11}}{\partial q_i} = a_i + 2\sum_j A_{ij}\, q_j \tag{16a}$$

$$\frac{\partial \varepsilon_{22}}{\partial q_i} = b_i + 2\sum_j B_{ij}\, q_j \tag{16b}$$

$$\frac{\partial \varepsilon_{12}}{\partial q_i} = c_i + 2\sum_j C_{ij}\, q_j \tag{16c}$$

$$\frac{\partial k_{11}}{\partial q_i} = p_i + 2\sum_j P_{ij}\, q_j \tag{16d}$$

$$\frac{\partial k_{22}}{\partial q_i} = s_i + 2\sum_j S_{ij}\, q_j \tag{16e}$$

$$\frac{\partial k_{12}}{\partial q_i} = t_i + 2\sum_j T_{ij}\, q_j \tag{16f}$$

Now, Eqs. (15), (A.13)–(A.23) and (16a)–(16f) lead to [2]

$$\varepsilon_{11}\frac{\partial \varepsilon_{11}}{\partial q_i}=\left[\sum_j a_j\, q_j+\sum_j\sum_k A_{jk}\, q_j\, q_k\right]\left[a_i+2\sum_k A_{ik}\, q_k\right] \tag{17a}$$

$$\varepsilon_{11}\frac{\partial \varepsilon_{11}}{\partial q_i}=\sum_j a_{ij}\, q_j+\sum_j\sum_k A_{ijk}\, q_j\, q_k+\sum_j\sum_k\sum_s A_{ijks}\, q_j\, q_k\, q_s \tag{17b}$$

Where,

$$a_{ij}=a_i\, a_j \tag{17c}$$

$$A_{ijk}=a_i\, A_{jk}+a_j\, A_{ki}+a_k\, A_{ij} \tag{17d}$$

$$A_{ijks}=2\, A_{jk}\, A_{is} \tag{17e}$$

Following the same reasoning, we get (See Appendix A) [2]

$$\varepsilon_{22}\frac{\partial \varepsilon_{22}}{\partial q_i}=\sum_j b_{ij}\, q_j+\sum_j\sum_k B_{ijk}\, q_j\, q_k+\sum_j\sum_k\sum_s B_{ijks}\, q_j\, q_k\, q_s \tag{18}$$

$$\varepsilon_{12}\frac{\partial \varepsilon_{12}}{\partial q_i}=\sum_j c_{ij}\, q_j+\sum_j\sum_k C_{ijk}\, q_j\, q_k+\sum_j\sum_k\sum_s C_{ijks}\, q_j\, q_k\, q_s \tag{19}$$

$$k_{11}\frac{\partial k_{11}}{\partial q_i}=\sum_j p_{ij}\, q_j+\sum_j\sum_k P_{ijk}\, q_j\, q_k+\sum_j\sum_k\sum_s P_{ijks}\, q_j\, q_k\, q_s \tag{20}$$

$$k_{22}\frac{\partial k_{22}}{\partial q_i}=\sum_j s_{ij}\, q_j+\sum_j\sum_k S_{ijk}\, q_j\, q_k+\sum_j\sum_k\sum_s S_{ijks}\, q_j\, q_k\, q_s \tag{21}$$

$$k_{12}\frac{\partial k_{12}}{\partial q_i}=\sum_j t_{ij}\, q_j+\sum_j\sum_k T_{ijk}\, q_j\, q_k+\sum_j\sum_k\sum_s T_{ijks}\, q_j\, q_k\, q_s \tag{22}$$

$$\varepsilon_{11}\frac{\partial \varepsilon_{22}}{\partial q_i}=\sum_j d_{ij}\, q_j+\sum_j\sum_k D_{ijk}\, q_j\, q_k+\sum_j\sum_k\sum_s D_{ijks}\, q_j\, q_k\, q_s \tag{23}$$

$$\varepsilon_{22}\frac{\partial \varepsilon_{11}}{\partial q_i}=\sum_j e_{ij}\, q_j+\sum_j\sum_k E_{ijk}\, q_j\, q_k+\sum_j\sum_k\sum_s E_{ijks}\, q_j\, q_k\, q_s \tag{24}$$

$$k_{11}\frac{\partial k_{22}}{\partial q_i}=\sum_j u_{ij}\, q_j+\sum_j\sum_k U_{ijk}\, q_j\, q_k+\sum_j\sum_k\sum_s U_{ijks}\, q_j\, q_k\, q_s \tag{25}$$

$$k_{22}\frac{\partial k_{11}}{\partial q_i}=\sum_j v_{ij}\, q_j+\sum_j\sum_k V_{ijk}\, q_j\, q_k+\sum_j\sum_k\sum_s V_{ijks}\, q_j\, q_k\, q_s \tag{26}$$

By inserting Eqs. (17)–(26) into Eq. (14), one obtains

$$\frac{\partial V}{\partial q_i} = \sum_j k_{ij} q_j + \sum_j \sum_k k_{ijk} q_j q_k + \sum_j \sum_k \sum_s k_{ijks} q_j q_k q_s \tag{27}$$

Where [2]

$$k_{ij} = \int_0^L \int_0^{2\pi} \Big\{ C\left[a_{ij} + b_{ij} + \nu\left(d_{ij} + e_{ij}\right) + 2(1-\nu) c_{ij} \right] + D\left[p_{ij} + s_{ij} + \nu\left(u_{ij} + v_{ij}\right) + 2(1-\nu) t_{ij} \right] \Big\} R\, dx\, d\theta \tag{28a}$$

$$k_{ijk} = \int_0^L \int_0^{2\pi} \Big\{ C\left[A_{ijk} + B_{ijk} + \nu\left(D_{ijk} + E_{ijk}\right) + 2(1-\nu) C_{ijk} \right] + D\left[P_{ijk} + S_{ijk} + \nu\left(U_{ijk} + V_{ijk}\right) + 2(1-\nu) T_{ijk} \right] \Big\} R\, dx\, d\theta \tag{28b}$$

$$k_{ijks} = \int_0^L \int_0^{2\pi} \Big\{ C\left[A_{ijks} + B_{ijks} + \nu\left(D_{ijks} + E_{ijks}\right) + 2(1-\nu) C_{ijks} \right] + D\left[P_{ijks} + S_{ijks} + \nu\left(U_{ijks} + V_{ijks}\right) + 2(1-\nu) T_{ijks} \right] \Big\} R\, dx\, d\theta \tag{28c}$$

$$i, j, k, s = 1, 2, .., N.$$

After developing the total kinetic and elastic strain energy and substituting Eqs. (7), (12) and (27) into the Lagrange equations (5), we obtain the dynamic behaviour of an empty cylindrical shell in the absence of external loads, in terms of the following nonlinear modal equations [2]:

$$\sum_j m_{ij}\, \ddot{q}_j + \sum_j k_{ij}\, q_j + \sum_j \sum_k k_{ijk}\, q_j\, q_k + \sum_j \sum_k \sum_s k_{ijks}\, q_j\, q_k\, q_s = 0 \tag{29}$$

In Eqs. (15)–(29), the subscripts $"i, j"$, $"i, j, k"$ and $"i, j, k, s"$ represent, respectively, the coupling between two, three and four different modes.

4.3. Linear part

The shell is subdivided into several cylindrical elements. Each element is defined by two line-nodes, i and j and the boundaries of the nodal surface. Each node has four degrees of freedom: three displacements (axial, circumferential and radial) and one rotation oriented, as shown in Fig.4.2. The theory developed by Lakis and Paidoussis [9] is a hybrid type of FEM, which is much more precise than the usual FEM because the displacement functions are derived from exact solutions of Sanders' shell equilibrium equations rather than an approximation with polynomial functions. The major advantage of this approach is that very accurate results [9] are obtained using a small number of finite elements.

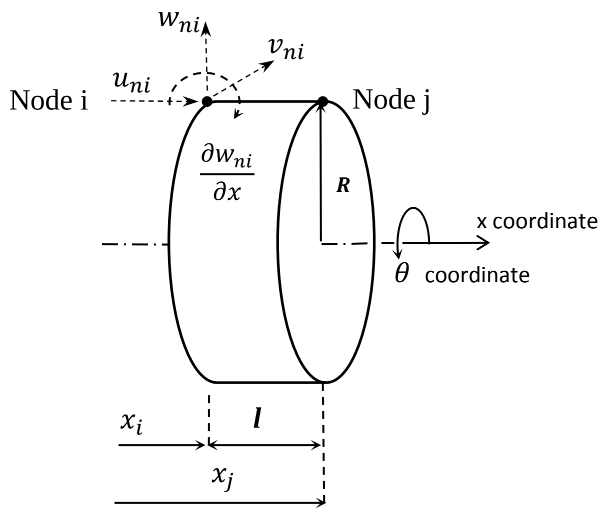

Figure 4.2: Nodal displacements of a cylindrical F.E

The linear strain vector according to Sanders theory [9] in the cylindrical coordinate system is expressed in terms of axial U, radial W, and circumferential V mid-surface displacements as follows:

$$\begin{Bmatrix} \varepsilon_x \\ \varepsilon_\theta \\ 2\varepsilon_{x\theta} \\ k_x \\ k_\theta \\ 2k_{x\theta} \end{Bmatrix} = \begin{Bmatrix} \dfrac{\partial U}{\partial x} \\ \dfrac{1}{R}\dfrac{\partial V}{\partial \theta} + \dfrac{W}{R} \\ \dfrac{\partial V}{\partial x} + \dfrac{1}{R}\dfrac{\partial U}{\partial \theta} \\ -\dfrac{\partial^2 W}{\partial x^2} \\ -\dfrac{1}{R^2}\dfrac{\partial^2 W}{\partial \theta^2} + \dfrac{1}{R^2}\dfrac{\partial V}{\partial \theta} \\ -\dfrac{2}{R}\dfrac{\partial^2 W}{\partial x \partial \theta} + \dfrac{3}{2R}\dfrac{\partial V}{\partial x} - \dfrac{1}{2R^2}\dfrac{\partial U}{\partial \theta} \end{Bmatrix} \tag{30}$$

where ε_x and ε_θ represent strain components in the axial and circumferential directions, respectively. $\varepsilon_{x\theta}$ represents the shear strain in the $x\theta$ plane. k_x, k_θ are the change of curvature of the normal mid-surface and $k_{x\theta}$ is the modified twisting strain. The stress–strain relation is given by:

$$\{\sigma\} = [P]\{\varepsilon\} \tag{31}$$

where $[P]$ is the elasticity matrix of order (6×6) for an anisotropic material. Its components for an isotropic shell are given in Appendix B.

The equilibrium equations of anisotropic cylindrical shells are expressed in terms of axial, tangential and radial displacements of the mean surface [9]. They are given fully in Appendix B, using three linear partial differential operators $L_k\,(k=1,2,3)$, they are thus defined as

$$L_k\left(U,W,V,P_{ij}\right) = 0 \tag{32}$$

where $L_k\left(U,W,V,P_{ij}\right)_{k=1,2,3}$ are the linear partial differential equations of an anisotropic cylindrical shell given in Appendix B. P_{ij} are the elements of the elasticity matrix $[P]$. From Eq. (32), we can define the displacement functions as periodic functions, which can be expressed as a Fourier series (see Ref. 9 for more details). The displacement field can therefore be defined for the n^{th} wave number by the following expressions:

$$U(x,\theta) = u_n(x)\cos(n\theta) \tag{33a}$$

$$W(x,\theta) = w_n(x)\cos(n\theta) \tag{33b}$$

$$V(x,\theta) = v_n(x)\sin(n\theta) \tag{33c}$$

Here n represents the circumferential wave number, and u_n, v_n, w_n are the magnitudes of displacements that depend only on the x coordinate, as follows [9]:

$$u_n(x) = A e^{\lambda x/R} \tag{34a}$$

$$v_n(x) = B e^{\lambda x/R} \tag{34b}$$

$$w_n(x) = C e^{\lambda x/R} \tag{34c}$$

By introducing Eqs. (33) and (34) into the Sanders' equilibrium equations (32), the following system of equations in terms of displacement parameters is obtained:

$$\begin{bmatrix} H_{11} & H_{12} & H_{13} \\ H_{21} & H_{22} & H_{23} \\ H_{31} & H_{32} & H_{33} \end{bmatrix} \begin{Bmatrix} A \\ B \\ C \end{Bmatrix} = \begin{Bmatrix} 0 \\ 0 \\ 0 \end{Bmatrix} \tag{35}$$

Expressions of matrix $\left[H_{ij}\right]$ are provided in Appendix B. For the nontrivial solution of Eq. (35), the determinant of $\left[H_{ij}\right]$ must vanish, yielding the following characteristic equation:

$$a\lambda^8 + b\lambda^6 + c\lambda^4 + d\lambda^2 + e = 0 \tag{36}$$

Coefficients $(a, b, c, d \text{ and } e)$ vary according to material properties, geometry and the circumferential mode n. Their mathematical expressions are given in Ref. 9. Each root λ_i of the characteristic equation represents a solution of Eqs. (32). Complete solution of the spatial displacement function is obtained by summation of the eight roots of the characteristic equation and constants A_i, B_i and C_i $(i = 1, 2, .., 8)$ as follows:

$$u_n(x) = \sum_{i=1}^{8} A_i \, e^{\lambda_i x/R} \tag{37a}$$

$$v_n(x) = \sum_{i=1}^{8} B_i \, e^{\lambda_i x/R} \tag{37b}$$

$$w_n(x) = \sum_{i=1}^{8} C_i \, e^{\lambda_i x/R} \tag{37c}$$

Let us return now to Eq. (35). Since the solution of this equation is nontrivial, A_i, B_i and C_i are not independent. This allows us to express A_i and B_i in terms of C_i as follows: $A_i = \alpha_i C_i$ and $B_i = \beta_i C_i$. Where α_i and β_i are complex numbers. More detail on the hybrid method is available in Ref. 9. The displacement functions may therefore be written as

$$\begin{Bmatrix} U(x,\theta) \\ W(x,\theta) \\ V(x,\theta) \end{Bmatrix} = [T][R]\{C\} \tag{38}$$

Where matrices $[T]$ of order (3×3) and $[R]$ of order (3×8) are given in Appendix B, and vector $\{C\} = \{C_1, C_2, ..., C_8\}^T$.

We are now in position to determine the constants $C_j\left(j=1,2,..,8\right)$, which may be replaced by the finite element nodal displacements vector using the eight boundary conditions of each finite element (four at each node) as follows:

$$\begin{Bmatrix}\delta_i\\ \delta_j\end{Bmatrix}=\left\{u_{ni}\ ,w_{ni},\partial w_{ni}/\partial x,v_{ni},u_{nj},w_{nj},\partial w_{nj}/\partial x,v_{nj}\right\}^T=\left[A\right]\left\{C\right\} \tag{39}$$

Recall that the cylindrical frustum is defined by two line-nodes, i and j. Thus, the terms of matrix $\left[A\right]$ are obtained using Eqs. (37a)–(37c), where x in matrix $\left[R\right]$ is replaced by definite coordinate values x_i and x_j corresponding, respectively, to nodes i and j, (see Fig.4.2). The components of matrix $\left[A\right]_{8\times 8}$ are defined in Ref. 9.

By multiplying Eq. (39) from either side by $\left[A\right]^{-1}$, one obtains the vector $\left\{C\right\}$ as a function of the nodal displacements of the considered finite element, as follows:

$$\left\{C\right\}=\left[A\right]^{-1}\begin{Bmatrix}\delta_i\\ \delta_j\end{Bmatrix} \tag{40}$$

Substituting Eq. (40) into Eq. (38), one obtains the displacement functions expressed in terms of nodal displacements as follows:

$$\begin{Bmatrix}U\left(x,\theta\right)\\ W\left(x,\theta\right)\\ V\left(x,\theta\right)\end{Bmatrix}=\left[T\right]\left[R\right]\left[A\right]^{-1}\begin{Bmatrix}\delta_i\\ \delta_j\end{Bmatrix}=\left[N\right]\begin{Bmatrix}\delta_i\\ \delta_j\end{Bmatrix} \tag{41}$$

By introducing Eqs. (33a)–(33c) and (37a)–(37c) into Eq. (30) and using Eq. (40), the strain vector expression is expressed as

$$\left\{\varepsilon\right\}=\begin{bmatrix}[T] & [0]\\ [0] & [T]\end{bmatrix}\left[Q\right]\left[A\right]^{-1}\begin{Bmatrix}\delta_i\\ \delta_j\end{Bmatrix}=\left[B\right]\begin{Bmatrix}\delta_i\\ \delta_j\end{Bmatrix} \tag{42}$$

Where the components of matrix $\left[Q\right]$ are given in Ref. 9. Now, the components of the stress vector may be written in terms of nodal displacements using Eqs. (31) and (42) as

$$\{\sigma\} = [P][B]\begin{Bmatrix}\delta_i \\ \delta_j\end{Bmatrix} \tag{43}$$

The elementary mass $[m]_s^e$ and stiffness $[k]_s^e$ matrices of the cylindrical finite element are subsequently calculated based on the standard finite element approach. Their relations are thus defined as

$$[k]_s^e = \int_0^l \int_0^{2\pi} [B]^T [P][B] R\, dx\, d\theta \tag{44}$$

$$[m]_s^e = \rho h \int_0^l \int_0^{2\pi} [N]^T [N] R\, dx\, d\theta \tag{45}$$

Where ρ is the density of the solid shell, h is the wall thickness, l is the length of the finite element and R is the mean radius of the cylindrical shell (See Fig.4.1),

Using Eqs. (41) and (42) in (44) and (45) then integrating over θ, one obtains

$$[k]_s^e = \left[[A]^{-1}\right]^T \left[\pi R \int_0^l [Q]^T [P][Q] dx\right] [A]^{-1} \tag{46}$$

$$[m]_s^e = \rho h \left[[A]^{-1}\right]^T \left[\pi R \int_0^l [R]^T [R] dx\right] [A]^{-1} \tag{47}$$

4.4. Nonlinear part

Before we embark on matrix formulation, note that the structure is assumed to be perfectly cylindrical in order to neglect the effect of the initial geometric imperfections.

In this section, the nonlinear stiffness matrices are evaluated through the development of the modal coefficients obtained based on the Lagrange method and expressed according to the spatial components of the field of displacement. The spatial functions (f_i, g_i, h_i) presented in Eqs. (4a)–(4c) are replaced by linear ones (U_i, V_i, W_i) relating to Eqs. (33a)–(33c). We obtain [2]:

$$u = \sum_i q_i\left(t\right).U_i\left(x,\theta\right) \tag{48a}$$

$$v = \sum_i q_i\left(t\right).\,V_i\left(x,\theta\right) \tag{48b}$$

$$w = \sum_i q_i\left(t\right).\,W_i\left(x,\theta\right) \tag{48c}$$

Each modal coefficient of Eqs. (A.10)–(A.23b) can be evaluated separately as follows [2]:

$$a_i = A_i\, e^{\lambda_i x/R}\, \frac{\lambda_i}{R}\, cos\left(n\theta\right) = \alpha_i\, C_i\, e^{\lambda_i x/R}\, \frac{\lambda_i}{R}\, cos\left(n\theta\right) \tag{49}$$

$$b_i = \frac{1}{R}\left[B_i e^{\lambda_i x/R} n\, cos\left(n\theta\right) + C_i e^{\lambda_i x/R} cos\left(n\theta\right)\right] = \frac{1}{R} C_i e^{\lambda_i x/R} cos\left(n\theta\right)\left[1+\beta_i n\right] \tag{50}$$

$$c_i = \frac{1}{2}\left[B_i\, \frac{\lambda_i}{R}\, e^{\lambda_i x/R}\, sin\left(n\theta\right) - \frac{1}{R} A_i\, e^{\lambda_i x/R}\; n\, sin\left(n\theta\right)\right] = \frac{1}{2R} C_i\, e^{\lambda_i x/R} sin\left(n\theta\right)\left[\beta_i\, \lambda_i - \alpha_i\, n\right] \tag{51}$$

$$p_i = -C_i\left(\frac{\lambda_i}{R}\right)^2 e^{\lambda_i x/R}\, cos\left(n\theta\right) \tag{52}$$

$$s_i = \frac{1}{R^2} C_i\, e^{\lambda_i x/R}\, cos\left(n\theta\right)\left[n^2 + \alpha_i\, \lambda_i + \beta_i\, n\right] \tag{53}$$

$$t_i = \frac{1}{R^2} C_i\;\; e^{\lambda_i x/R}\, sin\left(n\theta\right)\left[2\,\lambda_i\, n + \alpha_i\, n + \beta_i\, \lambda_i\right] \tag{54}$$

Similarly, we obtain

$$A_{ij} = C_i\, a'_{ij}\, e^{\left(\lambda_i+\lambda_j\right)x/R}\, C_j \tag{55a}$$

Where

$$a'_{ij} = \frac{1}{2R^2}\left[a_{ij}^{(1)}\, cos^2\left(n\theta\right) + a_{ij}^{(2)}\, sin^2\left(n\theta\right)\right] \tag{55b}$$

with,

$$a_{ij}^{(1)} = \left(1+\alpha_i\, \alpha_j\right)\lambda_i\, \lambda_j \tag{55c}$$

$$a_{ij}^{(2)} = \beta_i\, \beta_j\, \lambda_i\, \lambda_j \tag{55d}$$

The coefficients $B_{ij}, C_{ij}, P_{ij}, S_{ij}, T_{ij}$ are determined by following the same development (see Appendix C).

We proceed to evaluate the coefficients of the modal equations related to the second-order stiffness matrix [2]. Inserting Eqs. (49) and (55) into (17d) leads to the following expression:

$$A_{ijk} = \frac{1}{R} C_i C_j C_k e^{\left(\lambda_i + \lambda_j + \lambda_k\right)x/R} cos\left(n\theta\right) \left[\lambda_i \alpha_i a'_{jk} + \lambda_j \alpha_j a'_{ki} + \lambda_k \alpha_k a'_{ij} \right] \qquad (56)$$

The remaining coefficients are determined using the same approach illustrated above (see Appendix C for more details). Due to the axisymmetric nature of the model, the second-order stiffness matrix is equal to zero [2], which prompts us to eliminate the quadratic terms from the nonlinear modal equations of motion (29).

Turning now to the terms of the stiffness matrix of order three, inserting Eq. (55) into Eq. (17e) results in the following expression:

$$A_{ijks} = 2 C_i C_j C_k C_s a'_{is} a'_{jk} e^{\left(\lambda_i + \lambda_j + \lambda_k + \lambda_s\right)x/R} \qquad (57)$$

This completes the development of all the coefficients which constitute the expression of the nonlinear stiffness matrix (see Appendix C). It is written in the following form [2]:

$$\left[k^{NL3}\right] = \frac{\pi}{8R^2} \left[A^{-1}\right]^T \left[k^*_{NL}\right] \left[A^{-1}\right] \qquad (58)$$

The (i,k) term in matrix $\left[k^*_{NL}\right]$ is written as [2]:

$$k^*_{NL}(i,k) = \left\{ \begin{array}{ll} \displaystyle\sum_{s=1}^{8} \sum_{j=1}^{8} \frac{\tau_{sj}}{\lambda_i + \lambda_j + \lambda_k + \lambda_s} G(i,k) \left[e^{\left(\lambda_i + \lambda_j + \lambda_k + \lambda_s\right) l/R} - 1 \right] & \text{if } \lambda_i + \lambda_j + \lambda_k + \lambda_s \neq 0 \\ \displaystyle\sum_{s=1}^{8} \sum_{j=1}^{8} \tau_{sj} G(i,k) \frac{l}{R} & \text{if } \lambda_i + \lambda_j + \lambda_k + \lambda_s = 0 \end{array} \right\} \qquad (59)$$

τ_{sj} is the term (s, j) of matrix E, where $[E] = \left[A^{-1}\right]\left[A^{-1}\right]^T$, and $G(i,k)$ is a coefficient in conjunction with α, β, λ and elements C, D of matrix $[P]$. The general expression of $G(i,k)$ is given by

$$G(i,k)=C\Big\{3\Big[a_{is}^{(1)}a_{jk}^{(1)}+b_{is}^{(1)}b_{jk}^{(1)}+a_{is}^{(2)}a_{jk}^{(2)}+b_{is}^{(2)}b_{jk}^{(2)}+\nu\Big(b_{is}^{(1)}a_{jk}^{(1)}+a_{is}^{(1)}b_{jk}^{(1)}+b_{is}^{(2)}a_{jk}^{(2)}+a_{is}^{(2)}b_{jk}^{(2)}\Big)\Big]$$
$$+a_{is}^{(2)}a_{jk}^{(1)}+a_{is}^{(1)}a_{jk}^{(2)}+b_{is}^{(2)}b_{jk}^{(1)}+b_{is}^{(1)}b_{jk}^{(2)}+\nu\Big(b_{is}^{(2)}a_{jk}^{(1)}+b_{is}^{(1)}a_{jk}^{(2)}+a_{is}^{(1)}b_{jk}^{(2)}+a_{is}^{(2)}b_{jk}^{(1)}\Big)$$
$$+2(1-\nu)\Big(c_{is}^{(1)}+c_{is}^{(2)}\Big)\Big(c_{jk}^{(1)}+c_{jk}^{(2)}\Big)\Big\}+\frac{4D}{R^2}\Big\{3\Big[p_{is}^{(1)}p_{jk}^{(1)}+s_{is}^{(1)}s_{jk}^{(1)}+p_{is}^{(2)}p_{jk}^{(2)}+s_{is}^{(2)}s_{jk}^{(2)}$$
$$+\nu\Big(s_{is}^{(1)}p_{jk}^{(1)}+p_{is}^{(1)}s_{jk}^{(1)}+s_{is}^{(2)}p_{jk}^{(2)}+p_{is}^{(2)}s_{jk}^{(2)}\Big)\Big]+p_{is}^{(1)}p_{jk}^{(2)}+p_{is}^{(2)}p_{jk}^{(1)}+s_{is}^{(1)}s_{jk}^{(2)}+s_{is}^{(2)}s_{jk}^{(1)}$$
$$+\nu\Big(s_{is}^{(2)}p_{jk}^{(1)}+s_{is}^{(1)}p_{jk}^{(2)}+p_{is}^{(1)}s_{jk}^{(2)}+p_{is}^{(2)}s_{jk}^{(1)}\Big)+2(1-\nu)t_{is}^{(1)}t_{jk}^{(1)}\Big\} \qquad (60)$$

where the terms $a_{ij}^{(1)}$ and $a_{ij}^{(2)}$ are given by Eqs. (55c) and (55d); terms $b_{ij}^{(1)}$, $b_{ij}^{(2)}$, $c_{ij}^{(1)}$, $c_{ij}^{(2)}$, $p_{ij}^{(1)}$, $p_{ij}^{(2)}$, $s_{ij}^{(1)}$, $s_{ij}^{(2)}$ and $t_{ij}^{(1)}$ are coefficients appearing in expressions for the elements $B_{ij}, C_{ij}, P_{ij}, S_{ij}$ and T_{ij} of Eqs. (C.1a)–(C.5c) given in Appendix C and C, D are the terms of the elasticity matrix.

4.5. Numerical solution

In the case of axisymmetric structures (with symmetrical mechanics in the transverse direction), the system turns out to be devoid of quadratic terms, and the equations of motion (29) are reduced accordingly to:

$$\sum_j m_{ij}\,\ddot{q}_j+\sum_j k_{ij}\,q_j+\sum_j\sum_k\sum_s k_{ijks}\,q_j\;q_k\;q_s=0 \qquad (61)$$

Since the complete shell is subdivided into a number of cylindrical frustum finite elements, we proceed to superimpose the elementary mass and stiffness matrixes, which have already been calculated in Eqs. (46), (47) and (58) to obtain the global matrices for the whole shell. The assembly is done in such a way that all the equations of motion and the continuity of displacement at each node are satisfied. By considering the coupling between different modes, Eq. (61) is written in matrix form as follows:

$$[M]\{\ddot{\delta}\}+[K]\{\delta\}+\Big[K^{(NL3)}\Big]\{\delta\}^{\otimes 3}=\{0\} \qquad (62)$$

Where $\{\delta\}$ is the displacement vector and $[M],[K]$ and $\Big[K^{(NL3)}\Big]$ are, respectively, the mass, linear and nonlinear stiffness matrices of the whole system [2].

$\{\delta\}^{\otimes 3}$ is the Kronecker product power 3 of vector $\{\delta\}$ $\Big(\text{e.g.}\{\delta\}^{\otimes 2}=\{\delta\}\otimes\{\delta\}\Big)$.

In practice, specific conditions are applied to the shell boundaries. Thus the matrices cited above are reduced to square matrices of order $\mathrm{NREDUC} = \mathrm{NDF} * (\mathrm{NEL}+1) - J$, where J represents the number of essential constraints, NDF is the number of degrees of freedom and NEL designates the number of elements. Hence, the equations of motion (62) become

$$\left[M^{(r)}\right]\left\{\ddot{\delta}^{(r)}\right\}+\left[K^{(r)}\right]\left\{\delta^{(r)}\right\}+\left[K_{NL3}^{(r)}\right]\left\{\delta^{(r)}\right\}^{\otimes 3}=\{0\} \tag{63}$$

Where the superscript $"r"$ means, “reduced”, and

$$\left\{\delta^{(r)}\right\}=[\Phi]\{q\} \tag{64}$$

where $[\Phi]$ represents the square matrix for eigenvectors of the linear system and $\{q\}$ is a time-related vector.

Substituting Eq. (64) into (63) and multiplying by $[\Phi]^T$, one obtains

$$[\Phi]^T\left[M^{(r)}\right][\Phi]\{\ddot{q}\}+[\Phi]^T\left[K^{(r)}\right][\Phi]\{q\}+[\Phi]^T\left[K_{NL3}^{(r)}\right]\left([\Phi]\{q\}\right)^{\otimes 3}=\{0\} \tag{65}$$

The matrix product $[\Phi]^T\left[M^{(r)}\right][\Phi]$ and $[\Phi]^T\left[K^{(r)}\right][\Phi]$ represent diagonal matrices, written as $\left[M^{(D)}\right]$ and $\left[K^{(D)}\right]$, respectively. The system of Eqs. (65) becomes

$$\left[M^{(D)}\right]\{\ddot{q}\}+\left[K^{(D)}\right]\{q\}+[\Phi]^T\left[K_{NL3}^{(r)}\right]\left([\Phi]\{q\}\right)^{\otimes 3}=\{0\} \tag{66}$$

Eq. (66) can then be written as:

$$m_{ii}\,\ddot{q}_i+k_{ii}\,q_i+\sum_j\sum_k\sum_s \mathbb{k}_{ijks}\,q_j\,q_k\,q_s=0 \tag{67}$$

With $[\mathbb{k}]=[\Phi]^T\left[K_{NL3}^{(r)}\right]\left[\Phi^3\right]$

Let us now consider that

$$\Lambda_{ij}=\sum_k\sum_s \mathbb{k}_{ijks}\,q_k\,q_s \tag{68}$$

By introducing Eq. (68) into Eq. (67), one obtains [2]:

$$m_{ii}\,\ddot{q}_i + k_{ii}\,q_i + \sum_j \Lambda_{ij}\,q_j = 0 \tag{69}$$

By neglecting the cross-terms in the tensor $[\Lambda]$, Eq. (69) becomes

$$m_{ii}\,\ddot{q}_i + \left(k_{ii} + \Lambda_{ii}\right) q_i = 0 \tag{70}$$

Eq. (70) can be solved using the direct iteration method; the step-by-step procedure is stated as follows:

(1) Scale up the amplitude ratio A/h and multiply the desired value by the normalized first-mode shape vector.

(2) Determine matrix Λ_{ij} using the scaled-up eigenvector and applying numerical integration.

(3) Solve the nonlinear eigenvalue equation (Eq.(70)) and obtain the new frequency and the new corresponding eigenvector.

(4) Repeat steps (1)–(3) until convergence; the accuracy of the resulting frequency reached 10^{-5}.

4.6. Results and discussion

Before beginning our analysis of the results, we conducted a convergence test and a validation study to quantify the accuracy of this hybrid method and the rigor of the model developed above. The obtained linear frequency of vibration was compared with those of three cases calculated using numerical analysis, two of which are performed by ANSYS (case 1 and 2). The results are shown in Fig.4.3, Table 4.1 and Table 4.2. Validation of the nonlinear results as well as presentation of the effects of various parameters on the dynamic behavior of the cylindrical shells are discussed while referring to cases 4, 5, 6 and 7. The different cases are defined as follows:

- ✓ **Case 1:** A clamped-free cylindrical shell with an axial length $L = 0.231\ \text{m}$, radius $R = 7.725\ \text{cm}$ and thickness $h = 1.5\ \text{mm}$. The mechanical characteristics of the shell are, respectively: Young's modulus $E = 206\ \text{GPa}$, Poisson's ratio $\nu = 0.3$ and density $\rho = 7800\ \text{kg/m}^3$.

- ✓ **Case 2:** A cylindrical shell clamped at both ends. Its geometrical and mechanical proprieties are, respectively: axial length $L = 0.664$ m, rayon $R = 0.175$ m, thickness $h = 1$ mm, Young's modulus $E = 206$ GPa, Poisson's ratio $\nu = 0.3$ and density $\rho = 7680\ \text{kg/m}^3$.

- ✓ **Case 3:** A cylindrical shell clamped at both ends. Its geometrical and mechanical proprieties are respectively: $L/R = 20$ and $h/R = 0.01$, Young's modulus $E = 200$ GPa, Poisson's ratio $\nu = 0.3$ and density $\rho = 7850\ \text{kg/m}^3$.

- ✓ **Case 4:** A simply-supported $(u = v = w = 0, \text{ and } \partial w/\partial x \neq 0)$, axisymmetric isotropic cylindrical shell with the following dimensions: $L = 0.04$ m, $R = 2.54E-02$ m, $h = 0.254E\text{-}03$ m, and mechanical properties: $E = 205$ GPa, $\nu = 0.3$ and $\rho = 7833.57\ \text{kg/m}^3$. The number of axial and circumferential waves in this case is, respectively $m = 1$ and $n = 4$.

- ✓ **Case 5:** A freely simply-supported cylindrical shell $(v = w = 0,\ u \neq 0 \text{ et } \partial w/\partial x \neq 0)$ with the following characteristics: $\psi = \left(n^2 h/R\right)^2 = 1.0$, $\xi = \pi R m/(nL) = 2.0$ and $\nu = 0.3$.

- ✓ **Case 6:** A freely simply-supported cylindrical shell $(v = w = 0,\ u \neq 0 \text{ et } \partial w/\partial x \neq 0)$ with the following properties: $\psi = \left(n^2 h/R\right)^2 = 1.0$, and $\xi = \pi R m/(nL) = 0.5$ and $\nu = 0.3$.

- ✓ **Case 7:** A freely simply- supported cylindrical shell $(v = w = 0,\ u \neq 0 \text{ et } \partial w/\partial x \neq 0)$ with the following properties: $\psi = \left(n^2 h/R\right)^2 = 0.01$, and $\xi = \pi R m/(nL) = 2.0$ and $\nu = 0.3$.

4.6.1. Convergence test

The hybrid approach, presented above to model the linear dynamic behavior of axially thin cylindrical shells, provides very accurate results using a small number of finite elements [9]. The convergence study consists of determining the relative error of natural frequencies as a function of the number of finite elements (see Fig.4.3). The first set of calculations was depicted using the shell of case 1. Fig.4.3 shows the variation of the percentage error of natural frequencies relative to the requisite mesh size (30 F.E) $(\omega_{NFE}-\omega_{30FE})/\omega_{NFE}\times 100$ versus the number of cylindrical finite elements. The results were calculated using a regular mesh for four axial modes from $m=1$ to 4 and for two fundamental circumferential modes $n=2$ and 3.

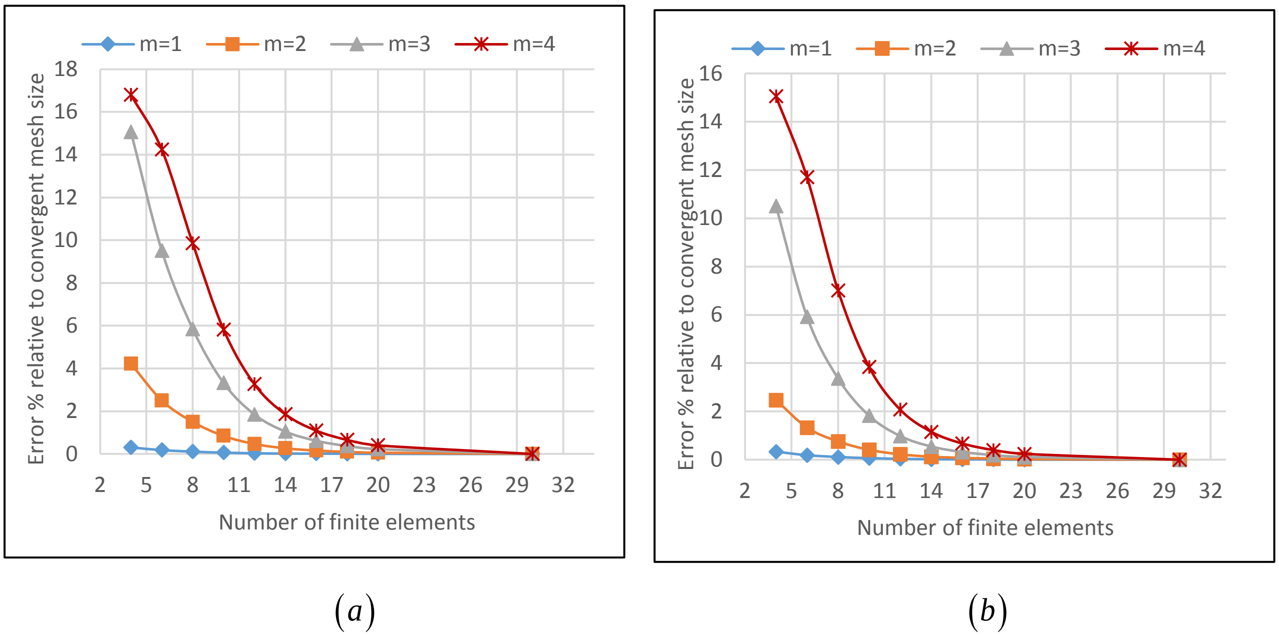

Figure 4.3: Variation of the relative error of natural frequencies versus the number of cylindrical finite elements (a) $n=2$, (b) $n=3$ with $Error(\%)=(\omega_{NFE}-\omega_{30FE})/\omega_{NFE}\times 100$

It is clear from the figure that the fundamental mode requires a very small number of finite elements, while the higher modes require a more refined mesh. This phenomenon is observed for the two numbers of circumferential waves considered in this case. Based on these results, we can conclude that, in the case of our model, only 20 finite elements are sufficient to ensure convergence for the case of cylindrical shells.

4.6.2. Linear free vibration of cylindrical shell

The second example studied here is related to case 2. Validation of our linear model is obtained by comparing the natural frequencies resulting from a numerical analysis carried out by ANSYS and those found using the linear hybrid FEM developed by Lakis and Paidoussis [9], for which only 20 elements are necessary to obtain good convergence. Excellent agreement between the two results is illustrated in Table 4.1.

Table 4.1: Comparison of the first five natural frequencies (Hz) of a thin cylindrical shell clamped on both ends [99]

Mode number		Frequency (Hz)	
m	n	ANSYS (Shell 63) Mesh (30×24)	Lakis and Paidoussis [9] 20 Hybrid FEM
1	4	380	380.6
	5	318	318.4
	6	340	340.3
	7	417	417.4
	8	528	528.1

Moreover, the nondimensional frequency parameter $\Omega = R\omega\sqrt{\left(1-\nu^2\right)\rho/E}$ for the isotropic cylindrical shell of case 3, obtained using the hybrid of finite element and classical shell theories developed by Lakis and Paidoussis [9], is compared with the beam modal function model as indicated in Table 4.2. The results demonstrate good agreement between the two methods.

Table 4.2: Comparison of the non-dimensional frequencies for an isotropic cylindrical shell clamped on both sides (m=1)

n	Lakis and Paidoussis [9] 30 Hybrid FEM	Masood and Ahmad [114]	Error(%)
2	0.013945	0.014062	-0.8417
3	0.022746	0.022732	0.0610
4	0.042425	0.042275	0.3537
5	0.068756	0.068117	0.9295

4.6.3. Nonlinear free vibration of cylindrical shell

4.6.3.1. Validation

Validation of the nonlinear model presented in this paper was first based on a comparative study highlighting the characteristics of nonlinear vibrations of the cylindrical shell of case 4, reported by Nowinski [78], Raju and Rao [91] and Selmane *et al.* [95] (see Fig.4.4). The numbers of axial and circumferential waves in this case are respectively $m=1$ and $n=4$. The fundamental frequency of natural linear vibration obtained in our study is 8536.091 Hz versus 8553.5972 Hz reported by Raju and Rao [91], which represents an error of 0.2%. From a first view of Fig.4.4, we notice a dependence between the nonlinear frequencies and the amplitude of oscillations.

This dependence is characterized by a hardening trend of the nonlinear behavior, which is demonstrated by an increase of the relative nonlinear frequency ω_{NL}/ω_L as the ratios A/h increase. These variations seem to be small for values of the ratio A/h below 1.0.

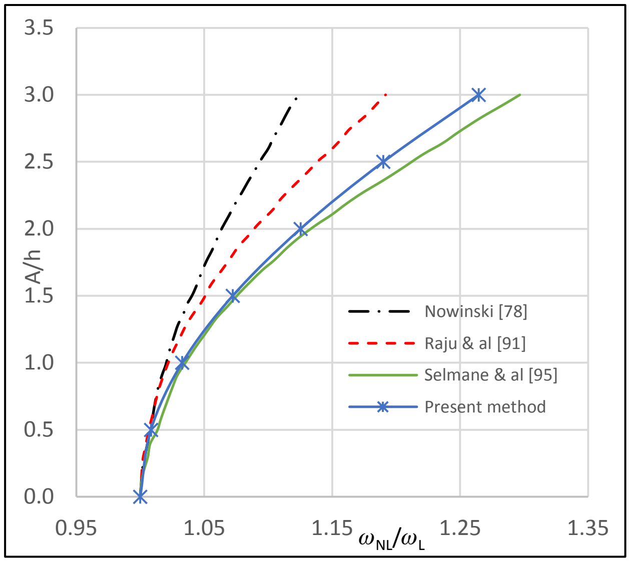

Figure 4.4: Evolution of the ratio ω_{NL}/ω_L as a function of A/h by comparing the present model to those of Nowinski [78], Raju & al [91] and to that of Selmane [95] with $m=1$ et $n=4$

It can be seen from the figure that the curve resulting from this study lies between those reported by Raju and Rao [91] and Selmane *et al.* [95], while being closer to the latter. We postulate that the difference between the results obtained by this study and those reported by Refs. 78, 91 and 95 may be due to the fact that Nowinski [78] used Donnell's type of nonlinearities in his study. He neglected in-plane inertia and assumed the mode shapes to have two components; a harmonic and a time-variable component. Alternatively, Raju and Rao [91] and Selmane *et al.* [95] employed Sander's theory, taking into account the nonlinear rotations around the normal to the surface plane. Moreover, Raju and Rao [91] expressed the displacements of components along the shell generator in polynomial form. The second example of comparison in this paper is shown in Fig.4.5. The cylindrical shell considered is that of case 5 and case 7. Fig.4.5(a) shows that the nonlinearity in this case leads to hardening-type characteristics. It highlights the variation of the relative nonlinear frequency as a function of dimensionless amplitude A/h calculated using the present method and compared it to the results of Atluri [83], Chu [76] and the work of Selmane *et al.* [95]. It can be seen that the curve resulting from this study is located between that of Chu and of Selmane *et al.*

We were able to ascertain that the differences between the curves might be due to the fact that the work of Atluri is based on Donnell's equations. He used a modal expansion for the normal displacement that satisfies the boundary conditions. He also employed the Galerkin technique to reduce the problem to a nonlinear ordinary differential equation for the modal amplitudes. As for Chu, he assumed a single mode, which satisfies the simple-support boundary conditions on w.

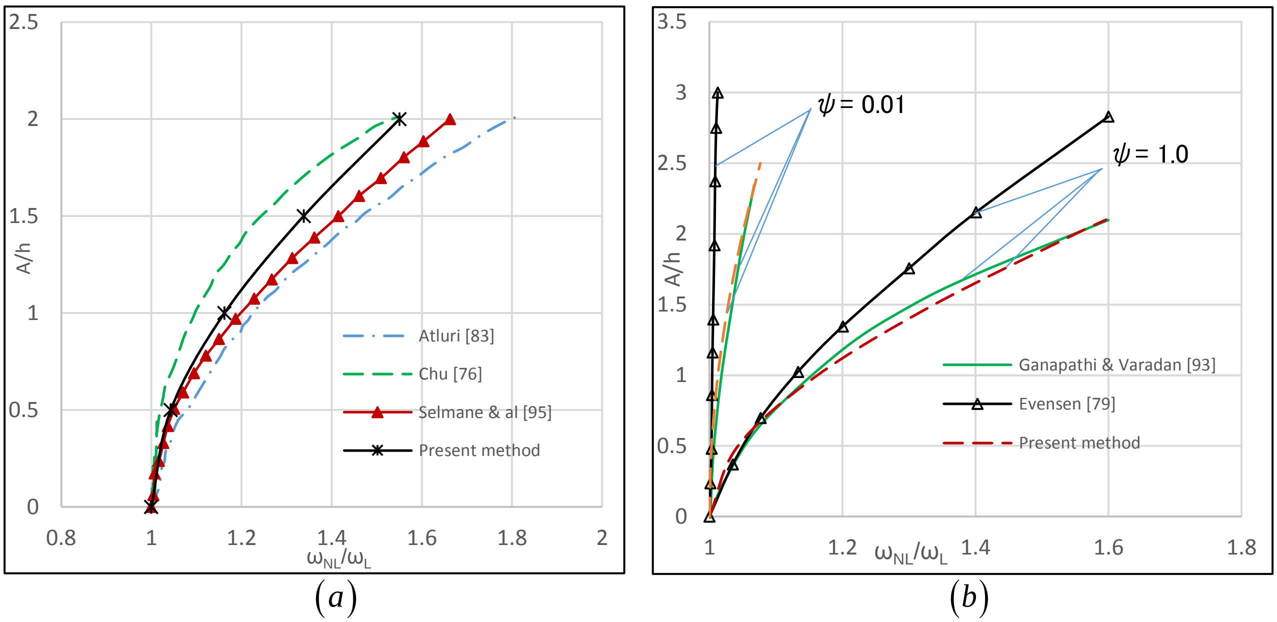

Figure 4.5: Characteristic of nonlinear vibrations relating to different methods for a freely simply supported cylindrical shell $(v=w=0)$, $\xi=(\pi Rm/(Ln))=2.0$, $\upsilon=0.3$, (a) $\psi=(n^2h/R)^2=1.0$, (b) $\psi=1.0$ and 0.01

However, the boundary conditions for the axial in-plane displacement u and the conditions of circumferential continuity of the circumferential in-plane displacement v were not satisfied. Numerical results for $\psi=1.0$ and $\psi=0.01$ presented in Fig.4.5(b) show the same nonlinear trend as Fig.4.5(a); a hardening behaviour is revealed. Comparison with Evensen's results [79] and those of Ganapathi and Varadan [93] demonstrates that the backbone curve of this study is very close to that reported in Ref. [93]. This is explained by the fact that Ganapathi and Varadan developed a finite element formulation to investigate the nonlinear free flexural vibrations of thin circular cylindrical shells using a C_0 continuous, QUAD-4 shear flexible shell element, based on the field consistency principle. Evensen, on the other hand, analyzed the nonlinear flexural vibrations of thin-walled circular cylinders by assuming two vibration modes. His equation was obtained using the Galerkin procedure. It is observed from Fig.4.5 that the results generated using the present method are in a good agreement with those of the other authors.

4.6.3.2. Effect of nonlinear coupling

The study of the dynamic behavior of geometrically nonlinear structures highlights the omnipresence of typically nonlinear phenomena, namely the phenomenon of coupling between modes. The case 4 example is considered in this section. It can be seen from Fig.4.6 that the curve exhibiting coupling is more pronounced than the curve without coupling, which shows that this phenomenon accentuates the hardening character of nonlinear vibrations. Moreover, coupling manifests itself by a transfer of energy between the different modes [115].

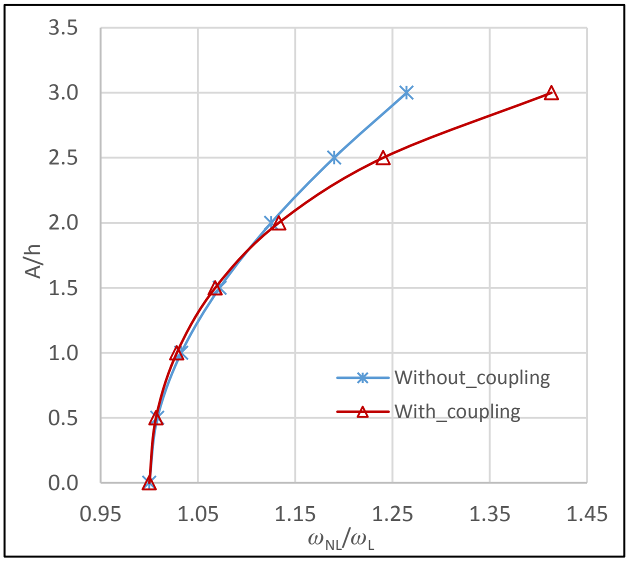

Figure 4.6: Coupling effect between the different modes, on the nonlinear dynamic behaviour of a simply-supported cylindrical shell $(u = v = w = 0,\ \text{and}\ \partial w/\partial x \neq 0)$

The figure also shows that the nonlinear coupling effect between different modes starts at the ratio $A/h = 2.0$ and becomes progressively more pronounced as the vibration amplitude becomes considerable.

4.6.3.3. Effect of axial wave number *m*

The effect of the axial mode on the nonlinear vibrations of the cylindrical shell defined in case 6 was investigated. Fig.4.7 presents the variation in the relative nonlinear frequency as a function of A/h for m varying from 1 to 5.

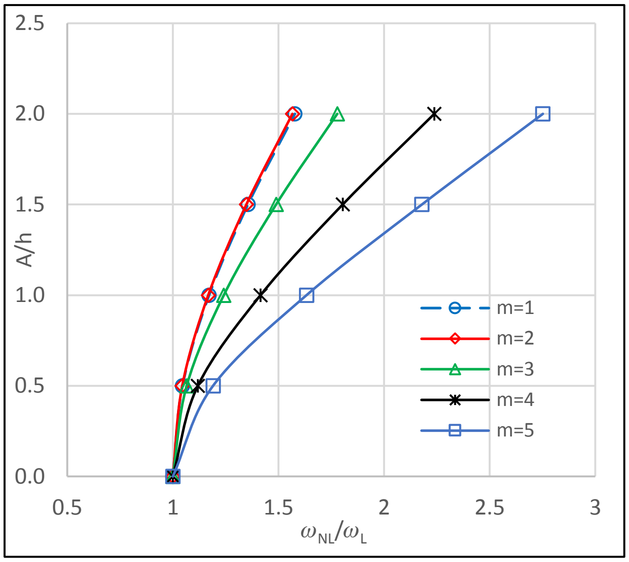

Figure 4.7: Variation of the relative nonlinear frequency ω_{NL}/ω_L as a function of the ratio A/h for different values of the axial mode m considering that $n=10$

The figure also indicates that the curves for $m=1$ and $m=2$ are almost coincident and deviate from the other curves. It can be seen that the nonlinear response becomes stronger for the higher axial modes. One can also notice that the gap revealed between the different curves increases as high frequencies (rising m) are reached.

4.6.3.4. Effect of circumferential wave number *n*

Fig.4.8 shows the variation of nonlinear frequency as a function of A/h for different circumferential mode numbers; $n=6-10$, for the freely simply-supported cylindrical shell of case 6. It can be seen from Fig.4.8(a) that for a fixed value of the ratio A/h, the relative nonlinear frequency increases as n increases, and the gap between the different curves is amplified when n is greater than 9. Moreover, the curve corresponding to $n=10$ turns out to be the most pronounced. Fig.4.8b shows that the linear frequencies decrease as a function of the number of circumferential waves up to a certain value and then increase further. (This is well illustrated in the figure when we examine the linear frequencies fluctuation along the vertical to the curve corresponding to $A/h=0$, for which the fundamental mode corresponds to $n=8$). By plotting the absolute frequencies against the non-dimensional amplitude of vibration, we notice that the curves corresponding to the different n overlap as the amplitude of vibration increases, illustrating a phenomenological behavior which stipulates that the fundamental frequency depends closely on the amplitude of the vibrations once we leave the domain of small vibrations. It can also be seen from Fig.4.8(b) that the minimum value of the frequency corresponds to $n=8$, for all the values of amplitude ratios $A/h \in [0,2[$. When A/h reaches the value 2.0, the minimum value of the frequency is assigned to mode $n=7$ ($f=1204.459$ Hz for $n=7$ vs $f=1207.016$ Hz for $n=8$). We deduce that nonlinear analysis of thin structures is a crucial step in order to characterize the system with more precision.

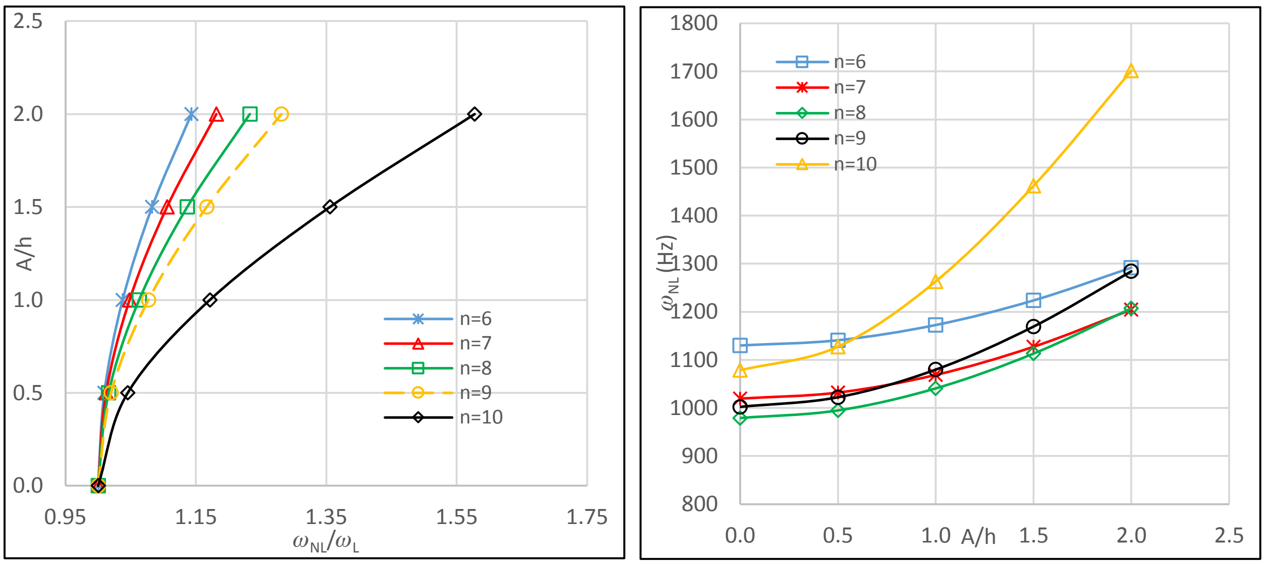

(a) (b)

Figure 4.8: Variation of nonlinear frequency for different circumferential wave numbers $(n=6-10)$ for a freely simply supported cylindrical shell: (a) backbone curve, (b) nonlinear frequency (Hz).

4.6.3.5. Geometry effect

In this section, we examine the effect of variation of geometric characteristics on the nonlinear dynamic behavior of thin-walled cylindrical shells. The study begins by examining the effect of varying the L/R ratio as a function of the nonlinear frequency while also varying the amplitude of oscillation. We then examine the evolution of the relative nonlinear frequency as a function of the structure thickness while taking into account the influence of vibration amplitude.

✓ *L/R Ratio effect*

By considering the shell mentioned in case 4 and varying the L/R ratio (L is variable and R is kept fixed) for the following different values: 0.5, 1.0, 1.57, 2.0, 2.5 and 3.0, we first follow the evolution of the relative nonlinear frequency ω_{NL}/ω_L for dimensionless amplitudes varying from 0.5 to 3.0 in steps of 0.5 (see Fig.4.9(a)). In a further step, we examine the fluctuation of the nonlinear frequency for the same range of variation of the ratio L/R (see Fig.4.9(b)).

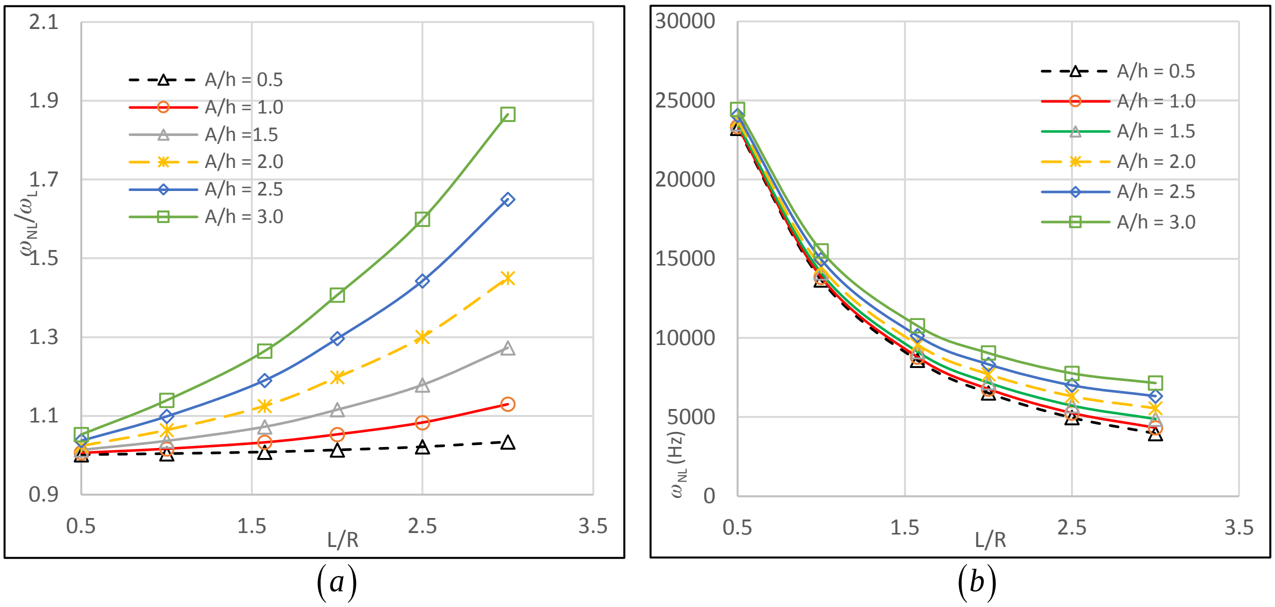

Figure 4.9: Variation of the nonlinear frequency (a) ω_{NL}/ω_L and (b) ω_{NL}, as a function of L/R for different values of the dimensionless amplitude A/h

Since the structure is slender, this last figure exhibits an exponential decrease in the nonlinear frequency. It can also be noted that for low values of the ratio L/R, the curves are tight, while the effect of the vibration amplitude increases as the length of the structure increases. Fig.4.9(a) shows the variation in the relative nonlinear frequency as a function of L/R. It can be seen that all the curves present an increasing pace, demonstrating a drastic decrease in linear frequency compared to nonlinear as the shells become more slender. The figure also shows a gradual increase in the gap between the different curves as the length of the shells increases. This highlights the effect of the vibration amplitude, which becomes considerable with augmentation of the structure's length (the curves are tight for low values of L/R and deviate as the structures increase in length).

✓ h/R *Ratio effect*

The cylindrical geometry and material properties are selected here to be the same as Case 4. This time, by varying the ratio h/R (the thickness is variable while the radius is kept constant), we investigate the effect of the shell's thickness on its nonlinear dynamic behavior for different values of the A/h ratio.

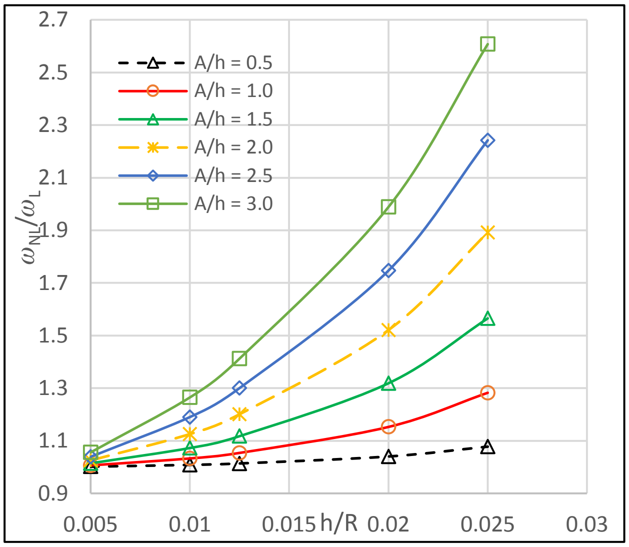

Figure 4.10: Variation of the relative nonlinear frequency ω_{NL}/ω_L as a function of h/R for different values of the dimensionless amplitude A/h

Fig.4.10 is plotted by choosing the following singular points of the ratio R/h : 200, 100, 80, 50 and 40. The dimensionless amplitude A/h increases from 0.5 to 3.0 in steps of 0.5. The figure shows that the relative nonlinear frequencies increase as the shell thickness becomes progressively bigger. As can be seen, thicker shells are more affected by increasing the nonlinear vibration amplitude. To illustrate this notion, we calculated the gap between the ratios ω_{NL}/ω_L corresponding to the dimensionless amplitudes $A/h = 1.0$ and $A/h = 3.0$. The gap between these relative nonlinear frequencies increases from 18.33% at $h/R = 0.01$ to reach 50.82% at $h/R = 0.025$.

4.6.3.6. Boundary conditions effect

In order to investigate the influence of the boundary conditions on the nonlinear free vibration behavior, the relative nonlinear frequencies ω_{NL}/ω_L were computed as a function of ratios A/h for the simply-supported cylindrical shell quoted in case 4. We examine the influence of various boundary conditions using Tong's convention as presented in Table 4.3.

Table 4.3: Different types of boundary conditions according to the Tong Convention [116]

Name	u	v	w	$\partial w/\partial x$
F	Free	Free	Free	Free
SS0	0	Free	Free	Free
SS1	Free	Free	0	Free
SS2	0	Free	0	Free
SS3	Free	0	0	Free
SS4	0	0	0	Free
CC1	Free	Free	0	0
CC2	0	Free	0	0
CC3	Free	0	0	0
CC4	0	0	0	0

Fig.4.11 clearly shows that this model has the advantage of supporting a variety of boundary conditions. An observation reveals a hardening trend in nonlinear behavior for all boundary conditions. It can also be seen from the curve that the more the degrees of freedom are constrained, the more the nonlinear behavior proves to be less hardening. This is clearly seen for the simply-supported case as well as for the clamped case (the relative nonlinear frequency increases for the same dimensionless amplitude as the boundaries are less restrictive).

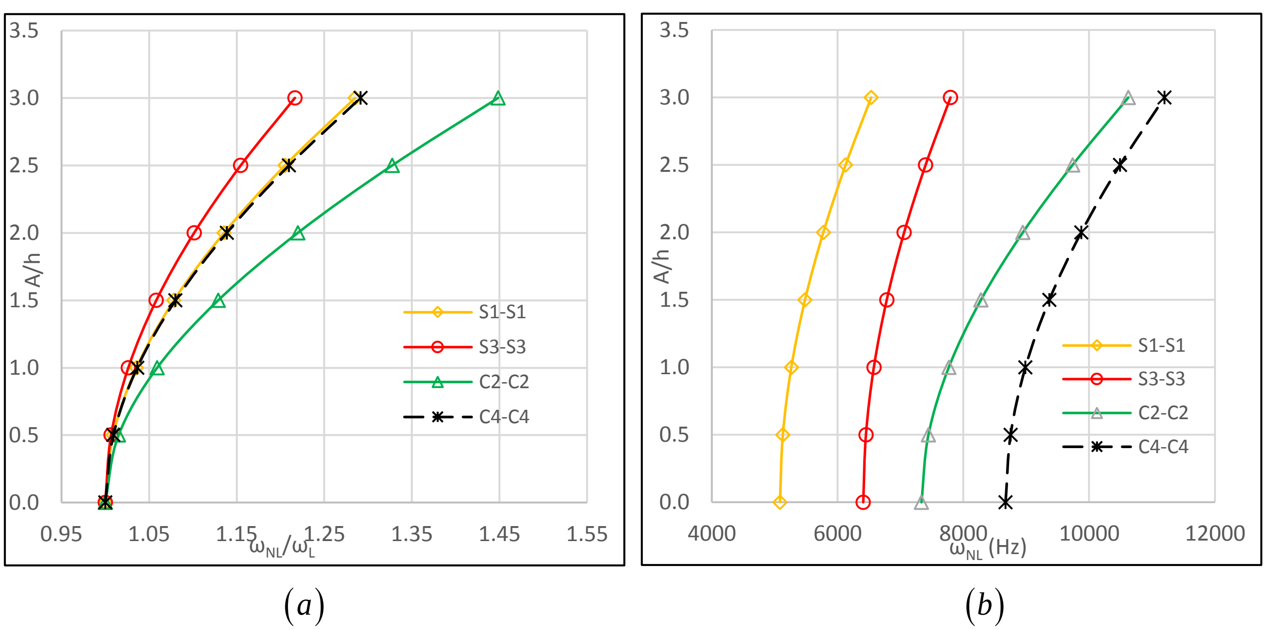

Figure 4.11: Variation of (a) the relative nonlinear frequency ω_{NL}/ω_L and (b) the nonlinear frequency as a function of A/h ratio for different boundary conditions

Therefore, we notice that the clamped C2–C2 boundary condition demonstrates a stronger hardening behavior than the clamped C4–C4 and the same behavior can be observed for the simply-supported shells S1–S1 in comparison to S3–S3. Fig.4.11(b) shows that the linear (corresponding to $A/h = 0$) and nonlinear frequencies increase when the boundary conditions are more restrictive. However, this evolution is not proportional for the case of two responses of different boundary conditions (C2–C2 vs C4–C4), which induces an evolution ratio whose value is different from 1.0. This aspect is well illustrated in Fig.4.11(a), which shows a more hardening behavior of the C2–C2 response compared to that of C4–C4, although the linear and nonlinear frequencies of the second case are higher than those of the first case. (See Fig.4.11(a)).

4.7. Conclusion

This study investigates the nonlinear free vibration of thin cylindrical shells employing Novozhilov nonlinear kinematics. This theory takes into consideration the curvature effect of the displacement field in the circumferential direction and also the initial geometric imperfections. The mathematical development used here highlights the influence of nonlinear coupling between the different modes and demonstrates that the equations of motion do not include quadratic terms because of the mechanical symmetry of the shell. The formulation began with a general form of the displacement field; this reveals that one of its strengths is the ability to support various forms of discretization. The mass and linear stiffness matrices are derived from a hybrid FEM for which the displacement functions are found from exact solution of Sander’s shell theory rather than approximated by polynomial functions. The nonlinear stiffness matrix is obtained based on the coefficients of the modal equations, which are employed by utilizing the strain-displacement relations of the Novozhilov nonlinear shell theory. The mass and stiffness matrices obtained apply to only one element. The global matrices are determined after superimposing the elementary matrices of the structure and introducing the boundary conditions. The governing equation of the motion has been derived using the Lagrange approach and solved by a direct iterative method. The nonlinear results are validated against those published in the literature and found to have very good agreement. The analysis therefore continues to study the effect of several parameters. Results show that an increase in the number of circumferential waves accentuates the hardening character of nonlinear dynamic behavior. It is also revealed that the fundamental frequency depends closely on the amplitude of vibration once we leave the domain of small vibrations. This study also shows that the relative nonlinear frequency increases when the shells are more slender or thicker. Finally, the model shows its ability to consider several boundary conditions and an analysis of case studies reveals that the nonlinear trend becomes more hardening when the edges are less constraining. The method developed in this paper may be applied to investigate the nonlinear response of cylindrical shells under dynamic loads.

4.8. Appendix

4.8.1. Appendix A

According to the Novozhilov nonlinear shell theory, β, ψ and χ are determined as follows:

$$\beta = -\frac{\partial(w+w_0)}{\partial x}\left(1+\frac{\partial u}{\partial x}+\frac{w}{R}\right)+\left(\frac{\partial(w+w_0)}{R\partial\theta}-\frac{v}{R}\right)\frac{\partial u}{R\partial\theta}-\frac{\partial w}{\partial x}\frac{w_0}{R} \qquad (A.1)$$

$$\psi = -\left(\frac{\partial(w+w_0)}{R\partial\theta}-\frac{v}{R}\right)\left(1+\frac{\partial u}{\partial x}\right)+\frac{\partial(w+w_0)}{\partial x}\frac{\partial v}{\partial x} \qquad (A.2)$$

$$\chi \cong \frac{\partial u}{\partial x}+\frac{\partial v}{R\partial\theta}+\frac{w+w_0}{R}+\frac{\partial u}{\partial x}\left(\frac{\partial v}{R\partial\theta}+\frac{w+w_0}{R}\right)-\frac{\partial u}{R\partial\theta}\frac{\partial v}{\partial x} \qquad (A.3)$$

The middle surface strain–displacement relationships corresponding to the Novozhilov nonlinear shell theory of circular shells

$$\varepsilon_{x,0} = \frac{\partial u}{\partial x}+\frac{1}{2}\left[\left(\frac{\partial u}{\partial x}\right)^2+\left(\frac{\partial v}{\partial x}\right)^2+\left(\frac{\partial w}{\partial x}\right)^2\right]+\frac{\partial w}{\partial x}\frac{\partial w_0}{\partial x}, \qquad (A.4)$$

$$\begin{aligned}\varepsilon_{\theta,0} = {} & \frac{\partial v}{R\partial\theta}+\frac{w}{R}+\frac{1}{2R^2}\left[\left(\frac{\partial u}{\partial\theta}\right)^2+\left(\frac{\partial v}{\partial\theta}+w\right)^2+\left(\frac{\partial w}{\partial\theta}-v\right)^2\right] \\ & +\frac{1}{R^2}\left[\frac{\partial w_0}{\partial\theta}\left(\frac{\partial w}{\partial\theta}-v\right)+w_0\left(w+\frac{\partial v}{\partial\theta}\right)\right],\end{aligned} \qquad (A.5)$$

$$\gamma_{x\theta,0} = \frac{\partial v}{\partial x}+\frac{\partial u}{R\partial\theta}+\frac{1}{R}\left[\frac{\partial u}{\partial x}\frac{\partial u}{\partial\theta}+\frac{\partial v}{\partial x}\left(\frac{\partial v}{\partial\theta}+w\right)+\left(\frac{\partial w}{\partial x}+\frac{\partial w_0}{\partial x}\right)\left(\frac{\partial w}{\partial\theta}-v\right)+\frac{\partial w}{\partial x}\frac{\partial w_0}{\partial\theta}+\frac{\partial v}{\partial x}w_0\right] \qquad (A.6)$$

$$k_x = -\frac{\partial^2 w}{\partial x^2} + \frac{\partial v}{R\partial x}\left(-\frac{\partial u}{R\partial\theta} + \frac{\partial v}{\partial x} - \frac{\partial^2 \left(w+w_0\right)}{\partial x\partial\theta}\right) + \frac{\partial\left(w+w_0\right)}{\partial x}\frac{\partial^2 u}{\partial x^2} + \frac{\partial^2 u}{R\partial x\partial\theta}\left(-\frac{v}{R} + \frac{\partial\left(w+w_0\right)}{R\partial\theta}\right)$$
$$+\frac{\partial^2\left(w+w_0\right)}{R\partial x\partial\theta}\frac{\partial u}{R\partial\theta} - \frac{\partial^2\left(w+w_0\right)}{\partial x^2}\left(\frac{w}{R} + \frac{\partial v}{R\partial\theta} + \frac{\partial u}{\partial x}\right) - \frac{\partial^2 w}{\partial x^2}\frac{w_0}{R}, \qquad (A.7)$$

$$k_\theta = -\frac{\partial^2 w}{R^2\partial\theta^2} + \frac{\partial u}{R\partial x} + \frac{\partial v}{R^2\partial\theta} - \frac{\left(w+w_0\right)}{R}\left(\frac{\partial^2 w}{R^2\partial\theta^2} - \frac{\partial v}{R^2\partial\theta} - 2\frac{\partial u}{R\partial x}\right) - \frac{w}{R}\left(\frac{\partial^2 w_0}{R^2\partial\theta^2}\right)$$
$$-\frac{\partial u}{R^2\partial\theta}\left(\frac{\partial u}{R\partial\theta} + \frac{\partial v}{\partial x} + \frac{\partial^2\left(w+w_0\right)}{\partial x\partial\theta}\right) + \frac{\partial v}{R^2\partial\theta}\left(\frac{\partial v}{R\partial\theta} + 3\frac{\partial u}{\partial x} - \frac{\partial^2\left(w+w_0\right)}{R\partial\theta^2}\right)$$
$$+\frac{\partial^2 v}{R^3\partial\theta^2}\left(\frac{\partial\left(w+w_0\right)}{\partial\theta} - v\right) + \frac{\partial\left(w+w_0\right)}{R^2\partial\theta}\left(-\frac{v}{R} + \frac{\partial w}{R\partial\theta}\right) - \frac{\partial^2\left(w+w_0\right)}{R^2\partial\theta^2}\frac{\partial u}{\partial x}$$
$$+\frac{\partial w}{R^2\partial\theta}\frac{\partial w_0}{R\partial\theta} + \frac{\partial\left(w+w_0\right)}{\partial x}\frac{\partial^2 v}{R\partial x\partial\theta} + \frac{\partial v}{\partial x}\frac{\partial^2\left(w+w_0\right)}{R\partial x\partial\theta}, \qquad (A.8)$$

$$k_{x\theta} = -2\frac{\partial^2 w}{R\partial x\partial\theta} - \frac{\partial u}{R^2\partial\theta} + \frac{\partial v}{R\partial x} + \frac{\partial u}{R^2\partial\theta}\left(-\frac{\partial u}{\partial x} + \frac{\partial^2\left(w+w_0\right)}{R\partial\theta^2} - \frac{\partial v}{R\partial\theta}\right) + \frac{\partial^2\left(w+w_0\right)}{\partial x^2}\frac{\partial v}{\partial x}$$
$$-\frac{v}{R^2}\left(\frac{\partial^2 u}{R\partial\theta^2} + \frac{\partial^2 v}{\partial x\partial\theta} + \frac{\partial\left(w+w_0\right)}{\partial x}\right) + \frac{\partial\left(w+w_0\right)}{R^2\partial\theta}\left(\frac{\partial^2 u}{R\partial\theta^2} + \frac{\partial w}{\partial x} + \frac{\partial^2 v}{\partial x\partial\theta}\right) + \frac{\partial w}{R^2\partial\theta}\frac{\partial w_0}{\partial x}$$
$$+\frac{\partial v}{R\partial x}\left(\frac{w+w_0}{R} + 2\frac{\partial v}{R\partial\theta} - \frac{\partial^2\left(w+w_0\right)}{R\partial\theta^2} + 2\frac{\partial u}{\partial x}\right) + \frac{\partial\left(w+w_0\right)}{\partial x}\left(\frac{\partial^2 u}{R\partial x\partial\theta} + \frac{\partial^2 v}{\partial x^2}\right)$$
$$-2\frac{\partial^2\left(w+w_0\right)}{R\partial x\partial\theta}\left(\frac{w}{R} + \frac{\partial v}{R\partial\theta} + \frac{\partial u}{\partial x}\right) - 2\frac{\partial^2 w}{R^2\partial x\partial\theta}w_0. \qquad (A.9)$$

By introducing the displacement functions (4a)–(4c) into the middle surface strain–displacement relationships of Novozhilov (A.4)–(A.9), one obtains for $\varepsilon_{x,0}$:

$$\varepsilon_{x,0} = \sum_i q_i f_{i,1} + \frac{1}{2}\left[\left(\sum_i q_i f_{i,1}\right)^2 + \left(\sum_i q_i g_{i,1}\right)^2 + \left(\sum_i q_i h_{i,1}\right)^2\right] + \sum_i q_i h_{i,1}\sum_j \delta_j h_{j,1}. \qquad (A.10)$$

By further developing this expression, we obtain:

$$\varepsilon_{x,0} = \sum_i q_i f_{i,1} + \frac{1}{2}\left[\sum_i\sum_j f_{i,1}f_{j,1}q_i q_j + \sum_i\sum_j g_{i,1}g_{j,1}q_i q_j + \sum_i\sum_j h_{i,1}h_{j,1}q_i q_j\right] + \sum_i h_{i,1}\left(\sum_j \delta_j h_{j,1}\right)q_i. \quad (A.11)$$

A simplification of this expression leads to

$$\varepsilon_{x,0} = \sum_i \left[f_{i,1} + h_{i,1}\left(\sum_j \delta_j h_{j,1}\right)\right] q_i + \sum_i \sum_j \frac{1}{2}\left[f_{i,1} f_{j,1} + g_{i,1} g_{j,1} + h_{i,1} h_{j,1}\right] q_i q_j . \qquad (A.12)$$

The expression then takes the form of (see Eq. (15) in the main text)

$$\varepsilon_{x,0} = \sum_i a_i q_i + \sum_i \sum_j A_{ij} q_i q_j ,$$

where

$$a_i = f_{i,1} + h_{i,1}\left(\sum_j \delta_j h_{j,1}\right), \qquad (A.13a)$$

$$A_{ij} = \frac{1}{2}\left[f_{i,1} f_{j,1} + g_{i,1} g_{j,1} + h_{i,1} h_{j,1}\right]. \qquad (A.13b)$$

We then follow the same strategy to determine the other strain–displacement relationships. We find that

$$\varepsilon_{\theta,0} = \varepsilon_{22} = \sum_i b_i q_i + \sum_i \sum_j B_{ij} q_i q_j , \qquad (A.14)$$

where

$$b_i = \frac{1}{R}\left(g_{i,2} + h_i\right) + \frac{1}{R^2}\left(\left(h_{i,2} - g_i\right)\left(\sum_j \delta_j h_{j,2}\right) + \left(h_i + g_{i,2}\right)\left(\sum_j \delta_j h_j\right)\right), \qquad (A.15a)$$

$$B_{ij} = \frac{1}{2R^2}\left[f_{i,2} f_{j,2} + \left(h_i + g_{i,2}\right)\left(h_j + g_{j,2}\right) + \left(h_{i,2} - g_i\right)\left(h_{j,2} - g_j\right)\right], \qquad (A.15b)$$

$$\varepsilon_{x\theta,0} = \varepsilon_{12} = \sum_i c_i q_i + \sum_i \sum_j C_{ij} q_i q_j \ , \qquad (A.16)$$

where

$$c_i = \frac{1}{2}\left[g_{i,1} + \frac{1}{R} f_{i,2} + \frac{1}{R}\left(h_{i,2} - g_i\right)\left(\sum_j \delta_j h_{j,1}\right) + \frac{1}{R} g_{i,1}\left(\sum_j \delta_j h_j\right) + \frac{1}{R} h_{i,1}\left(\sum_j \delta_j h_{j,2}\right)\right], \qquad (A.17a)$$

$$C_{ij} = \frac{1}{2R}\left[f_{i,1} f_{j,2} + g_{i,1} g_{j,2} + g_{i,1} h_j + h_{i,1} h_{j,2} - h_{i,1} g_j \right], \qquad (A.17b)$$

$$k_{x,0} = k_{11} = \sum_i p_i q_i + \sum_i \sum_j P_{ij} q_i q_j , \qquad (A.18)$$

Where

$$p_i = -h_{i,11} + \left(-\frac{1}{R} g_{i,1} + \frac{1}{R^2} f_{i,2}\right)\left(\sum_j \delta_j h_{j,12}\right) + f_{i,11}\left(\sum_j \delta_j h_{j,1}\right) + \frac{1}{R^2} f_{i,12}\left(\sum_j \delta_j h_{j,2}\right)$$
$$-\left(\frac{1}{R} h_i + \frac{1}{R} g_{i,2} + f_{i,1}\right)\left(\sum_j \delta_j h_{j,11}\right) - \frac{1}{R} h_{i,11}\left(\sum_j \delta_j h_j\right), \qquad (A.19a)$$

$$P_{ij} = \frac{1}{R} g_{i,1}\left(-\frac{1}{R} f_{j,2} + g_{j,1} - h_{j,12}\right) + h_{i,1} f_{j,11} - \frac{1}{R^2} f_{i,12} g_j + \frac{1}{R^2} f_{i,12} h_{j,2} + \frac{1}{R^2} h_{i,12} f_{j,2}$$
$$-h_{i,11}\left(\frac{1}{R} h_j + \frac{1}{R} g_{j,2} + f_{j,1}\right), \qquad (A.19b)$$

$$k_{\theta,0} = k_{22} = \sum_i s_i q_i + \sum_i \sum_j S_{ij} q_i q_j \;, \qquad (A.20)$$

$$s_i = -\frac{1}{R^2} h_{i,22} + \frac{1}{R} f_{i,1} + \frac{1}{R^2} g_{i,2} + \left(\sum_j \delta_j h_j\right)\left(-\frac{1}{R^3} h_{i,22} + \frac{1}{R^3} g_{i,2} + \frac{2}{R^2} f_{i,1}\right)$$
$$+\left(\sum_j \delta_j h_{j,22}\right)\left(-\frac{1}{R^3} h_i - \frac{1}{R^3} g_{i,2} - \frac{1}{R^2} f_{i,1}\right) + \left(\sum_j \delta_j h_{j,12}\right)\left(-\frac{1}{R^2} f_{i,2} + \frac{1}{R} g_{i,1}\right)$$
$$+\left(\sum_j \delta_j h_{j,2}\right)\left(\frac{1}{R^3} g_{i,22} - \frac{1}{R^3} g_i + \frac{2}{R^3} h_{i,2}\right) + \left(\sum_j \delta_j h_{j,1}\right)\frac{1}{R} g_{i,12}, \qquad (A.21a)$$

$$S_{ij} = h_i\left[-\frac{1}{R^3} h_{j,22} + \frac{1}{R^3} g_{j,2} + \frac{2}{R^2} f_{j,1}\right] - f_{i,2}\left[\frac{1}{R^3} f_{j,2} + \frac{1}{R^2} g_{j,1} + \frac{1}{R^2} h_{j,12}\right]$$
$$+g_{i,2}\left[\frac{1}{R^3} g_{j,2} + \frac{3}{R^2} f_{j,1} - \frac{1}{R^3} h_{j,22}\right] + g_{i,22}\left[\frac{1}{R^3} h_{j,2} - \frac{1}{R^3} g_j\right] + h_{i,2}\left[-\frac{1}{R^3} g_j + \frac{1}{R^3} h_{j,2}\right]$$
$$-\frac{1}{R^2} h_{i,22} f_{j,1} + \frac{1}{R} h_{i,1} g_{j,12} + \frac{1}{R} g_{i,1} h_{j,12} \;, \qquad (A.21b)$$

$$k_{x\theta,0} = k_{12} = \sum_i t_i q_i + \sum_i \sum_j T_{ij} q_i q_j \;, \qquad (A.22)$$

where

$$t_i = \frac{-2}{R} h_{i,12} - \frac{1}{R^2} f_{i,2} + \frac{1}{R} g_{i,1} + \left(\sum_j \delta_j h_{j,22}\right)\left(\frac{1}{R^3} f_{i,2} - \frac{1}{R^2} g_{i,1}\right) + g_{i,1}\left(\sum_j \delta_j h_{j,11}\right)$$
$$+\left(\sum_j \delta_j h_{j,1}\right)\left(-\frac{1}{R^2} g_i + \frac{1}{R^2} h_{i,2} + \frac{1}{R} f_{i,12} + g_{i,11}\right) + \left(\sum_j \delta_j h_{j,2}\right)\left(\frac{1}{R^3} f_{i,22} + \frac{1}{R^2} h_{i,1} + \frac{1}{R^2} g_{i,12}\right)$$
$$+\left(\sum_j \delta_j h_j\right)\left(\frac{1}{R^2} g_{i,1} - \frac{2}{R^2} h_{i,12}\right) + \left(\sum_j \delta_j h_{j,12}\right)\left(-\frac{2}{R^2} h_i - \frac{2}{R^2} g_{i,2} - \frac{2}{R} f_{i,1}\right), \tag{A.23a}$$

$$T_{ij} = f_{i,2}\left(-\frac{1}{R^2} f_{j,1} + \frac{1}{R^3} h_{j,22} - \frac{1}{R^3} g_{j,2}\right) + h_{i,11} g_{j,1} - g_i\left(\frac{1}{R^3} f_{j,22} + \frac{1}{R^2} g_{j,12} + \frac{1}{R^2} h_{j,1}\right)$$
$$+h_{i,2}\left(\frac{1}{R^3} f_{j,22} + \frac{1}{R^2} h_{j,1} + \frac{1}{R^2} g_{j,12}\right) + g_{i,1}\left(\frac{1}{R^2} h_j + \frac{2}{R^2} g_{j,2} - \frac{1}{R^2} h_{j,22} + \frac{2}{R} f_{j,1}\right) + h_{i,1}\left(\frac{1}{R} f_{j,12} + g_{j,11}\right)$$
$$-h_{i,12}\left(\frac{2}{R^2} h_j + \frac{2}{R^2} g_{j,2} + \frac{2}{R} f_{j,1}\right). \tag{A.23b}$$

The coefficients $a_i, b_i, c_i, \ldots$etc. are functions of the spatial coordinates x, θ and are obtained from the strain–displacement relations of the Novozhilov nonlinear shell theory.

Equations (18)–(26) lead to

$$b_{ij} = b_i\, b_j,\; B_{ijk} = b_i\, B_{jk} + b_j\, B_{ki} + b_k\, B_{ij},\; B_{ijks} = 2 B_{jk}\, B_{is} \tag{A.24}$$

$$c_{ij} = c_i\, c_j,\; C_{ijk} = c_i\, C_{jk} + c_j\, C_{ik} + c_k\, C_{ji},\; C_{ijks} = 2 C_{jk}\, C_{is} \tag{A.25}$$

$$p_{ij} = p_i\, p_j,\; P_{ijk} = p_i\, P_{jk} + p_j\, P_{ik} + p_k\, P_{ji},\; P_{ijks} = 2 P_{jk}\, P_{is} \tag{A.26}$$

$$s_{ij} = s_i\, s_j,\; S_{ijk} = s_i\, S_{jk} + s_j\, S_{ik} + s_k\, S_{ji},\; S_{ijks} = 2 S_{jk}\, S_{is} \tag{A.27}$$

$$t_{ij} = t_i\, t_j,\; T_{ijk} = t_i\, T_{jk} + t_j\, T_{ik} + t_k\, T_{ji},\; T_{ijks} = 2 T_{is}\, T_{jk} \tag{A.28}$$

$$d_{ij} = b_i\, a_j,\; D_{ijk} = b_i\, A_{jk} + a_j\, B_{ki} + a_k\, B_{ij},\; D_{ijks} = 2 A_{jk}\, B_{is} \tag{A.29}$$

$$e_{ij} = a_i\, b_j,\; E_{ijk} = a_i\, B_{jk} + b_j\, A_{ki} + b_k\, A_{ij},\; E_{ijks} = 2 A_{is}\, B_{jk} \tag{A.30}$$

$$u_{ij} = p_j\, s_i,\; U_{ijk} = s_i\, P_{jk} + p_j\, S_{ik} + p_k\, S_{ji},\; U_{ijks} = 2 P_{jk}\, S_{is} \tag{A.31}$$

$$v_{ij} = p_i\, s_j,\; V_{ijk} = s_j\, P_{ik} + s_k\, P_{ji} + p_i\, S_{jk},\; V_{ijks} = 2 P_{is}\, S_{jk} \tag{A.32}$$

All coefficients in the nonlinear modal equations (29) can now be computed, once suitable trial functions f_i, g_i, h_i, are chosen.

4.8.2. Appendix B

Matrix $[P]$:

The elasticity matrix $[P]$ of order (6×6) for an anisotropic material is expressed as

$$[P]=\begin{bmatrix} P_{11} & P_{12} & 0 & P_{14} & P_{15} & 0 \\ P_{21} & P_{22} & 0 & P_{24} & P_{25} & 0 \\ 0 & 0 & P_{33} & 0 & 0 & P_{36} \\ P_{41} & P_{42} & 0 & P_{44} & P_{45} & 0 \\ P_{51} & P_{52} & 0 & P_{54} & P_{55} & 0 \\ 0 & 0 & P_{63} & 0 & 0 & P_{66} \end{bmatrix}. \qquad (B.1)$$

In the case of isotropic material, the matrix of elasticity becomes

$$[P]=\begin{bmatrix} C & \nu C & 0 & 0 & 0 & 0 \\ \nu C & C & 0 & 0 & 0 & 0 \\ 0 & 0 & \frac{C(1-\nu)}{2} & 0 & 0 & 0 \\ 0 & 0 & 0 & D & \nu D & 0 \\ 0 & 0 & 0 & \nu D & D & 0 \\ 0 & 0 & 0 & 0 & 0 & \frac{D(1-\nu)}{2} \end{bmatrix}, \qquad (B.2)$$

Where $C=\dfrac{Eh}{1-\nu^2}$, $D=\dfrac{Eh^3}{12(1-\nu^2)}$, E is Young's modulus, ν is Poisson's ratio and h is the shell thickness.

After integrating each component of the stress vector over the thickness of the shell, the normal stress resultant and moment resultant for an isotropic cylindrical shell can be written as

$$\{\sigma\} = \begin{Bmatrix} N_x \\ N_\theta \\ N_{x\theta} \\ M_x \\ M_\theta \\ M_{x\theta} \end{Bmatrix} = [P] \begin{Bmatrix} \varepsilon_x \\ \varepsilon_\theta \\ 2\varepsilon_{x\theta} \\ k_x \\ k_\theta \\ 2k_{x\theta} \end{Bmatrix}. \tag{B.3}$$

Sander's linear equations for thin anisotropic cylindrical shell in terms of axial, tangential, and circumferential displacements are as follows:

$$L_1\left(U,V,W,P_{ij}\right) = P_{11}\frac{\partial^2 U}{\partial x^2} + \frac{P_{12}}{R}\frac{\partial^2 U}{\partial x^2}\left(\frac{\partial^2 V}{\partial x\partial\theta} + \frac{\partial W}{\partial x}\right) - P_{14}\frac{\partial^3 W}{\partial x^3} + \frac{P_{15}}{R^2}\left(\frac{\partial^3 W}{\partial x\partial\theta^2} + \frac{\partial^2 V}{\partial x\partial\theta}\right)$$
$$+\left(\frac{P_{33}}{R} - \frac{P_{63}}{2R^2}\right)\left(\frac{\partial^2 V}{\partial x\partial\theta} + \frac{1}{R}\frac{\partial^2 U}{\partial\theta^2}\right) + \left(\frac{P_{36}}{R^2} - \frac{P_{66}}{2R^3}\right)\left(-2\frac{\partial^3 W}{\partial x\partial\theta^2} + \frac{3}{2}\frac{\partial^2 V}{\partial x\partial\theta} - \frac{1}{2R}\frac{\partial^2 U}{\partial\theta^2}\right), \tag{B.4}$$

$$L_2\left(U,V,W,P_{ij}\right) = \left(\frac{P_{21}}{R} - \frac{P_{51}}{R^2}\right)\frac{\partial^2 U}{\partial x\partial\theta} + \frac{1}{R}\left(\frac{P_{22}}{R} + \frac{P_{52}}{R^2}\right)\left(\frac{\partial^2 V}{\partial\theta^2} + \frac{\partial W}{\partial\theta}\right) - \left(\frac{P_{24}}{R} + \frac{P_{54}}{R^2}\right)\frac{\partial^3 W}{\partial x^2\partial\theta}$$
$$+\frac{1}{R^2}\left(\frac{P_{25}}{R} + \frac{P_{55}}{R^2}\right)\left(-\frac{\partial^3 W}{\partial\theta^3} + \frac{\partial^2 V}{\partial\theta^2}\right) + \left(P_{33} + \frac{3P_{63}}{2R}\right)\left(\frac{\partial^2 V}{\partial x^2} + \frac{\partial^2 U}{R\partial x\partial\theta}\right)$$
$$+\frac{1}{R}\left(P_{36} + \frac{3P_{66}}{2R}\right)\left(-2\frac{\partial^3 W}{\partial x^2\partial\theta} + \frac{3}{2}\frac{\partial^2 V}{\partial x^2} - \frac{1}{2R}\frac{\partial^2 U}{\partial x\partial\theta}\right), \tag{B.5}$$

$$L_3\left(U,V,W,P_{ij}\right) = P_{41}\frac{\partial^3 U}{\partial x^3} + \frac{P_{42}}{R}\left(\frac{\partial^3 V}{\partial x^2\partial\theta} + \frac{\partial^2 W}{\partial x^2}\right) - P_{44}\frac{\partial^4 W}{\partial x^4} + \frac{P_{45}}{R^2}\left(-\frac{\partial^4 W}{\partial x^2\partial\theta^2} + \frac{\partial^3 V}{\partial x^2\partial\theta}\right)$$
$$+\frac{2P_{63}}{R}\left(\frac{1}{R}\frac{\partial^3 U}{\partial x\partial\theta^2} + \frac{\partial^3 V}{\partial x^2\partial\theta}\right) + \frac{2P_{66}}{R^2}\left(-2\frac{\partial^4 W}{\partial x^2\partial\theta^2} + \frac{3}{2}\frac{\partial^3 V}{\partial x^2\partial\theta} - \frac{1}{2R}\frac{\partial^3 U}{\partial x\partial\theta^2}\right) + \frac{P_{51}}{R^2}\frac{\partial^3 U}{\partial x\partial\theta^2}$$
$$+\frac{P_{52}}{R^3}\left(\frac{\partial^3 V}{\partial\theta^3} + \frac{\partial^2 W}{\partial\theta^2}\right) + \frac{P_{55}}{R^4}\left(-\frac{\partial^4 W}{\partial\theta^4} + \frac{\partial^3 V}{\partial\theta^3}\right) - \frac{P_{21}}{R}\frac{\partial U}{\partial x} - \frac{P_{54}}{R^2}\frac{\partial^4 W}{\partial x^2\partial\theta^2} + \frac{P_{22}}{R^2}\left(\frac{\partial V}{\partial\theta} + W\right)$$
$$+\frac{P_{24}}{R^2}\frac{\partial^2 W}{\partial\theta^2} - \frac{P_{25}}{R^3}\left(-\frac{\partial^2 W}{\partial\theta^2} + \frac{\partial V}{\partial\theta}\right). \tag{B.6}$$

Expression of matrix $\left[H_{ij}\right]$:

As mentioned above, the A_i and B_i can be expressed in terms of C_i, through the coefficients α_i and β_i which are interconnected, so that the system of equations (35) may therefore be simplified as follows:

$$\begin{bmatrix} H_{11} & H_{12} \\ H_{21} & H_{22} \end{bmatrix} \begin{Bmatrix} \alpha_j \\ \beta_j \end{Bmatrix} = \begin{Bmatrix} -H_{13} \\ -H_{23} \end{Bmatrix}, \tag{B.7}$$

where

$$H_{11} = \left[\lambda_j^2 - \frac{(1-\nu)}{2} n^2 \left(1 + \frac{\kappa}{4} \right) \right], \tag{B.8a}$$

$$H_{12} = \frac{n\lambda_j}{2} \left[\nu \left(1 + \frac{3\kappa}{4} \right) + \left(1 - \frac{3\kappa}{4} \right) \right], \tag{B.8b}$$

$$H_{21} = H_{12}, \tag{B.8c}$$

$$H_{22} = \left[-\frac{(1-\nu)}{2} \lambda_j^2 + n^2 (1+\kappa) - \frac{9(1-\nu)}{8} \kappa \lambda_j^2 \right], \tag{B.8d}$$

$$H_{23} = \left[n\left(1 + n^2\kappa\right) - \frac{(3-\nu)}{2} \kappa n \lambda_j^2 \right], \tag{B.8e}$$

$$H_{13} = \left[\nu \lambda_j - \frac{(1-\nu)}{2} \kappa \lambda_j n^2 \right], \tag{B.8f}$$

Noting that

$$H_{11}H_{22} - H_{21}H_{12} = -\frac{(1-\nu)}{2} \left(\lambda^2 - n^2 \right)^2 \neq 0, \text{ with } \kappa = (1/12)(h/R)^2. \tag{B.9}$$

Matrix $[T]$:

$$[T] = \begin{bmatrix} \cos n\theta & 0 & 0 \\ 0 & \cos n\theta & 0 \\ 0 & 0 & \sin n\theta \end{bmatrix}. \tag{B.10}$$

Matrix $[R]$:

$$[R] = \begin{bmatrix} \alpha_1 e^{(\lambda_1 x/R)} & \alpha_2 e^{(\lambda_2 x/R)} & \alpha_3 e^{(\lambda_3 x/R)} & \alpha_4 e^{(\lambda_4 x/R)} & \alpha_5 e^{(\lambda_5 x/R)} & \alpha_6 e^{(\lambda_6 x/R)} & \alpha_7 e^{(\lambda_7 x/R)} & \alpha_8 e^{(\lambda_8 x/R)} \\ e^{(\lambda_1 x/R)} & e^{(\lambda_2 x/R)} & e^{(\lambda_3 x/R)} & e^{(\lambda_4 x/R)} & e^{(\lambda_5 x/R)} & e^{(\lambda_6 x/R)} & e^{(\lambda_7 x/R)} & e^{(\lambda_8 x/R)} \\ \beta_1 e^{(\lambda_1 x/R)} & \beta_2 e^{(\lambda_2 x/R)} & \beta_3 e^{(\lambda_3 x/R)} & \beta_4 e^{(\lambda_4 x/R)} & \beta_5 e^{(\lambda_5 x/R)} & \beta_6 e^{(\lambda_6 x/R)} & \beta_7 e^{(\lambda_7 x/R)} & \beta_8 e^{(\lambda_8 x/R)} \end{bmatrix} \tag{B.11}$$

4.8.3. Appendix C

The coefficients of modal equations are given by

$$B_{ij} = C_i\, b'_{ij}\, e^{\left(\lambda_i+\lambda_j\right)x/R}\, C_j\,, \tag{C.1a}$$

where

$$b'_{ij} = \frac{1}{2R^2}\left[b_{ij}^{(1)} \cos^2\left(n\theta\right) + b_{ij}^{(2)} \sin^2\left(n\theta\right)\right], \tag{C.1b}$$

with

$$b_{ij}^{(1)} = 1 + \left(\beta_i + \beta_j\right)n + \beta_i\,\beta_j\,n^2\,, \tag{C.1c}$$

$$b_{ij}^{(2)} = \left(1+\alpha_i\,\alpha_j\right)n^2 + \left(\beta_i+\beta_j\right)n + \beta_i\,\beta_j\,. \tag{C.1d}$$

$$C_{ij} = C_i\, c'_{ij}\, e^{\left(\lambda_i+\lambda_j\right)x/R}\, C_j\,, \tag{C.2a}$$

where,

$$c'_{ij} = -\frac{1}{2R^2}\left[c_{ij}^{(1)} + c_{ij}^{(2)}\right] \cos\left(n\theta\right)\,\sin\left(n\theta\right), \tag{C.2b}$$

with

$$c_{ij}^{(1)} = \left(1+\alpha_i\,\alpha_j - \beta_i\,\beta_j\right)\lambda_i\,n\,, \tag{C.2c}$$

$$c_{ij}^{(2)} = \left(\beta_j - \beta_i\right)\lambda_i\,. \tag{C.2d}$$

$$P_{ij} = C_i\, p'_{ij}\, e^{\left(\lambda_i+\lambda_j\right)x/R}\, C_j\,, \tag{C.3a}$$

where,

$$p'_{ij} = \frac{1}{R^3}\left[p_{ij}^{(1)} \cos^2\left(n\theta\right) + p_{ij}^{(2)} \sin^2\left(n\theta\right)\right], \tag{C.3b}$$

with

$$p_{ij}^{(1)} = \alpha_j\,\lambda_i\,\lambda_j^2 - \lambda_i^2 - \beta_j\,\lambda_i^2\,n - \alpha_j\,\lambda_i^2\,\lambda_j\,, \tag{C.3c}$$

$$p_{ij}^{(2)} = \left(\alpha_i+\alpha_j\right)\lambda_i\,n^2 + \left(\beta_i\,\alpha_j + \beta_i\,\lambda_j + \alpha_i\,\beta_j\right)\lambda_i\,n + \beta_i\,\beta_j\,\lambda_i\,\lambda_j\,. \tag{C.3d}$$

Also, we have

$$S_{ij} = C_i\, s'_{ij}\, e^{(\lambda_i+\lambda_j)x/R}\, C_j\ , \tag{C.4a}$$

Assume that

$$s'_{ij} = \frac{1}{R^3}\left[s^{(1)}_{ij}\, cos^2(n\theta) + s^{(2)}_{ij}\, sin^2(n\theta)\right], \tag{C.4b}$$

with

$$s^{(1)}_{ij} = \beta_i\ n^3 + \left(1+\beta_i\,\beta_j + \alpha_j\,\lambda_j\right)\, n^2 + \left(\beta_j + 3\beta_i\,\alpha_j\,\lambda_j + \beta_j\,\lambda_i\,\lambda_j\right)\, n + 2\alpha_j\,\lambda_j\ , \tag{C.4c}$$

$$s^{(2)}_{ij} = \beta_i\, n^3 + \left(1+\beta_i\,\beta_j - \alpha_i\,\alpha_j - \alpha_i\,\lambda_j\right)\, n^2 + \left(\alpha_i\,\beta_j\,\lambda_j + \beta_j - \beta_i\,\lambda_i\,\lambda_j\right)\, n\ . \tag{C.4d}$$

Finally,

$$T_{ij} = C_i\, t'_{ij}\, e^{(\lambda_i+\lambda_j)x/R}\, C_j\ , \tag{C.5a}$$

where

$$t'_{ij} = \frac{1}{R^3}\ t^{(1)}_{ij}\, cos(n\theta)\ sin(n\theta), \tag{C.5b}$$

with

$$\begin{aligned} t^{(1)}_{ij} = &\left(\alpha_i + \alpha_j\right) n^3 + \left(\alpha_i\,\beta_j + \beta_i\,\alpha_j - \beta_j\,\lambda_j + \beta_i\,\lambda_i + 2\,\beta_j\,\lambda_i\right)\, n^2 \\ &+ \left(\alpha_i\,\alpha_j\,\lambda_j - \beta_i\,\beta_j\,\lambda_j - \lambda_j + 2\,\beta_i\,\beta_j\,\lambda_i - \alpha_j\,\lambda_i\,\lambda_j + 2\lambda_i + 2\alpha_j\,\lambda_j\,\lambda_i\right)\, n + \beta_j\lambda_i^2\lambda_j \\ &- \beta_i\,\lambda_j + \beta_i\,\lambda_i + 2\,\beta_i\,\alpha_j\,\lambda_i\,\lambda_j + \beta_j\,\lambda_i\,\lambda_j^2\ . \end{aligned} \tag{C.5c}$$

The terms, which constitute the nonlinear stiffness matrix of order two, are

$$B_{ijk} = \frac{1}{R} C_i\, C_j\, C_k\, e^{(\lambda_i+\lambda_j+\lambda_k)x/R}\, cos(n\theta)\left[\left(1+\beta_i\, n\right)\, b'_{jk} + \left(1+\beta_j\, n\right) b'_{ki} + \left(1+\beta_k\, n\right) b'_{ij}\right], \tag{C.6}$$

$$\begin{aligned} C_{ijk} = &\frac{1}{2R} C_i\, C_j\, C_k\, e^{(\lambda_i+\lambda_j+\lambda_k)x/R}\, sin(n\theta)\left[c'_{jk}\left(\beta_i\,\lambda_i - \alpha_i\, n\right) + c'_{ik}\left(\beta_j\,\lambda_j - \alpha_j\, n\right)\right. \\ &\left. + c'_{ji}\left(\beta_k\,\lambda_k - \alpha_k\, n\right)\right], \end{aligned} \tag{C.7}$$

$$P_{ijk} = -\frac{1}{R^2}\ C_i\, C_j\, C_k\, e^{(\lambda_i+\lambda_j+\lambda_k)x/R}\, cos(n\theta)\left[\lambda_i^2\ p'_{jk} + \lambda_j^2\ p'_{ik} + \lambda_k^2\ p'_{ji}\right], \tag{C.8}$$

$$\begin{aligned} S_{ijk} = &\frac{1}{R^2}\ C_i\, C_j\, C_k\, e^{(\lambda_i+\lambda_j+\lambda_k)x/R}\ cos(n\theta)\left[s'_{jk}\ \left(n^2 + \alpha_i\,\lambda_i + \beta_i\, n\right) + s'_{ik}\ \left(n^2 + \alpha_j\,\lambda_j + \beta_j\, n\right)\right. \\ &\left. + s'_{ji}\ \left(n^2 + \alpha_k\,\lambda_k + \beta_k\, n\right)\right], \end{aligned} \tag{C.9}$$

$$\begin{aligned} T_{ijk} = &\frac{1}{R^2} C_i\, C_j\, C_k\, e^{(\lambda_i+\lambda_j+\lambda_k)x/R}\, sin(n\theta)\left[t'_{jk}\left(2\,\lambda_i\, n + \alpha_i\, n + \beta_i\,\lambda_i\right) + t'_{ik}\left(2\,\lambda_j\, n + \alpha_j\, n + \beta_j\,\lambda_j\right)\right. \\ &\left. + t'_{ji}\left(2\,\lambda_k\, n + \alpha_k\, n + \beta_k\,\lambda_k\right)\right], \end{aligned} \tag{C.10}$$

$$D_{ijk} = \frac{1}{R} C_i C_j C_k e^{(\lambda_i+\lambda_j+\lambda_k)x/R} cos(n\theta) \left[\alpha_j \lambda_j b'_{ki} + \alpha_k \lambda_k b'_{ij} + a'_{jk} (1+\beta_i n)\right], \qquad (C.11)$$

$$E_{ijk} = \frac{1}{R} C_i C_j C_k e^{(\lambda_i+\lambda_j+\lambda_k)x/R} cos(n\theta) \left[a'_{ki} (1+\beta_j n) + a'_{ij} (1+\beta_k n) + b'_{jk} \alpha_i \lambda_i\right], \qquad (C.12)$$

$$U_{ijk} = \frac{1}{R^2} C_i C_j C_k e^{(\lambda_i+\lambda_j+\lambda_k)x/R} cos(n\theta) \left[p'_{jk} \left(n^2 + \beta_i n + \alpha_i \lambda_i\right) - s'_{ik} \lambda_j^2 - s'_{ji} \lambda_k^2\right], \qquad (C.13)$$

$$V_{ijk} = \frac{1}{R^2} C_i C_j C_k e^{(\lambda_i+\lambda_j+\lambda_k)x/R} cos(n\theta) \Big[p'_{ik} \left(n^2 + \beta_j n + \alpha_j \lambda_j\right) + p'_{ji} \left(n^2 + \beta_k n + \alpha_k \lambda_k\right)$$
$$- s'_{jk} \lambda_i^2 \Big]. \qquad (C.14)$$

The terms, which constitute the nonlinear stiffness matrix of order three, are

$$B_{ijks} = 2 C_i C_j C_k C_s b'_{is} b'_{jk} e^{(\lambda_i+\lambda_j+\lambda_k+\lambda_s)x/R}, \qquad (C.15)$$

$$C_{ijks} = 2 C_i C_j C_k C_s c'_{is} c'_{jk} e^{(\lambda_i+\lambda_j+\lambda_k+\lambda_s)x/R}, \qquad (C.16)$$

$$P_{ijks} = 2 C_i C_j C_k C_s p'_{is} p'_{jk} e^{(\lambda_i+\lambda_j+\lambda_k+\lambda_s)x/R}, \qquad (C.17)$$

$$S_{ijks} = 2 C_i C_j C_k C_s s'_{is} s'_{jk} e^{(\lambda_i+\lambda_j+\lambda_k+\lambda_s)x/R}, \qquad (C.18)$$

$$T_{ijks} = 2 C_i C_j C_k C_s t'_{is} t'_{jk} e^{(\lambda_i+\lambda_j+\lambda_k+\lambda_s)x/R}, \qquad (C.19)$$

$$D_{ijks} = 2 C_i C_j C_k C_s a'_{jk} b'_{is} e^{(\lambda_i+\lambda_j+\lambda_k+\lambda_s)x/R}, \qquad (C.20)$$

$$U_{ijks} = 2 C_i C_j C_k C_s p'_{jk} s'_{is} e^{(\lambda_i+\lambda_j+\lambda_k+\lambda_s)x/R}, \qquad (C.22)$$

$$V_{ijks} = 2 C_i C_j C_k C_s p'_{is} s'_{jk} e^{(\lambda_i+\lambda_j+\lambda_k+\lambda_s)x/R}. \qquad (C.23)$$

CHAPITRE 5 ARTICLE 3: EFFECT OF GEOMETRIC NONLINEARITY ON THE DYNAMIC BEHAVIOR OF THIN CYLINDRICAL SHELLS SUBJECTED TO SUPERSONIC FLOW

(Submitted to Thin-Walled Structures, July 9th, 2021)

Yacine Ben-Youssef, Youcef Kerboua, Aouni A. Lakis

5.1. Abstract

This paper presents a numerical model for the analysis of the aeroelastic stability of a thin cylindrical shell subjected to external supersonic airflow by considering the effects of geometric nonlinearity. The nonlinear stiffness matrix is based on an approach developed using Novozhilov's nonlinear shell theory and taking into account the effects of the curvature of the displacement field in the circumferential direction, the initial geometric imperfections and nonlinear coupling between the different modes. The linear mass and stiffness matrices are derived based on a hybrid method, which is a combination of Sander's thin shell theory and the classic finite element method. The aerodynamic damping and stiffness matrices are evaluated using the first–order potential (piston) theory. The initial stiffening effects due to radial pressure and/or axial loading is also taken into account. The numerical studies illustrate the effects of different parameters including internal pressure, nonlinear coupling, circumferential wave number and shell's geometry. Good agreement is found between the results obtained using the present approach and those published in the literature.

Keywords

Thin cylindrical shell, geometry nonlinearity, finite element, nonlinear Novozhilov theory, flutter, Stress stiffening.

5.2. Introduction

Thin-walled cylindrical shells are one of the key structures that are widely employed in several high-tech sectors such as the aerospace industry. These structures are frequently used in the fuselage and engine nacelles of airplanes and in the skin of space shuttles. When these structures are exposed to external aerodynamic pressure in a supersonic environment, they become prone to dynamic instability including flutter induced by high-Mach number gas flow. This self-excited oscillation manifests itself by large-amplitude vibrations that arise at a critical pressure, above which the structure loses its dynamic stability, which may lead to its collapse. Aeroelastic instability is one of the primary design criteria that must be considered by aeronautical engineers to prevent this behavior. In the literature, several studies present experimental and analytical analyses that highlight the supersonic flutter of cylindrical shells using structural linear models. Many researchers have studied this aspect, including Dowell, Olson and Fung and Barr and Stearman. However, a notable discrepancy is observed between linear analysis and experimental results for the prediction of dynamic instability and the corresponding behavior of the structure during flutter. This prompted researchers to lean towards nonlinear analysis of these structures in order to design a model that more faithfully represents reality. Few research studies have been published during past decades dealing with the aeroelastic stability of cylindrical shells subjected to supersonic flow using a nonlinear structural model. The first is attributed to Librescu [19, 20], who investigated the stability of shallow panels and finite-length circular cylindrical shells using Donnell's nonlinear shallow shell theory and a simple mode expansion. It included nonlinear terms which are associated with the supersonic flow pressure and calculated by piston theory. Olson and Fung [21] used a simplified form of Donnell's nonlinear shallow-shell theory and a simple two-mode expansion to model simply-supported shells. At the NASA Ames Research Center, California, in 1962 and 1964, Olson and Fung [22] performed a complete experimental study of supersonic flutter of pressurized and axially compressed circular cylindrical shells. The researchers reported a peculiar behavior of the flutter boundary versus shell pressurization. Amabili and Pellicano [23] analyzed the aeroelastic stability of simply-supported, circular cylindrical shells in supersonic flow. They employed Donnell's nonlinear shallow-shell theory to model nonlinearities caused by large-amplitude shell motion. Their study also accounts for the effect of viscous structural damping. The fluid structure interaction was described via the linear piston theory using two different formulations. The authors revealed that the system loses stability by standing wave flutter through supercritical bifurcation. Amabili and Pellicano [24] later developed a model using a larger mode expansion involving up to 22 modes and the third-order piston theory. They emphasized that differences between linear and third-order piston theory were found to be negligible for a Mach number of three. Librescu et al [25] studied the flutter and post-flutter of infinitely-long thin-walled cylindrical panels in supersonic/hypersonic flow. The aeroelastic equations were derived based on nonlinear shell theory in conjunction with third–order piston theory and shock wave aerodynamics. Oh and Lee [26] applied a nonlinear finite element method based on multifield layerwise theory to investigate the dynamic instability of piezolaminated cylindrical panels subjected to thermal and piezoelectric loads. Kurilov and Mikhlin [27] investigated the nonlinear behaviour of elastic cylindrical shells using the theory of shallow shells. They analyzed the effect of the flow and the initial deflections on the vibrations of the shell. Jansen [28] developed a theory that includes the combined effects of finite vibration amplitudes, nonlinear static deformation and initial geometric imperfections in an investigation of the nonlinear dynamic response of laminated cylindrical shells. Haddadpour et al [29] analyzed the supersonic flutter prediction of functionally graded cylindrical shells for different sets of boundary conditions by considering the nonlinear structural model coupled with linearized piston theory. The study highlighted the effect of temperature and internal pressure on the flutter boundaries of a simply-supported FG cylindrical structure. Kubenko and Koval'chuk [30] presented results of their study of the stability and nonlinear vibration of thin cylindrical shells interacting with fluid flow. They analyzed the effect of initial geometrical imperfections, boundary conditions, added concentrated masses and longitudinal and transverse static loads on the critical velocities. Liu et al [31] analyzed the nonlinear dynamic behaviour of a simply-supported FGM cylindrical shell under harmonic excitation, compressive in-plane force combined with supersonic aerodynamic and thermal loads by taking into account the effect of small initial geometric imperfections of the cylindrical shell. Mahmoudkhani et al [32] analyzed the aero-thermoelastic stability of layered cylindrical shells with viscoelastic cores. The model is developed using Donnell's theory and first-order shear deformation theory in conjunction with the Von Karman-Donnell kinematic nonlinearity. The results establish that pre-deformation could significantly influence the flutter boundaries for high temperatures. In another paper, Mahmoudkhani [33] examined the supersonic flutter of functionally graded cylindrical shells under thermal loadings, taking into account the effect of geometric imperfections. His numerical study exhibited changes to the trend of variation of the flutter pressure with temperature due to the effect of imperfections. Chen and Li [34] studied the nonlinear aeroelastic flutter and the nonlinear dynamic behaviour of a composite circular cylindrical shell under the combined action of compressive in-plane force and radial harmonic excitation when subjected to supersonic airflow. Asadi and Wang [35] examined the nonlinear instability of a pressurized functionally graded carbon-nanotube reinforced composite (FG-CNTRC) cylindrical shell subjected to supersonic airflow. Asadi [36] extended his study to investigate the aero-thermoelastic flutter and buckling instabilities of an FG-CNRC cylindrical shell. His numerical results revealed that temperature rise has a significant effect on the aero-thermoelastic flutter characteristics of the FG-CNRC cylindrical structure. Avramov et al [37] developed a new model of nonlinear vibration of functionally graded CNT-reinforced composite cylindrical shells to analyze stability of the trivial equilibrium of the cylindrical shell. The numerical results showed that a significant decrease in the self-sustained vibrations is obtained due to growth of the volume fraction of the CNTs. Fazilati et al [38] studied the aero-thermoelastic behavior of a cylindrical curved panel under high supersonic airflow taking into consideration the structural nonlinearity effect using Von Karman-Donnell strain-displacement relations and third-order piston theory to assess the aeroelastic stability of the structure. Khudayarov and Turaev [39] investigated the dynamic response of orthotropic cylindrical shells in supersonic flow including consideration of the viscoelastic properties of material and geometric nonlinearities. The numerical results indicated that a decrease in the critical flutter velocities is caused by the viscoelastic properties of shell material. Baghdasaryan et al [40] examined the nonlinear aeroelastic response and stability of closed cylindrical shells subjected to supersonic flow and placed in an inhomogeneous temperature field. Their numerical solutions showed that the critical velocity is inversely proportional to the relative thickness of the shell. In another paper, Baghdasaryan et al [41] investigated the nonlinear vibrations of an isotropic cylindrical shallow shell in supersonic gas flow, taking into consideration both types of nonlinearities: geometric and aerodynamic. Torki et al [117] studied the dynamic stability of cantilevered, functionally graded cylindrical shells under axial follower forces. The equations of motion were derived based on the Hamilton principle and using the first-order shear deformation theory. The stability analysis was performed using the extended Galerkin method. Flutter boundaries and their corresponding critical circumferential mode number were calculated for different volume fraction and length-to-radius, and thicknesses-to-radius ratios. Yazdi [118] examined the flutter of geometrical imperfect functionally graded carbon nanotubes (FG-CNTs) doubly curved shell subjected to a supersonic flow. Large deflection flutter was evaluated based on the piston theory and von Karman geometrical nonlinearity terms. Numerical results showed the preponderant effect of shell imperfection on flutter pressure compared to CNTs volume fraction and distributions.

The formulations developed in this area lack precision due to the complexity of the studied problem, which prompted the need to develop a nonlinear model focused on speed of convergence, reduction of processing costs and accuracy of results. In order to meet this objective, a new geometrically non-linear model is presented, in this manuscript, in order to characterize the dynamic instability and nonlinear behaviour of a thin isotropic cylindrical shell under internal pressure and axial compression load and subjected to external supersonic flow. The nonlinear model presented in this research, accounts for the effect of initial geometric imperfections, the shell curvature effect in the circumferential direction of the orthogonal displacements as well as the phenomenon of coupling between different modes. The linear analysis is performed here to identify natural modes, which are then used in the nonlinear analysis as a spatial function. Therefore, this manuscript is structured in three main steps as follows:

- ✓ The first step deals with linear analysis of thin-walled cylindrical shell dynamic behaviour based on the hybrid method developed by Lakis and Paidoussis in order to determine the displacement functions as well as the mass and linear stiffness matrices. (All details of the method are presented in reference [9]). This step also includes modeling the initial stiffening effect by assessing the expression of the potential energy.
- ✓ The second step involves computation of the modal coefficients according to the functions of displacement resulting from the linear analysis. The nonlinear stiffness matrices for an empty finite element are consequently calculated based on an analytical integration with respect to modal coefficients. The second and third-order nonlinear stiffness matrices, once calculated, are overlaid on the linear system.
- ✓ The last step consists of modeling the structure-fluid interaction by determining the aerodynamic pressure loading due to the supersonic airflow based on linearized first-order potential theory with (or without) the curvature correction term, and by using the shape function matrix deduced from linear structural analysis. We finally proceed to determine the aerodynamic damping and aerodynamic stiffness matrices.

The approach, on which this analysis was based, stands out for its high accuracy by sweeping high and low frequencies, and its speed of convergence for the treatment of axisymmetric shells using a small number of finite elements. This is due to the fact that the displacement functions are derived in the linear part from exact solutions of Sanders' shell equilibrium equations rather than an approximation with polynomial functions. The nonlinear study based on Novozhilov's shell theory also benefits from this hybrid method given that modal coefficients are obtained based on the shape functions induced by the linearized equations of motion. The hybrid method also shows its ability to deal with various boundary conditions. The aerodynamic pressure induced by supersonic airflow and modeled using first-order piston theory, can be assessed at any point in the structure with exactitude due to this hybrid method.

5.3. Structural modeling

5.3.1. Linear solution and hybrid finite element formulation

The shell is subdivided into several cylindrical elements. Each element is defined by two line-nodes, i and j and the boundaries of the nodal surface. Each node has four degrees of freedom; three displacements (axial U, circumferential V and radial W) and one rotation $\partial W/\partial x$ oriented as shown in Figure 5.1.

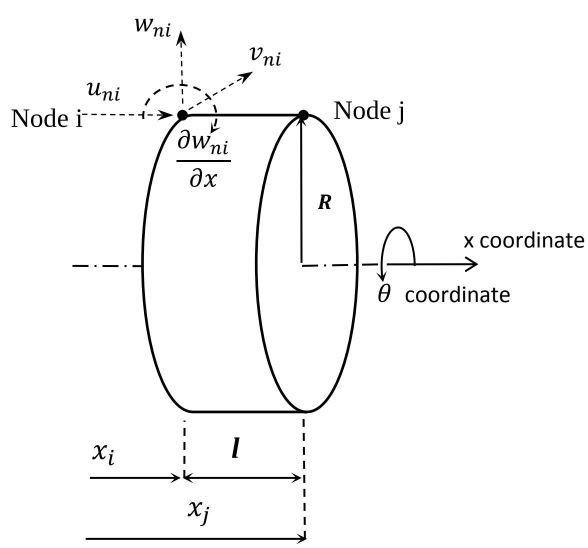

Figure 5.1: Nodal displacements of a cylindrical Finite Element

The linear strain vector according to Sanders theory [9] in the cylindrical coordinate system is expressed in terms of axial, radial, and circumferential mid-surface displacements as follows:

$$\begin{Bmatrix} \varepsilon_x \\ \varepsilon_\theta \\ 2\varepsilon_{x\theta} \\ k_x \\ k_\theta \\ 2k_{x\theta} \end{Bmatrix} = \begin{Bmatrix} \dfrac{\partial U}{\partial x} \\ \dfrac{1}{R}\dfrac{\partial V}{\partial \theta} + \dfrac{W}{R} \\ \dfrac{\partial V}{\partial x} + \dfrac{1}{R}\dfrac{\partial U}{\partial \theta} \\ -\dfrac{\partial^2 W}{\partial x^2} \\ -\dfrac{1}{R^2}\dfrac{\partial^2 W}{\partial \theta^2} + \dfrac{1}{R^2}\dfrac{\partial V}{\partial \theta} \\ -\dfrac{2}{R}\dfrac{\partial^2 W}{\partial x \partial \theta} + \dfrac{3}{2R}\dfrac{\partial V}{\partial x} - \dfrac{1}{2R^2}\dfrac{\partial U}{\partial \theta} \end{Bmatrix} \tag{1}$$

In Equation (1), ε_x and ε_θ represent strain components in the axial and circumferential directions, respectively. $\varepsilon_{x\theta}$ represents the shear strain in the $x\theta$ plane. k_x, k_θ are the change of curvature of the normal mid-surface and $k_{x\theta}$ is the modified twisting strain. The stress-strain relation is given by:

$$\{\sigma\} = [P]\{\varepsilon\} \tag{2}$$

Where $[P]$ is the elasticity matrix of order (6×6) for an anisotropic material [9]. Its components for an isotropic shell are given in Appendix A.

The equilibrium equations of anisotropic cylindrical shells are expressed in terms of axial, tangential and radial displacements of the mean surface [9]. They are given fully in Appendix A, using three linear partial differential operators $L_k\left(k=1,2,3\right)$, they are thus defined as;

$$L_k\left(U,W,V,P_{ij}\right)=0 \tag{3}$$

Where $L_k\left(U,W,V,P_{ij}\right)_{k=1,2,3}$ are the linear partial differential equations of an anisotropic cylindrical shell given in Appendix A, and P_{ij} are the elements of the elasticity matrix [P]. From Equation (3), we can define the displacement functions as periodic functions, which can be expressed in Fourier series (see reference [9]). Thus the displacement field is defined for the n^{th} wave number by the following expressions:

$$U\left(x,\theta\right)=\sum_{n}u_{n}\left(x\right)\cos\left(n\theta\right) \qquad (4.a)$$

$$W\left(x,\theta\right)=\sum_{n}w_{n}\left(x\right)\cos\left(n\theta\right) \qquad (4.b)$$

$$V\left(x,\theta\right)=\sum_{n}v_{n}\left(x\right)\sin\left(n\theta\right) \qquad (4.c)$$

Here n represents the circumferential wave number, and u_n, v_n, w_n are the magnitudes of displacements that depend only on the *x* coordinate. By introducing Equations (4) into the Sanders equilibrium Equations (3), and by resolving the characteristic equation, Lakis and Paidoussis [9] found the exact analytical solution for displacement functions which have a final form as follows (see ref [9] for more details):

$$\begin{Bmatrix} U\left(x,\theta\right) \\ W\left(x,\theta\right) \\ V\left(x,\theta\right) \end{Bmatrix}=\left[T\right]\left[R\right]\left[A\right]^{-1}\begin{Bmatrix} \delta_i \\ \delta_j \end{Bmatrix}=\left[N\right]\begin{Bmatrix} \delta_i \\ \delta_j \end{Bmatrix} \qquad (5)$$

Where the finite element nodal displacements vector using the eight boundary conditions of each finite element, four at each node is defined as follows:

$$\begin{Bmatrix} \delta_i \\ \delta_j \end{Bmatrix}=\left\{u_{ni}\ , w_{ni}, \partial w_{ni}/\partial x, v_{ni}, u_{nj}, w_{nj}, \partial w_{nj}/\partial x, v_{nj}\right\}^{T}=\left[A\right]\left\{C\right\} \qquad (6)$$

Matrices $\left[T\right]$ of order $\left(3\times3\right)$, $\left[R\right]$ of order $\left(3\times8\right)$ and the components of matrix $\left[A\right]_{8\times8}$ are given in Appendix A, and vector $\left\{C\right\}=\left\{C_1, C_2, ..., C_8\right\}^{T}$ is defined in reference [9].

By introducing Equations (5) into Equation (1), the strain vector expression is expressed as;

$$\left\{\varepsilon\right\}=\begin{bmatrix} \left[T\right] & \left[0\right] \\ \left[0\right] & \left[T\right] \end{bmatrix}\left[Q\right]\left[A\right]^{-1}\begin{Bmatrix} \delta_i \\ \delta_j \end{Bmatrix}=\left[B\right]\begin{Bmatrix} \delta_i \\ \delta_j \end{Bmatrix} \qquad (7)$$

Where the components of matrix $\left[Q\right]$ are given in Appendix A. Now the components of the stress vector may be written in terms of nodal displacements using Equations (2) and (7) as:

$$\left\{\sigma\right\}=\left[P\right]\left[B\right]\begin{Bmatrix} \delta_i \\ \delta_j \end{Bmatrix} \qquad (8)$$

The elementary mass $\left[m\right]_s^e$ and stiffness $\left[k\right]_s^e$ matrices of the cylindrical finite element are consequently, calculated based on the standard finite element approach. Their relations are thus defined as [9]:

$$\left[k\right]_s^e = \int_0^l \int_0^{2\pi} \left[B\right]^T \left[P\right]\left[B\right] R\, dx\, d\theta \tag{9}$$

$$\left[m\right]_s^e = \rho h \int_0^l \int_0^{2\pi} \left[N\right]^T \left[N\right] R\, dx\, d\theta \tag{10}$$

Where ρ is the density of the solid shell, h its wall thickness, l is the length of the finite element and R is the mean radius of the cylindrical shell. (See Figure 5.1). Further information concerning the derivation of the linear stiffness and mass matrix equations can be found in ref [9]. The global mass $\left[M_s\right]$ and linear stiffness $\left[K_s\right]$ matrices for the entire shell are consequently developed using standard assembling techniques for different boundary conditions.

5.3.2. Nonlinear analysis

The nonlinear analysis presented in this manuscript is based on the formulation developed by Ben Youssef et al [2] with particular attention to geometric nonlinearities. The structure is assumed to be perfectly cylindrical in order to neglect the effect of the initial geometric imperfections. Development of the nonlinear stiffness matrix is done through evaluation of the coefficients of the modal equations, which were obtained using the Lagrange method based on an energy approach. The nonlinear stiffness matrix, once calculated, was overlaid onto the linear system.

The approach followed by the method cited in [2] begins by expressing the displacement functions of points on the middle surface of the shell as a sum of product of the generalized coordinates $q_i\left(t\right)$ with the spatial functions U, V, W given in Equations (4.a – 4.c) [2].

$$u = \sum_i q_i\left(t\right).U_i\left(x,\theta\right) \tag{11.a}$$

$$v = \sum_i q_i\left(t\right).\, V_i\left(x,\theta\right) \tag{11.b}$$

$$w = \sum_i q_i\left(t\right).\, W_i\left(x,\theta\right) \tag{11.c}$$

By introducing the displacement functions (11.a - 11.c) into the middle-surface strain-displacement relationships of Novozhilov for circular shells (see Appendix B), one can express the deformation vector of an arbitrary point belonging to the mean surface as a function of the generalized coordinates in the following form [2]:

$$\varepsilon_{x,0} = \sum_j a_j q_j + \sum_j \sum_k A_{jk} q_j q_k \tag{12.a}$$

$$\varepsilon_{\theta,0} = \sum_j b_j q_j + \sum_j \sum_k B_{jk} q_j q_k \tag{12.b}$$

$$\varepsilon_{x\theta,0} = \sum_j c_j q_j + \sum_j \sum_k C_{jk} q_j q_k \tag{12.c}$$

$$k_{x,0} = \sum_j p_j q_j + \sum_j \sum_k P_{jk} q_j q_k \tag{12.d}$$

$$k_{\theta,0} = \sum_j s_j q_j + \sum_j \sum_k S_{jk} q_j q_k \tag{12.e}$$

$$k_{x\theta,0} = \sum_j t_j q_j + \sum_j \sum_k T_{jk} q_j q_k \tag{12.f}$$

The expressions of the coefficients $a_j, b_j, c_j, \ldots$etc. are thus derived in terms of the spatial functions of Equations (4.a – 4.c) (see Appendix B).

$\varepsilon_{x,0}$, $\varepsilon_{\theta,0}$, $\varepsilon_{x\theta,0}$ are the middle surface strain components, and $k_{x,0}$, $k_{\theta,0}$, $k_{x\theta,0}$ are the changes in curvature and torsion of the middle surface.

Using Equations (11.a – 11.c), the Lagrange equations which follow from Hamilton's variational principle, can thus be written in the generalized coordinates $q_i(t)$:

$$\frac{d}{dt}\left(\frac{\partial T}{\partial \dot{q}_i}\right) - \frac{\partial T}{\partial q_i} + \frac{\partial V}{\partial q_i} = Q_i, \qquad i = 1, 2, .., N. \tag{13}$$

Here N is the number of degrees of freedom, and can be chosen according to the desired accuracy, T is the total kinetic energy, V represents the total elastic strain energy of deformation and the Q_i 's are the generalized forces.

Once the total kinetic and elastic strain energy are calculated using Equations (11.a – 11.c) and (12.a – 12.f) respectively, they will subsequently be inserted into the Lagrange equations (Equation

13) to assess the dynamic behaviour of an empty cylindrical shell in the absence of external loads. The nonlinear modal equations are defined as follows [2]:

$$\sum_j m_{ij}\, \ddot{q}_j + \sum_j k_{ij}\, q_j + \sum_j \sum_k \sum_s k_{ijks}\, q_j\, q_k\, q_s = 0 \tag{14}$$

The subscripts $"i, j"$, $"i, j, k"$ and $"i, j, k, s"$ represent, respectively, the coupling between two, three and four different modes. m_{ij}, k_{ij} are the terms of mass and linear stiffness matrices given by Equations (9) and (10); the term k_{ijks}, which represents the nonlinear stiffness is given by the following integral for the case of an isotropic closed cylindrical shell [2]:

$$\begin{aligned} k_{ijks} = \int_0^l \int_0^{2\pi} \Big\{ & C\left[A_{ijks} + B_{ijks} + \nu\left(D_{ijks} + E_{ijks}\right) + 2(1-\nu)C_{ijks} \right] \\ & + D\left[P_{ijks} + S_{ijks} + \nu\left(U_{ijks} + V_{ijks}\right) + 2(1-\nu)T_{ijks} \right] \Big\}\, R\, dx\, d\theta \end{aligned} \tag{15}$$

Where C and D are the terms of the elasticity matrix $[P]$ given in Appendix A, and the terms $A_{ijks}, B_{ijks}, C_{ijks}, D_{ijks}, E_{ijks}, P_{ijks}, S_{ijks}, T_{ijks}, U_{ijks}$ and V_{ijks} represent the coefficients of the modal equations. These coefficients are given by the following equations [2]:

$$A_{ijks} = 2\, A_{jk}\, A_{is} \tag{16}$$

$$B_{ijks} = 2\, B_{jk}\, B_{is} \tag{17}$$

$$C_{ijks} = 2\, C_{jk}\, C_{is} \tag{18}$$

$$P_{ijks} = 2\, P_{jk}\, P_{is} \tag{19}$$

$$S_{ijks} = 2\, S_{jk}\, S_{is} \tag{20}$$

$$T_{ijks} = 2\, T_{is}\, T_{jk} \tag{21}$$

$$D_{ijks} = 2\, A_{jk}\, B_{is} \tag{22}$$

$$E_{ijks} = 2\, A_{is}\, B_{jk} \tag{23}$$

$$U_{ijks} = 2\, P_{jk}\, S_{is} \tag{24}$$

$$V_{ijks} = 2\, P_{is}\, S_{jk} \tag{25}$$

By introducing Equation (5) into (B.13) and after carrying out some development we obtain;

$$A_{ij} = C_i \, a'_{ij} \, e^{\left(\lambda_i+\lambda_j\right)x/R} \, C_j \tag{26}$$

where,

$$a'_{ij} = \frac{1}{2R^2}\left[a_{ij}^{(1)} \cos^2\left(n\theta\right) + a_{ij}^{(2)} \sin^2\left(n\theta\right) \right] \tag{27}$$

with,

$$a_{ij}^{(1)} = \left(1+\alpha_i \, \alpha_j\right)\lambda_i \, \lambda_j \tag{28.a}$$

$$a_{ij}^{(2)} = \beta_i \, \beta_j \, \lambda_i \, \lambda_j \qquad \left(i, j = 1,....,8\right) \tag{28.b}$$

$\lambda_i \left(i=1,..,8\right)$ are the roots of characteristic Equation (see reference [9]). α_i, β_i and $C_i \left(i=1,..8\right)$, the constant of vector $\{C\}$ are developed in detail in Ref [9]. n is the circumferential wave number of the shell and R its mean radius.

In the same manner, we proceed to determine the terms $B_{ij}, C_{ij}, P_{ij}, S_{ij}$ and T_{ij}, which can be written as a function of α, β, λ, n, R, x and θ. Their expressions are given in Appendix B.

After introducing Equations (26-28) into Equation (16), and Equations (B.19 – B.33) into Equations (17-25), one can evaluate separately each coefficient of Equation (15). The double integral over the middle surface of the shell can be calculated to obtain an explicit expression for the nonlinear stiffness matrix that manifests in the following form [2]:

$$\left[k^{NL3}\right] = \frac{\pi}{8R^2}\left[A^{-1}\right]^T \left[k_{NL}^*\right]\left[A^{-1}\right] \tag{29}$$

The (i,k) term in matrix $\left[k_{NL}^*\right]$ is written as [2]:

$$k_{NL}^*\left(i,k\right) = \begin{cases} \displaystyle\sum_{s=1}^{8}\sum_{j=1}^{8} \frac{\tau_{sj}}{\lambda_i+\lambda_j+\lambda_k+\lambda_s} G\left(i,k\right)\left[e^{\left(\lambda_i+\lambda_j+\lambda_k+\lambda_s\right)l/R} - 1\right] & \text{if } \lambda_i+\lambda_j+\lambda_k+\lambda_s \neq 0 \\ \displaystyle\sum_{s=1}^{8}\sum_{j=1}^{8} \tau_{sj} \, G\left(i,k\right)\frac{l}{R} & \text{if } \lambda_i+\lambda_j+\lambda_k+\lambda_s = 0 \end{cases} \tag{30}$$

τ_{sj} is the term $\left(s, j\right)$ of matrix $\left[E\right]$, where $[E] = \left[A^{-1}\right]\left[A^{-1}\right]^T$, and $G\left(i,k\right)$ is a coefficient in conjunction with α, β, λ and elements C, D of matrix $\left[P\right]$. The general expression of $G\left(i,k\right)$ is given by:

$$G(i,k)=C\Big[\!\Big[3\Big[a_{is}^{(1)}a_{jk}^{(1)}+b_{is}^{(1)}b_{jk}^{(1)}+a_{is}^{(2)}a_{jk}^{(2)}+b_{is}^{(2)}b_{jk}^{(2)}+\nu\left(b_{is}^{(1)}a_{jk}^{(1)}+a_{is}^{(1)}b_{jk}^{(1)}+b_{is}^{(2)}a_{jk}^{(2)}+a_{is}^{(2)}b_{jk}^{(2)}\right)\Big]$$
$$+a_{is}^{(2)}a_{jk}^{(1)}+a_{is}^{(1)}a_{jk}^{(2)}+b_{is}^{(2)}b_{jk}^{(1)}+b_{is}^{(1)}b_{jk}^{(2)}+\nu\left(b_{is}^{(2)}a_{jk}^{(1)}+b_{is}^{(1)}a_{jk}^{(2)}+a_{is}^{(1)}b_{jk}^{(2)}+a_{is}^{(2)}b_{jk}^{(1)}\right)$$
$$+2(1-\nu)\left(c_{is}^{(1)}+c_{is}^{(2)}\right)\left(c_{jk}^{(1)}+c_{jk}^{(2)}\right)\Big]\!\Big]+\frac{4D}{R^2}\Big[\!\Big[3\Big[p_{is}^{(1)}p_{jk}^{(1)}+s_{is}^{(1)}s_{jk}^{(1)}+p_{is}^{(2)}p_{jk}^{(2)}+s_{is}^{(2)}s_{jk}^{(2)}$$
$$+\nu\left(s_{is}^{(1)}p_{jk}^{(1)}+p_{is}^{(1)}s_{jk}^{(1)}+s_{is}^{(2)}p_{jk}^{(2)}+p_{is}^{(2)}s_{jk}^{(2)}\right)\Big]+p_{is}^{(1)}p_{jk}^{(2)}+p_{is}^{(2)}p_{jk}^{(1)}+s_{is}^{(1)}s_{jk}^{(2)}+s_{is}^{(2)}s_{jk}^{(1)}$$
$$+\nu\left(s_{is}^{(2)}p_{jk}^{(1)}+s_{is}^{(1)}p_{jk}^{(2)}+p_{is}^{(1)}s_{jk}^{(2)}+p_{is}^{(2)}s_{jk}^{(1)}\right)+2(1-\nu)t_{is}^{(1)}t_{jk}^{(1)}\Big]\!\Big] \qquad (31)$$

where the terms $a_{ij}^{(1)}$ and $a_{ij}^{(2)}$ are given by Equations (28.a) and (28.b), and the terms $b_{ij}^{(1)}$, $b_{ij}^{(2)}$, $c_{ij}^{(1)}$, $c_{ij}^{(2)}$, $p_{ij}^{(1)}$, $p_{ij}^{(2)}$, $s_{ij}^{(1)}$, $s_{ij}^{(2)}$ and $t_{ij}^{(1)}$ are coefficients appearing in the expressions of $B_{ij}, C_{ij}, P_{ij}, S_{ij}$ and T_{ij} of Equations (B.19 - B.33), given in the Appendix B.

Finally, the global nonlinear stiffness matrix $\left[K^{NL3}\right]$ is found using the assembling procedure.

5.4. Stress stiffening

The initial stiffening stresses in axisymmetric shells result from radial pressure and axial load. Their effect is estimated here by calculating the potential energy using direct membrane forces per unit width and rotations about the orthogonal axes. It is assumed that the shell is under equilibrium condition and has not reached its buckling state. The initial in-plane shear, static bending and transverse shear are ignored. The strain energy is thus expressed [68]:

$$U_i=\frac{1}{2}\iint\left[\bar{N}_x\,\varphi_{xx}^2+\bar{N}_\theta\,\varphi_{\theta\theta}^2+\left(\bar{N}_x+\bar{N}_\theta\right)\varphi_{nn}^2\right]dA \qquad (32)$$

where

$\bar{N}_x$ and $\bar{N}_\theta$ are the resultant membrane loads due to a differential radial pressure. P_m and axial load P_x may be expressed respectively by:

$$\bar{N}_\theta=P_m\,R \text{ and } \bar{N}_x=-\frac{P_x}{2\pi R} \qquad (33)$$

φ_{xx}, $\varphi_{\theta\theta}$ and φ_{nn} are the elastic rotations and are defined according to Sanders' shell theory as follows [62]:

$$\varphi_{xx} = -\frac{\partial W}{\partial x} \tag{34.a}$$

$$\varphi_{\theta\theta} = \frac{1}{R}\left(V - \frac{\partial W}{\partial \theta}\right) \tag{34.b}$$

$$\varphi_{nn} = \frac{1}{2}\left(-\frac{1}{R}\frac{\partial U}{\partial \theta} + \frac{\partial V}{\partial x}\right) \tag{34.c}$$

By introducing Equation (5) into Equation (34), the expression of the elastic strain energy in terms of nodal degrees of freedom is generated [119]:

$$U_i = \frac{1}{2}\int_0^l \int_0^{2\pi} \{Z\}^T \begin{bmatrix} \bar{N}_x & 0 & 0 \\ 0 & \bar{N}_\theta & 0 \\ 0 & 0 & \bar{N}_x + \bar{N}_\theta \end{bmatrix} \{Z\}\ R\,dx\,d\theta \tag{35}$$

where,

$$\{Z\} = \begin{Bmatrix} \varphi_{xx} \\ \varphi_{\theta\theta} \\ \varphi_{nn} \end{Bmatrix} = \begin{bmatrix} 0 & -\frac{\partial}{\partial x} & 0 \\ 0 & -\frac{1}{R}\frac{\partial}{\partial \theta} & \frac{1}{R} \\ -\frac{1}{2R}\frac{\partial}{\partial \theta} & 0 & \frac{1}{2}\frac{\partial}{\partial x} \end{bmatrix} \begin{Bmatrix} U \\ W \\ V \end{Bmatrix} = [C_0][N]\begin{Bmatrix} \delta_i \\ \delta_j \end{Bmatrix} \tag{36}$$

The initial stress stiffness matrix for each cylindrical finite element becomes [119]:

$$[k_I] = \int_0^l \int_0^{2\pi} [N]^T [C_0]^T \begin{bmatrix} \bar{N}_x & 0 & 0 \\ 0 & \bar{N}_\theta & 0 \\ 0 & 0 & \bar{N}_x + \bar{N}_\theta \end{bmatrix} [C_0][N]\ R\,dx\,d\theta \tag{37}$$

After assembling the whole initial stiffness matrix $[K_I]$, it is added to the global stiffness matrix generated from Equation (9).

5.5. Aerodynamic modeling

Piston theory, introduced into aeroelasticity in the linearized form by Ashley and Zartarian [120], is a powerful tool that furnishes an approximation for aerodynamic pressure acting on a slightly deformed cylindrical shell in a supersonic airstream. It is equivalent to modelling the pressure on a piston moving in a one-dimensional channel and generating an isentropic simple wave. The local pressure is therefore expressed as:

$$\frac{P}{P_\infty} = \left\{1 + \left[(\gamma - 1)/2\right]\left(\bar{w}/a_\infty\right)\right\}^{2\gamma/(\gamma-1)} \tag{38}$$

where,

P is the aerodynamic pressure,

P_∞ is the freestream static pressure,

γ is the adiabatic exponent of air,

$\bar{w}$ is the velocity of the piston,

a_∞ is the freestream speed of sound.

The piston velocity is therefore modeled by rallying the convective rate of displacement due to the surface gradient in the freestream direction, with the time-dependent local surface velocity arising from airfoil motion. This is expressed by [121, 122]:

$$\bar{w} = \frac{\partial W}{\partial t} + U_\infty \frac{\partial W}{\partial x} \tag{39}$$

where U_∞ is the freestream velocity and W represents the radial displacement.

$U_\infty \frac{\partial W}{\partial x}$ consists of "convection" terms that translate the contribution from body shape and angle of attack.

$\frac{\partial W}{\partial t}$ represents the contribution from body motion.

By considering the linear terms in the binomial expansion of Equation (38), the expression of the aerodynamic pressure on the cylindrical shell wall can be expressed with (or without) the curvature correction term[123]:

$$P_a = \frac{\gamma p_\infty M^2}{\left(M^2 - 1\right)^{1/2}} \left[\frac{\partial W}{\partial x} + \frac{M^2 - 2}{M^2 - 1}\frac{1}{U_\infty}\frac{\partial W}{\partial t} - \frac{W}{2R\left(M^2 - 1\right)^{1/2}}\right] \tag{40}$$

where M is the Mach number. For sufficiently high Mach numbers $(M \geq 2)$ and neglecting the curvature term $W\Big/\left[2R\left(M^2-1\right)^{1/2}\right]$, this expression simplifies to the so-called linear piston theory[120]:

$$P_a = -\gamma P_\infty \left[M \frac{\partial W}{\partial x} + \frac{1}{a_\infty}\frac{\partial W}{\partial t} \right] \tag{41}$$

Considering the radial displacement assumed to be the same as that of Equation (5):

$$W = \sum_{j=1}^{8} C_j \, e^{i\left(\lambda_j x/R + \omega t\right)} \cos\left(n\theta\right) = \sum_{j=1}^{8} W_j = \left[T\right]\left[R_f\right]\left[A^{-1}\right]\begin{Bmatrix}\delta_i \\ \delta_j\end{Bmatrix} \tag{42}$$

where λ_j is the complex root of the characteristic equation given in Ref. [9], ω is the oscillation frequency of the shell, n is the circumferential wave number and the elements of matrix $\left[R_f\right]$ are given in Appendix C.

By introducing Equation (42) into Equation (41), the aerodynamic pressure field vector in terms of nodal degrees of freedom may be defined as:

$$\left\{P_a\right\} = \begin{Bmatrix} 0 \\ P_{radial} \\ 0 \end{Bmatrix} = -\gamma \frac{P_\infty}{a_\infty}\left[T\right]\left[R_f\right]\left[A^{-1}\right]\begin{Bmatrix}\dot{\delta}_i \\ \dot{\delta}_j\end{Bmatrix} - \left(i\frac{\lambda_j}{R}\right)\gamma P_\infty M \left[T\right]\left[R_f\right]\left[A^{-1}\right]\begin{Bmatrix}\delta_i \\ \delta_j\end{Bmatrix} \tag{43}$$

Following the same reasoning and introducing Equation (42) into Equation (40), the aerodynamic pressure, including the curvature term, can be expressed as follows:

$$\begin{aligned}\left\{P_a\right\} = \begin{Bmatrix} 0 \\ P_{radial} \\ 0 \end{Bmatrix} &= \frac{-\rho_\infty U_\infty^2}{\left(M^2-1\right)^{1/2}}\frac{1}{U_\infty}\left(\frac{M^2-2}{M^2-1}\right)\left[T\right]\left[R_f\right]\left[A^{-1}\right]\begin{Bmatrix}\dot{\delta}_i \\ \dot{\delta}_j\end{Bmatrix} + \left(i\frac{\lambda_j}{R}\right)\frac{-\rho_\infty U_\infty^2}{\left(M^2-1\right)^{1/2}}\left[T\right]\left[R_f\right]\left[A^{-1}\right]\begin{Bmatrix}\delta_i \\ \delta_j\end{Bmatrix} \\ &- \frac{-\rho_\infty U_\infty^2}{\left(M^2-1\right)^{1/2}}\left(\frac{1}{2R\left(M^2-1\right)^{1/2}}\right)\left[T\right]\left[R_f\right]\left[A^{-1}\right]\begin{Bmatrix}\delta_i \\ \delta_j\end{Bmatrix}\end{aligned} \tag{44}$$

Where ρ_∞ is the freestream air density. It should be noted that the correlation existing between the freestream static pressure and velocity is acquired using the expressions:

$$U_\infty = M \cdot a_\infty \tag{45}$$

$$a_\infty = \sqrt{\gamma \frac{P_\infty}{\rho_\infty}} \tag{46}$$

The general force vector due to the pressure field is written as:

$$\{F_p\} = \iint [N]^T \{P_a\} dA \tag{47}$$

Substituting Equations (5) and (43) into the above relation, the aerodynamic damping $\left[c_f\right]$ and stiffness $\left[k_f\right]$ matrices for each element are obtained:

$$\left[c_f\right] = \left[A^{-1}\right]^T \left[D_f\right]\left[A^{-1}\right] \tag{48}$$

$$\left[k_f\right] = \left[A^{-1}\right]^T \left[G_f\right]\left[A^{-1}\right] \tag{49}$$

Where,

$$\left[D_f\right] = -\frac{\gamma}{a_\infty} P_\infty \pi R \int_0^l [R]^T \left[R_f\right] dx \tag{50}$$

$$\left[G_f\right] = -i\frac{\lambda_j}{R} \gamma P_\infty M \pi R \int_0^l [R]^T \left[R_f\right] dx \tag{51}$$

For the case including the curvature correction term, we follow the same procedure and introduce Equations (5) and (44) into Equation (47) and derive the expressions of the local damping and stiffness matrices, similar to those defined in Equations (48) and (49), with the expressions of D_f and G_f defined, this time, as follows:

$$\left[D_f\right] = \frac{-\rho_\infty U_\infty^2}{\left(M^2-1\right)^{1/2}} \frac{1}{U_\infty} \left(\frac{M^2-2}{M^2-1}\right) \pi R \int_0^l [R]^T \left[R_f\right] dx \tag{52}$$

$$\left[G_f\right] = \frac{-\rho_\infty U_\infty^2}{\left(M^2-1\right)^{1/2}} \pi R \int_0^l [R]^T \left[R_f\right] dx \left(\left(i\frac{\lambda_j}{R}\right) - \frac{1}{2R\left(M^2-1\right)^{1/2}}\right) \tag{53}$$

Finally, the global aerodynamic stiffness $\left[K_f\right]$ and viscous damping $\left[C_f\right]$ are found using the assembly procedure in FEM and added to the equations of motion.

5.6. Numerical solution

The governing equation of motion of a thin cylindrical shell subjected to an external supersonic airflow may be expressed by considering the initial stiffening effect, as follows:

$$[M_s]\{\ddot{q}\}-\left[C_f\right]\{\dot{q}\}+\left[[K_s]+[K_I]-\left[K_f\right]\right]\{q\}+\left[K^{(NL3)}\right]\{q\}^{\otimes 3}=\{0\} \tag{54}$$

Where the subscripts s and f refer to a shell in vacuo and fluid, respectively, and I refers to a shell under axial compression and/or radial pression and $\{q\}$ is the degrees of freedom vector corresponding to total nodes. $\{q\}^{\otimes 3}$ is the Kronecker product power 3 of vector $\{q\}$.

In practice, the matrices cited in the motion equation are reduced to square matrices of order $NREDUC=\bar{N}=NDF\times(NEL+1)-J$, where J represents the number of essential constraints, NDF is the number of degrees of freedom and NEL designates the number of elements. Therefore, Equation (54) becomes:

$$\left[M_s^{(r)}\right]\{\ddot{q}\}-\left[C_f^{(r)}\right]\{\dot{q}\}+\left[\left[K_s^{(r)}\right]+\left[K_I^{(r)}\right]-\left[K_f^{(r)}\right]\right]\{q\}+\left[K_{(NL3)}^{(r)}\right]\{q\}^{\otimes 3}=\{0\} \tag{55}$$

Where the subscript $"r"$ means, ‘reduced’.

Equation (55) can still be written in the index form as follows:

$$\sum_{j=1}^{\bar{N}}\left[m_{ij}\,\ddot{q}_j-c_{ij}\,\dot{q}_j+k_{ij}^{TOTAL}q_j\right]+\sum_{j,k,l=1}^{\bar{N}}k_{ijkl}^{NL3}\,q_jq_kq_l=0 \qquad i=1,\dots,\bar{N} \tag{56}$$

$k_{ij}^{TOTAL}=k_{ij}^{s}+k_{ij}^{I}-k_{ij}^{f}$, and m_{ij}, c_{ij}, k_{ij}^{TOTAL} are respectively the linear coefficients and k_{ijkl}^{NL3} is the cubic coefficients.

By further developing Equation (56), we obtain:

$$\sum_{j=1}^{\bar{N}}\left[m_{ij}\,\ddot{q}_j-c_{ij}\,\dot{q}_j+k_{ij}^{TOTAL}q_j\right]+\sum_{j=1}^{\bar{N}}n_{3_{ij}}\,q_j=0 \tag{57}$$

Where,

$$n_{3_{ij}}(q,q)=\sum_{k,l=1}^{\bar{N}}k_{ijkl}^{NL3}\,q_kq_l$$

Equation (57) can then be written as:

$$\sum_{j=1}^{\bar{N}}\left\{m_{ij}\,\ddot{q}_j - c_{ij}\,\dot{q}_j + \left[k_{ij}^{TOTAL} + n_{3_{ij}}\left(q,q\right)\right]q_j\right\} = 0 \tag{58}$$

Thus, Equation (58) is written as:

$$\left[M_s^{(r)}\right]\{\ddot{q}\} - \left[C_f^{(r)}\right]\{\dot{q}\} + \left(\left[K_{TOTAL}^{(r)}\right] + \left[N_3\left(q,q\right)\right]\right)\{q\} = \{0\} \tag{59}$$

Where N_3 denotes the cubic nonlinear stiffness matrix of dimension $\left(\bar{N}\times\bar{N}\right)$

Equation (59) can be solved using the direct iteration method; the step-by-step procedure is stated below:

1) Scale up the amplitude ratio A/h and multiply the desired value by the normalized first-mode shape vector.

2) Determine matrix $\left[N_3\left(q,q\right)\right]$ using the scaled-up eigenvector

3) Solve the nonlinear eigenvalue equation (Equation 59) using the equation reduction method and obtain the new frequency and the new corresponding eigenvector as follows:

   Rewrite Equation (59) as:

$$\begin{bmatrix} [0] & \dfrac{1}{\omega_0}\left[M_s^{(r)}\right] \\ \dfrac{1}{\omega_0^2}\left[M_s^{(r)}\right] & \dfrac{1}{\omega_0}\left[C_f^{(r)}\right] \end{bmatrix}\begin{Bmatrix}\ddot{q}\\ \dot{q}\end{Bmatrix} + \begin{bmatrix} -\dfrac{1}{\omega_0}\left[M_s^{(r)}\right] & [0] \\ [0] & [K] \end{bmatrix}\begin{Bmatrix}\dot{q}\\ q\end{Bmatrix} = \{0\} \tag{60}$$

Where ω_0 represents the first element of the elasticity matrix in Equation (A.2) and $[K]$ is the total stiffness matrix defined as follows:

$$[K] = \left[K_{TOTAL}^{(r)}\right] + \left[N_3\left(q,q\right)\right] \tag{61}$$

Thus, the corresponding eigenvalue problem is given by:

$$\left|\left[DD\right]-\frac{1}{\omega_0\Lambda}\left[I\right]\right|=0 \tag{62}$$

Where $\left[I\right]$is the identity matrix, Λ is the eigenvalue representing the complex frequency of the system and $\left[DD\right]$is defined as:

$$\left[DD\right]=\begin{bmatrix} \left[0\right] & \left[I\right] \\ \frac{1}{\omega_0^2}\left[K^{-1}\right]\left[M_s^{(r)}\right] & -\frac{1}{\omega_0}\left[K^{-1}\right]\left[C_f^{(r)}\right] \end{bmatrix} \tag{63}$$

4) Repeat steps (1–3) until convergence; the accuracy of the resulting frequency reached 10^{-5}

5.7. Results and Discussion

Before starting an analysis of our results, we conducted a convergence test and a validation study to quantify the accuracy of this hybrid method in the presence of fluid and to prove the rigour of the model developed above. Validation of the linear study is performed by calculating the critical freestream static pressure of a pressurized cylindrical shell subjected to supersonic airflow and comparing it to existing experimental data and analytical and numerical solutions. Validation of our nonlinear results as well as presentation of the effects of various parameters on the dynamic behaviour of cylindrical shells are conducted by highlighting the backbone curves in terms of variation of the relative nonlinear frequency as a function of dimensionless amplitude calculated using the present method. All of these studies refer to Cases I and II, in which the shell geometry and flow parameters have the following physical properties: $E=1.6\times10^7$ lb/in. , $\nu=0.35$, $h=0.0040$ *in.*, $L=15.4$ *in.*, $R=8.00$ *in.*, $\rho=0.000833$ lb.s^2/in.^{4} , $M=3.00$, $a_\infty=8400$ in./s and $T_{t\infty}=120^\circ$F. This set of data originates from the experimental study done by Olson and Fung [21] in the NASA Ames Research Center (It is referred to as case I). It is important to mention that some other studies, such as the case referred to Carter and Stearman [124], have different values for $L=16$ in., $E=13\times10^6$ lb/in.^{2} and $\nu=0.33$ (referred to as case II).

5.7.1. Convergence test

The convergence study presents a crucial step in finite element analysis since the results are strongly influenced by the number of finite elements. A study was conducted using the simply-supported $\left(\text{SS4}: u = v = w = 0,\ \text{and}\ \partial w/\partial x \neq 0\right)$ cylindrical shell of case I subjected to supersonic airflow. The linearized first-order piston theory including the curvature correction term is used in this case to evaluate the freestream static pressure $P_\infty = 0.1\text{psi}$. Only the first three axial modes $m = 1, 2$ and 3 are shown for $n = 23$. As seen in Figure 5.2, only twenty finite elements are sufficient to ensure convergence for the case of cylindrical shells.

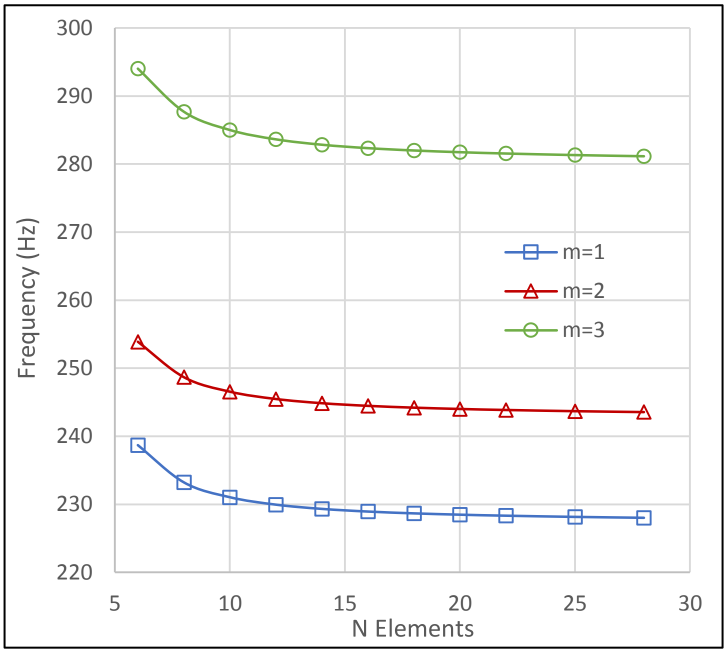

Figure 5.2: Natural frequencies versus the number of cylindrical finite elements for $n = 23$

5.7.2. Validation

This sub-section presents a validation of the results from our linear and nonlinear models in terms of boundary flutter used to characterize the onset of aeroelastic instability. The homogenous isotropic simply-supported cylindrical shell of case II is considered, with SS1 BC's $\left(u \neq 0,\ w = 0,\ \partial w/\partial x \neq 0 \text{ and } v \neq 0\right)$, under internal pressure and subjected to external supersonic airflow. The study consists in detecting, for each internal pressure applied to the structure, the values of the parameters characterizing its instability and triggering the onset of flutter. This corresponds to determining the minimum circumferential wave number $n_{\min}$ and its corresponding critical freestream static pressure P_{cr}. The results are compared with those of Carter and Stearman [124] and Haddadpour et al [29] as shown in Figure 5.3. As seen in Figure 5.3, there is a good agreement between results with a very minor difference in the critical circumferential wave number between our results and those of the other authors. It should also be noted that for all the cases considered in this study, the minimum freestream static pressure at which flutter occurs is evaluated using Equation (44). It corresponds to coalescence of the lowest and the second frequencies. Another comparison study was carried out here to validate the minimum value of the critical freestream static pressure that triggers instability of the structure.

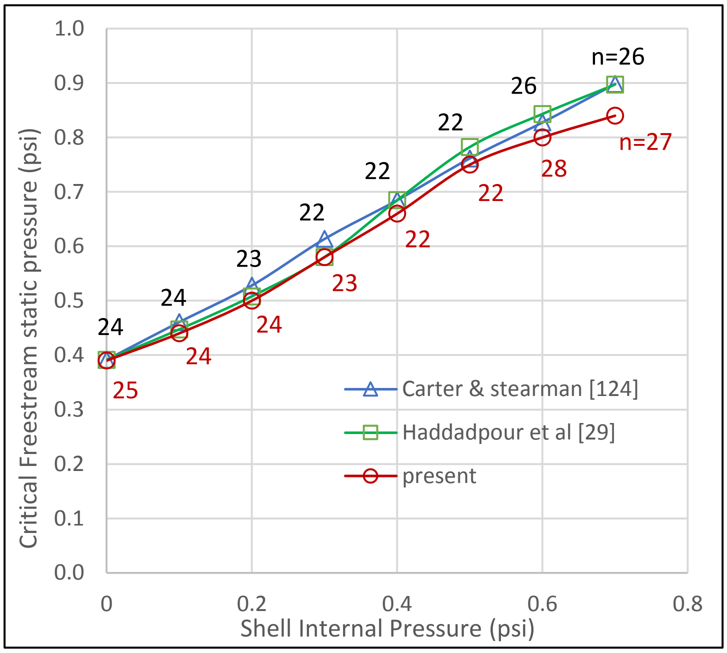

Figure 5.3: Validation of flutter boundaries for thin cylindrical shell using Haddadpour et al [29] and Carter and Stearman [124] results

It was found among the critical values calculated for different circumferential wave numbers (see Table 5.1). For both cases (I and II) with free simply-supported boundary conditions $\left(\mathrm{SS3}: u \neq 0,\ w = 0,\ \partial w/\partial x \neq 0 \text{ and } v = 0\right)$, the numerical results calculated using our approach were compared with experimental, theoretical, and numerical analyses available in the literature and a very good agreement was found with experimental data and analytical results as shown in Table 5.1.

Figure 5.4 illustrates the variation of the flutter boundary of a cylindrical shell subjected to internal pressure. The results of the stability boundary derived using our method were compared with the analytical and experimental data of Olson and Fung [21] and the numerical results of Pourya et al [125]. It should be noted that the different curves show the same tendency for different values of internal pressure. They manifest as an exponential evolution of the critical pressure as a function of the internal pressure.

Table 5.1: Comparison of the shell flutter boundary for different experimental, theoretical and numerical linear analyses

	$P_{\infty}^{cr}\,(\mathrm{Psi})$	n_{cr}	Cas N°
Experimental results [22]	0.380 -0.420	20	I
Analytical results [124]	0.42	24	II
Analytical results [21]	0.55	25	I
Analytical results [23]	0.33	27	I
FEM results [126]	0.5621	25	II
FEM results [126]	0.5621	26	I
FEM results [33]	0.5401	25	I
FEM results [32]	0.39971	25	II
FEM results [125]	0.5497	***	I
FEM results [125]	0.4033	***	II
Present results	0.521	25	I
Present results	0.382	25	II

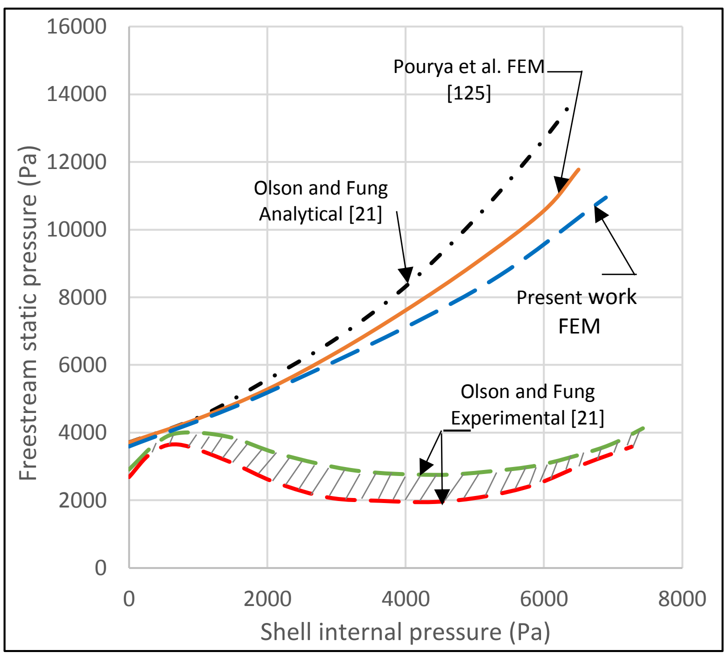

Figure 5.4: Variation of flutter boundary versus shell internal pressure for the freely simply-supported cylindrical shell of case I

The gap between the different critical pressures increases as the structures are increasingly pressurized. Furthermore, Figure 5.4 shows good agreement between the critical pressure predicted by the present study and the numerical results in the work of Pourya et al [125] in comparison to the analytical results in the work of Olson and Fung [21]. It can also be seen from the Figure that the results of the theoretical and numerical analyses demonstrate a predominant effect of the internal pressure in terms of stabilization of the structure in comparison to experimental data. The final example of validation consists in determining the geometrically nonlinear dynamic behaviour of the pressurized $(P_m = 0.5 \text{ Psi})$ freely simply-supported cylindrical shell of case I for $(n = 23)$ at the moment of the onset of flutter. It is especially interesting to note that the aerodynamic pressure is evaluated in this case using Equations (43) and (44).

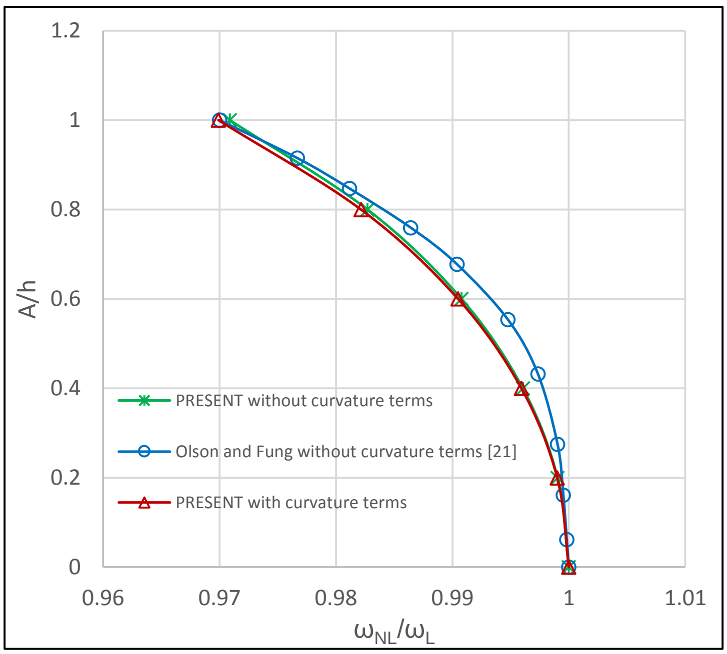

Figure 5.5: Variation of the relative nonlinear frequency ω_{NL}/ω_L as a function of the flutter dimensionless amplitude for the pressurized freely simply-supported cylindrical shell of case I for $n = 23$

Figure 5.5 shows the dependence between the nonlinear flutter frequencies and the amplitude of oscillations, which results in a softening trend curve characterizing the nonlinear behaviour. We note that the flutter relative nonlinear frequency ω_{NL}/ω_L, calculated with the first longitudinal mode, is seen to decrease slowly as the ratio A/h increases. Good agreement is seen between the present model and that of Reference [21]. The critical pressure calculated by Equation (43) is $P_\infty^{cr} = 1.28\,\text{psi}$ while that corresponding to Equation (44) reaches $P_\infty^{cr} = 1.01\,\text{psi}$. It can also be seen from the figure that the backbone curves calculated using this model, with and without the curvature correction term, are very close. This demonstrates that consideration of the curvature correction terms has no effect on the evolution of the relative flutter frequency.

5.7.3. Nonlinear dynamic behaviour during flutter

This sub-section presents an analysis of the nonlinear dynamic behavior of a cylindrical structure during two stages neighbouring the critical mode, which is characterized by the lowest critical static freestream pressure leading to the appearance of flutter. The stability region preceding the onset of flutter is characterized by a pressure equal to $P_\infty = 0.8 \times P_\infty^{cr}$ while the post-instability zone is defined by a pressure equal to $P_\infty = 1.5 \times P_\infty^{cr}$. The freely simply-supported cylindrical shell of case I is considered. The flutter boundary of the pressurized shell $(P_m = 0.5 \text{ psi})$ occurs at $P_\infty^{cr} = 0.992 \text{ psi}$, corresponding to a critical circumferential wave number equal to $n_{cr} = 22$. In Figure 5.6, a slow decrease of the relative nonlinear frequency ω_{NL}/ω_L with an increase of the ratio A/h is revealed for all the curves, which highlights a typical behaviour characterizing the softening type of nonlinearity.

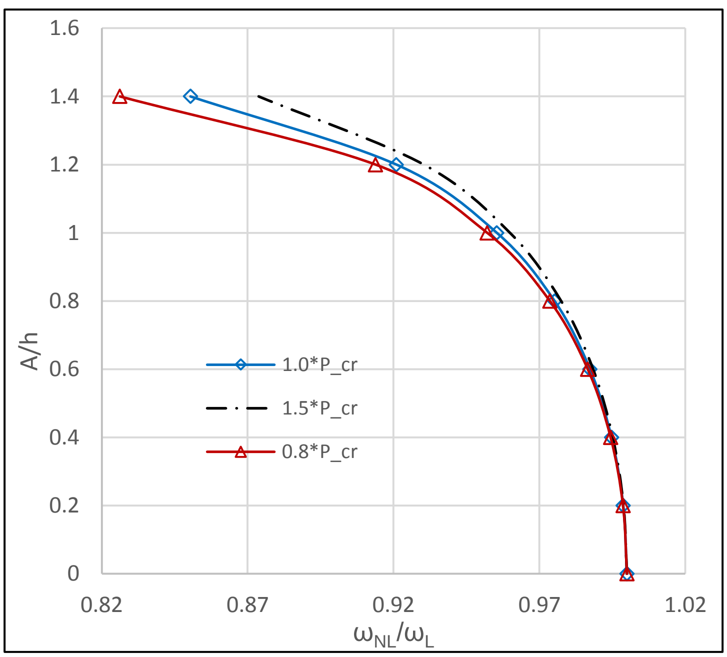

Figure 5.6: Variation of the relative nonlinear frequency ω_{NL}/ω_L as a function of ratio A/h for different freestream static pressures located in the neighbourhood of the flutter onset region

The figure also demonstrates that the curve corresponding to the lowest value of aerodynamic pressure $\left(P_\infty = 0.8\times P_\infty^{cr}\right)$ is the most pronounced. As seen in the figure, the variation of the flutter frequency corresponding to different pressures neighbouring the critical value is negligible for low values of vibration amplitude. This variation becomes significant for large values of the A/h ratio. It can also be noticed that the nonlinear frequency increases as the pressure applied to the structure grows (this can be illustrated by plotting the horizontal corresponding to A/h fixed; the ratio ω_{NL}/ω_L increases as the value of the applied aerodynamic pressure grows).

5.7.4. Effect of internal pressure on the nonlinear dynamic behaviour of a cylindrical shell during flutter

The initial stiffening effect due to internal pressure on the geometrical nonlinear dynamic behaviour of the cylindrical shell of case I is investigated in this sub-section. For both data sets (pressurized and unpressurized shell) the free simply-supported boundary is considered.

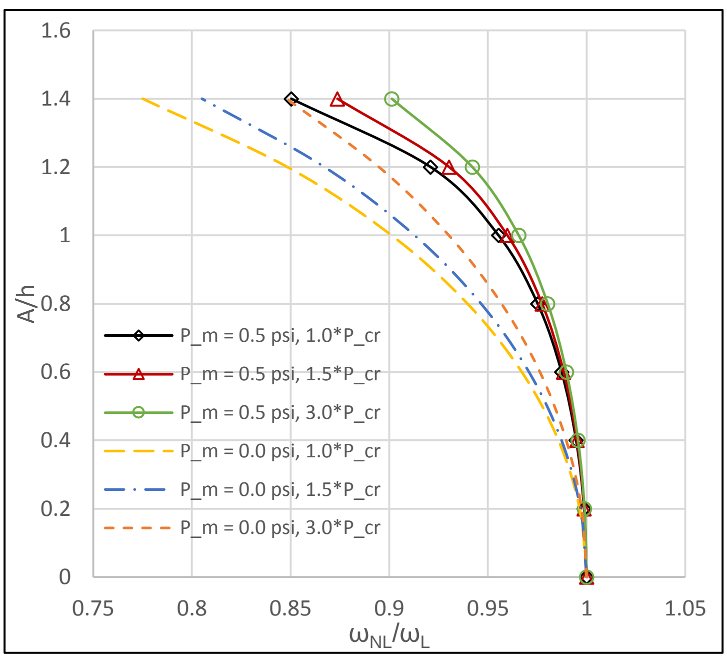

Figure 5.7: Backbone curve during the stage following the onset of flutter for the cylindrical shells of case I with and without internal pressure (P_m)

The minimum value of the critical freestream static pressure for the pressurized shell is evaluated at $P_\infty^{cr} = 0.992$ psi for its corresponding critical circumferential wave number equal to $n_{cr} = 22$

while the critical aerodynamic pressure of the unpressurized shell is equal to $P_\infty^{cr} = 0.521$ psi for $n_{cr} = 25$. Two values of aerodynamic pressure $P_\infty = 1.5 \times P_\infty^{cr}$ and $P_\infty = 3 \times P_\infty^{cr}$ are considered here to assess the dynamic behaviour of the shell during the stage following the onset of flutter. The first remark that can be deduced from numerical results is the stabilizing effect of the internal pressure. $P_\infty^{cr} = 0.992 > P_\infty^{cr} = 0.521$ which supports the results found by Olson and Fung [21] and Amabilli and Pellicano [23,24]. We also note that the trend of nonlinearity revealed in Figure 5.7, for all the cases studied, is of a softening type and the curves of the unpressurized shells are more accentuated.

5.7.5. Effect of nonlinear coupling

This study of the dynamic behaviour of geometrically nonlinear structures highlights the omnipresence of typically nonlinear phenomena, namely the phenomenon of nonlinear coupling between generalized coordinates. The effect of this phenomenon is emphasized in this section through analysis of the dynamic behaviour of pressurized freely simply-supported cylindrical shells subjected to supersonic flow whose geometry characteristics and flow parameters are those of case I for $n = 23$. As shown in Figure 5.8, the numerical results derived from this study exhibit a nonlinear trend of a softening type for the two cases (with and without coupling).

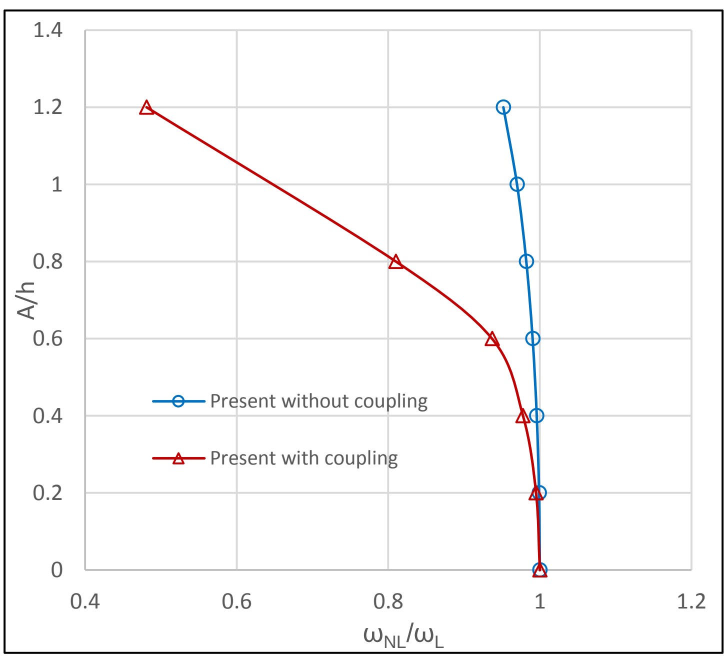

Figure 5.8: Coupling effect between the different modes, on the nonlinear dynamic behaviour of a pressurized cylindrical shell with free simply-supported boundary

It can also be seen from Figure 5.8 that the curve exhibiting coupling is more pronounced than the curve without coupling, which demonstrates that the effect of this phenomenon is an accentuation of the softening character of nonlinear dynamic behaviour. Moreover, the coupling manifests itself by a transfer of energy between the different modes [115]. The figure also shows that the nonlinear coupling effect starts at the ratio $A/h = 0.2$ and becomes progressively more pronounced as the vibration amplitude increases, indicating the presence of a bifurcation of the backbone curve with coupling at the ratio $A/h = 0.6$.

5.7.6. Effect of circumferential wave number n

We evaluate here the effect of the variation of the circumferential wave number n on the nonlinear dynamic behaviour of a cylindrical shell subjected to supersonic flow. Note that for all the cases studied here, the structure has lost its dynamic stability and the aerodynamic pressure of the flow is indeed the critical freestream static pressure of flutter. Figure 5.9 presents the variation of flutter frequency as a function of flutter amplitude for different circumferential wave numbers: $n = 24 - 29$ for the pressurized $\left(P_m = 0.5 \text{ psi}\right)$, freely simply-supported cylindrical shell of case I.

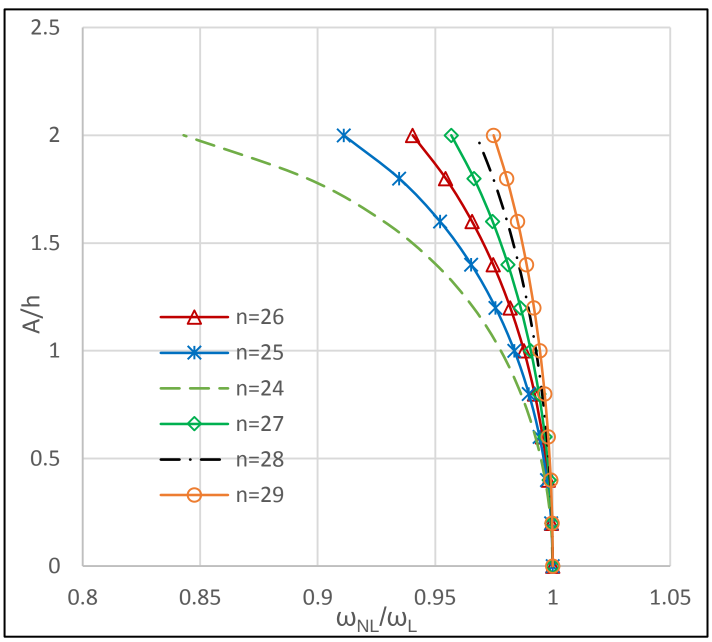

Figure 5.9: Variation of the dimensionless flutter frequency ω_{NL}/ω_L as a function of ratio A/h for a freely simply-supported cylindrical shell at different circumferential wave numbers

As seen from the figure, for a fixed value of the ratio A/h, the relative nonlinear frequency decreases as n decreases, and the gap between the different curves is decreasing as the circumferential wave number becomes larger. Moreover, the curve corresponding to $n = 24$ is the most pronounced.

5.7.7. Geometry effect

In this section, we analyze the effect of variation of the length-to-radius and the radius-to-thickness ratios of a pressurized thin cylindrical shell subjected to external supersonic airflow, on its nonlinear dynamic behaviour corresponding to the onset of flutter and during flutter stages.

5.7.7.1. Effect of L/R ratio on supersonic flutter

To assess the effect of the variation of the shell length on its nonlinear dynamic behaviour, a study was conducted in this sub-section highlighting the analysis of the nonlinear vibration of a thin pressurized cylindrical shell $(P_m = 0.5\,\text{psi})$ subjected to supersonic airflow as a function of the variation of its slenderness. The shell considered is freely simply-supported corresponding to case I. The study revolves around three main steps stipulating the variation of the L/R ratio according to the fundamental parameters influencing instability: the applied freestream static pressure and the circumferential wave number. The first step is to vary the ratio L/R (variation of L keeping R constant). For each length L, the corresponding minimum circumferential wave number (n_{cr}) and the critical freestream static pressure (P_∞^{cr}) are sought. In the second step, the value of L is varied while fixing the circumferential wave number at $(n = 22)$ and looking for the critical pressure for each L. The third step consists in keeping the same number n fixed as in step 2 and choosing the aerodynamic pressure P_∞ so that it is greater than all the critical pressures corresponding to step 2. Figure 5.10 shows the variation of the relative flutter frequency as a function of the dimensionless amplitude A/h for different values of the L/R ratio varying as follows: 3.0, 3.5, 4.0 and 5.0. The first remark, which is obvious when examining Figure 5.10, is the softening tendency that characterizes all the curves of the different cases studied. Furthermore, focusing on the curves that follow from step 2 and 3 previously described, we notice that, for structures that are increasingly slender, the nonlinear dynamic behaviour is less softening.

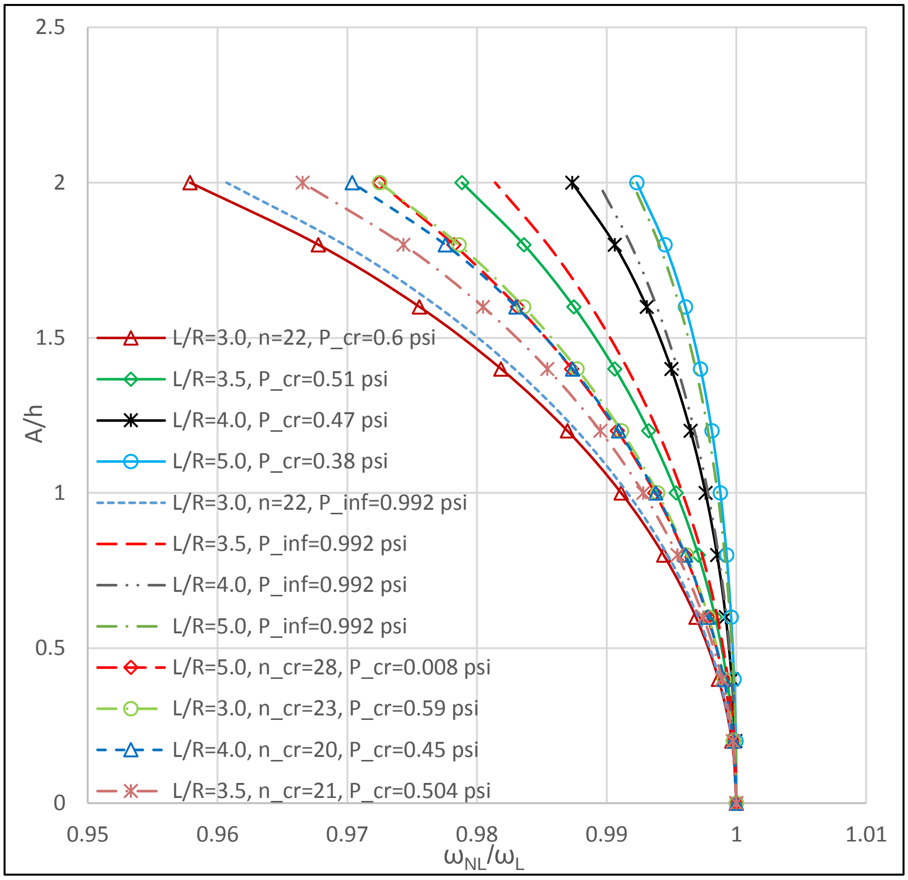

Figure 5.10: Variation of the dimensionless flutter frequency ω_{NL}/ω_L as a function of ratio A/h for a pressurized, freely simply-supported cylindrical shell at different L/R ratios

This is accompanied by an equally important phenomenon which resides in the gradual decrease of the gap between the different curves for large amplitudes of vibration, since the structure is more slender $\left(L/R\,\text{growing}\right)$. This can be illustrated by plotting the horizontal corresponding to a fixed value of A/h and detecting, accordingly, the spread that lies between the different ω_{NL}/ω_L ratios corresponding to the different *L/R* values. Another remark that is revealed by analyzing Figure 5.10 is the existence of a synergism between the different curves corresponding to the ratios *L/R*=3.0, 4.0 and 5.0 for curves generated based on the criteria of step1. We notice that the dispersion between these curves is much less intense compared to those resulting from step 2 and 3. The curves are almost merged, which shows an absence of the effect of variation of the shell length for these cases. Nevertheless, the effect of length increases for *L/R*=3.5. The figure also shows that the curves for step 2 appear more pronounced compared to those for step 3 for the different *L/R* ratios, except for one corresponding to *L/R*=5.0, where the curve of step 3 is more pronounced than that of step 2.

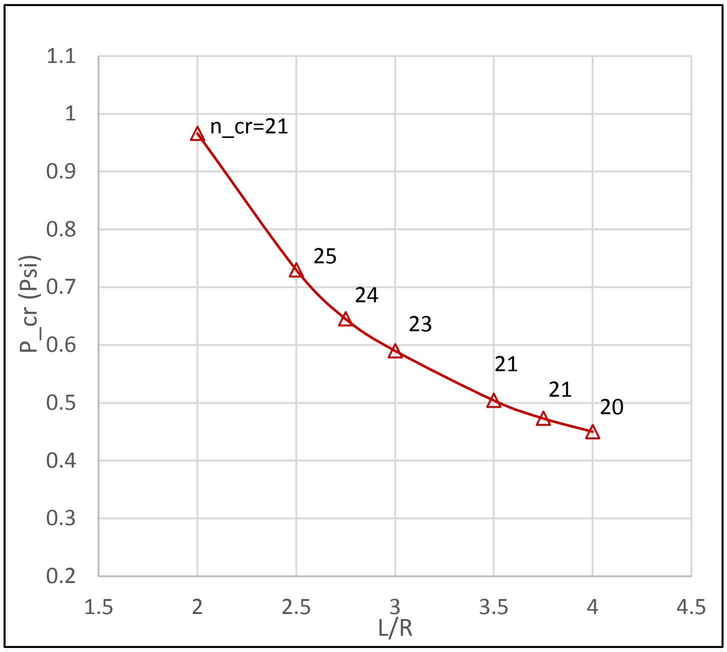

Figure 5.11: Variation of the flutter boundary with ratio L/R for the pressurized freely simply-supported cylindrical shell of case I

Figure 5.11 presents the variation of the critical pressure as a function of the *L/R* ratio relative to step1. It is important to note that the results illustrated in Figure 5.11 also show the existence of a correlation between the lowest critical pressure applied on the structure and the variation of its length. As depicted in the figure, the lowest critical value of freestream static pressure for each circumferential wave number becomes larger when the L/R ratio is decreased. This is demonstrated by a sudden decrease in critical pressure for small values of structure length (the slope of the tangent to the curve is pronounced for low *L/R* ratios) and a slight decrease in the critical pressure value as the length of the structure becomes more significant. We may thus conclude that the more slender the structure, the more vulnerable it will be to instability.

5.7.7.2. Effect of R/h ratio on supersonic flutter

Numerical calculations have been conducted to examine the effect of the variation of the radius-to-thickness ratio R/h (R is variable and h is kept fixed) on the nonlinear dynamic behaviour of a thin, pressurized $\left(P_m = 0.5\,\text{psi}\right)$ freely simply-supported cylindrical shell subjected to external supersonic airflow, corresponding to case I. Following the same approach mentioned in the section 5.7.7.1, three main steps are applied here, involving variation of the radius *R* in accordance with certain particularities relating to each step: the first step consists in finding, for each *R*, the minimum value of the circumferential wave number and the corresponding critical freestream static pressure. The second step is completed by fixing the number n $(n=22)$ and searching for the critical pressure corresponding to each R. In the third step, we fix both the number n $(n=22)$ and the aerodynamic pressure so that the latter is greater than the maximum of the critical freestream static pressures detected in step 2 to ensure that the structure is in its instability phase. Figure 5.12 shows the variation of the dimensionless amplitude A/h as a function of the flutter relative frequency for different values of the ratio R/h: $R/h = 875, 1125, 1250$ and 1750. It is clear from the figure that all the curves have a nonlinear softening character.

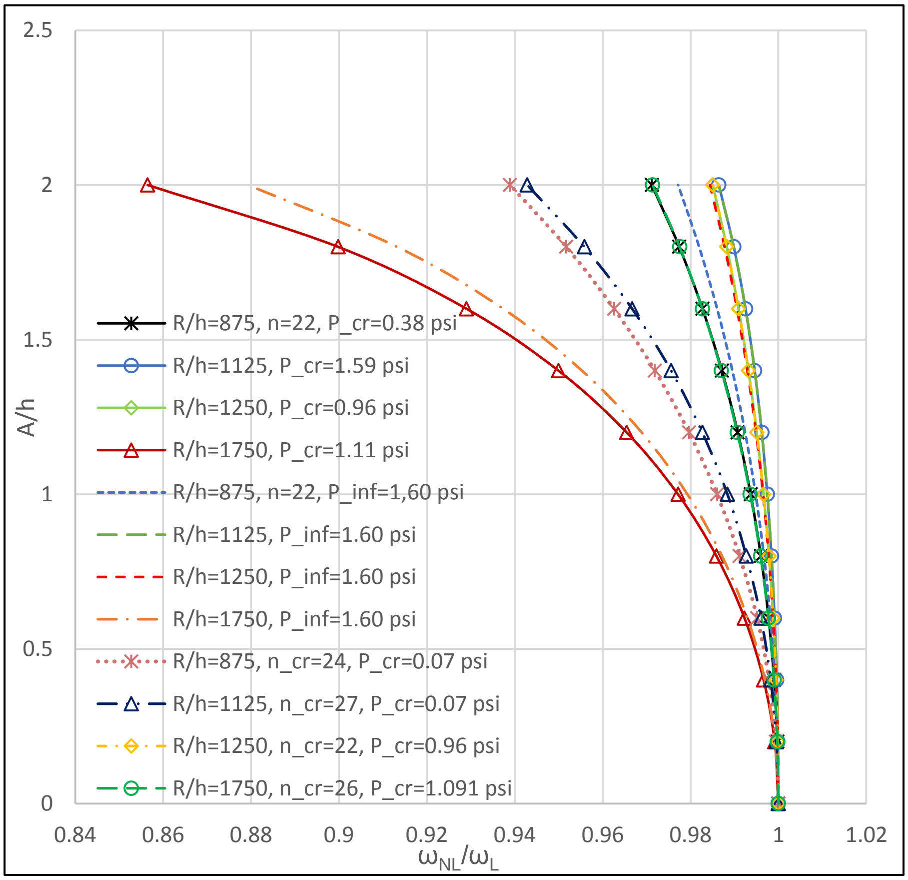

Figure 5.12: Effect of the radius-to-thickness ratio on the nonlinear dynamic behaviour of a pressurized freely simply-supported cylindrical shell

By examining Figure 5.12 we note that the trend of the curves corresponding to step 2 becomes more softening as the radius of the shell increases except for the case $R/h = 875$. The same behaviour is observed for the curves related to step 3 (which occurred during the instability of the shell) by discerning a more softening trend for the curves corresponding to step 2 (performed at the onset of flutter). Figure 5.12 also shows that the curve corresponding to $R/h = 1750$ resulting from step 2 seems to be the most pronounced. Additionally, it is important to note that the curves corresponding to $R/h = 875$ and $R/h = 1125$ relating to step 1, appear to have the same value of the critical pressure with a difference in the minimum value of the circumferential wave number $\left(n_{cr} = 24 \text{ and } n_{cr} = 27 \text{ respectively}\right)$, which seems to be the most pronounced for the curve with the smallest radius.

5.7.8. Effect of boundary conditions

In order to illustrate the effect of boundary conditions on the nonlinear behaviour of a thin cylindrical shell exposed to supersonic flow, the flutter boundaries were obtained for the pressurized and unpressurized shells of case I and the relative nonlinear frequencies were computed as a function of dimensionless amplitude A/h. It should be noted that the boundary conditions are defined based on Tong's convention [116] presented in Table 5.2.

Table 5.2: Boundary conditions according to the Tong's convention [116]

Name	u	v	w	$\partial w/\partial x$
F	Free	Free	Free	Free
SS0	0	Free	Free	Free
SS1	Free	Free	0	Free
SS2	0	Free	0	Free
SS3	Free	0	0	Free
SS4	0	0	0	Free
CC1	Free	Free	0	0
CC2	0	Free	0	0
CC3	Free	0	0	0
CC4	0	0	0	0

The analysis consists of determining, for each boundary condition, the minimum value of the critical freestream static pressure P_{cr} and its corresponding circumferential wave number n_{cr}, for each case of pressurized $\left(P_m = 0.5\,\text{psi}\right)$ and unpressurized shells as presented in Table 5.3. The numerical results highlight the ability of the developed model to support a variety of boundary conditions. As seen in Figure 5.13, all the curves present a softening trend of nonlinear dynamic behaviour occurring at the onset of flutter. Table 5.3 shows the effects of different simply-supported and clamped boundary conditions (BCs) on the stability of the structure.

Table 5.3: Critical freestream static pressure giving onset of flutter of a thin cylindrical shell under different boundary conditions $\left(P_x = 0.0\,\text{psi}\right)$

B.C	$P_m\,(\text{psi})$	$P_\infty^{cr}\,(\text{psi})$	n_{cr}
S1-S1	0.5	0.980	22
S2-S2		1.076	25
S3-S3		0.992	22
S4-S4		1.085	25
C1-C1		1.000	22
C2-C2		1.086	25
C3-C3		1.000	22
C4-C4		1.088	25
S1-S1	0.0	0.520	25
S2-S2		0.652	28
S3-S3		0.521	25
S4-S4		0.654	28
C1-C1		0.540	26
C2-C2		0.656	28
C3-C3		0.543	26
C4-C4		0.656	28

Observation of Table 5.3 reveals that, for the case with the least constraints at the ends among the eight sets of BCs (the case with out-of-plane constraint: SS1), the critical static pressure is the lowest. This remains valid for pressurized and non-pressurized shells. Another remark that can be highlighted from Table 5.3 concerning the cases without any axial constraints at the ends; the shell is more vulnerable to instability for these configurations (SS3 vs SS4 and CC3 vs CC4) whether it is for a pressurized shell or a structure without internal pressure. According to Figure 5.13, for boundary conditions with in-plane constraints at the ends, the backbone curves are merged (SS4 and CC4). Looking further, we note that the curve with the SS3 boundary condition is the most pronounced. It is also imperative to note that the gap between the curves corresponding to SS3 and SS4 boundary conditions is significant for large vibration amplitudes corresponding to unpressurized shells. This gap is reduced when the structures are subjected to internal pressures. The result presented in Figure 5.14.a, it leads to the observation that case CC3 which is not constrained in the axial direction presents a more softening trend compared to case CC4.

This is clearly demonstrated for the unpressurized shell as well as for those subjected to internal pressure. The same behaviour is revealed in Figure 5.14.b for the simply-supported case.

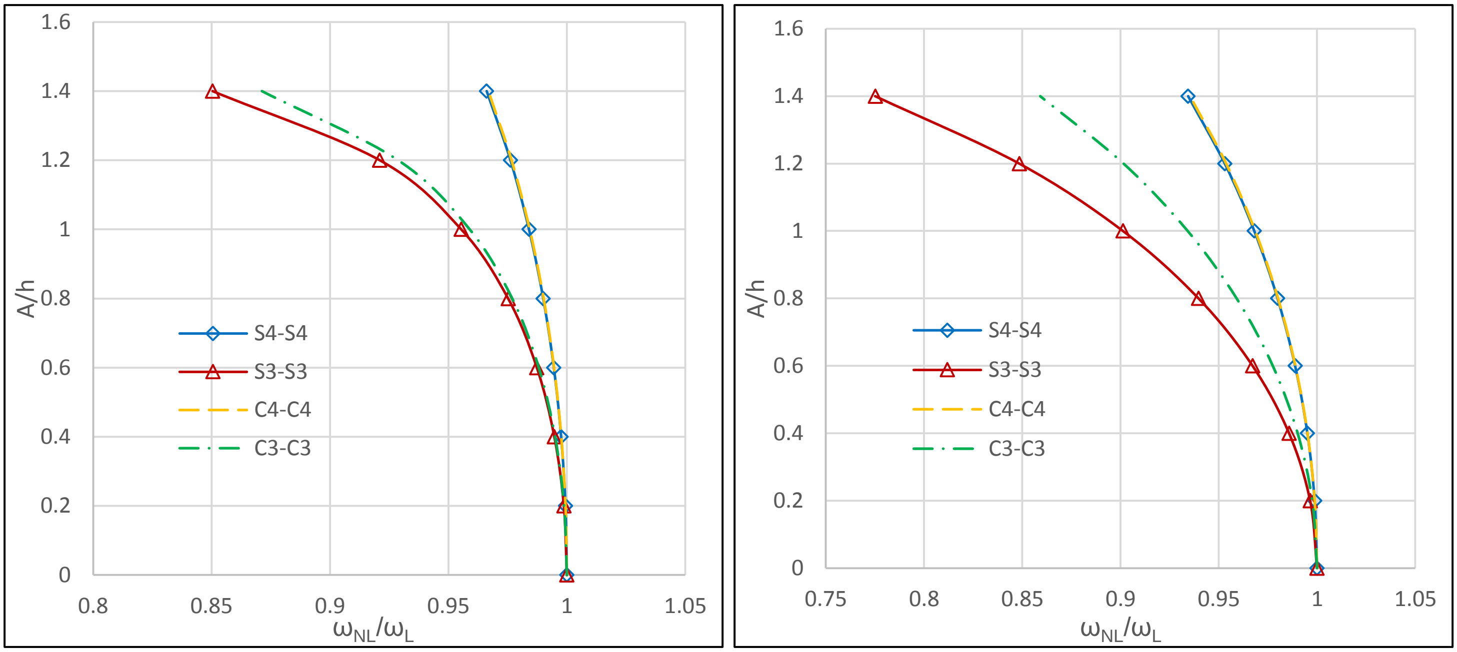

(*a*) (*b*)

Figure 5.13: Effect of boundary conditions on the nonlinear aeroelastic behaviour of a (*a*) pressurized (*b*) unpressurized cylindrical shell at the onset of flutter (C: clamped, S: simply supported)

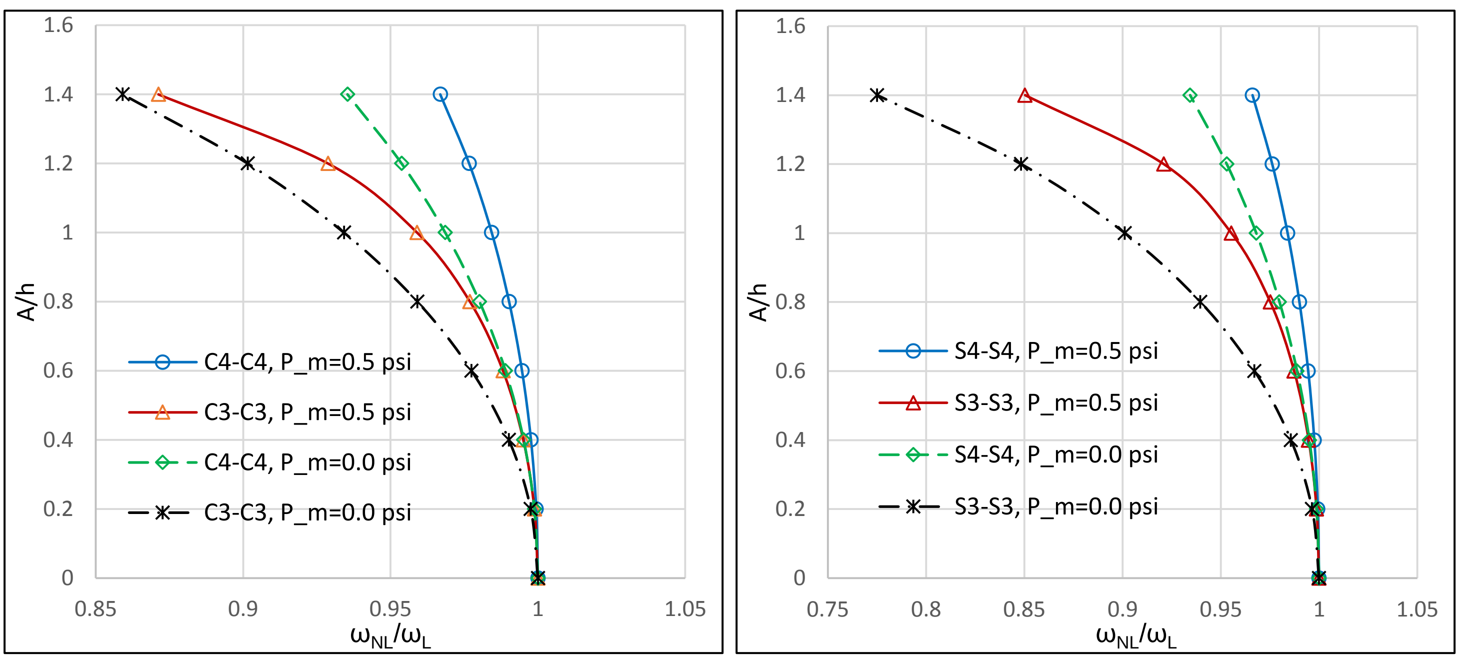

(*a*) (*b*)

Figure 5.14: Variation of the relative flutter frequency as a function of the dimensionless amplitude of a (*a*) clamped and (*b*) simply-supported cylindrical shell for cases P_m=0.0 psi and P_m=0.5 psi

It can also be seen from Figure 5.14 that, by considering the same boundary condition, the softening character of the nonlinear dynamic behaviour of unpressurized shells is more accentuated compared to that of pressurized shells, which reinforces the results found in sub-section 5.7.4. Furthermore, we note that the gap between the curves corresponding to case CC3 of pressurized and unpressurized shells decreases remarkably for the large vibration amplitudes considered at the onset of flutter (the gap becomes more contiguous at $A/h = 1.4$). This is unlike case CC4, which shows an increase in the gap between the relative frequencies for large A/h ratios. For the simply-supported case, the gap between the SS3 curves, corresponding to pressurized and unpressurized shells, is significant.

5.8. Conclusion

A semi-analytical FEM is implemented in this paper to investigate the effect of geometric nonlinearities on the dynamic behaviour of a thin cylindrical shell subjected to external supersonic flow. The study is performed by considering the effects of stress stiffness due to internal pressure and axial loading on the flutter boundaries. The geometric nonlinearities are highlighted due to the theory developed in this paper based on the Novozhilov nonlinear kinematics and taking into account the curvature effect of the displacement field in the circumferential direction, the initial geometric imperfections and the influence of nonlinear coupling between the different modes. Linear analysis is performed to identify the shape functions, which are found from exact solution of Sander's shell theory and then used in the nonlinear analysis as a spatial function. The linearized first-order potential (piston) theory, with and without a correction factor for curvature, is also used for aerodynamic modeling to derive aerodynamic damping and stiffness matrices. The governing nonlinear aeroelastic equations are derived using the Lagrange approach and solved by a direct iterative method. The method benefits from the advantages of the finite element technique, which facilitates the study of complex shells, and the precision of results obtained by analytical means. This concept results in fast and efficient convergence when applied to investigate the dynamic stability and the dynamic behaviour of shells during the flutter stage. Numerical studies are conducted for different shell boundary conditions and geometries to examine the nonlinear dynamic behaviour of cylindrical shells at the onset of flutter and during the stage beyond the appearance of flutter. Results are provided and discussed in detail for isotropic thin cylindrical shells. Finally, it is important to point out the capability of the model developed in this paper to analyze the nonlinear dynamic behaviour of cylindrical structures during their instability phase, which is not possible if linear analysis is employed. It is also shown that this aeroelastic model gives accurate results but needs to be used to deal with aerodynamic nonlinearities to improve the consistency of the FEM package.

5.9. Appendix

5.9.1. Appendix A

Matrix $[P]$

The elasticity matrix $[P]$ of order (6×6) for an anisotropic material is expressed as:

$$[P]=\begin{bmatrix} P_{11} & P_{12} & 0 & P_{14} & P_{15} & 0 \\ P_{21} & P_{22} & 0 & P_{24} & P_{25} & 0 \\ 0 & 0 & P_{33} & 0 & 0 & P_{36} \\ P_{41} & P_{42} & 0 & P_{44} & P_{45} & 0 \\ P_{51} & P_{52} & 0 & P_{54} & P_{55} & 0 \\ 0 & 0 & P_{63} & 0 & 0 & P_{66} \end{bmatrix} \qquad (A.1)$$

In the case of isotropic material, the matrix of elasticity becomes:

$$[P]=\begin{bmatrix} C & \nu C & 0 & 0 & 0 & 0 \\ \nu C & C & 0 & 0 & 0 & 0 \\ 0 & 0 & \dfrac{C(1-\nu)}{2} & 0 & 0 & 0 \\ 0 & 0 & 0 & D & \nu D & 0 \\ 0 & 0 & 0 & \nu D & D & 0 \\ 0 & 0 & 0 & 0 & 0 & \dfrac{D(1-\nu)}{2} \end{bmatrix} \qquad (A.2)$$

where $C=\dfrac{Eh}{1-\nu^2}$, $D=\dfrac{Eh^3}{12\left(1-\nu^2\right)}$, E is Young's modulus, ν is Poisson's ratio and h the shell thickness.

After integrating each component of the stress vector over the thickness of the shell, the normal stress resultant and moment resultant for an isotropic cylindrical shell can be written as:

$$\{\sigma\}=\begin{Bmatrix} N_x \\ N_\theta \\ N_{x\theta} \\ M_x \\ M_\theta \\ M_{x\theta} \end{Bmatrix}=[P]\begin{Bmatrix} \varepsilon_x \\ \varepsilon_\theta \\ 2\varepsilon_{x\theta} \\ k_x \\ k_\theta \\ 2k_{x\theta} \end{Bmatrix} \qquad (A.3)$$

Sander's linear equations for thin anisotropic cylindrical shell in terms of axial, tangential, and circumferential displacements are as follows:

$$L_1\left(U,V,W,P_{ij}\right)=P_{11}\frac{\partial^2 U}{\partial x^2}+\frac{P_{12}}{R}\frac{\partial^2 U}{\partial x^2}\left(\frac{\partial^2 V}{\partial x\partial\theta}+\frac{\partial W}{\partial x}\right)-P_{14}\frac{\partial^3 W}{\partial x^3}+\frac{P_{15}}{R^2}\left(\frac{\partial^3 W}{\partial x\partial\theta^2}+\frac{\partial^2 V}{\partial x\partial\theta}\right)$$
$$+\left(\frac{P_{33}}{R}-\frac{P_{63}}{2R^2}\right)\left(\frac{\partial^2 V}{\partial x\partial\theta}+\frac{1}{R}\frac{\partial^2 U}{\partial\theta^2}\right)+\left(\frac{P_{36}}{R^2}-\frac{P_{66}}{2R^3}\right)\left(-2\frac{\partial^3 W}{\partial x\partial\theta^2}+\frac{3}{2}\frac{\partial^2 V}{\partial x\partial\theta}-\frac{1}{2R}\frac{\partial^2 U}{\partial\theta^2}\right) \qquad (A.4)$$

$$L_2\left(U,V,W,P_{ij}\right)=\left(\frac{P_{21}}{R}-\frac{P_{51}}{R^2}\right)\frac{\partial^2 U}{\partial x\partial\theta}+\frac{1}{R}\left(\frac{P_{22}}{R}+\frac{P_{52}}{R^2}\right)\left(\frac{\partial^2 V}{\partial\theta^2}+\frac{\partial W}{\partial\theta}\right)-\left(\frac{P_{24}}{R}+\frac{P_{54}}{R^2}\right)\frac{\partial^3 W}{\partial x^2\partial\theta}$$
$$+\frac{1}{R^2}\left(\frac{P_{25}}{R}+\frac{P_{55}}{R^2}\right)\left(-\frac{\partial^3 W}{\partial\theta^3}+\frac{\partial^2 V}{\partial\theta^2}\right)+\left(P_{33}+\frac{3P_{63}}{2R}\right)\left(\frac{\partial^2 V}{\partial x^2}+\frac{\partial^2 U}{R\partial x\partial\theta}\right)$$
$$+\frac{1}{R}\left(P_{36}+\frac{3P_{66}}{2R}\right)\left(-2\frac{\partial^3 W}{\partial x^2\partial\theta}+\frac{3}{2}\frac{\partial^2 V}{\partial x^2}-\frac{1}{2R}\frac{\partial^2 U}{\partial x\partial\theta}\right) \qquad (A.5)$$

$$L_3\left(U,V,W,P_{ij}\right)=P_{41}\frac{\partial^3 U}{\partial x^3}+\frac{P_{42}}{R}\left(\frac{\partial^3 V}{\partial x^2\partial\theta}+\frac{\partial^2 W}{\partial x^2}\right)-P_{44}\frac{\partial^4 W}{\partial x^4}+\frac{P_{45}}{R^2}\left(-\frac{\partial^4 W}{\partial x^2\partial\theta^2}+\frac{\partial^3 V}{\partial x^2\partial\theta}\right)$$
$$+\frac{2P_{63}}{R}\left(\frac{1}{R}\frac{\partial^3 U}{\partial x\partial\theta^2}+\frac{\partial^3 V}{\partial x^2\partial\theta}\right)+\frac{2P_{66}}{R^2}\left(-2\frac{\partial^4 W}{\partial x^2\partial\theta^2}+\frac{3}{2}\frac{\partial^3 V}{\partial x^2\partial\theta}-\frac{1}{2R}\frac{\partial^3 U}{\partial x\partial\theta^2}\right)+\frac{P_{51}}{R^2}\frac{\partial^3 U}{\partial x\partial\theta^2}$$
$$+\frac{P_{52}}{R^3}\left(\frac{\partial^3 V}{\partial\theta^3}+\frac{\partial^2 W}{\partial\theta^2}\right)+\frac{P_{55}}{R^4}\left(-\frac{\partial^4 W}{\partial\theta^4}+\frac{\partial^3 V}{\partial\theta^3}\right)-\frac{P_{21}}{R}\frac{\partial U}{\partial x}-\frac{P_{54}}{R^2}\frac{\partial^4 W}{\partial x^2\partial\theta^2}+\frac{P_{22}}{R^2}\left(\frac{\partial V}{\partial\theta}+W\right)$$
$$+\frac{P_{24}}{R^2}\frac{\partial^2 W}{\partial\theta^2}-\frac{P_{25}}{R^3}\left(-\frac{\partial^2 W}{\partial\theta^2}+\frac{\partial V}{\partial\theta}\right) \qquad (A.6)$$

Matrices $[T]_{3\times3}, [R]_{3\times8}, [A]_{8\times8}$ and $[Q]_{6\times8}$ are defined as

Matrix $[T]$

$$[T]=\begin{bmatrix} \cos n\theta & 0 & 0 \\ 0 & \cos n\theta & 0 \\ 0 & 0 & \sin n\theta \end{bmatrix} \qquad (A.7)$$

Matrix $[R]$

$$[R]=\begin{bmatrix} \alpha_1 e^{(\lambda_1 x/R)} & \alpha_2 e^{(\lambda_2 x/R)} & \alpha_3 e^{(\lambda_3 x/R)} & \alpha_4 e^{(\lambda_4 x/R)} & \alpha_5 e^{(\lambda_5 x/R)} & \alpha_6 e^{(\lambda_6 x/R)} & \alpha_7 e^{(\lambda_7 x/R)} & \alpha_8 e^{(\lambda_8 x/R)} \\ e^{(\lambda_1 x/R)} & e^{(\lambda_2 x/R)} & e^{(\lambda_3 x/R)} & e^{(\lambda_4 x/R)} & e^{(\lambda_5 x/R)} & e^{(\lambda_6 x/R)} & e^{(\lambda_7 x/R)} & e^{(\lambda_8 x/R)} \\ \beta_1 e^{(\lambda_1 x/R)} & \beta_2 e^{(\lambda_2 x/R)} & \beta_3 e^{(\lambda_3 x/R)} & \beta_4 e^{(\lambda_4 x/R)} & \beta_5 e^{(\lambda_5 x/R)} & \beta_6 e^{(\lambda_6 x/R)} & \beta_7 e^{(\lambda_7 x/R)} & \beta_8 e^{(\lambda_8 x/R)} \end{bmatrix} \quad (A.8)$$

Matrix $[A]$

$$A(1,i)=\alpha_i,\ A(2,i)=1,\ A(3,i)=\frac{\lambda_i}{R},\ A(4,i)=\beta_i,\ A(5,i)=\alpha_i e^{\lambda_i l/R},\ A(6,i)=e^{\lambda_i l/R},$$

$$A(7,i)=\frac{\lambda_i}{R}e^{\lambda_i l/R},\ A(8,i)=\beta_i e^{\lambda_i l/R} \qquad i=1,2,...,8. \qquad (A.9)$$

Matrix $[Q]$

$$Q(1,i)=\alpha_i\frac{\lambda_i}{R}e^{\lambda_i x/R}, \qquad Q(2,i)=\frac{1}{R}(n\beta_i+1)e^{\lambda_i x/R}, \qquad Q(3,i)=\frac{1}{R}(\beta_i\lambda_i-n\alpha_i)e^{\lambda_i x/R},$$

$$Q(4,i)=-\left(\frac{\lambda_i}{R}\right)^2 e^{\lambda_i x/R},\ Q(5,i)=\frac{1}{R^2}\left(n^2+\beta_i n\right)e^{\lambda_i x/R},$$

$$Q(6,i)=\frac{1}{R^2}\left(2n\lambda_i+\frac{3}{2}\beta_i\lambda_i+\frac{1}{2}n\alpha_i\right)e^{\lambda_i x/R} \qquad i=1,2,...,8 \qquad (A.10)$$

5.9.2. Appendix B

The middle surface strain-displacement relationships corresponding to the Novozhilov nonlinear shell theory of circular shells:

$$\varepsilon_{x,0}=\frac{\partial u}{\partial x}+\frac{1}{2}\left[\left(\frac{\partial u}{\partial x}\right)^2+\left(\frac{\partial v}{\partial x}\right)^2+\left(\frac{\partial w}{\partial x}\right)^2\right]+\frac{\partial w}{\partial x}\frac{\partial w_0}{\partial x}, \qquad (B.1)$$

$$\varepsilon_{\theta,0}=\frac{\partial v}{R\partial\theta}+\frac{w}{R}+\frac{1}{2R^2}\left[\left(\frac{\partial u}{\partial\theta}\right)^2+\left(\frac{\partial v}{\partial\theta}+w\right)^2+\left(\frac{\partial w}{\partial\theta}-v\right)^2\right]$$
$$+\frac{1}{R^2}\left[\frac{\partial w_0}{\partial\theta}\left(\frac{\partial w}{\partial\theta}-v\right)+w_0\left(w+\frac{\partial v}{\partial\theta}\right)\right], \qquad (B.2)$$

$$\gamma_{x\theta,0}=\frac{\partial v}{\partial x}+\frac{\partial u}{R\partial\theta}+\frac{1}{R}\left[\frac{\partial u}{\partial x}\frac{\partial u}{\partial\theta}+\frac{\partial v}{\partial x}\left(\frac{\partial v}{\partial\theta}+w\right)+\left(\frac{\partial w}{\partial x}+\frac{\partial w_0}{\partial x}\right)\left(\frac{\partial w}{\partial\theta}-v\right)+\frac{\partial w}{\partial x}\frac{\partial w_0}{\partial\theta}+\frac{\partial v}{\partial x}w_0\right], \qquad (B.3)$$

$$k_x = -\frac{\partial^2 w}{\partial x^2} + \frac{\partial v}{R\partial x}\left(-\frac{\partial u}{R\partial \theta} + \frac{\partial v}{\partial x} - \frac{\partial^2 \left(w + w_0 \right)}{\partial x \partial \theta} \right) + \frac{\partial \left(w + w_0 \right)}{\partial x}\frac{\partial^2 u}{\partial x^2} + \frac{\partial^2 u}{R\partial x \partial \theta}\left(-\frac{v}{R} + \frac{\partial \left(w + w_0 \right)}{R\partial \theta} \right)$$

$$+ \frac{\partial^2 \left(w + w_0 \right)}{R\partial x \partial \theta}\frac{\partial u}{R\partial \theta} - \frac{\partial^2 \left(w + w_0 \right)}{\partial x^2}\left(\frac{w}{R} + \frac{\partial v}{R\partial \theta} + \frac{\partial u}{\partial x} \right) - \frac{\partial^2 w}{\partial x^2}\frac{w_0}{R}, \qquad (B.4)$$

$$k_\theta = -\frac{\partial^2 w}{R^2 \partial \theta^2} + \frac{\partial u}{R\partial x} + \frac{\partial v}{R^2 \partial \theta} - \frac{\left(w + w_0 \right)}{R}\left(\frac{\partial^2 w}{R^2 \partial \theta^2} - \frac{\partial v}{R^2 \partial \theta} - 2\frac{\partial u}{R\partial x} \right) - \frac{w}{R}\left(\frac{\partial^2 w_0}{R^2 \partial \theta^2} \right)$$

$$- \frac{\partial u}{R^2 \partial \theta}\left(\frac{\partial u}{R\partial \theta} + \frac{\partial v}{\partial x} + \frac{\partial^2 \left(w + w_0 \right)}{\partial x \partial \theta} \right) + \frac{\partial v}{R^2 \partial \theta}\left(\frac{\partial v}{R\partial \theta} + 3\frac{\partial u}{\partial x} - \frac{\partial^2 \left(w + w_0 \right)}{R\partial \theta^2} \right)$$

$$+ \frac{\partial^2 v}{R^3 \partial \theta^2}\left(\frac{\partial \left(w + w_0 \right)}{\partial \theta} - v \right) + \frac{\partial \left(w + w_0 \right)}{R^2 \partial \theta}\left(-\frac{v}{R} + \frac{\partial w}{R\partial \theta} \right) - \frac{\partial^2 \left(w + w_0 \right)}{R^2 \partial \theta^2}\frac{\partial u}{\partial x}$$

$$+ \frac{\partial w}{R^2 \partial \theta}\frac{\partial w_0}{R\partial \theta} + \frac{\partial \left(w + w_0 \right)}{\partial x}\frac{\partial^2 v}{R\partial x \partial \theta} + \frac{\partial v}{\partial x}\frac{\partial^2 \left(w + w_0 \right)}{R\partial x \partial \theta}, \qquad (B.5)$$

$$k_{x\theta} = -2\frac{\partial^2 w}{R\partial x \partial \theta} - \frac{\partial u}{R^2 \partial \theta} + \frac{\partial v}{R\partial x} + \frac{\partial u}{R^2 \partial \theta}\left(-\frac{\partial u}{\partial x} + \frac{\partial^2 \left(w + w_0 \right)}{R\partial \theta^2} - \frac{\partial v}{R\partial \theta} \right) + \frac{\partial^2 \left(w + w_0 \right)}{\partial x^2}\frac{\partial v}{\partial x}$$

$$- \frac{v}{R^2}\left(\frac{\partial^2 u}{R\partial \theta^2} + \frac{\partial^2 v}{\partial x \partial \theta} + \frac{\partial \left(w + w_0 \right)}{\partial x} \right) + \frac{\partial \left(w + w_0 \right)}{R^2 \partial \theta}\left(\frac{\partial^2 u}{R\partial \theta^2} + \frac{\partial w}{\partial x} + \frac{\partial^2 v}{\partial x \partial \theta} \right) + \frac{\partial w}{R^2 \partial \theta}\frac{\partial w_0}{\partial x}$$

$$+ \frac{\partial v}{R\partial x}\left(\frac{w + w_0}{R} + 2\frac{\partial v}{R\partial \theta} - \frac{\partial^2 \left(w + w_0 \right)}{R\partial \theta^2} + 2\frac{\partial u}{\partial x} \right) + \frac{\partial \left(w + w_0 \right)}{\partial x}\left(\frac{\partial^2 u}{R\partial x \partial \theta} + \frac{\partial^2 v}{\partial x^2} \right)$$

$$- 2\frac{\partial^2 \left(w + w_0 \right)}{R\partial x \partial \theta}\left(\frac{w}{R} + \frac{\partial v}{R\partial \theta} + \frac{\partial u}{\partial x} \right) - 2\frac{\partial^2 w}{R^2 \partial x \partial \theta} w_0 . \qquad (B.6)$$

<u>The general expressions of the coefficients relating to the middle surface strain-displacement relationships of Novozhilov for circular shells:</u>

$$a_i = \frac{\partial U_i}{\partial x} \qquad (B.7)$$

$$b_i = \frac{1}{R}\left(\frac{\partial V_i}{\partial \theta} + W_i \right) \qquad (B.8)$$

$$c_i = \frac{1}{2}\left(\frac{\partial V_i}{\partial x} + \frac{1}{R}\frac{\partial U_i}{\partial \theta} \right) \qquad (B.9)$$

$$p_i = -\frac{\partial^2 W_i}{\partial x^2} \qquad (B.10)$$

$$s_i = -\frac{1}{R^2}\frac{\partial^2 W_i}{\partial \theta^2} + \frac{1}{R}\frac{\partial U_i}{\partial x} + \frac{1}{R^2}\frac{\partial V_i}{\partial \theta} \qquad (B.11)$$

$$t_i = -\frac{2}{R}\frac{\partial^2 W_i}{\partial x \partial \theta} - \frac{1}{R^2}\frac{\partial U_i}{\partial \theta} + \frac{1}{R}\frac{\partial V_i}{\partial x} \tag{B.12}$$

$$A_{ij} = \frac{1}{2}\left[\frac{\partial U_i}{\partial x}\frac{\partial U_j}{\partial x} + \frac{\partial V_i}{\partial x}\frac{\partial V_j}{\partial x} + \frac{\partial W_i}{\partial x}\frac{\partial W_j}{\partial x}\right] \tag{B.13}$$

$$B_{ij} = \frac{1}{2R^2}\left[\frac{\partial U_i}{\partial \theta}\frac{\partial U_j}{\partial \theta} + \left(W_i + \frac{\partial V_i}{\partial \theta}\right)\left(W_j + \frac{\partial V_j}{\partial \theta}\right) + \left(\frac{\partial W_i}{\partial \theta} - V_i\right)\left(\frac{\partial W_j}{\partial \theta} - V_j\right)\right] \tag{B.14}$$

$$C_{ij} = \frac{1}{2R}\left[\frac{\partial U_i}{\partial x}\frac{\partial U_j}{\partial \theta} + \frac{\partial V_i}{\partial x}\frac{\partial V_j}{\partial \theta} + \frac{\partial V_i}{\partial x}W_j + \frac{\partial W_i}{\partial x}\frac{\partial W_j}{\partial \theta} - \frac{\partial W_i}{\partial x}V_j\right] \tag{B.15}$$

$$\begin{aligned} P_{ij} = {} & \frac{1}{R}\frac{\partial V_i}{\partial x}\left[-\frac{1}{R}\frac{\partial U_j}{\partial \theta} + \frac{\partial V_j}{\partial x} - \frac{\partial^2 W_j}{\partial x \partial \theta}\right] + \frac{\partial W_i}{\partial x}\frac{\partial^2 U_j}{\partial x^2} - \frac{1}{R^2}\frac{\partial^2 U_i}{\partial x \partial \theta}V_j + \frac{1}{R^2}\frac{\partial^2 U_i}{\partial x \partial \theta}\frac{\partial W_j}{\partial \theta} \\ & + \frac{1}{R^2}\frac{\partial^2 W_i}{\partial x \partial \theta}\frac{\partial U_j}{\partial \theta} - \frac{\partial^2 W_i}{\partial x^2}\left[\frac{1}{R}W_j + \frac{1}{R}\frac{\partial V_j}{\partial \theta} + \frac{\partial U_j}{\partial x}\right] \end{aligned} \tag{B.16}$$

$$\begin{aligned} S_{ij} = {} & W_i\left[-\frac{1}{R^3}\frac{\partial^2 W_j}{\partial \theta^2} + \frac{1}{R^3}\frac{\partial V_j}{\partial \theta} + \frac{2}{R^2}\frac{\partial U_j}{\partial x}\right] - \frac{\partial U_i}{\partial \theta}\left[\frac{1}{R^3}\frac{\partial U_j}{\partial \theta} + \frac{1}{R^2}\frac{\partial V_j}{\partial x} + \frac{1}{R^2}\frac{\partial^2 W_j}{\partial x \partial \theta}\right] \\ & + \frac{\partial V_i}{\partial \theta}\left[\frac{1}{R^3}\frac{\partial V_j}{\partial \theta} + \frac{3}{R^2}\frac{\partial U_j}{\partial x} - \frac{1}{R^3}\frac{\partial^2 W_j}{\partial \theta^2}\right] + \frac{\partial^2 V_i}{\partial \theta^2}\left[\frac{1}{R^3}\frac{\partial W_j}{\partial \theta} - \frac{1}{R^3}V_j\right] + \frac{\partial W_i}{\partial \theta}\left[-\frac{1}{R^3}V_j + \frac{1}{R^3}\frac{\partial W_j}{\partial \theta}\right] \\ & - \frac{1}{R^2}\frac{\partial^2 W_i}{\partial \theta^2}\frac{\partial U_j}{\partial x} + \frac{1}{R}\frac{\partial W_i}{\partial x}\frac{\partial^2 V_j}{\partial x \partial \theta} + \frac{1}{R}\frac{\partial^2 W_j}{\partial x \partial \theta}\frac{\partial V_i}{\partial x} \end{aligned} \tag{B.17}$$

$$\begin{aligned} T_{ij} = {} & \frac{\partial U_i}{\partial \theta}\left(-\frac{1}{R^2}\frac{\partial U_j}{\partial x} + \frac{1}{R^3}\frac{\partial^2 W_j}{\partial \theta^2} - \frac{1}{R^3}\frac{\partial V_j}{\partial \theta}\right) + \frac{\partial^2 W_i}{\partial x^2}\frac{\partial V_j}{\partial x} - V_i\left(\frac{1}{R^3}\frac{\partial^2 U_j}{\partial \theta^2} + \frac{1}{R^2}\frac{\partial^2 V_j}{\partial x \partial \theta} + \frac{1}{R^2}\frac{\partial W_j}{\partial x}\right) \\ & + \frac{\partial W_i}{\partial \theta}\left(\frac{1}{R^3}\frac{\partial^2 U_j}{\partial \theta^2} + \frac{1}{R^2}\frac{\partial W_j}{\partial x} + \frac{1}{R^2}\frac{\partial^2 V_j}{\partial x \partial \theta}\right) + \frac{\partial V_i}{\partial x}\left(\frac{1}{R^2}W_j + \frac{2}{R^2}\frac{\partial V_j}{\partial \theta} - \frac{1}{R^2}\frac{\partial^2 W_j}{\partial \theta^2} + \frac{2}{R}\frac{\partial U_j}{\partial x}\right) \\ & + \frac{\partial W_i}{\partial x}\left(\frac{1}{R}\frac{\partial^2 U_j}{\partial x \partial \theta} + \frac{\partial^2 V_j}{\partial x^2}\right) - \frac{\partial^2 W_i}{\partial x \partial \theta}\left(\frac{2}{R^2}W_j + \frac{2}{R^2}\frac{\partial V_j}{\partial \theta} + \frac{2}{R}\frac{\partial U_j}{\partial x}\right) \end{aligned} \tag{B.18}$$

where U, V and W denote the spatial functions determined by Equations (4.a – 4.c)

<u>The terms $B_{ij}, C_{ij}, P_{ij}, S_{ij}$ and T_{ij} of modal equations are defined as follows:</u>

$$B_{ij} = C_i\, b'_{ij}\, e^{(\lambda_i + \lambda_j)x/R}\, C_j \tag{B.19}$$

where,

$$b'_{ij} = \frac{1}{2R^2}\left[b_{ij}^{(1)} \cos^2(n\theta) + b_{ij}^{(2)} \sin^2(n\theta)\right] \tag{B.20}$$

with,

$$b_{ij}^{(1)} = 1 + \left(\beta_i + \beta_j\right) n + \beta_i\, \beta_j\, n^2 \qquad (B.21a)$$

$$b_{ij}^{(2)} = \left(1 + \alpha_i\, \alpha_j\right) n^2 + \left(\beta_i + \beta_j\right) n + \beta_i\, \beta_j \qquad (B.21b)$$

$$C_{ij} = C_i\, c'_{ij}\, e^{\left(\lambda_i + \lambda_j\right) x/R}\, C_j \qquad (B.22)$$

where,

$$c'_{ij} = -\frac{1}{2R^2}\left[c_{ij}^{(1)} + c_{ij}^{(2)} \right] cos\left(n\theta\right)\, sin\left(n\theta\right) \qquad (B.23)$$

with,

$$c_{ij}^{(1)} = \left(1 + \alpha_i\, \alpha_j - \beta_i\, \beta_j\right) \lambda_i\, n \qquad (B.24a)$$

$$c_{ij}^{(2)} = \left(\beta_j - \beta_i\right)\, \lambda_i \qquad (B.24b)$$

$$P_{ij} = C_i\, p'_{ij}\, e^{\left(\lambda_i + \lambda_j\right) x/R}\, C_j \qquad (B.25)$$

where,

$$p'_{ij} = \frac{1}{R^3}\left[p_{ij}^{(1)}\, cos^2\left(n\theta\right) + p_{ij}^{(2)}\, sin^2\left(n\theta\right) \right] \qquad (B.26)$$

with,

$$p_{ij}^{(1)} = \alpha_j\, \lambda_i\, \lambda_j^2 - \lambda_i^2 - \beta_j\, \lambda_i^2\, n - \alpha_j\, \lambda_i^2\, \lambda_j \qquad (B.27a)$$

$$p_{ij}^{(2)} = \left(\alpha_i + \alpha_j\right) \lambda_i\, n^2 + \left(\beta_i\, \alpha_j + \beta_i\, \lambda_j + \alpha_i\, \beta_j\right) \lambda_i\, n + \beta_i\, \beta_j\, \lambda_i\, \lambda_j \qquad (B.27b)$$

also, we have:

$$S_{ij} = C_i\, s'_{ij}\, e^{\left(\lambda_i + \lambda_j\right) x/R}\, C_j \qquad (B.28)$$

assuming that,

$$s'_{ij} = \frac{1}{R^3}\left[s_{ij}^{(1)}\, cos^2\left(n\theta\right) + s_{ij}^{(2)}\, sin^2\left(n\theta\right) \right] \qquad (B.29)$$

with,

$$s_{ij}^{(1)} = \beta_i\, n^3 + \left(1 + \beta_i\, \beta_j + \alpha_j\, \lambda_j\right) n^2 + \left(\beta_j + 3\beta_i\, \alpha_j\, \lambda_j + \beta_j\, \lambda_i\, \lambda_j\right) n + 2\alpha_j\, \lambda_j \qquad (B.30.a)$$

$$s_{ij}^{(2)} = \beta_i\, n^3 + \left(1 + \beta_i\, \beta_j - \alpha_i\, \alpha_j - \alpha_i\, \lambda_j\right) n^2 + \left(\alpha_i\, \beta_j\, \lambda_j + \beta_j - \beta_i\, \lambda_i\, \lambda_j\right) n \qquad (B.30.b)$$

Finally:

$$T_{ij} = C_i\, t'_{ij}\, e^{\left(\lambda_i + \lambda_j\right) x/R}\, C_j \qquad (B.31)$$

where,

$$t'_{ij} = \frac{1}{R^3}\, t_{ij}^{(1)}\, cos\left(n\theta\right)\, sin\left(n\theta\right) \qquad (B.32)$$

with,

$$t_{ij}^{(1)} = \left(\alpha_i + \alpha_j\right) n^3 + \left(\alpha_i \beta_j + \beta_i \alpha_j - \beta_j \lambda_j + \beta_i \lambda_i + 2\beta_j \lambda_i\right) n^2$$
$$+ \left(\alpha_i \alpha_j \lambda_j - \beta_i \beta_j \lambda_j - \lambda_j + 2\beta_i \beta_j \lambda_i - \alpha_j \lambda_i \lambda_j + 2\lambda_i + 2\alpha_j \lambda_j \lambda_i\right) n + \beta_j \lambda_i^2 \lambda_j$$
$$- \beta_i \lambda_j + \beta_i \lambda_i + 2\beta_i \alpha_j \lambda_i \lambda_j + \beta_j \lambda_i \lambda_j^2 \qquad (B.33)$$

5.9.3. Appendix C

Matrix $\left[R_f\right]_{3\times 8}$ is given by:

$$\left[R_f\right] = \begin{bmatrix} 0 & \cdots & 0 \\ e^{i\lambda_1 x/R} & e^{i\lambda_j x/R} & e^{i\lambda_8 x/R} \\ 0 & \cdots & 0 \end{bmatrix}_{3\times 8} \qquad (C.1)$$

CHAPITRE 6 DISCUSSION GÉNÉRALE

L'objectif ultime de cette thèse était de développer un outil capable d'analyser le comportement nonlinéaire des structures cylindriques minces isotropes et fermées à vide et lorsqu'elles sont soumises à un flux d'air supersonique tout en tenant compte de l'effet des contraintes initiales de raidissement induites par des pressions radiales et/ou des forces axiales. Cet outil est capable aussi de prédire le début de flottement et de décrire la tendance de nonlinéarité des structures cylindriques au moment et pendant leurs phases d'instabilité.

La majorité des méthodes jusqu'alors développées utilisent la théorie des coques surbaissées de Donnell ou celle de Sanders-Koiter pour étudier les vibrations nonlinéaires libres et forcées des coques cylindriques et ce à cause de leur simplicité. Très peu d'études qui se sont penchées vers la théorie de Flügge-Lur'e-Byrne ou encore celle de Novozhilov qui représentent une cinématique plus complexe qui tient compte des nonlinéarités membranaires quant aux expressions des changements de courbures et de torsion reliées à leurs champs de déformation. Ce résultat a été élucidé par Amabili [97] à travers une étude comparative qu'il a menée, entre les cinq théories qui sont pratiquement considérées les seules généralement appliquées pour résoudre les problèmes géométriquement nonlinéaires parmi toutes les théories qui emploient trois variables cinématiques (trois déplacements). Amabili a considéré dans le même article que les formulations de Flügge-Lur'e-Byrne et celle de Novozhilov s'avèrent les plus raffinées parmi les différentes théories citées et a mentionné dans son livre [3] que les expressions de changement de courbure et de torsion de Novozhilov acquiert une forme plus complexe suite à la prise en compte des termes d'approximations quadratiques de l'inverse de rayon de courbures négligées par la théorie de Flügge-Lur'e-Byrne.

Le modèle proposé dans cette étude est basé sur une approche hybride combinant la méthode des éléments finis classique et la théorie des coques minces de Novozhilov. Une formulation analytique est développée en la matière, basée sur les équations cinématiques nonlinéaires de Novozhilov pour déceler les matrices de masse et celles de rigidité linéaires et nonlinéaires quadratiques et cubiques. L'originalité d'une telle formulation réside dans sa capacité de considérer à la fois l'effet de courbure au niveau du champ de déplacement circonférentiel, l'effet des imperfections géométriques initiales et l'effet du couplage nonlinéaire entre les différents modes. Ce dernier a été souvent négligé dans les modèles trouvés dans la littérature dans le but de simplifier le calcul numérique. Une application de la méthode développée a été menée en remplaçant les fonctions spatiales du champ de déplacement par les fonctions de forme provenant des solutions exactes qui découlent des équations d'équilibre de Sanders ce qui acquiert au modèle plus de fiabilité et plus de précision au niveau de ces résultats en les comparant à ceux relatifs aux autres approches qui se basent sur des approximations polynomiales. Cette approche est adoptée du fait que la théorie linéaire d'élasticité de Novozhilov et celle de Sanders fournissent des résultats qui sont étroitement similaires au point de vue fréquences linéaires [10]. Ce qui nous a conduit entre autre à adopter cette dernière pour la détermination des matrices de masse et de rigidité linéaire tel qu'il a été développé dans l'article de Lakis et Païdoussis [9]. Les calculs ont conduit à la nullité de la matrice de rigidité quadratique ce qui est en bonne concordance avec les résultats des autres auteurs. Un avantage attrayant du modèle établit réside dans son flexibilité supérieure à supporter des différentes conditions aux limites. Plusieurs paramètres ont été examinés en la matière mettant en exergue l'effet prépondérant du nombre d'ondes axiales et circonférentielles et des différents paramètres géométriques sur le caractère nonlinéaire du comportement dynamique. Tous les cas étudiés ont montré une tendance nonlinéaire de type raidissante, ce caractère est accentué lors de la présence d'un couplage entre les différents modes nonlinéaires. Lequel couplage prend d'ampleur au fur et à mesure que l'amplitude de vibration augmente et il se manifeste sous forme d'une interaction entre les orbites périodiques définissant les modes nonlinéaires. Ces orbites se présentent sous forme de famille de solutions périodiques représentant les sous espaces invariants de l'espace des phases qui sont tangents aux modes linéaires plan en chacun des points d'équilibre. Le croisement entre les différents modes nonlinéaires engendre des superpositions des déformées modales ce qui donne naissance à des mouvements complexes. La considération de l'effet de la nonlinéarité structurale est une étape cruciale permettant de mieux caractériser les structures cylindriques du fait de sa répercussion sur les modes fondamentaux (fréquence minimale et le nombre d'ondes circonférentiel correspondant). En effet, l'augmentation de l'amplitude de vibration induit des chevauchements entre les différentes courbes traduisant ainsi la variation de la fréquence nonlinéaire en fonction de l'amplitude adimentionnelle. Ceci fait révéler un comportement phénoménologique qui stipule que le mode fondamentale dépend étroitement de l'amplitude de vibration une fois qu'on quitte le domaine des petites perturbations. Un autre point sur lequel on peut mettre l'accent est la chute de fréquence linéaire qui s'avère draconienne en la comparant à celle nonlinéaire et ce au fur et mesure que les structures sont élancées. D'autant plus, l'effet de la variation de l'amplitude de vibration est négligeable pour les coques cylindriques courtes alors qu'il devient prononcé lorsque les coques deviennent de plus en plus élancées.

L'effet des contraintes initiales de raidissement induites par la présence de pression radiales et/ou des forces axiales appliquées sur des coques axisymétriques est l'un des phénomènes fondamentaux analysés dans cette recherche. L'étude a mis en exergue l'effet des forces axiales de tension et de compression ainsi que des pressions radiales internes et externes sur l'instabilité des structures cylindriques et coniques et ce pour différents rapports géométriques. L'étude a marqué son originalité à travers l'analyse du comportement dynamique linéaire des structures axisymétriques de forme complexes soumises à l'effet des forces axiales et des pressions radiales par le biais d'un model combiné cylindrique-conique. Une étude exhaustive a été dressée dans l'article 1. Les résultats ont montré que les structures cylindriques soumises à des pressions externes deviennent vulnérables à l'instabilité au fur et à mesure que leurs rayons de courbure augmentent. Alors que l'augmentation du ratio r/h n'a pas d'influence sur la valeur de la force critique de flambement dynamique (l'instabilité se manifeste par une divergence). On peut aussi souligner le fait que l'augmentation de l'angle du tronc de cône relatif aux coques coniques favorise l'instabilité de ces dernières. Les résultats ont aussi montré que l'effet des contraintes de raidissement initial s'avère prépondérant lorsque le comportement flexionnel gouverne (n grand) alors qu'il diminue drastiquement lorsque le comportement membranaire gouverne.

Dans une optique à traiter le problème aéroélastique nonlinéaire par étapes, l'article 3, a englobé tous les aspects étudiés préalablement, en leur rajoutant l'effet de l'interaction fluide-structure à travers l'étude des vibrations nonlinéaires des structures cylindriques soumises à un écoulement supersonique en tenant compte de l'effet des contraintes de raidissement initiales. Ceci est considéré comme une étape cruciale pour évaluer la fiabilité de la formulation développée et tester en conséquence, l'aptitude du logiciel maison conçu pour l'analyse des phénomènes d'interaction fluide-structure. Seulement la nonlinéarité structurale est considérée dans ce troisième article ce qui a déjà été largement étudiée dans l'article 2. Quant à la nonlinéarité de fluide, elle est négligée en se basant sur les résultats se trouvant dans la littérature [127] ce qui nous a conduits à se concentrer seulement sur la forme linéaire de l'écoulement supersonique. Plusieurs paramètres ont été considérés dans cette analyse, tels que les termes géométriques et les conditions aux limites pour le cas des coques pressurisées et non pressurisées. La validation des résultats numériques a montré une excellente concordance avec ceux présents dans la littérature. L'analyse a souligné l'effet prépondérant de la pression interne pour la stabilisation des coques cylindriques en poussant leurs pressions critiques de flottement vers les valeurs supérieures comparées aux coques non pressurisées. La tendance nonlinéaire révélée dans tous les cas étudiés est de type assouplissante et le couplage nonlinéaire a montré une autre fois son effet épinant dans l'accentuation du caractère nonlinéaire. L'instabilité des coques est aussi examinée dans cette étude à travers la détermination des pressions et des modes critiques déclenchant le flottement et en évaluant le comportement dynamique nonlinéaire de ses structures pendant leurs phases d'instabilité. La considération des termes de correction de courbure a apporté quelques amendements en matière de caractérisation de la valeur critique de la pression aérodynamique cependant l'étude a montré l'absence de l'effet de ces termes sur la tendance du comportement dynamique nonlinéaire. Les résultats ont montré aussi l'absence de l'effet de la variation du ratio L/R sur le caractère assouplissant du comportement dynamique nonlinéaire (une synergie entre les différentes courbes a été révélée) pour les coques cylindriques examinées durant les phases les plus critique en termes de P_{cr} et n_{cr} (limite de flottement). En outre, on peut noter que les structures deviennent vulnérables au flottement au fur et à mesure qu'elles sont élancées.

CHAPITRE 7 CONCLUSION ET RECOMMENDATIONS

Une bonne analyse du phénomène de flottement des coques cylindriques exige une approche raisonnable du problème étudié et mène à une approximation fiable de leur comportement dynamique nonlinéaire afin d'acquérir une évaluation réaliste et un dimensionnement plus rigoureux de la structure. C'est dans cette optique qu'une formulation a été développée dans cette thèse basée sur la théorie des coques minces de Novozhilov couronnée par la conception d'un logiciel maison ralliant à la fois la précision des résultats et la rapidité de convergence du fait de son fondement sur une approche hybride des éléments finis. Le logiciel développé dans cette thèse est un outil puissant et assez complet pour être utilisé dans le design des structures aérospatiales. Il permet de :

- ✓ Étudier efficacement le comportement linéaire des structures cylindriques minces pour différents paramètres géométriques et mécaniques et pour des différentes conditions aux limites complexes et ce pour les basses et hautes fréquences ;
- ✓ Analyser l'effet des contraintes initiales de raidissement induites par les pressions radiales et/ou des forces axiales sur le comportement dynamique linéaire des coques axisymétriques de formes complexes ;
- ✓ Prédire le comportement dynamique nonlinéaire des structures cylindriques à vide pour différents propriétés géométriques et mécaniques et pour différentes conditions aux limites, et d'analyser l'évolution de la fréquence nonlinéaire en fonction de l'amplitude de vibration;
- ✓ Modéliser le comportement dynamique linéaire et nonlinéaire des structures cylindriques minces et isotropes soumises à un écoulement supersonique externe ;
- ✓ Analyser la stabilité des coques cylindriques minces et isotropes lorsqu'elles sont soumises à un écoulement d'air supersonique, prédire le début de flottement et caractériser la tendance du comportement nonlinéaire de ces structures pendant les phases qui suivent le début de l'instabilité dynamique ;
- ✓ Modéliser l'effet de correction de courbures pour le calcul de la pression aérodynamique ;
- ✓ Analyser l'effet des contraintes initiales de raidissement sur le comportement aéroélastique nonlinéaire des structures cylindriques.

La formulation développée dans cette thèse, mise à part sa capacité à considérer différents paramètres tel que l'effet de courbure du champ de déplacement dans la direction circonférentielle, l'effet du couplage nonlinéaire et l'effet des imperfections géométriques initiales, se caractérise par son aptitude à employer différentes formes de discrétisation de la structure cylindrique et ce à travers la forme de son champ de déplacement que revête un aspect général.

Il convient par ailleurs de signaler que le logiciel développé présente un pas en avant dans le domaine de l'analyse numérique des engins spatiaux et il peut être considéré comme un outil qui mise sur la performance et la précision avec coût de temps réduit comparé aux autres logiciels commerciaux.

7.1. Travaux futurs et Recommandations

Le domaine de modélisation et d'analyse numérique des phénomènes aéroélastiques des plaques et coques est un secteur fortifié et complexe qui fait appel à plusieurs disciplines et qui exige une prise en considération de plusieurs paramètres en même temps lors de la modélisation du comportement de la structure ou lors de l'analyse des phénomènes qui lui sont liés. Ceci dans le but de concevoir des modèles fiables qui se rapprochent le plus possible de la réalité. Plusieurs axes de recherche peuvent être révélés parmi lesquels on trouve l'effet de la température qui est sans doute un paramètre substantiel pour le design des, structures en aérospatiale du fait de son effet sur la stabilité dynamique des aéronefs. Un autre aspect sur lequel on peut mettre l'accent est la prise en compte des imperfections géométriques initiales d'une manière quantitative et d'analyser leur répercussion sur les valeurs critiques de flottement. Rappelons que ces imperfections géométriques ont été considéré dans la formulation développée dans cette thèse cependant et par motif d'alléger les calculs, la géométrie a été supposée parfaite dans l'étude numérique. Un autre aspect tout aussi important que les précédents réside dans la considération du couplage entre les nonlinéarités géométriques et matérielles incitées par les grands déplacements et par les grandes déformations et pour lequel les relations déformation-déplacement et celles des contraintes-déformations sont considérées comme nonlinéaires. En réalité ces phénomènes sont souvent ralliés et la considération d'un tel couplage s'avère impératif et une étape cruciale pour le design des aéronefs afin d'assurer la fiabilité et la sécurité de ces structures.

REFERENCES

[1] D. Gero. "Military Aviation Disasters". Patrick Stephens, London, 1999.

[2] Ben Youssef, Yacine, Aouni Lakis, and Youcef Kerboua. "Développement d’une formulation pour l’étude du comportement dynamique non linéaire des coques cylindriques isotropes." (2020). (Rapport technique n° EPM-RT-2020-01). https://publications.polymtl.ca/5321/1/EPM-RT-2020-01_BenYousef.pdf

[3] Amabili, Marco. "Nonlinear vibrations and stability of shells and plates". Cambridge University Press, 2008. Doi: 10.1017/CBO9780511619694.

[4] Donnell, Lloyd H. "A new theory for the buckling of thin cylinders under axial compression and bending." (1934): 86.

[5] Ginsberg, J. H. "Large amplitude forced vibrations of simply supported thin cylindrical shells", *J. Appl. Mech*., 40.2, (1973): 471-477. https://doi.org/10.1115/1.3423008

[6] Novozhilov, V. V. "Foundations of the Nonlinear Theory of Elasticity (in Russian), Gostekhteorizdat." *English translation* (1953).

[7] Sanders Jr, J. Lyell. "Nonlinear theories for thin shells." *Quarterly of Applied Mathematics*, 21.1 (1963): 21-36. https://doi.org/10.1090/qam/147023

[8] Koiter, Warner Tjardus. "On the nonlinear theory of thin elastic shells." *Proc. Koninkl. Ned. Akad. van Wetenschappen, Series B* 69 (1966): 1-54.

[9] Lakis, Aouni A., and M. P. Paidoussis. "Dynamic analysis of axially non-uniform thin cylindrical shells." *Journal of Mechanical Engineering Science* 14.1 (1972): 49-71. https://doi.org/10.1243/JMES_JOUR_1972_014_009_02.

[10] Leissa, Arthur W. *Vibration of shells*. Vol. 288. Scientific and Technical Information Office, National Aeronautics and Space Administration, 1973. ID-19730018197

[11] Garrick, I. E., and Wilmer H. Reed III. "Historical development of aircraft flutter." *Journal of Aircraft* 18.11 (1981): 897-912. https://doi.org/10.2514/3.57579

[12] Von Baumhauer, Albert G., and C. Koning. "On the stability of oscillations of an airplane wing." *NACA TM 223*, (1923).

[13] Keldysh, M. V. "Vibrations of a wing with bracing struts in airflow." *Trudy Tsentr. Aerogidrodinam. Inst* 357 (1938): 304-341.

[14] Morino, Luigi. "A general theory of unsteady compressible potential aerodynamics." (1974). NASA-CR-2464

[15] Hedgepeth, John, and E. Widmayer. "Dynamic and aeroelastic problems of lifting re-entry bodies." *Aerospace Engineering* 22.1 (1963): 148-153.

[16] Dugundji, J. "Effect of quasi-steady air forces on incompressible bending-torsion flutter." *Journal of the Aerospace Sciences* 25.2 (1958): 119-121.
https://doi.org/10.2514/8.7525

[17] Robinson, Brian A., John T. Batina, and Henry TY Yang. "Aeroelastic analysis of wings using the Euler equations with a deforming mesh." *Journal of Aircraft* 28.11 (1991): 781-788. https://doi.org/10.2514/3.46096

[18] Dowell, Earl H. "Nonlinear oscillations of a fluttering plate. II." *AIAA journal* 5.10 (1967): 1856-1862. https://doi.org/10.2514/3.4316

[19] Librescu, Liviu. "Aeroelastic Stability of Orthotropic Heterogeneous Thin Panels In Vicinity of Flutter Critical Boundary. 1. Simply Supported Panels." *Journal de Mécanique* 4.1 (1965): 51-76.

[20] Librescu, L. "Aeroelastic stability of orthotropic heterogeneous thin panels in the vicinity of the flutter critical boundary. II (Boundary conditions influence on flutter critical boundary character considering nonlinearities of physical nature)." *Journal de Mécanique* 6.1 (1967): 133-152.

[21] Olson, Mervyn D., and Y. C. Fung. "Comparing theory and experiment for the supersonic flutter of circular cylindrical shells." *AIAA Journal* 5.10 (1967): 1849-1856.
https://doi.org/10.2514/3.4315.

[22] Olson, Mervyn D., and Y. C. Fung. "Supersonic flutter of circular cylindrical shells subjected to internal pressure and axial compression." *AIAA Journal* 4.5 (1966): 858-864. https://doi.org/10.2514/3.3558.

[23] Amabili, Marco, and Francesco Pellicano. "Nonlinear supersonic flutter of circular cylindrical shells." *AIAA journal* 39.4 (2001): 564-573. https://doi.org/10.2514/2.1365.

[24] Amabili, M., and Francesco Pellicano. "Multimode approach to nonlinear supersonic flutter of imperfect circular cylindrical shells." *J. Appl. Mech.* 69.2 (2002): 117-129. https://doi.org/10.1115/1.1435366

[25] Librescu, Liviu, Piergiovanni Marzocca, and Walter A. Silva. "Supersonic/hypersonic flutter and postflutter of geometrically imperfect circular cylindrical panels." *Journal of Spacecraft and Rockets* 39.5 (2002): 802-812. https://doi.org/10.2514/2.3882.

[26] Oh, Il-Kwon, and In Lee. "Supersonic flutter suppression of piezolaminated cylindrical panels based on multifield layerwise theory." *Journal of Sound and Vibration* 291.3-5 (2006): 1186-1201. https://doi.org/10.1016/j.jsv.2005.07.033.

[27] Kurilov, E. A., and Yu V. Mikhlin. "Nonlinear vibrations of cylindrical shells with initial imperfections in a supersonic flow." *International Applied Mechanics* 43.9 (2007): 1000-1008. https://doi.org/10.1007/s10778-007-0099-2

[28] Jansen, E. L. "Effect of boundary conditions on nonlinear vibration and flutter of laminated cylindrical shells." *Journal of vibration and acoustics* 130.1 (2008). https://doi.org/10.1115/1.2775512.

[29] Haddadpour, H., S. Mahmoudkhani, and H. M. Navazi. "Supersonic flutter prediction of functionally graded cylindrical shells." *Composite Structures* 83.4 (2008): 391-398. https://doi.org/10.1016/j.compstruct.2007.05.011.

[30] Kubenko, V. D., and P. S. Koval'chuk. "Stability and nonlinear vibrations of closed cylindrical shells interacting with a fluid flow." *International applied mechanics* 51.1 (2015): 12-63. DOI 10.1007/s10778-015-0672-z.

[31] Liu, Y. Z., et al. "Nonlinear dynamics of initially imperfect functionally graded circular cylindrical shell under complex loads." *Journal of Sound and Vibration* 348 (2015): 294-328. https://doi.org/10.1016/j.jsv.2015.03.023.

[32] Mahmoudkhani, S., M. Sadeghmanesh, and Hassan Haddadpour. "Aero-thermo-elastic stability analysis of sandwich viscoelastic cylindrical shells in supersonic airflow." *Composite Structures* 147 (2016): 185-196. https://doi.org/10.1016/j.compstruct.2016.03.020.

[33] Mahmoudkhani, S. "Aerothermoelastic analysis of imperfect FG cylindrical shells in supersonic flow." *Composite Structures* 225 (2019): 111160. https://doi.org/10.1016/j.compstruct.2019.111160.

[34] Chen, Jie, and Qiu-Sheng Li. "Nonlinear aeroelastic flutter and dynamic response of composite laminated cylindrical shell in supersonic air flow." *Composite Structures* 168 (2017): 474-484. https://doi.org/10.1016/j.compstruct.2017.02.019.

[35] Asadi, Hamed, and Quan Wang. "Dynamic stability analysis of a pressurized FG-CNTRC cylindrical shell interacting with supersonic airflow." *Composites Part B: Engineering* 118 (2017): 15-25. https://doi.org/10.1016/j.compositesb.2017.03.001.

[36] Asadi, Hamed. "Numerical simulation of the fluid-solid interaction for CNT reinforced functionally graded cylindrical shells in thermal environments." *Acta Astronautica* 138 (2017): 214-224. https://doi.org/10.1016/j.actaastro.2017.05.039.

[37] Avramov, K. V., et al. "Self-sustained vibrations of functionally graded carbon nanotubes-reinforced composite cylindrical shells in supersonic flow." *Nonlinear Dynamics* 98.3 (2019): 1853-1876. https://doi.org/10.1007/s11071-019-05292-z.

[38] Fazilati, Jamshid, Vahid Khalafi, and Hossein Shahverdi. "Three-dimensional aero-thermo-elasticity analysis of functionally graded cylindrical shell panels." *Proceedings of the Institution of Mechanical Engineers, Part G: Journal of Aerospace Engineering* 233.5 (2019): 1715-1727. https://doi.org/10.1177/0954410018763861.

[39] Khudayarov, B. A., and F. Zh Turaev. "Nonlinear supersonic flutter for the viscoelastic orthotropic cylindrical shells in supersonic flow." *Aerospace Science and Technology* 84 (2019): 120-130. https://doi.org/10.1016/j.ast.2018.08.044.

[40] Baghdasaryan, G. Y., et al. "Nonlinear flutter response of cylindrical shell in thermal field and supersonic gas flow." *IOP Conference Series: Materials Science and Engineering*. Vol. 927. No. 1. IOP Publishing, (2020), Sept, Alushta, Russia. p. 012022.

[41] Baghdasaryan, G. Y., et al. "Influence of supersonic flow on nonlinear oscillations of a cylindrical shell." *Journal of Physics: Conference Series*. Vol. 1474. No. 1. IOP Publishing, (2020), Feb, Dilijan, Armenia. p. 012007.

[42] Fung, Y. C., E. E. Sechler, and A. Kaplan. "On the vibration of thin cylindrical shells under internal pressure." *Journal of the Aeronautical Sciences* 24.9 (1957): 650-660. https://doi.org/10.2514/8.3934

[43] Miserentino, Robert, and Louis F. Vosteen. "*Vibration tests of pressurized thin-walled cylindrical shells*". National Aeronautics and Space Administration, NASA. Washington, DC, Report No. TN-D-3066, 1966.

[44] Reissner, Eric. "*Non-linear effects in vibrations of cylindrical shells*". Ramo-Wooldridge Corporation, Guided Missile Research Division, Aeromechanics Section, Los Angeles, CA. 1955.

[45] Weingarten, V. I. "The effect of internal or external pressure on the free vibrations of conical shells." *International Journal of Mechanical Sciences* 8.2 (1966): 115-124. https://doi.org/10.1016/0020-7403(66)90070-1

[46] Dixon, Sidney C., and M. Latrelle Hudson. "*Flutter, vibration, and buckling of truncated orthotropic conical shells with generalized elastic edge restraint*". National Aeronautics and Space Administration, NASA, Washington, DC, Report No. TN-D-5759. 1970.

[47] Miserentino, Robert. "*Vibration and flutter tests of a pressurized thin-walled truncated conical shell*". National Aeronautics and Space Administration, NASA, Washington, DC, Report No. TN-D-6106. 1971.

[48] Ueda, Tetsuhiko, Shigeo Kobayashi, and Masatoma Kihira. "Supersonic flutter of truncated conical shells." *Trans. Jpn. Soc. Aeronaut. Space Sci* 20.47 (1977): 13-30.

[49] Tong, L. "Effect of axial load on free vibration of orthotropic truncated conical shells." *Trans. ASME*, 118.2 (1996): 164-168. https://doi.org/10.1115/1.2889644

[50] Lam, K. Y., and Li Hua. "Influence of initial pressure on frequency characteristics of a rotating truncated circular conical shell." *International journal of mechanical sciences* 42.2 (2000): 213-236. https://doi.org/10.1016/S0020-7403(98)00125-8

[51] Zhang, Yong Liang, Daniel G. Gorman, and Jason M. Reese. "Vibration of prestressed thin cylindrical shells conveying fluid." *Thin-Walled Structures* 41.12 (2003): 1103-1127. https://doi.org/10.1016/S0263-8231(03)00108-3

[52] Lindholm, Ulric S., Daniel D. Kana, and H. NORMAN ABRAMSON. "Breathing vibrations of a circular cylindrical shell with an internal liquid." *Journal of the Aerospace Sciences* 29.9 (1962): 1052-1059. https://doi.org/10.2514/8.9693

[53] Sofiyev, A. H., M. H. Omurtag, and E. Schnack. "The vibration and stability of orthotropic conical shells with non-homogeneous material properties under a hydrostatic pressure." *Journal of Sound and Vibration* 319.3-5 (2009): 963-983. https://doi.org/10.1016/j.jsv.2008.06.033

[54] Heydarpour, Y., P. Malekzadeh, and M. M. Aghdam. "Free vibration of functionally graded truncated conical shells under internal pressure." *Meccanica* 49.2 (2014): 267-282. https://doi.org/10.1007/s11012-013-9791-y

[55] Chiba, M., Yamaki, N., and Tani, J., "Free Vibration of a Clamped-Free Circular Cylindrical Shell Partially Filled With Liquid—Part I: Theoretical Analysis," *Thin-Walled Struct*., 2.3 (1984): 265–284. https://doi.org/10.1016/0263-8231(84)90022-3

[56] Chiba, M., Yamaki, N., and Tani, J., "Free Vibration of a Clamped-Free Circular Cylindrical Shell Partially Filled With Liquid—Part II: Numerical Results," *Thin-Walled Struct.*, 2.4 (1984): 307–324. https://doi.org/10.1016/0263-8231(84)90002-8

[57] Chiba, M., Yamaki, N., and Tani, J., "Free Vibration of a Clamped-Free Circular Cylindrical Shell Partially Filled With Liquid—Part III: Experimental Results," *Thin-Walled Struct.*, 3.1 (1985): 1–14. https://doi.org/10.1016/0263-8231(85)90016-3

[58] Yamaki, N., Tani, J., and Yamaji, T., "Free-Vibration of a Clamped Clamped Circular Cylindrical-Shell Partially Filled With Liquid," *Journal of Sound and Vibration*, 94.4 (1984): 531–550.

[59] Chiba, M., and H. Osumi. "Free vibration and buckling of a partially submerged clamped cylindrical tank under compression." *Journal of sound and vibration* 209.5 (1998): 771-796. https://doi.org/10.1006/jsvi.1997.1282

[60] Tani, J., H. Haiji, and M. Chiba. "Free Vibration of Fluid-Coupled Coaxial Cylindrical Shells, Shells, Membranes and Space Frames." *Proceedings of the IASS Symposium*. Vol. 1. Osaka, Japan. 1986, Sept. 15–19: 57–64.

[61] Chiba, M. "Free vibration of a partially liquid-filled and partially submerged, clamped-free circular cylindrical shell." *The Journal of the Acoustical Society of America* 100.4 (1996): 2170-2180. https://doi.org/10.1121/1.417494

[62] Sanders Jr, J. Lyell. "An improved first-approximation theory for thin shells." *NASA Washington*, DC, Report No. R-24. (1959).

[63] Toorani, M. H., and A. A. Lakis. "General equations of anisotropic plates and shells including transverse shear deformations, rotary inertia and initial curvature effects." *Journal of Sound and Vibration* 237.4 (2000): 561-615.
https://doi.org/10.1006/jsvi.2000.3073

[64] Flügge, Wilhelm. "Buckling of Shells." *Stresses in Shells*. Springer, Berlin, Heidelberg, 1973. 433-506.

[65] Lakis, A. A., P. Van Dyke, and H. Ouriche. "Dynamic analysis of anisotropic fluid-filled conical shells." *Journal of fluids and structures* 6.2 (1992): 135-162.
https://doi.org/10.1016/0889-9746(92)90042-2

[66] Kerboua, Y., A. A. Lakis, and M. Hmila. "Vibration analysis of truncated conical shells subjected to flowing fluid." *Applied Mathematical Modelling* 34.3 (2010): 791-809.
https://doi.org/10.1016/j.apm.2009.06.028

[67] Lakis, A. A., and Ouriche, H., "Dynamic Analysis of Anisotropic Conical Shells," *École Polytechnique de Montréal, Montreal, PQ, Canada*, (1986). (Report No. EPM/RT-86-36).

[68] MacNeal, R. H. "The NASTRAN Theoretical Manual, NASA.", Washington, DC, *Report No. SP-221 (01)* (1972).

[69] Kerboua, Youcef, and Aouni A. Lakis. "Numerical model to analyze the aerodynamic behavior of a combined conical–cylindrical shell." *Aerospace Science and Technology* 58 (2016): 601-617. https://doi.org/10.1016/j.ast.2016.09.019

[70] Mazúch, T., et al. "Natural modes and frequencies of a thin clamped–free steel cylindrical storage tank partially filled with water: fem and measurement." *Journal of Sound and Vibration* 193.3 (1996): 669-690. https://doi.org/10.1006/jsvi.1996.0307

[71] Kohnke, Peter. "Theory reference for the mechanical APDL and mechanical applications." *Ansys Inc, release* 12, Canonsburg, PA. (2009) .

[72] Jawad, M. H. "Design of conical shells under external loads.", *ASME Journal of Pressure Vessel Technology*. 102.2 (1980): 230-238. https://doi.org/10.1115/1.3263325

[73] Singer, Josef. "Buckling of circular conical shells under axisymmetrical external pressure." *Journal of Mechanical Engineering Science* 3.4 (1961): 330-339. https://doi.org/10.1243/JMES_JOUR_1961_003_045_02

[74] Seide, Paul. "Axisymmetrical buckling of circular cones under axial compression." *ASME Journal of Applied Mechanics*. 23.4 (1956): 625-628. https://doi.org/10.1115/1.4011410

[75] Grigolyuk, E. I., and Prikladnaya Matematika i Mekhanika. "Vibrations of circular cylindrical panels subjected to finite deflections." *Prikladnaya Matematika i Mekhanika* 19 (1955): 376-382.

[76] Chu, Hu-Nan. "Influence of large amplitudes on flexural vibrations of a thin circular cylindrical shell." *Journal of the Aerospace Sciences* 28.8 (1961): 602-609. https://doi.org/10.2514/8.9113

[77] Cummings, Benjamin E. "Large-amplitude vibration and response of curved panels." *AIAA Journal* 2.4 (1964): 709-716. https://doi.org/10.2514/3.2392

[78] Nowinski, J. L. "Nonlinear transverse vibrations of orthotropic cylindrical shells." *AIAA Journal* 1.3 (1963): 617-620. https://doi.org/10.2514/3.1604

[79] Evensen, David A. "Some observations on the nonlinear vibration of thin cylindrical shells." *AIAA Journal* 1.12 (1963): 2857-2858. https://doi.org/10.2514/3.2188

[80] Matsuzaki, Y. "An analytical study of the nonlinear flexural vibration of thin circular cylindrical shells." *J. Jpn. Soc. Aero. Space Sci.* 17.187 (1969): 308.

[81] Matsuzaki Y and Kobayashi S, "A theoretical and experimental study of the nonlinear flexural vibration of thin circular cylindrical shells with clamped ends", *Transactions of the Japan Society for Aeronautical and Space Sciences* 12.21 (1969): 55–62.

[82] Dowell, E. H., and C. S. Ventres. "Modal equations for the nonlinear flexural vibrations of a cylindrical shell." *International Journal of Solids and Structures* 4.10 (1968): 975-991. https://doi.org/10.1016/0020-7683(68)90017-6

[83] Atluri, Satyanadham. "A perturbation analysis of non-linear free flexural vibrations of a circular cylindrical shell." *International Journal of Solids and Structures* 8.4 (1972): 549-569. https://doi.org/10.1016/0020-7683(72)90022-4

[84] Dowell EH, Ventres CS, and Tang D. "Modal equations for the nonlinear flexural vibrations of a cylindrical shell", *Duke Univ*. (1998). Research Report, DT 98-1.

[85] Varadan, T. K., G. Prathap, and H. V. Ramani. "Nonlinear free flexural vibration of thin circular cylindrical shells." *AIAA journal* 27.9 (1989): 1303-1304. https://doi.org/10.2514/3.10263

[86] Prathap, G., and Evensen DA. "Comments on The Large Amplitude Asymmetric Vibrations of Some Thin Shells of Revolution." *Journal of Sound and Vibration*, 56.2 (1978): 303-308.

[87] El-Zaouk, B. R., and Clive L. Dym. "Non-linear vibrations of orthotropic doubly-curved shallow shells." *Journal of Sound and Vibration* 31.1 (1973): 89-103. https://doi.org/10.1016/S0022-460X(73)80251-2

[88] Ginsberg, J. H. "Nonlinear axisymmetric free vibration in simply supported cylindrical shells." *Journal of Applied Mechanics*, 41.1 (1974): 310-312.

[89] Radwan, Hatem, and Joseph Genin. "Non-linear modal equations for thin elastic shells." *International Journal of Non-linear Mechanics* 10.1 (1975): 15-29.

https://doi.org/10.1016/0020-7462(75)90026-8

[90] Radwan, H. R., and J. Genin. "Nonlinear vibrations of thin cylinders." *ASME Journal of Applied Mechanics*, 43 (1976): 370-372.

[91] Raju, K. Kanaka, and G. Venkateswara Rao. "Large amplitude asymmetric vibrations of some thin shells of revolution." *Journal of Sound and Vibration* 44.3 (1976): 327-333. https://doi.org/10.1016/0022-460X(76)90505-8

[92] Chiba, M. "Non-linear hydroelastic vibration of a cantilever cylindrical tank—I. Experiment (empty case)." *International journal of non-linear mechanics* 28.5 (1993): 591-599. https://doi.org/10.1016/0020-7462(93)90050-U

[93] Ganapathi, M., and T. K. Varadan. "Large amplitude vibrations of circular cylindrical shells." *Journal of sound and vibration* 192.1 (1996): 1-14. https://doi.org/10.1006/jsvi.1996.0172

[94] Selmane, A., and A. A. Lakis. "Influence of Geometric Non-linearities on the Free Vibrations of Orthotropic Open Cylindrical Shells." *International Journal for Numerical Methods in Engineering* 40.6 (1997): 1115-1137. https://doi.org/10.1002/(SICI)1097-0207(19970330)40:6<1115::AID-NME105>3.0.CO;2-H

[95] Lakis, A. A., A. Selmane, and A. Toledano. "Non-linear free vibration analysis of laminated orthotropic cylindrical shells." *International journal of mechanical sciences* 40.1 (1998): 27-49. https://doi.org/10.1016/S0020-7403(97)00029-5

[96] Amabili, M., Francesco Pellicano, and M. P. Paidoussis. "Nonlinear vibrations of simply supported, circular cylindrical shells, coupled to quiescent fluid." *Journal of Fluids and Structures* 12.7 (1998): 883-918. https://doi.org/10.1006/jfls.1998.0173

[97] Amabili, M. "A comparison of shell theories for large-amplitude vibrations of circular cylindrical shells: Lagrangian approach." *Journal of Sound and Vibration* 264.5 (2003): 1091-1125. https://doi.org/10.1016/S0022-460X(02)01385-8

[98] Liu, Yanqi, and Fulei Chu. "Nonlinear vibrations of rotating thin circular cylindrical shell." *Nonlinear Dynamics* 67.2 (2012): 1467-1479. https://doi.org/10.1007/s11071-011-0082-7

[99] Ramzi, Redouane, and Aouni Lakis. "Effect of geometric nonlinearities on nonlinear vibrations of closed cylindrical shells." *International Journal of Structural Stability and Dynamics* 13.04 (2013): 1250078. https://doi.org/10.1142/S0219455412500782

[100] Sofiyev, A. H. "Nonlinear free vibration of shear deformable orthotropic functionally graded cylindrical shells." *Composite Structures* 142 (2016): 35-44. https://doi.org/10.1016/j.compstruct.2016.01.066

[101] Sofiyev, A. H., Z. Karaca, and Z. Zerin. "Non-linear vibration of composite orthotropic cylindrical shells on the non-linear elastic foundations within the shear deformation theory." *composite structures* 159 (2017): 53-62. https://doi.org/10.1016/j.compstruct.2016.09.048

[102] Dey, Tanish, and L. S. Ramachandra. "Non-linear vibration analysis of laminated composite circular cylindrical shells." *composite structures* 163 (2017): 89-100. https://doi.org/10.1016/j.compstruct.2016.12.018

[103] Hasrati, E., R. Ansari, and H. Rouhi. "Nonlinear free vibration analysis of shell-type structures by the variational differential quadrature method in the context of six-parameter shell theory." *International Journal of Mechanical Sciences* 151 (2019): 33-45. https://doi.org/10.1016/j.ijmecsci.2018.10.053

[104] Kurylov, Ye, and M. Amabili. "Polynomial versus trigonometric expansions for nonlinear vibrations of circular cylindrical shells with different boundary conditions." *Journal of Sound and Vibration* 329.9 (2010): 1435-1449. https://doi.org/10.1016/j.jsv.2009.10.038

[105] Kamaloo, Abbas, et al. "Nonlinear free vibration analysis of delaminated composite circular cylindrical shells." *Journal of Vibration and Control* 26.19-20 (2020): 1697-1707. https://doi.org/10.1177/1077546320902556

[106] Nguyen, Thi Phuong, et al. "Nonlinear vibration of full-filled fluid corrugated sandwich functionally graded cylindrical shells." *Journal of Vibration and Control* 27.9-10 (2021): 1020-1035. https://doi.org/10.1177/1077546320936537

[107] Khuc, Phu Van, Bich Huy Dao, and Doan Xuan Le. "Analysis of nonlinear thermal dynamic responses of sandwich functionally graded cylindrical shells containing fluid." *Journal of Sandwich Structures & Materials* 21.6 (2019): 1953-1974. https://doi.org/10.1177/1099636217737235

[108] Zhu, Chang-Song, et al. "Surface energy effect on nonlinear free vibration behavior of orthotropic piezoelectric cylindrical nano-shells." *European Journal of Mechanics-A/Solids* 66 (2017): 423-432. https://doi.org/10.1016/j.euromechsol.2017.08.001

[109] Van Dung, Dao, and Vu Hoai Nam. "Nonlinear dynamic analysis of eccentrically stiffened functionally graded circular cylindrical thin shells under external pressure and surrounded by an elastic medium." *European Journal of Mechanics-A/Solids* 46 (2014): 42-53. https://doi.org/10.1016/j.euromechsol.2014.02.008

[110] Foroutan, Kamran, and Habib Ahmadi. "Nonlinear Static and Dynamic Buckling Analyses of Imperfect FGP Cylindrical Shells Resting on Nonlinear Elastic Foundation Under Axial Compression." *International Journal of Structural Stability and Dynamics* 20.07 (2020): 2050074. https://doi.org/10.1142/S0219455420500741.

[111] Xu, Jie, et al. "Nonlinear vibrations of thermo-hyperelastic moderately thick cylindrical shells with 2: 1 internal resonance." *International Journal of Structural Stability and Dynamics* 20.05 (2020): 2050067. https://doi.org/10.1142/S0219455420500674.

[112] Wang, Yan Qing, Yun Fei Liu, and T. H. Yang. "Nonlinear thermo-electro-mechanical vibration of functionally graded piezoelectric nanoshells on Winkler–Pasternak foundations via nonlocal Donnell's nonlinear shell theory." *International Journal of Structural Stability and Dynamics* 19.09 (2019): 1950100. https://doi.org/10.1142/S0219455419501001.

[113] Phuong, Nguyen Thi, et al. "Nonlinear stability of sandwich functionally graded cylindrical shells with stiffeners under axial compression in thermal environment." *International Journal of Structural Stability and Dynamics* 19.07 (2019): 1950073. https://doi.org/10.1142/S0219455419500731

[114] Mohandes, Masood, and Ahmad Reza Ghasemi. "A new approach to reinforce the fiber of nanocomposite reinforced by CNTs to analyze free vibration of hybrid laminated cylindrical shell

using beam modal function method." *European Journal of Mechanics-A/Solids* 73 (2019): 224-234.

[115] Touzé, Cyril, Marina Vidrascu, and Dominique Chapelle. "Direct finite element computation of non-linear modal coupling coefficients for reduced-order shell models." *Computational Mechanics* 54.2 (2014): 567-580. https://doi.org/10.1007/s00466-014-1006-4

[116] Tong, Liyong. "Free vibration of orthotropic conical shells." *International Journal of Engineering Science* 31.5 (1993): 719-733. https://doi.org/10.1016/0020-7225 (93)90120-J

[117] Torki, Mohammad Ebrahim, et al. "Dynamic stability of cantilevered functionally graded cylindrical shells under axial follower forces." *Thin-Walled Structures* 79 (2014): 138-146. https://doi.org/10.1016/j.tws.2013.12.005

[118] AminYazdi, Ali. "Flutter of geometrical imperfect functionally graded carbon nanotubes doubly curved shells." *Thin-Walled Structures* 164 (2021): 107798 https://doi.org/10.1016/j.tws.2021.107798

[119] Ben-Youssef, Y., Kerboua, Y., & Lakis, A. A. "Numerical Modeling of Initial Stress Stiffening Effect on the Dynamic Behavior of Axisymmetric Shells". *Journal of Pressure Vessel Technology*, 143.5 (2021): 051303. https://doi.org/10.1115/1.4050092

[120] Ashley, Holt, and Garabed Zartarian. "Piston theory-a new aerodynamic tool for the aeroelastician." *Journal of the Aeronautical Sciences* 23.12 (1956): 1109-1118. https://doi.org/10.2514/8.3740

[121] Dowell, Earl H. "Flutter of infinitely long plates and shells. II-Cylindrical shell." *AIAA Journal* 4.9 (1966): 1510-1518. https://doi.org/10.2514/3.3728

[122] Dowell, E. H. "Aeroelasticity of plates and shells, Noordhoff Int." *Publishing, Leyden, The Netherlands* (1975).

[123] Krumhaar, H. "The accuracy of linear piston theory when applied to cylindrical shells". *AIAA Journal*, 1.6, (1963): 1448-1449. https://doi.org/10.2514/3.1832

[124] Carter, L. L., and R. O. Stearman. "Some aspects of cylindrical shell panel flutter." *AIAA Journal* 6.1 (1968): 37-43. https://doi.org/10.2514/3.4438

[125] Zarifian, P., Ovesy, H. R., & Firouz-Abadi, R. D. "Sloshing effects on supersonic flutter characteristics of a circular cylindrical shell partially filled with liquid". *International Journal for Numerical Methods in Engineering*, 117.8 (2019): 901-925. https://doi.org/10.1002/nme.5984

[126] Ganapathi, M., Varadan, T. K., & Jijen, J. "Field-consistent element applied to flutter analysis of circular cylindrical shells". *Journal of sound and vibration*, 171.4 (1994): 509-527. https://doi.org/10.1006/jsvi.1994.1137

[127] Ramzi, R., and A. Lakis. "Effect of Geometric and Fluid Flow Nonlinearities On Cylindrical Shells Subjected to a Supersonic Flow." *International Journal of Numerical Methods and Applications* 9.1 (2013): 1.